STRAIN AGE EMBRITTLEMENT IN REINFORCING STEELS

A thesis

presented for the Degree of

Doctor of Philosophy

in

Mechanical Engineering

in the University of Canterbury

by

Lakshman Nissanka Pussegoda

University of Canterbury,

Christchurch, New Zealand.

1978.

To Appachi (Dad),

in appreciation of his interest in my future.

ACKNOWLEDGEMENTS

The author wishes to record his appreciation of the support and guidance provided by Dr L. A. Erasmus during his supervision of this project. His encouragement, suggestions and time spent in discussion have been much appreciated.

I also extend my gratitude to Professor D. C. Stevenson, Head of the Mechanical Engineering Department, for the use of facilities for this study.

I wish to thank other academic and technical staff of the Mechanical Engineering Department, particularly Mr D. Somerville for his assistance with the chemical analysis, Mr E. D. Retallick for the preparation of test specimens, and Mrs J. Ritchie for her care in preparation of the diagrams and photographs.

The project was financially supported by the Ministry of Works and Development, and the author wishes to gratefully acknowledge this assistance. Also the interest shown by its Structural Engineers at the Head Office and the academic staff of the Civil Engineering Department have been much appreciated.

The support for this project by the Management of Pacific Steel Limited in making all the experimental steels is gratefully acknowledged. I also wish to acknowledge the financial assistance received from them during my stay in Auckland.

Finally, I wish to thank Mrs P. Dowell for typing the manuscript.

ABSTRACT

The object of this thesis is to examine the effect of strain ageing on the tensile and fracture properties of reinforcing steels and to determine economically feasible methods of reducing strain age embrittlement in reinforcing bar contained in reinforced concrete structures.

The effect of titanium and vanadium additions to normal reinforcing steels on strain ageing has been investigated by obtaining the resultant changes in mechanical properties. Both these transition elements have been effective in reducing strain ageing to a negligible level when present in sufficient quantities, while titanium also reduces the as-rolled transition temperature and increases the Luder's strain.

Examined in detail also is the effect of strain ageing on the mechanical properties of a normal reinforcing steel and a similar titanium-bearing steel after variation of plastic strain, ageing temperature and ageing time. Due to the stabilizing effect of the titanium addition, this steel exhibits superior impact properties over the normal steel when strained and then aged at or below $100^{\circ}C$. When the ageing temperature is increased above $100^{\circ}C$, these stabilized characteristics are gradually removed and hence the fracture properties tend to that of the normal steel.

A critical study of the existing standards for bends in deformed reinforcing bar shows the necessity for modification of these standards to eliminate the possibility of brittle fracture at bends as a result of strain age embrittlement. Recommendations for these modifications are made from the determination of safe bend diameters obtained using data from field failures at bends.

CONTENTS

CHAPTER			Page
1	INTRODUCTION		1
2	THE SIGNIFICANCE OF STRAIN AGEING IN REINFORCED CONCRETE STRUCTURES		6
	2.1	Design Philosophy	6
	2.2	Ductility Requirements for Reinforcing Steels	7
	2.3	Susceptibility of Reinforcing Steels to Strain Age Embrittlement	7
	2.4	Critical Effects of Strain Ageing on the Design Philosophy	8
3	STRAIN AGEING AND EMBRITTLEMENT IN LOW CARBON STEELS		11
	3.1	The Yield Point in Low Carbon Steels	11
	3.2	General Features of Strain Ageing	15
	3.3	Mechanism of Strain Ageing	17
	3.4	Effects of Carbon and Nitrogen	20
	3.5	Type and Extent of Pre-strain	23
	3.6	Effect of Ageing Temperature	25
	3.7	Strain Hardening	27
	3.8	Effects of Strain Ageing on Mechanical Properties	27
		3.8.1 Tensile Properties	27
		3.8.2 Strain Age Embrittlement	31
4	METHODS OF PREVENTING STRAIN AGEING		38
	4.1	Comparison of Methods Available	38
	4.2	Effect of Nitride Forming Elements	40
		4.2.1 Aluminium	40
		4.2.2 Boron	47
		4.2.3 Titanium	49
		4.2.4 Vanadium	53
		4.2.5 Niobium	59
		4.2.6 Zirconium	64
	4.3	Summary	65

CHAPTER			Page
5	EFFECT OF TITANIUM ADDITIONS TO AS-ROLLED C-Mn REINFORCING STEELS		66
	5.1	Preparation of the Steels	66
	5.2	Stabilization of Nitrogen by Titanium	66
	5.3	Grain Refinement and Luder's Strain	66
	5.4	Effect of Titanium Content on Strain Ageing Characteristics	70
		5.4.1 Tensile Properties	70
		5.4.2 Impact Properties	70
	5.5	Summary	73
6	EFFECT OF VANADIUM ADDITIONS TO AS-ROLLED C-Mn REINFORCING STEELS - EXPERIMENTAL PROCEDURE, RESULTS AND DISCUSSION		76
	6.1	Preparation of the Steels	76
	6.2	Chemical Analysis	76
		6.2.1 Composition of the Steels	76
		6.2.2 Determination of Nitrogen in the Steels	77
	6.3	Grain Size Measurements	80
	6.4	Tensile Test Results	80
	6.5	Charpy V-notch Impact Test Results	81
	6.6	Discussion of Results	84
		6.6.1 Stabilisation of Nitrogen by Vanadium	84
		6.6.2 Effect of Vanadium Content on As-Rolled Tensile Properties	86
		6.6.3 Effect of Vanadium on Changes in Tensile Properties due to Strain Ageing	88
		6.6.4 Effect of Vanadium on the As-Rolled Transition Temperature	94
		6.6.5 Effect of Vanadium on Strain Age Embrittlement	94
	6.7	Summary	99

CHAPTER			Page
7	STRAIN AGEING CHARACTERISTICS OF NORMAL AND TITANIUM-BEARING AS-ROLLED REINFORCING STEELS - EXPERIMENTAL PROCEDURE, RESULTS AND DISCUSSION		102
	7.1	Introduction	102
	7.2	Experimental Procedure	102
	7.3	As-Rolled Mechanical Properties	103
	7.4	Tensile Test Results	105
		7.4.1 Effect of Pre-strain	105
		7.4.2 Effect of Ageing Temperature and Time	105
	7.5	Charpy V-notch Impact Test Results	105
		7.5.1 Effect of Pre-strain	105
		7.5.2 Effect of Ageing Temprature and Time	112
	7.6	Discussion of Results	112
		7.6.1 The Effect of Pre-Strain	112
		7.6.2 Effect of Pre-strain within the Yield Strain Region	119
		7.6.3 Effect of Ageing Temperature and Time	121
	7.7	Summary	135
8	EMBRITTLEMENT IN COLD BEND REINFORCING BAR		136
	8.1	Embrittlement Testing of Deformed Reinforcing Bar	136
		8.1.1 Chemical Analysis	136
		8.1.2 Testing Procedure	136
	8.2	Estimation of Plastic Strain in Cold Bent Reinforcing Bar	140
		8.2.1 Specimen Preparation	140
		8.2.2 Quantitative Metallographic Estimation of Plastic Strain	140
	8.3	Examination of Fracture Profiles	143
	8.4	Examination of Fracture Surfaces	145
	8.5	Discussion	147

CHAPTER				Page
8		8.5.1	Embrittlement Test Results	147
		8.5.2	Cleavage Fracture at Bends	151
		8.5.3	The Mechanism of Fracture	153
		8.5.4	Methods of Reducing the Susceptibility of Cleavage Fracture	156
9	CONCLUSIONS AND RECOMMENDATIONS			163
	9.1	The Significant Effects of Strain Ageing		163
		9.1.1	The Effect of Increase in Yield Strength	163
		9.1.2	The Effect of Strain Age Embrittlement	163
	9.2	The Advantages of Non-Strain Ageing Steels		165
		9.2.1	The Effect of Increase in Yield Strength	165
		9.2.2	The Effect of Strain Age Embrittlement	165
	9.3	Comparison of the Elements that may be used to prevent Strain Ageing		166
REFERENCES				169
APPENDIX A		Detailed Procedures for Chemical Analysis		A.1
APPENDIX B		Details of Test Specimen Preparation		B.1
APPENDIX C		Safe Bend Radii for Deformed Reinforcing Bar to avoid failure by Strain Age Embrittlement		C.1

LIST OF FIGURES

FIGURE	DESCRIPTION	Page
3.1	A typical load-extension curve for a low carbon steel.	12
3.2	A typical load-extension curve for a non-ferrous steel.	12
3.3	Load-elongation curve for low carbon steel, showing the effect of strain ageing.	16
3.4	Effect of ageing time on changes in tensile properties due to strain ageing in low carbon steels.	18
3.5	Effect of interstitial content on strain ageing in low carbon steels.	19
3.6	Solubilities of nitrogen and carbon in iron.	22
3.7	Diffusion coefficients of nitrogen and carbon in α-iron.	22
3.8	Ageing curves for deep-drawing rimmed steel.	24
3.9	Effect of the degree of pre-strain on changes in tensile properties due to strain ageing.	24
3.10	Effect of strain ageing in a low carbon steel on the Hall-Petch relationship ($\sigma_y = \sigma_i + k_y d^{-\frac{1}{2}}$).	34
3.11	Effect of strain ageing on the impact transition curve.	34
3.12	Changes in Charpy V-notch impact transition temperature due to straining and subsequent ageing, in C-Mn steels.	37
4.1	Increase in yield stress after strain ageing with ageing temperature, in as-rolled C-Mn steel.	41
4.2	Increase in yield stress after strain ageing with ageing temperature, in normalised C-Mn steel.	41
4.3	Variation in impact transition temperature with grain size.	43
4.4	Variation in lower yield stress with grain size.	43
4.5	Preceipitation characteristics of AlN in a 0.08% aluminium steel.	46
4.6	Data on precipitation kinetics of AlN in low carbon steel.	46
4.7	Effect of Boron content on strain ageing in a low carbon steel.	48
4.8	Solubility products for BN, AlN, VN, and Si_3N_4.	48
4.9	Change in ΔY with pre-strain after strain ageing in HSLA steels.	56

FIGURE	DESCRIPTION	Page
4.10	Effect of the rolling variables and composition on the Hall-Petch relationship of a structural steel containing 0.09% vanadium.	56
4.11	Effect of finish rolling temperature on yield strength and impact transition temperature of 0.06% vanadium steels.	58
4.12	Effect of niobium content on ΔY after strain ageing in a low carbon steel.	61
4.13	Effect of the rolling variables on the Hall-Petch relationship of a structural steel containing 0.08% niobium.	61
4.14	Effect of niobium content on yield strength and impact transition temperature of a C-Mn steel at two finish rolling temperatures.	63
5.1	Effect of titanium content on the stabilisation of nitrogen in as-rolled reinforcing steel.	68
5.2	Effect of titanium content on grain size, at two manganese contents.	69
5.3	Effect of titanium content on Luder's strain, at two manganese contents.	69
5.4	Effect of titanium content on ΔY, at the lower manganese content.	71
5.5	Effect of titanium content on ΔU, at the lower manganese content.	71
5.6	Effect of titanium content on ΔEl, at the lower manganese content.	72
5.7	Effect of titanium content on ΔY, at the higher manganese content.	72
5.8	Effect of titanium content on impact transition temperature, at the lower manganese content.	74
5.9	Effect of titanium content on the impact transition temperature, at the higher manganese content.	74
6.1	Effect of vanadium content on the stabilisation of nitrogen in as-rolled reinforcing steel with (a) 0.025% Al_{sol}, and (b) 0.005% Al_{sol}.	85
6.2	Variation in LYS with vanadium content of as-rolled reinforcing steel having two levels of Al_{sol}.	87

FIGURE	DESCRIPTION	Page
6.3	Variation in Luder's strain with vanadium content of as-rolled reinforcing steels having two levels of Al_{sol}.	87
6.4	Variation in tensile strength with vanadium content of as-rolled reinforcing steels having two levels of Al_{sol}.	89
6.5	Effect of strain ageing on the changes in the stress-strain curves for (A) Normal Grade 275 steel, (B) 0.6% vanadium steel.	90
6.6(a)	Effect of vanadium content on the changes in tensile properties due to strain ageing in Group A steels	91
6.6(b)	Effect of vanadium content on changes in tensile properties due to strain ageing in Group B steels.	92
6.7	Effect of the V/N ratio on the fracture transition temperature (T_{27}) of as-rolled vanadium steels.	95
6.8	Effect of strain ageing on the fracture transition temperature as a function of vanadium content in reinforcing steel, with (a) 0.025% Al_{sol}, and (b) 0.005% Al_{sol}.	97
6.9	Effect of vanadium content on strain age embrittlement of as-rolled reinforcing steel with (a) 0.025% Al_{sol}, (b) 0.005% Al_{sol}.	98
7.1	Effect of pre-strain on changes in tensile properties due to strain ageing in normal and titanium steels.	113
7.2	Effect of strain ageing on the changes in the stress-strain curves for (A) normal steel; (B) Ti(a) steel.	114
7.3	Effect of pre-strain on ΔT_{27} due to strain ageing in normal and titanium steels.	117
7.4	Effect of pre-strain (including the yield strain region) on ΔY due to strain ageing in normal and Ti(a) steel.	117
7.5	Effect of pre-strain in the yield strain region on changes in the stress-strain curves after strain ageing, for (A) normal steel, (B) Ti(a) steel.	120
7.6	The relationship between pre-strain in the yield strain region and the first yield point elongation (YPE_1) after strain ageing in normal and Ti(a) steels.	120
7.7	Effect of ageing temperature on changes in tensile properties due to strain ageing in normal and Ti(a) steels.	122
7.8	Effect of strain ageing on changes in the stress-strain curve for Ti(a) steel, at (A) 150°C; (B) 200°C.	124

FIGURE	DESCRIPTION	Page
7.9	Effect of equivalent ageing time at 60°C as determined by Hundy's equation, on changes in tensile properties of normal steel.	126
7.10	Changes in tensile properties obtained from ageing temperature-time combinations, superimposed on the curves from Figure 7.7 using Hundy's equation, for normal and Ti(a) steel.	127
7.11	Changes in tensile properties obtained from ageing temperature-time combinations, superimposed on the curves from Figure 7.7 using Hundy's equation, for Ti(b) steel.	129
7.12	Effect of ageing temperature on ΔT_{27} due to strain ageing in normal and Ti(a) steel.	131
7.13	ΔT_{27} obtained from selected ageing temperature-time combinations, superimposed on the curves from Figure 7.12 using Hundy's equation, for normal and Ti(a) steel.	131
7.14	ΔT_{27} obtained from selected ageing temperature-time combinations superimposed on the curves from Figure 7.12 using Hundy's equation, for Ti(b) steel.	133
8.1	Photomicrographs of areas below (a) a notch root, and (b) a compression crack, formed adjacent to a deformation on the inner radii surface of bends in deformed reinforcing bar.	141
8.2	Initial fracture profiles of (a) an aged bend, (b) an unaged bend, in 28 mm deformed bar with a bend diameter of 2.5d, after re-straightening.	144
8.3	A ductile tear in a predominantely cleavage fracture of a 3.5d bend in 22 mm deformed bar.	146
8.4	A "compression crack" area adjacent to the inner radius surface of a 1.5d bend.	146
8.5	A transition area with "compression crack" facets preceding cleavage facets.	148
8.6	An area of high pre-strain adjacent to the "compression crack".	148
8.7	An area of low pre-strain close to the neutral axis of the 1.5d bend.	149
8.8	Cleavage fracture in 28 mm diameter deformed bar at a bend.	149
8,9	Localised plastic yielding from stress concentration points adjacent to deformations in reinforcing bar, during initial stages of re-straightening, shown by etching with Fry's reagent.	154

FIGURE	DESCRIPTION	Page
8.10	A "compression crack" area with the fracture surface tilted by 20°.	154
8.11	Variation in plastic strain on bend inner radius surface of 20 mm diameter plain reinforcing bar, with former diameter/bar diameter ratio.	157
8.12	Variation in plastic strain with former diameter/bar diameter ratio for 28 mm deformed bar, both at notch root and bend inner radius surface.	157
8.13	Variation in plastic strain with former diameter/bar diameter ratio for 22 mm deformed bar, both at notch root and bend inner radius surface.	158
8.14	Variation in plastic strain with former diameter/bar diameter ratio for 16 mm deformed bar, both at notch root and bend inner radius surface.	158

LIST OF TABLES

TABLE	DESCRIPTION	Page
5.1	Cast analysis of Grades 275 and 380 steels.	67
6.1	Approximate base compositions of the two groups of vanadium steels.	78
6.2	Vanadium and aluminium analysis of the vanadium steels.	78
6.3	Nitrogen determinations of the vanadium steels.	79
6.4	Grain size measurements of some vanadium steels.	79
6.5	Tensile properties of the vanadium steels.	82
6.6	Variation in tensile properties due to strain ageing in vanadium steels.	82
6.7	Charpy V-notch fracture transition temperature of as-rolled and strain aged vanadium steels.	83
7.1	The composition and nitrogen determinations of the titanium and normal steels.	104
7.2	Mechanical properties and ferrite grain size.	104
7.3	Effect of pre-strain on changes in tensile properties due to strain ageing in normal and titanium steels.	106
7.4	Effect of ageing temperature on changes in tensile properties due to strain ageing.	107
7.5	Equivalent ageing times for a one hour ageing time at higher temperatures as determined using Hundy's equation.	108
7.6	Combined effect of ageing temperature and time on changes in tensile properties due to strain ageing.	109
7.7	Effect of pre-strain on ΔT_{27} in normal and titanium steels.	110
7.8	Effect of ageing temperature on ΔT_{27} in normal and titanium steel.	110
7.9	Combined effect of ageing temperature and time on ΔT_{27} in normal and titanium steels.	111
8.1	Chemical analysis of commercially obtained reinforcing bar.	137
8.2	Results from slow bend tests on deformed reinforcing bar. (a) Grade 275; (b) Grade 380.	138,139
8.3	Tangential plastic strain at the inner surface radii of cold bend reinforcing bar.	142

SOME NOTATIONS OF FREQUENT OCCURRENCE

d	mean grain diameter or nominal reinforcing bar diameter
σ_y	lower yield stress (LYS)
σ_i	friction stress in Hall-Petch equation
k_y	the grain boundary strength coefficient in Hall-Petch equation
ΔY	increase in lower yield stress (LYS) on ageing
ΔU	increase in tensile strength (TS) on ageing
ΔEl	change in elongation at fracture (El) on ageing
σ_f	flow stress
T	Temperature
γ	free surface energy
γ_{eff}	'effective' surface energy
σ_F	fracture stress
T_{27}	27 Joule (or 20 ft lb) fracture transition temperature
ΔT_{27}	increase in the fracture transition temperature caused by strain ageing
N_{sol}	'acid soluble' nitrogen
N_{insol}	'acid insoluble' nitrogen
N_{tot}	total nitrogen
N_{AlN}	nitrogen in the form of AlN
N_{active}	'active' nitrogen
Al_{sol} or Al_{sol}	soluble aluminium
D	diameter of bend former

CHAPTER 1

INTRODUCTION

The principal requirement of a properly designed structure is that it, or any part of it, be able to support the loads that are applied during its operating life time. These loads may be separated and classed as static and dynamic loads. In case of reinforced concrete structural design, in most instances the main operating loads are static (i.e., the service loads). However, structures built in regions of the world which are liable to earthquakes should be capable of supporting dynamic seismic loading without catastrophic results.

As a result of economics and feasibility, both strength and energy dissipation characteristics of the system are utilised rather than the criteria of strength alone in the present philosophy of designing earthquake resistant structures[1]. The energy dissipation characteristics are utilised to absorb the dynamic loads encountered during earthquakes, and relies on a ductile performance of the structure in the post-elastic range. Therefore, it is essential that the steels used for reinforcement in these structures should be capable of accommodating significant amounts of plastic strain without failure (in certain regions of the structure), and so absorb and dissipate energy during seismic loading.

Consequently, the possibility of failure without energy dissipation, as may occur if the reinforcing steel fails in a brittle mode with little or no plastic strain, is of considerable concern to engineers involved in earthquake resistant structural design. Therefore a brittle failure at a standard bend in a column reinforcing (deformed) bar reported in 1972 has drawn attention to the problem of strain age embrittlement in reinforcing steel bar.

Since the above incident, similar failures have been reported from many parts of New Zealand; Invercargill, Manapouri, Auckland and Canterbury. These failures almost always occur when a designed bend or return in deformed reinforcing bar is being opened out or adjusted by decreasing the bend angle sometime after the initial bend was made. The occurrence of high tensile stresses closed to designed bends contained in reinforced concrete structures must always be a possibility during earthquakes as a result of seismic loading, and could result in similar brittle failures. Hence these reported failures have led to the urgent need for definitive information on the significance of strain ageing in earthquake resistant reinforced concrete structures and on precautions necessary to protect structures from such failures in service.

From a metallurgical viewpoint, an investigation on this problem is best directed in the following lines. Quantitative information be provided to engineers on the effects of strain ageing on the mechanical properties of reinforcing steels so that this information can be used at the design stage. This information, to some extent, will show the significance of strain ageing in earthquake resistant concrete structures. Work should also be carried out on an attempt to separate the contributory causes of embrittlement in plastically strained reinforcing bar and thus examine the possibilities of reducing the susceptibility of the present reinforcing steels to embrittlement.

Embrittlement in plastically strained reinforcing steels in concrete structures is caused by the combined effects of:

(a) Embrittlement due to plastic straining;

(b) Embrittlement due to subsequent ageing;

(c) In the case of deformed reinforcing bar, the notch effects of the deformations;

(d) Increases in the strain rate;

(e) A decrease in temperature.

Of these effects, (d) is predominantly dependent on the characteristics of earthquake ground motion and the structure design, while (e) is dependent on the environment temperature. Therefore, both these effects are independent of metallurgical factors. (a) and (b) are metallurgical phenomena, while (c) is partially affected by metallurgical behaviour. Therefore, in attempts to reduce embrittlement in plastically strained reinforcing steels, it is logical to investigate possibilities of reducing embrittlement resulting from (a), (b) and (c) above.

Strain ageing is a term used to describe a number of property changes which occur in low-carbon steels as a result of plastic straining followed by subsequent 'ageing' at ambient or elevated temperatures. These property changes are more accurately divided into a number of separate processes referred to as Strain Ageing, Strain Age Hardening, and Strain Age Embrittlement.

When a low-carbon steel is plastically strained and then aged naturally (at ambient temperature) or artificially (at an elevated temperature), there is a progressive return of the discontinuous yield point at a stress substantially above that of the unstrained steel. The return of the discontinuous yield point is caused by the 'locking' of mobile dislocations, introduced during plastic straining, by interstitial carbon and nitrogen atoms which diffuse to the dislocation sites during ageing[2, 3]. This increase in the lower yield stress is normally accompanied by an increase in the tensile strength and a decrease in elongation at fracture. These effects of strain ageing on tensile properties are normally referred to as strain age hardening. Associated with this strain age hardening is an increase in the ductile to brittle transition temperature, known as strain age embrittlement.

Natural strain ageing in slow cooled or as-rolled low-carbon steels

is caused by interstitial or 'active' nitrogen only[2, 3]. Therefore the addition of strong nitride formers to low-carbon steels should reduce their susceptibility to strain ageing.

Previous research work done in the Department of Mechanical Engineering at the University of Canterbury showed that additions of sufficient Titanium (a strong nitride former) to combine with the 'active' nitrogen in normal reinforcing steels almost completely eliminated natural strain ageing[4]. As these Titanium-bearing steels exhibit non-strain ageing characteristics in the hot-rolled condition, this method is both feasible and economical for a commercial scale operation. As Titanium is a strong deoxidizer, the product will have to be a fully killed steel.

Although published literature is available on the effect of strain ageing in low-carbon steels on both tensile and impact properties, these have been predominantly limited to the study of single aspects; e.g., the effect of ageing time, ageing temperature or interstitial content. These investigations were generally restricted to the effect of strain ageing on one particular mechanical property such as either the tensile properties or to the increase in the fracture transition temperature (which is a measure of strain age embrittlement).

Therefore, a complete systematic investigation of the effects of plastic straining, ageing temperature, ageing time and interstitial content on both tensile and impact properties due to strain ageing in as-rolled reinforcing steels, is not feasible from available data. An experimental investigation along these lines is essential for a detailed study of the separate causes of embrittlement due to plastic straining and subsequent ageing. Such an investigation will also result in quantitative data regarding the effects of strain ageing on the mechanical properties of reinforcing steels currently manufactured in New Zealand.

As a result of the preceding discussion, the scope of this thesis is given below:

(i) A systematic study of the effects of plastic strain, ageing temperature and ageing time on the mechanical properties of a normal grade 275 (NZS 3402 P, 1973) reinforcing steel and a similar Titanium-bearing non-strain ageing steel. From these results an attempt is made to separate the embrittlement effects of plastic straining and subsequent ageing.

(ii) As a Titanium-bearing steel has to be fully killed, the use of Vanadium (another strong nitride former) for eliminiating strain ageing in as-rolled reinforcing steels has also been investigated.

(iii) The present reinforcing bar bending practices in New Zealand have been critically examined and the brittle fracture at bends in deformed reinforcing bar studied in order to eliminate such failures in reinforced concrete structures.

To begin with, the significance of strain ageing in earthquake resistant reinforced concrete structures is discussed, followed by a detailed discussion of the literature on strain ageing in low-carbon steels. The literature available on the effect of the addition of nitride forming elements to low-carbon steels is also reviewed.

CHAPTER 2

THE SIGNIFICANCE OF STRAIN AGEING IN REINFORCED CONCRETE STRUCTURES

2.1 Design Philosophy

In the design of reinforced concrete structures, a significant consideration that may have to be added to strength and serviceability is ductility. It is important to ensure that in the extreme event of a structure being loaded to failure, it will not fail in a brittle manner (without warning) but will be capable of large deformation at near-maximum load carrying capacity. The large deformations at near-maximum load will give ample warning of failure, and by maintaining the load carrying capacity, total collapse may be prevented and lives saved.

In designing for seismic loading, ductility becomes an extremely important consideration. This is because the present philosophy of codes for seismic loading is to design structures to resist only relatively moderate earthquakes elastically; in the case of a severe earthquake, reliance is placed on the availability of sufficient ductility after yielding to enable the structure to survive without catastrophic failure[1]. These recommendations for seismic loading can be justified only if the structure has sufficient ductility to absorb and dissipate energy by post-elastic deformations when subjected to several cycles of loading well into the yield range.

In the present design philosophy, the ductility of the structure is ensured by the development of 'plastic hinges' in certain regions of the reinforced concrete frame[1, 5]. Plastic hinges are formed in regions where post-elastic deformations occur when the structure is subjected to seismic loading, i.e., the initial regions of flexural yielding in beams and/or columns. These hinges are designed to form in the beams adjacent to column-beam joints in preference to forming in the columns[1, 5]. Energy

dissipation is best provided by plastic hinging in beams because yielding is then spread through the frame and the ductility demands on individual plastic hinges are not so great. Hence the emphasis at present is for the design of strong column-weak beam joints.

2.2 Ductility Requirements for Reinforcing Steels

Reinforcing steel plays an extremely important role in earthquake resistant reinforced concrete structures. The longitudinal steel in a member determines the strength and ductility of the member, while transverse steel is provided to prevent shear failure (which is a brittle form of failure in structural members), to prevent buckling of longitudinal compression steel and to increase the ductility of the concrete by effective concrete confinement[1, 5].

The ductility requirements for reinforcing steel used in earthquake resistant concrete structures are significantly more demanding than for the case of normal reinforced concrete structures. This results from the design philosophy which requires absorption and dissiptation of energy by post-elastic deformation in regions such as plastic hinges, and is almost entirely dependent on the ductile performance of the reinforcing steel[1]. In extreme cases, the total energy dissipation may have to be carried by the longitudinal steel at the plastic hinges. For the survival of a reinforced structure without collapse during a severe earthquake, it is essential to completely eliminate brittle fracture in both longitudinal or transverse reinforcing steels. For example, concrete confinement depends upon the safe performance of transverse steel in the form of stirrups, hoops etc.

2.3 Susceptibility of Reinforcing Steels to Strain Age Embrittlement

The ductility requirements for reinforcing steels used in earthquake resistant concrete structures are provided by as-rolled reinforcing steels currently manufactured in New Zealand by the BEA process to grades 275 and

380 of NZS 3402 P (1973). However, this reinforcing steel is not always present in the as-rolled state in concrete structures. For example, most regions contain cold bent reinforcing bars in the form of standard bends, returns or hooks, generally for anchorage purposes, and stirrups for shear resistance, concrete confinement etc. These plastically strained bars strain age during service as these steels have sufficient 'active' nitrogen in the as-rolled state to cause strain ageing at ambient temperatures[4]. Therefore, although as-rolled reinforcing steels have sufficient ductility to perform satisfactorily in concrete structures during seismic loading, strain aged regions will be susceptible to brittle failure, which may cause catastrophic collapse of the structure. This possiblity has been illustrated by construction failures at bends in deformed reinforcing bars. These failures have been reported from many parts of New Zealand. A detailed investigation of one such field failure has shown that these failures (at bends) were by cleavage fracture resulting from strain age embrittlement and associated with the stress concentration effect of notches formed adjacent to the deformations (ribs) on the inner radius surface[6].

Strain ageing in longitudinal reinforcing bars will occur at plastic hinges formed by the first formidable earthquake the concrete structure is subjected to. This will result in an increase in the flexural strength of these plastic hinges as a result of the increase in yield strength of this steel during the ageing process. As a result of this increase in flexural strength, plastic hinges may be formed during subsequent earthquakes or 'after shocks', in regions which have not been designed as such. For example, the development of plastic hinges in regions which do not have sufficient transverse reinforcement can cause shear failure[1, 5].

2.4 Critical Effects of Strain Ageing on the Design Philosophy

To ensure that plastic hinges will form in the beams adjacent to

columns, the following conditions should be satisfied when designing strong column-weak beam joints:

(a) The column should have sufficient strength to withstand any 'over-strength' of the potential plastic hinge in the beam resulting from variations in mechanical properties of the reinforcing steel and concrete, section size etc.[1].

(b) Have sufficient transverse steel at designed plastic hinges mainly in the form of stirrups, to prevent shear failure, to prevent buckling of the longitudinal steel during cyclic loading and to increase the ductility of the concrete by applying a passive confinement pressure to the concrete[5].

Strain ageing can have adverse effects on both of the above conditions. Strain age embrittlement at bends in stirrups, ties etc. makes these transverse components susceptible to brittle fracture at the bends, especially in the case of a severe earthquake when large post-elastic cyclic strains are to be withstood by the longitudinal steel. Secondly, strain ageing of the longitudinal steel at the plastic hinges subsequent to the first formidable seismic loading, can increase the flexural strength at the plastic hinge sufficiently to cause plastic hinging in the column adjacent to the beam-column joint or result in a brittle shear type failure of the beam, due to unaccounted 'overstrength'[5].

Even with the strong column-weak beam joint concept, it is not feasible to completely eliminate the formation of plastic hinges in columns under certain conditions of seismic loading[1]. Because of the heavy axial compressive loading on columns, they are inherently less ductile than the beams in the post-elastic range[5]. The ductility of columns may be improved by passive concrete confinement using sufficient transverse steel in the form of stirrups, ties, hoops, or spirals adjacent to the column-

beam joint where the potential plastic hinge may be formed in columns in cases of extreme seismic loading[1]. It is also essential that these regions have sufficient transverse reinforcement to prevent brittle shear type failure. When stirrups are used for passive concrete confinement in columns, the stirrup bends are subjected to a bend opening load when the cover concrete falls and the stirrups arch between corners[1], causing tensile stresses at the inner surface radii of the bend, which can cause cleavage fracture[6].

Effective anchorage of reinforcement is an essential criteria for the ductile performance of the structure in response to seismic loading. In certain regions concrete confinement is beneficial to the anchorage of reinforcement and is obtained by transverse steel[1], once again showing the importance of the safe performance of transverse steel under seismic loading. Finally, in the case of a severe earthquake, failure of reinforcing steel in a brittle mode without gross plastic deformation is obviously *not* desirable.

CHAPTER 3

STRAIN AGEING AND EMBRITTLEMENT IN LOW CARBON STEELS

Strain ageing is a term used to describe a number of property changes which occur in low-carbon steels as a result of plastic straining followed by subsequent ageing at ambient (natural ageing) or elevated (artificial ageing) temperature. Under certain conditions, ageing also takes place simultaneously with straining, and is known as 'dynamic' strain ageing. However, when straining is done at ambient temperature, only very low strain rates will give rise to dynamic strain ageing.

As strain ageing is caused by the 'locking' of mobile dislocations by interstitial atoms which cause the return of the discontinuous yield point, to begin with, the discontinuous yield point in low-carbon steel is discussed.

3.1 The Yield Point in Low Carbon Steels

Low carbon steels show a clearly defined discontinuous yield point in contrast to many other non-ferrous metals. In these steels the yield phenomena can be characterised by an upper yield point (UYP), lower yield point (LYP) and Luder's strain (or yield point elongation) - see Figure 3.1 - whilst in most non-ferrous metals the yield point is generally taken as the stress required to produce 0.2% plastic strain (Figure 3.2).

At the upper yield point plastic deformation is initiated by a discrete band of plastically deformed metal from some stress concentration and this yielding propagates along the specimen to give the full yield point elongation. These discrete bands which are 45^{o} to the loading axis, are known as Luder bands. Further straining beyond this takes place with increased load due to strain hardening. The yield phenomena is affected by strain rate, surface finish, specimen shape, axiality of loading and machine stiffness[7].

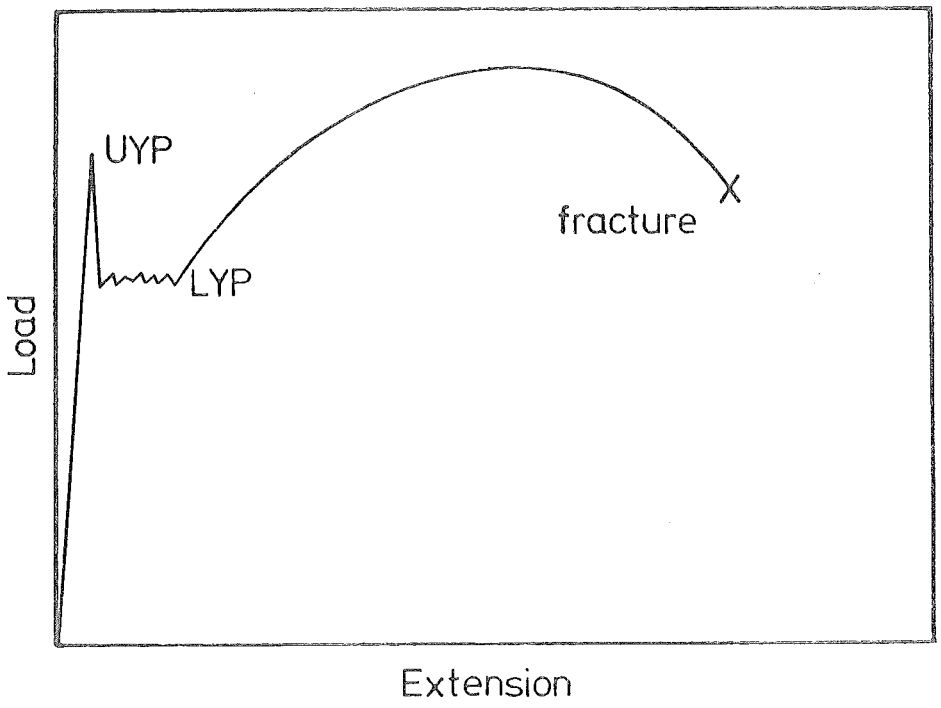

Figure 3.1: A typical load-extension curve for a low-carbon steel tested in tension.

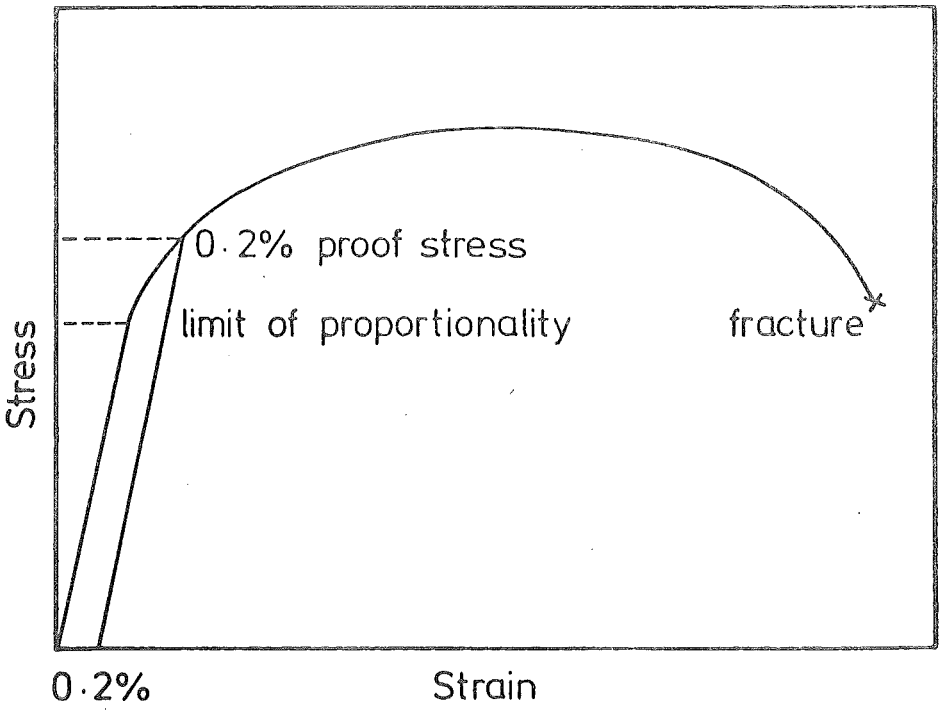

Figure 3.2: A typical load-extension curve for a non-ferrous metal tested in tension.

Reasons for this yielding phenomena in low carbon steels have been well established. The theory was initially due to Cottrell & Bilby[8], who suggested that the interstitial atoms in solid solution in ferrite segregate to dislocations locking them in position. The strain energy of the distorted bcc ferrite lattice (due to interstitial carbon and nitrogen atoms) could be relieved by the diffusion of carbon and nitrogen to the tension side of an edge dislocation. They estimated that a concentration of approximately 10^{-6} wt % carbon was sufficient to place one Carbon atom on each dislocation per atom plane at a normal dislocation density of 10^{8} cm^{-2} in an annealed ferrite. This would give a binding energy of approximately 0.5eV per atom plane, which has to be overcome by the applied strain energy assisted by thermal activation for yielding to occur by unlocking of the dislocation. But later it was found[9] by internal friction measurements, or electrical resistivity techniques, that the interstitial atoms per dislocation plane were usually in excess of 10. Therefore, it was suggested that the upper yield point correspond to the stress which caused the dislocations to break from their 'atmospheres' of interstitial atoms, multiplying to form the first Luder band.

The lower yield stress is the stress required for the propagation of Luder bands along the specimen. These dislocations, which have been unpinned from their locked positions, pile up against the grain boundary and cause a stress concentration in the next or adjoining grain. A blocked slip band of length ℓ can be considered to transfer a force $(\tau - \tau_i)$ to the next grain,

where τ = applied shear stress

τ_i = friction stress which opposes the glide of the slip band.

By analogy between the slip band and a crack, it can be shown from elastic theory that the stress concentration factor is $(\ell/4r)^{\frac{1}{2}}$ at a distance r ahead of the blocked slip band. If r is taken as the average distance

between the blocked slip band and the nearest locked dislocation source in the adjoining grain, then the pile-up of dislocation can make the adjoining grain yield if:

$$\tau_c = (\tau - \tau_i)\ (\ell/4r)^{\frac{1}{2}} \qquad 3.1$$

where τ_c is the critical shear stress to create dislocations from a locked source.

If $\ell = Ad$, where d is the mean grain diameter

and A is a constant,

Equation 3.1 could be written as

$$\tau_c = (\tau - \tau_i)\ (Ad/4r)^{\frac{1}{2}} \qquad 3.2$$

Assuming that the applied shear stress is equal to the lower yield shear stress when yielding is propagating across grains, and converting all shear stresses to their corresponding tensile stress:

$$\sigma_c = (\sigma_y - \sigma_i)\ (Ad/4r)^{\frac{1}{2}} \qquad 3.3$$

i.e. $$\sigma_y = \sigma_i + 2\sigma_c (r/A)^{\frac{1}{2}}\ d^{-\frac{1}{2}}$$

$$\sigma_y = \sigma_i + k_y\ d^{-\frac{1}{2}} \qquad 3.4$$

where $$k_y = 2\sigma_c\ (r/A)^{\frac{1}{2}} \qquad 3.4a$$

Equation 3.4 is known as the Hall-Petch equation[10].

Low carbon steels in the as-rolled or normalised state consist of a duplex ferrite/pearlite structure. When the volume fraction of pearlite is small, yielding takes place almost completely due to the movements of dislocations in the ferrite.

Later work by Fisher[11] and Cottrell[12] showed that, ageing caused k_y to increase to a saturation value k_{yo} which became independent of further

continued solute segregation to dislocations and changes in testing temperature. These results implied that dislocation pinning was by precipitates of Fe_3C and Fe_4N, and that mobile dislocations are not nucleated by unpinning when dislocation locking is strong, as if it was so, then σ_c and hence k_y should increase with continued solute segregation.

It has been suggested[12, 13], that these new dislocation sources may be grain boundaries. In this case, σ_c is regarded as a measure of the nucleation stress when dislocations are nucleated at the grain boundaries.

3.2 General Features of Strain Ageing

If a low carbon steel specimen (in annealed, normalised or as-rolled state) is strained to a point A in the strain hardening region - Figure 3.3, i.e. beyond the lower yield extension, unloaded and then immediately retested, the steel will behave elastically up to point A and follow the previous strain hardening curve (a). The new "yield point" A may be slightly rounded, but there will be no evidence of the initial discontinuous yield point of low carbon steel. In other words, the steel behaves in the same manner as a cold-worked non-ferrous metal (Figure 3.2). However, if the specimen is aged (either at room temperature or at an elevated temperature) after it has been unloaded at A and then re-tested in tension, the discontinuous yield behaviour returns with increases in LYS, an increase in TS, and loss in ductility ($\Delta E\ell$) as shown in the new stress-strain curve (b). (Figure 3.3). The new lower yield point is higher than the flow stress at the end of pre-straining. This increase in yield stress (ΔY) is the universal indication of strain ageing.

Other properties which are affected by strain ageing are the ductile/brittle transition temperature (or impact transition temperature), high temperature strength, fatigue strength and electrical and magnetic properties. Strain ageing and related phenomena have been extensively reviewed by Baird[2, 3].

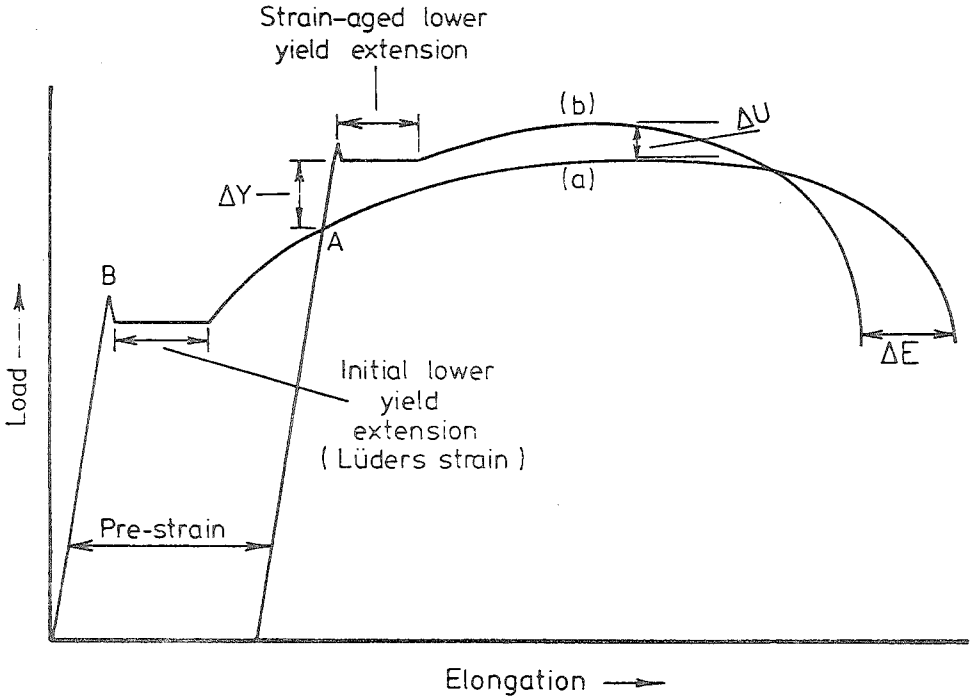

Figure 3.3: Load-elongation curve for low-carbon steel strained to point A, unloaded, and then re-strained immediately (curve a) and re-strained after ageing (curve b).

ΔY and ΔU are calculated on original area.

3.3 Mechanism of Strain Ageing

It is now universally accepted that interstitial carbon and nitrogen atoms, i.e. carbon and nitrogen in solid solution, are responsible for dislocation locking in low carbon steels. During strain ageing the newly formed dislocations resulting from plastic straining or deformation are locked in position by the segregation of interstitial atoms to these dislocation sites, and hence result in the re-emergence of the discontinuous yield point.

The kinetics of strain ageing have been explained by separating the ageing process into two main stages; namely, 'atmosphere formation' and 'precipitation on dislocations'[2]. During the first stage the interstitial solute atoms are assumed to migrate to the dislocation sites to form 'Cottrell atmospheres' around the dislocations. On the earlier interpretation of yielding[8] this should affect only the locking portion of the curve (i.e. UYP, LYP and the Luder strain) while the strain hardening portion (a) (Figure 3.3) remains unaltered, since on straining beyond the lower yield extension, the atmospheres are dispersed. Hence the TS and elongation at fracture are not affected during this stage (i.e. Stage 1 in Figure 3.4). With very low interstitial solute contents, only ageing up to this stage takes place - see Figure 3.5.

During the second stage of strain ageing, the interstitial solute atoms continue to segregate to the dislocations causing atmosphere formation to be exceeded to form precipitates along the dislocations. Since the dislocations are fully locked at the end of the first stage, the Luder strain is little affected during the second stage. However, precipitate formation raises the level of curve (b) (Figure 3.3), hence raising the TS. The corresponding increase in the work hardening rate causes a reduction in the elongation at fracture. In most cases this stage of ageing takes place unless the interstitial solute content is extremely low - see Figure 3.5.

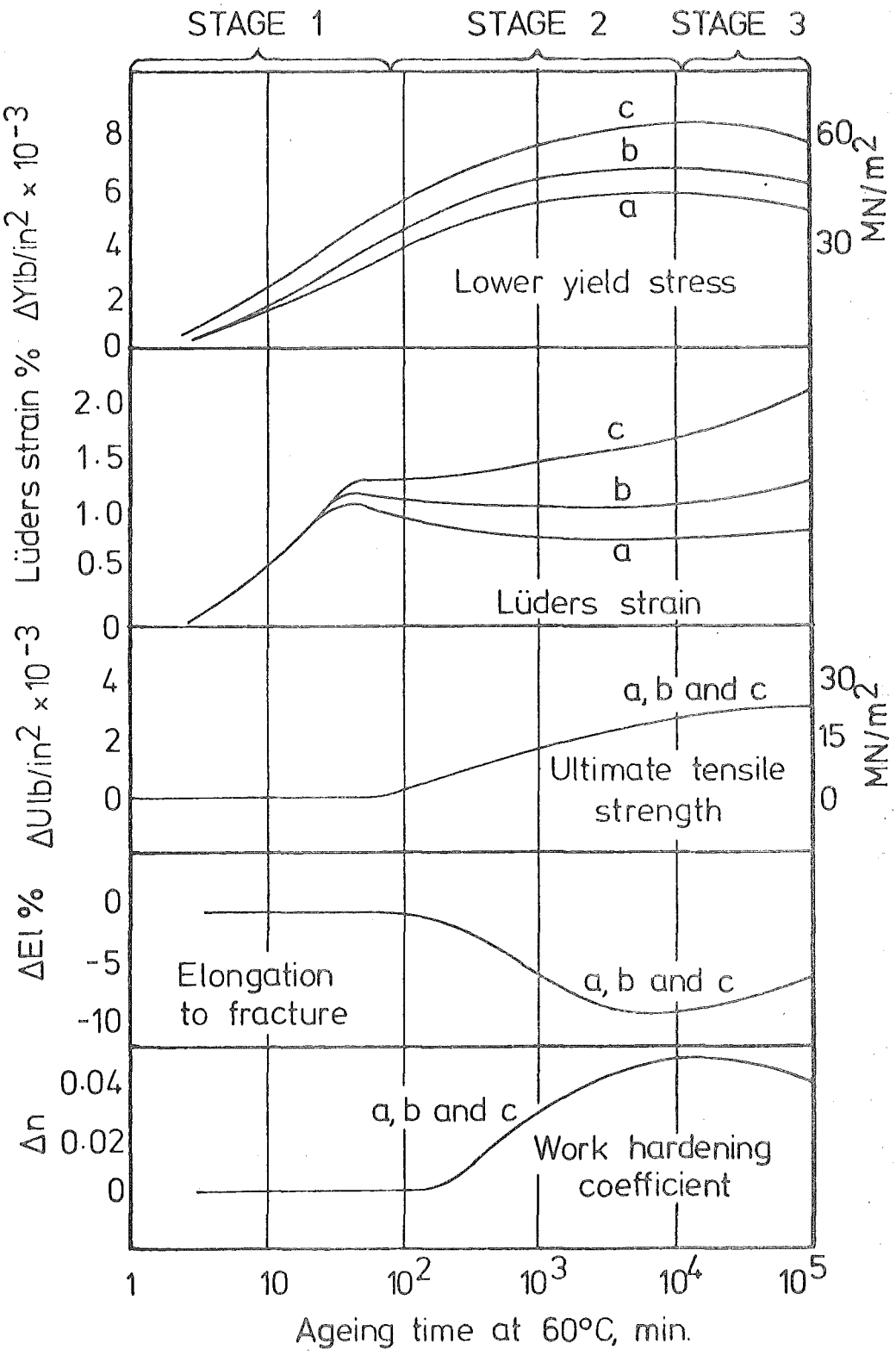

Figure 3.4: Effect of ageing time on changes in tensile properties due to strain ageing (pre-strain 4%) in low-carbon rimmed steels having grain sizes (grains/mm^2) (a) 50, (b) 195, (c) 1850. (Wilson and Russell[15]).

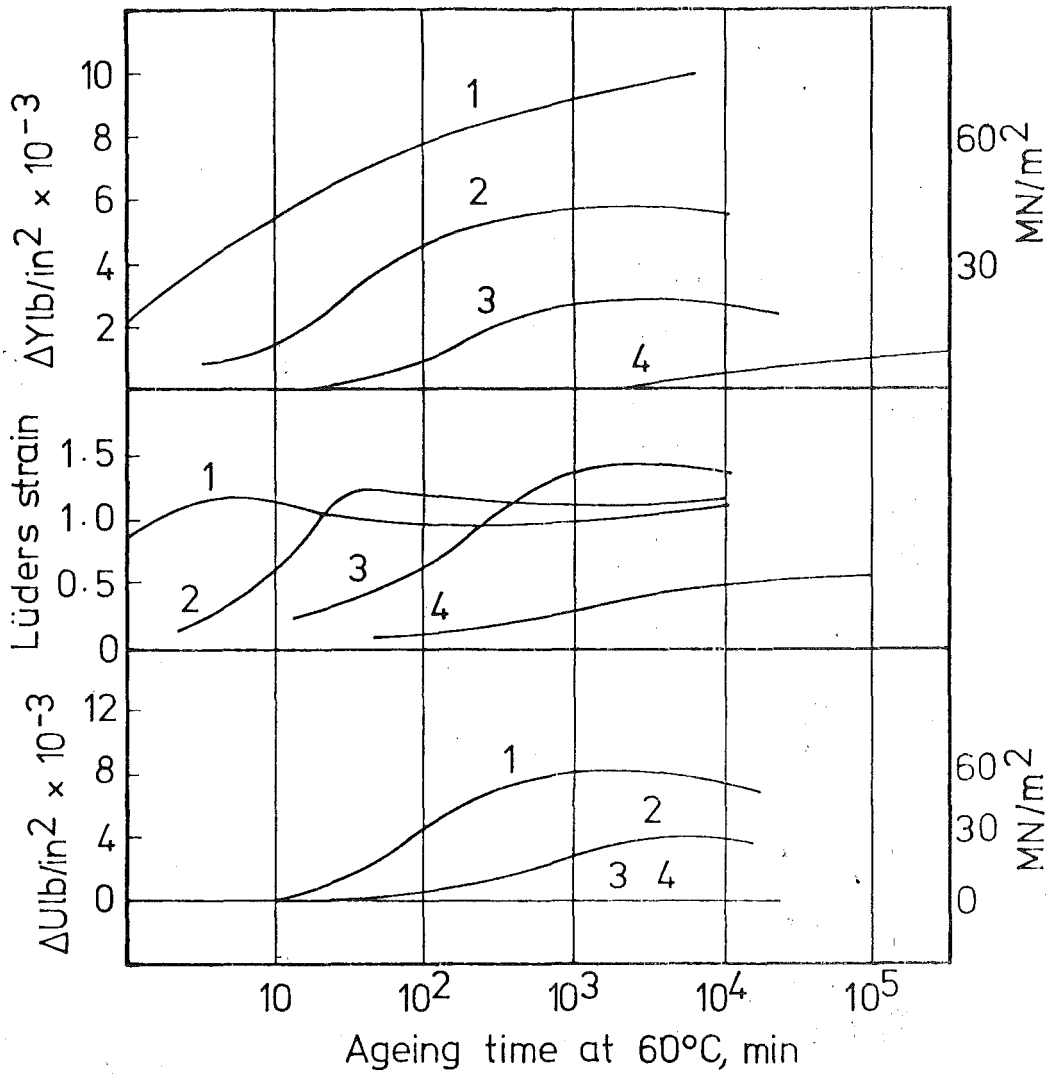

Figure 3.5: Effect of interstitial solute content on changes in tensile properties due to strain ageing (pre-strain 4%) in low-carbon rimmed steel. Interstitial solute contents (1) 0.014%, (2) 0.0022%, (3) 0.0005%, (4) <0.0002%. (Wilson and Russell[15]).

It is reported[2] that the observed type of kinetics can be explained if it is assumed that a rod-like precipitate is formed along the dislocation core and the rate of transfer of the interstitial solute across the interface to this precipitate slows down as segregation proceeds. It has been shown[14] that precipitates formed in this manner did not redissolve on heating as easily as the precipitates formed in low carbon steels during quench ageing. These observations show that at least in the early stages of precipitate formation (i.e., during stage 2 in Figure 3.4) the solute atoms are more tightly bound than if they were in the form of discrete carbide or nitride precipitates. This supports the view of Bullough and Newman's hypothesis that the dislocation precipitates are a specialised form, partly stabilized by the interaction with the elastic strain field associated with the dislocation[2]. Possibly in the latter stages of ageing, discrete particles of carbides and/or nitrides form on the dislocations. The possibility of these precipitates coarsening after long ageing times, especially at high temperatures, may be a possible cause for over-ageing as observed by Wilson and Russell[15, 16]. This over-ageing was characterised by a small drop in yield stress, decrease in TS, and a small rise in elongation at fracture, see Figure 3.4. Luder strain may increase, due to the decrease in the rate of work hardening.

3.4 Effects of Carbon and Nitrogen

The effectiveness of carbon and nitrogen in producing strain ageing is a function of

(a) their solubilities in ferrite;

(b) their diffusion coefficients; and

(c) the severity with which each locks dislocations.

The main difference between carbon and nitrogen arises from their widely differeing solubilities in ferrite. It is clear from Figure 3.6 that the solubility of nitrogen above 200^{o}C (where rapid precipitation can

take place), is higher than that of carbon, which is $<10^{-4}$ wt %. As a result, provided that well dispersed nucleii are present in which carbon atoms can precipitate, the quantity of carbon in interstitial solid solution will be very low below 200°C. However, as a result of its higher solubility, a reasonable proportion of nitrogen atoms may be held in super-saturated solid solution. In support of this, internal friction measurements show that in the absence of cold work, precipitation from such super-saturations is very slow[17]. The solubility of nitrogen at room temperature extrapolates to 10^{-4} to 10^{-5} wt % (Figure 3.6), but it is doubtful if this figure is ever approached, even on very slow cooling. It can be deduced[18] that precipitates of Fe_4N and less stable $Fe_{16}N_2$ should dissolve in the presence of dislocations to provide more nitrogen atoms for dislocation locking, especially for atmosphere formation. These observations suggest that the effect of nitrogen on strain ageing may not be greatly dependent on the prior heat treatment[19], and hence nitrogen can cause appreciable strain ageing when aged at 100°C or less.

From the solubility data on carbon (Figure 3.6), it may be said that interstitial carbon in solid solution at room temperature in normally cooled low-carbon steels is insufficient to cause strain ageing. Evidence from internal friction studies[20, 21], suggests that re-solution of carbide precipitates is much less extensive than nitride precipitates, as may be expected in view of the much greater stability of Fe_3C compared to Fe_4N. Further evidence[22] shows that carbon strain ageing in slowly cooled steels is negligible below 100°C. However, Low and Gensamer[23] have shown that carbon produces strain ageing at 200°C. It has also been shown[24, 25], that on ageing at temperatures above 100°C, there is evidence of fine carbide particles dissolving to produce extensive strain ageing. From these observations it appears that sufficient resolution of Fe_3C can occur in normally cooled steels at temperatures of 150°C and above to give appreciable strain ageing due to carbon dislocation locking. Strain ageing

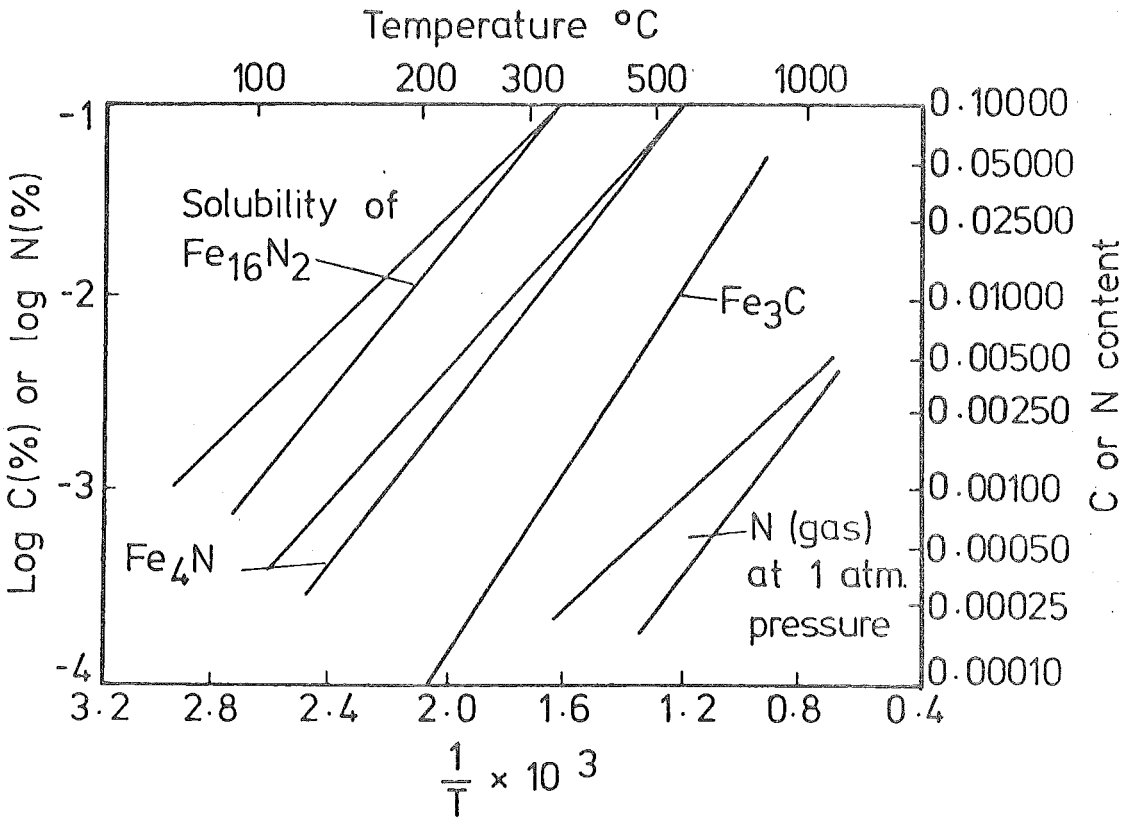

Figure 3.6: Solubilities of nitrogen and carbon in iron (Baird[2]).

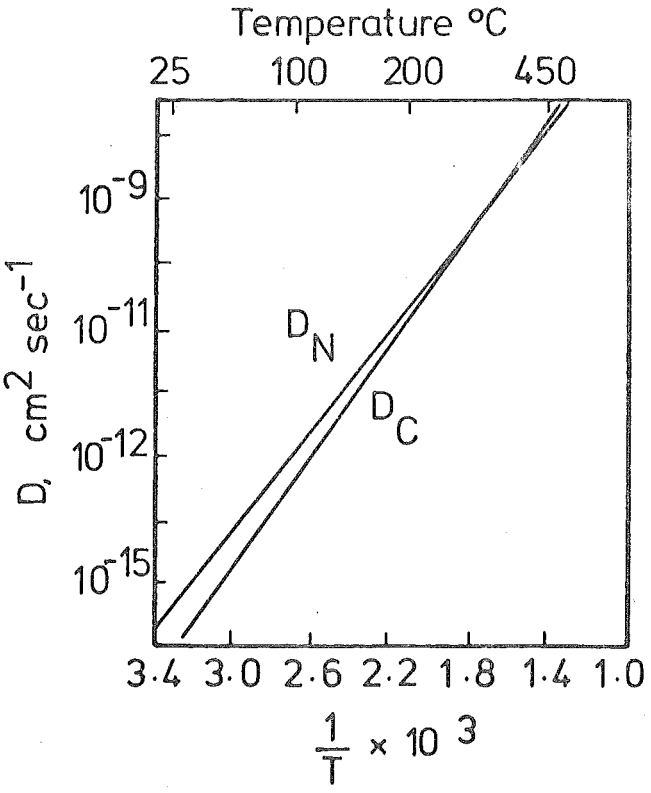

Figure 3.7: Diffusion coefficients of nitrogen (D_N) and carbon (D_C) in α - Iron (Baird[2]).

may also be caused by interstitial carbon below these temperatures due to it being held in super-saturated solid solution after rapid cooling from the austenite range.

Diffusion coefficient of nitrogen atoms in ferrite is given by:

$$D_N = 6.6 \times 10^{-3} \exp^{(-18,000/RT)} \quad cm^2/sec \qquad 3.5$$

and the diffusion coefficient of carbon atoms in iron is given by:

$$D_C = 0.02 \exp^{(-20,100/RT)} \quad cm^2/sec \qquad 3.6$$

which have been determined by internal friction methods[2]. Comparison of the results (Figure 3.7) shows only negligible difference between the two rates.

Considering the above aspects of carbon and nitrogen in causing strain ageing, it may be concluded that in normally cooled low carbon steels, ageing below about $100^{o}C$ is almost entirely due to nitrogen, while above $100^{o}C$ carbon appears to become increasingly effective.

Strain ageing phenomena begin to occur when the interstitial content reaches 0.0002 - 0.0005%. In this range of interstitials, partial first stage ageing can take place. When the interstitial content is ~.002%, ageing extends well into the second stage. Effects of further increases in interstitial content on mechanical properties are shown in Figure 3.5.

3.5 Type and Extent of Pre-strain

Normally susceptibility of strain ageing is obtained by pre-straining, and then retesting in the same direction after subsequent ageing. It has been shown by Hundy[26] and Tardif and Ball[27] that if the restraining direction is not the same as that of pre-straining, the return of lower yield elongation is retarded (Figure 3.8). However, they showed that the other property changes after ageing are not affected by the type of pre-strain, and

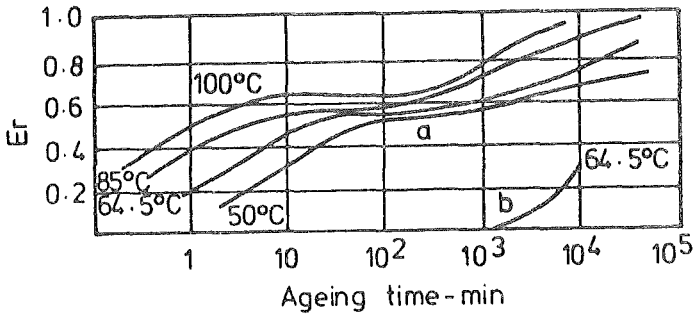

Figure 3.8: Ageing curves for deep-drawing rimmed steel. (pre-strain 5%).
Er = (strain aged Luder's strain)/(initial Luder's strain)
(a) direction of straining the same before and after ageing
(b) direction of straining after ageing transverse to pre-strain direction.
(Tardif and Ball[27]).

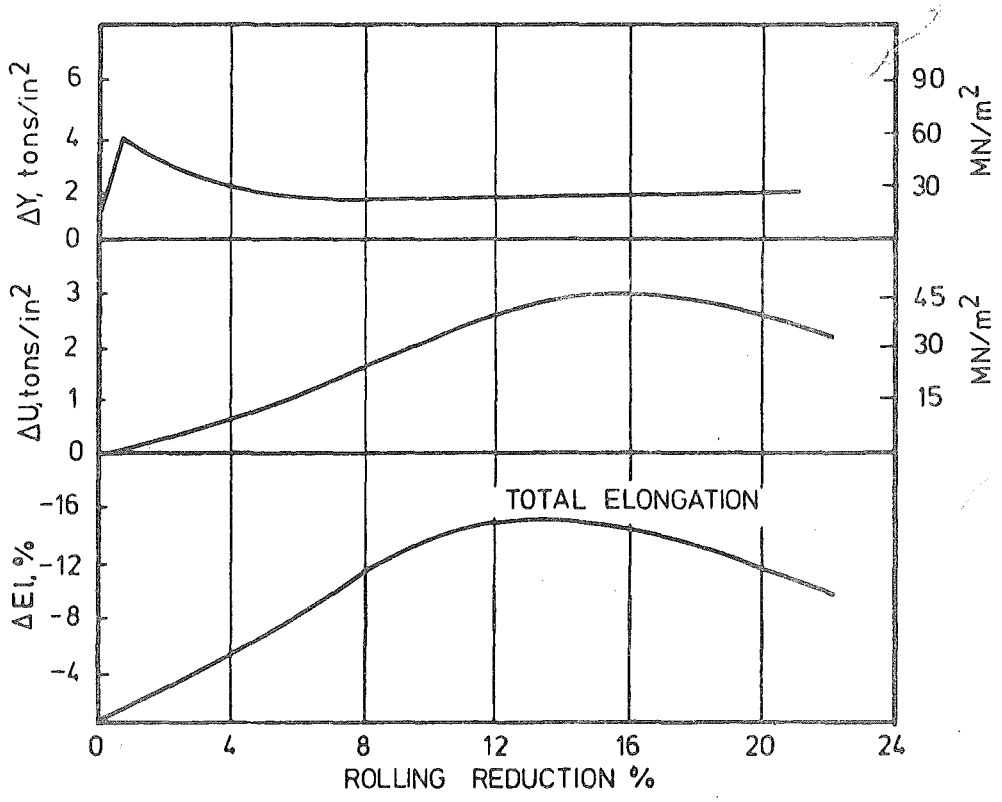

Figure 3.9: Effect of the degree of cold rolling (i.e. pre-strain) on changes in tensile properties due to strain ageing. (Ageing 3 months at room temperature.) (Hundy[29]).

suggested that this may be due to the presence of residual micro-stresses which are of suitable sign to cause premature yielding of some grains, in which case the return of yield point must be controlled by the rate of micro-stress relaxation. Later, Wilson and Orgram[28] have shown that:

(a) The return of yield point in 'reversed strain' conditions is controlled by the segreation of interstitial solute atoms to dislocations or dislocation sources and not other effects, such as recovery or relief or internal micro-stresses.

(b) The dislocations operative in forward and reverse straining are different, the latter requiring much more extensive segregation of solute to lock them than the former.

These results indicate that the change in the rate of return of discontinuous yield point is connected with the atmosphere formation stage as the other properties (due to precipitate formation) are not affected.

The effect of the amount of pre-strain has been investigated[15, 23, 29]. The change in yield stress (ΔY) is not particularly sensitive to the amount of pre-strain, provided it is greater than the lower yield extension. In contrast, the change in TS (ΔU) and elongation at fracture ($\Delta E\ell$) initially increase with pre-strain and then decrease with further increase in pre-strain, see Figure 3.9.

3.6 Effect of Ageing Temperature

The ageing temperature has two main effects on strain ageing, namely:

(a) alter the mechanical properties in the fully aged condition;

(b) change the rate at which strain ageing takes place.

In a low carbon steel where the interstitial nitrogen content is <.0005%, the properties in the fully aged condition will be significantly

different between specimens aged below 100°C and those aged around 250°C, due to the resolution of Fe_3C releasing Carbon atoms into solid solution and carbon hence being available for dislocation locking. Below 100°C the interstitial content may be sufficient to give very slight first stage ageing effects, while around 250°C the interstitial content will be sufficient to complete second stage ageing. But in steels containing sufficient interstitial nitrogen to complete second stage ageing, changes in ageing temperature may not show significant differences in mechanical properties in the fully aged condition.

The predominant effect of the ageing temperature is on the rate of the ageing process. Hundy[30], using the kinetics of strain ageing due to Cottrell and Bilby[8], derived the following relationship connecting strain ageing at different temperatures:

$$\text{Log}_{10}\ (t_r/t) = H\ (1/T_r - 1/T) - \text{Log}_{10}(T/T_r) \qquad 3.7$$

where t_r and t are the times taken to give the same degree of ageing at room temperature T_r(°K) and a higher temperature T(°K) respectively.

H = 4,400 for carbon atoms

H = 4,000 for nitrogen atoms.

Hundy found that Equation 3.7 satisfactorily described the effect of ageing temperature on the changes in proportional limit, yield point, total elongation and TS in a rimmed steel which had been either temper rolled 4% or strained 5% in tension.

As pointed out by Hundy in the derivation of this equation, it is assumed that the quantity of dissolved solute available to produce strain ageing is independent of temperature. The fact that this equation is applicable for a rimmed steel can be taken as an indication that this assumption appears to hold for a normally cooled low-carbon steel.

But in steels where interstitial nitrogen is <.0005%, strain ageing will be significantly different around 100°C and below as compared to ageing around 250°C, and equation 3.7 should therefore be used with caution.

3.7 Strain Hardening

When a low carbon steel (consisting mainly of ferrite) is strained beyond its lower yield point, the tensile load increases with further strain (Figure 3.1). This region of the tensile curve is known as the strain hardening region. Straining in this region results in the interaction of dislocations causing new dislocation sources, forming dislocation loops, networks, etc., and leads to a completely distorted grain structure with 'forests' or clouds of dislocations. Hence strain hardening produces an increase in dislocation density. Generally, the rate of strain hardening diminishes with increase in strain mainly due to recovery, which begins to occur as straining proceeds.

As shown in Figure 3.1, straining (without ageing) causes the flow stress to increase and the new flow stress may be given in the form:

$$\sigma_f = \sigma_j + k_j d^{-\frac{1}{2}} \quad [13] \qquad 3.8$$

where σ_j = friction stress on unlocked dislocations

k_j = corresponding value of k_y.

σ_j is greater than σ_i and increases with increase in pre-strain, due to increase in the resistance for the movement of unlocked dislocations caused by the increased dislocation density. k_j is smaller than k_y, due to the reduction in stress (σ_c) required to nucleate dislocations from grain boundaries after pre-straining[13].

3.8 Effects of Strain Ageing on Mechanical Properties

3.8.1 Tensile Properties

Qualitative studies on strain ageing have shown that tensile

properties are affected mainly in two stages:

(a) The first stage due to 'atmospheric formation' on dislocations only affect the yield point (LYS, UYS, etc.)

(b) During the second stage, due to precipitation on dislocations LYS, TS and elongation at fracture are all affected.

An attempt has been made by Wilson and Russell[16] to show the effect of strain ageing on the Hall-Petch relationship $\sigma_y = \sigma_i + k_y d^{-\frac{1}{2}}$. As suggested by equation 3.8, a pronounced increase in σ_i and a decrease in k_y were observed on pre-straining an annealed steel, see Figure 3.10. On subsequent ageing to the end of the first stage k_y increased while σ_i remained unaltered, while on full ageing there was no further change in k_y but σ_i increased. These results were expected on the basis of the existing theory at that time: that yielding took place by the unpinning of locked dislocations and k_y in the strain aged specimen never reached the initial value of the annealed specimen, attributed to the decrease in r, see equation 3.4(a).

But yielding in an annealed steel is now believed to take place at dislocation sources in grain boundaries[12] which leads to an unexplained reduction in k_y. This anomaly has since been explained by Wilson[13]. His work on yielding of strain aged steels showed that:

(a) The first stage of ageing is due to atmospheric locking of dislocations. The yield point behaviour during this stage is consistent with Cottrell's original suggestion that mobile dislocations are nucleated by the unpinning process. Thus the yield stress will depend on k_y during this stage which will, in turn, depend on dislocation atmosphere density.

(b) At the end of the first stage continued segregation of the

interstitial solute to dislocations has no further effect on k_y. Yielding by unpinning is very unlikely during this stage (second stage). Mobile dislocations are probably nucleated at grain boundary sources as in the initial stage (annealed, normalised, as-rolled, etc.).

(c) The lower value of k_y during the second stage, as compared to its initial value k_{yo} ($k_y = 0.65\ k_{yo}$) is explained by the assumption that pre-straining causes a reduction in stress σ_c required to nucleate dislocations from grain boundaries. Finally, a slow rise in k_y to the original value k_{yo} may take place due to long range diffusion of solute from grain interior to grain boundaries. This rate is clearly related to the interstitial content.

Erasmus[31] has suggested that the initial rapid rise of k_y from its value at the pre-strained condition to $0.65\ k_{yo}$ at the end of stage 1, is due to a rapid rise of σ_c to $0.65\ \sigma_{co}$, which follows as a result of some solute segregation to grain boundaries during this stage, causing an increase in σ_c from the pre-strained value. Further increases in σ_c will depend on long range diffusion of interstitials to grain boundaries at much slower rates.

These observations were made when specimens were pre-strained, aged, and then re-strained in the same direction. When these modes or directions are different, observations have shown that the rate of return of the discontinuous yield point is retarded while other properties are not affected[26, 27]. There appears to be no quantitative explanation for this phenomenon. As this effect is only found during the first stage, it may be possible to explain this by investigating the rate of increase in k_y during this stage, after different modes of pre-straining.

An attempt has been made to describe the strain ageing behaviour of steel using a dislocation model[32]. This model, developed on the basis that the mobile dislocation density is constant during plastic straining, gives the following relationship:

$$u = \frac{dc}{d\varepsilon} + \frac{dr_f}{d\varepsilon} + \frac{dr_l}{d\varepsilon} \qquad 3.9$$

where u = rate of dislocation immobilization,

$\frac{dc}{d\varepsilon}$ = rate of dislocation creation,

$\frac{dr_f}{d\varepsilon}$ = rate of re-mobilization of free immobile dislocations, and

$\frac{dr_l}{d\varepsilon}$ = rate of re-mobilization of locked immobile dislocations.

The above relationship is used to derive an expression relating the true stress (σ) and true strain (ε) of the strain aged steel. When comparing this theoretical expression with experimental data from a low-carbon steel, some interesting results are obtained[32]:

(a) On account of dislocation locking, the probability of the re-mobilization of the pre-strain introduced dislocations (Ω_p) decrease to zero within an hour at an ageing temperature of 65°C and the corresponding solute atmosphere density is about 5 atoms/dislocation plane. This stage of ageing is beyond the completion of the first stage.

(b) When the pre-strained introduced dislocations are completely locked, i.e. $\Omega_p = 0$, further ageing has no effect on Ω_p, although eventually, after long ageing times (35 days at 65°C) there appears to be a slight increase in Ω_p to about 1%, especially at lower pre-strains. This, in some way, may be related to overageing, suggested by Wilson and Russell[15].

3.8.2 Strain Age Embrittlement

Fracture of low carbon steels can take place in two distinctly different modes which are based on crystal shear or cleavage. Fracture by shear mode is classified as a ductile fracture and the fracture surface appearance is fibrous, while the cleavage mode is classified as a brittle fracture having a granular surface appearance. Ductile fracture takes place after considerable plastic deformation, whilst brittle fracture has very limited or no gross plastic deformation.

For a specific material, the mode of fracture may depend on:

(a) state of stress at position of fracture;

(b) temperature; and

(c) rate of application of strain.

Generally, in low carbon steels, the mode of fracture changes from ductile (micro-void coalescence) to brittle (cleavage) as the temperature is reduced under identical conditions of stress application at the position of fracture. A universal method of testing to investigate this change in fracture mode with reduction in temperature is the Charpy V-notch impact test. The temperature at which the mode changes is generally known as the impact transition temperature (ITT) or fracture transition temperature. It is well established that one of the factors which increase the ductile to brittle fracture transition temperature of low-carbon steels is strain-age hardening. This increase in fracture transition temperature is known as strain-age embrittlement.

Theories of brittle fracture in low-carbon steels are based on the same principal; i.e., on the energy balance relating the work done in the slip band which produces the growth of a micro-crack to the corresponding surface energy required for this crack growth.

Cottrell[33] has shown that for the unstable growth of such a micro-crack,

$$\sigma_F \, n \, a > 2\gamma \qquad 3.10$$

where σ_F = fracture stress

n = number of piled-up dislocations producing the crack

a = interatomic spacing

γ = surface energy

and predicts a ductile to brittle fracture transition when

$$\sigma_F \, n \, a = 2\gamma \qquad 3.11$$

Further, on the assumption that brittle fracture occurs at the yield point, and using the dislocation pile-up equation

$$\sigma_y - \sigma_i = \frac{2 \, n \, a \, \mu}{\ell} \qquad 3.12$$

where the pile-up length (ℓ) = A d, A being a constant and μ = shear modulus, it is shown that the ductile to brittle transiton point is defined by

$$(\sigma_i d^{\frac{1}{2}} + k_y) \, k_y = \beta \, \mu \, \gamma \qquad 3.13$$

where β = a constant dependent on the state of stress.

Petch[34] worked out an expression for the transition temperature (T_c) given by:

$$\varepsilon \, T_c = \sigma_i^* + C - (4\beta\mu\gamma/k - k) \, d^{-\frac{1}{2}} \qquad 3.14$$

where σ_i^* is the temperature independent friction stress given by:

$$\sigma_i = \sigma_i^* + C - \varepsilon T \text{ (C and } \varepsilon \text{ are constants)}$$

and k is given by $\sigma_f = \sigma_{i,f} + k \, d^{-\frac{1}{2}}$

where σ_f = flow stress at fracture; and

$\sigma_{i,f}$ = friction stress at fracture

Cottrell's equation has been later modified[35] to the form:

$$(\sigma_i d^{\frac{1}{2}} + k_y)\ k_s = \beta\mu\gamma \qquad 3.15$$

where $k_y = m\ k_s$, m being an orientation factor which expresses the average ratio of the normal to shear stress on the operative slip plane. It has also been considered appropriate to change equation 3.15 (in which it has been assumed that brittle fracture occurs at the yield point) to the form:

$$\sigma_f\ k_{s,f}\ d^{\frac{1}{2}} = \beta\mu\gamma \qquad 3.16$$

where $k_{s,f}$ is the corresponding value of k_s at fracture, in cases where fracture transition occurs after some plastic deformation[35]. Using Cottrell's theory of fracture transition, a similar relationship to equation 3.14 has been derived[36] and is given below:

$$\varepsilon T_c = \sigma_1^* + C - \left(\frac{\beta\mu\gamma}{k_y} - k_y\right) d^{-\frac{1}{2}} \qquad 3.17$$

Baird[2], using the results of Wilson and Russell[16] (Figure 3.10) obtained values for the L.H.S. of equation 3.13 and found that it is the highest in the annealed state and lowest in the strained state, while during ageing, it again begins to rise. On assuming that the surface energy (γ) does not change appreciably during straining and subsequent ageing, according to equation 3.13, transition temperature should decrease (as the L.H.S. decreases) after prestraining and increase during ageing, but will not reach the transition temperature of the annealed state even after full ageing. This is contrary to experimental observation, which shows an increase in the transition temperature after straining (though this condition cannot be strictly obtained in practice) and a further increase occurring

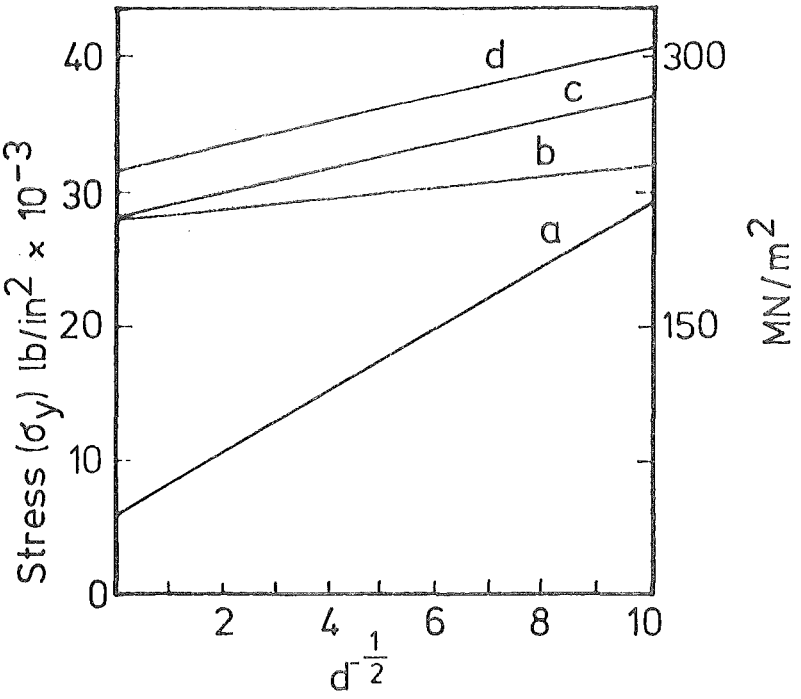

Figure 3.10: Effect of strain ageing in a low-carbon steel on the relationship between the lower yield stress (σ_y) and $d^{-\frac{1}{2}}$; where 2d is the mean grain diameter. (a) Annealed steel; (b) strained 4%; (c) strained 4% and aged to the end of stage 1; (d) strained 4% and fully aged (10^4min. at 60°C). (Wilson and Russell[16]).

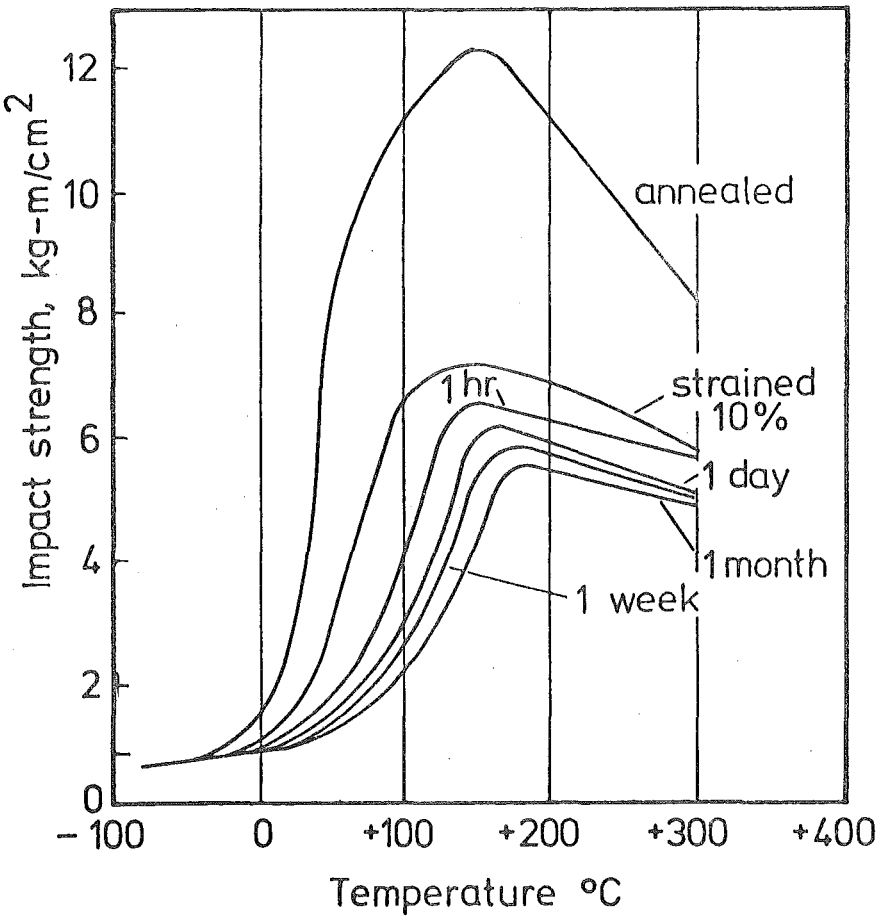

Figure 3.11: Effect of strain ageing in a basic Bessemer steel on the impact transition curve. (Pre-strained 10% and aged at 60°C). (Baird[2]).

during subsequent ageing[2, 3] (see Figure 3.11). Heslop and Petch[37] have suggested that:

$$\gamma = B\, k_y^{-a} \qquad 3.18$$

where B is a constant

and a = 1 to 2.

Taking this relationship into consideration, Cottrell's criteria for fracture transition is in even less agreement with the observed increase in transition temperature on pre-straining, but the rise in ITT on subsequent ageing should be enhanced.

Although the existing theories of brittle fracture give some indication of the causes for strain age embrittlement, the observed changes cannot be fully explained. Further investigation into the effects of plastic strain, subsequent ageing and temperature on σ_i, k_y, and γ, should be carried out for an attempt to be made on a comprehensive explanation of the observed changes. Also, the use of the dislocation pile-up equation 3.12 to determine the number of piled-up dislocations producing the crack (n) in the derivation of equation 3.13, appears to be questionable[38].

Although it is well established that strain ageing in low-carbon steels raises the fracture transition temperature, very few systematic studies have been carried out on this aspect. Literature on effects of plastic strain, ageing temperature, and interstitial solute content on strain age embrittlement in low-carbon steels is scarce. The effect of pre-straining and subsequent ageing for different times on the impact transition curve is shown in Figure 3.11. De Kazinczy and Axnaș[39] have attempted to separate the effects of plastic straining and subsequent ageing on embrittlement of a semi-killed Open Hearth carbon-manganese steel, both in the as-rolled and normalised conditions, see

Figure 3.12. In order to measure strain effects only, ageing was retarded by keeping the pre-strained specimens in dry ice (i.e. below -70^{o}C). When the ageing temperature is raised to 250^{o}C, the increase in transition temperature as a result of ageing shows a general increase, compared with ageing below 100^{o}C, especially in steels that would contain low interstitial nitrogen as the Nb-treated and the normalised Al-treated. This clear increase, as a result of ageing only, at 250^{o}C, in steels with low interstitial Nitrogen, may be due to the resolution of Fe_3C releasing Carbon atoms into solid solution and Carbon hence being available for dislocation locking.

Although overageing or softening characteristics were observed in tensile properties after long ageing times[15], no such recovery in impact properties (after strain ageing) has been reported[3]. Ageing for long periods at 230^{o}C gave no recovery in the impact properties, even though the tensile properties showed overageing characteristics.

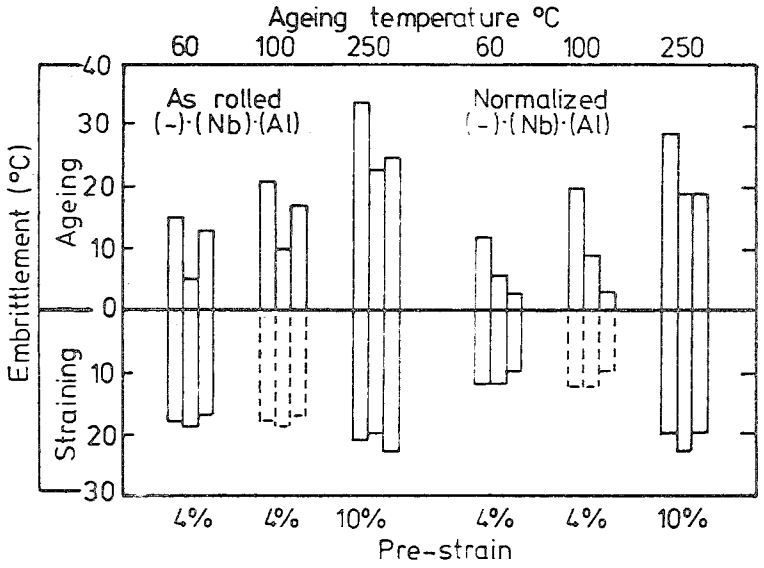

Figure 3.12: Changes in Charpy impact transition temperature (27 Joule) of semi-killed Open Hearth C-Mn steels due to straining and subsequent ageing. Sequence from left to right - base, Nb - treated, Al - treated. (Kazinczy and Axnäs[39])

CHAPTER 4

METHODS OF PREVENTING STRAIN AGEING

The prevention of strain ageing in low-carbon steel appears to have had little attention since the early 1960's. At that time strain ageing caused problems in the sheet metal processing industry, especially when forming automobile bodies.

The characteristic discontinuous yielding behaviour and the associated Luder bands in low carbon steels result in the formation of stretcher strains when processing low carbon sheet steels, and hence give an undesirable surface appearance. To overcome this effect, the sheet steels were temper rolled (a cold reduction of about 4%) so that the discontinuous yield point is eliminated before processing. However, when this sheet was allowed to age at room temperature or above for extended periods, the discontinuous yield point returned together with an increase of hardness and loss of ductility. The increase in hardness and loss of ductility also results in fracture problems during forming.

This differs from the present problem in New Zealand, which is mainly associated with strain age embrittlement of plastically strained reinforcing bar contained in concrete structures.

4.1 Comparison of Methods Available

Since strain ageing is caused by the locking of mobile dislocations by interstitial carbon and nitrogen atoms during ageing, methods of strain age inhibition should either reduce this interstitial content to <0.0005% or immobilise these atoms. The present problem in New Zealand is associated mainly with strain ageing at ambient temperature (i.e., natural strain ageing), and therefore only the interstitial nitrogen content in the steel is of major concern. This interstitial nitrogen content can be reduced or rendered inactive by the following methods:

(a) By annealing the steel in dry hydrogen[40].

(b) By retarding the rate of cooling from the austenite range. This may reduce the interstitial nitrogen content due to the possibility of attaining equilibrium solubility. A more effective method is by quench ageing in the region of 100 - 200°C[19], i.e., by rapid cooling from the austenite range to 100 - 200°C and holding at that temperature to attain equilibrium solubility. But the nitrogen precipitates (Fe_4N and $Fe_{16}N_2$), formed by this treatment, could re-dissolve in the presence of dislocations to again become effective in locking them, i.e., the 'active' nitrogen content (which includes nitrogen in solid solution and in the form of iron nitride) is not reduced by this treatment.

(c) The precipitation of 'active' nitrogen in an inactive form by the addition of nitride forming elements in the steel.

(d) Lowering the ageing temperature well below the ambient temperature, hence retarding the diffusion of interstitial nitrogen.

(e) By the addition of alloying elements which interact with nitrogen atoms[3] and hence restrict its mobility in the steel. These elements do not generally produce stable precipitates. Manganese and silicon belong to this catgeory[41, 42] and are present in reasonable amounts in reinforcing steels. The higher activation energy for strain ageing in steels containing sufficient manganese in solid solution may be a result of the interaction of nitrogen atoms with manganese and hence retard the ageing process[3]. A low carbon steel containing 0.48% manganese strain aged after a full ageing treatment at 110°C; however, a 1.68% manganese steel subcritically annealed at 650°C had negligible ageing after a similar ageing treatment[31]. This may be due to the precipitation of nitrogen as a Mn-Si-nitride as a result of the subcritical annealing treatment[43]. A manganese content of 1.33% in a hot rolled reinforcing steel had no effect

on strain ageing after a full ageing treatment of three hours at 100°C[4].

When examining these methods in the context of controlling or preventing strain ageing in as-rolled reinforcing steels, the only practical method is to use additions of strong nitride forming elements, the other methods being uneconomical.

4.2 Effect of Nitride Forming Elements

Most nitride formers are also carbide formers, the main exceptions being aluminium and boron. The efficiency of a nitride forming element in precipitating the nitrogen in steels depends on:

(a) The solubility product of the nitride in steel under equilibrium conditions, especially in the austenite temperature range.

(b) Its affinity to combine with the nitrogen.

(c) The kinetics of precipitation of the nitride under non-equlibrium conditions.

The other strong nitride forming elements are titanium, vanadium, niobium and zirconium.

4.2.1 Aluminium

Because aluminium is a strong nitride forming element, there is a belief that Al-killed steels are non-strain ageing. However, for aluminium to be a strain age inhibitor, it should be able to combine with all or most of the nitrogen in the steel, bringing the 'active' nitrogen level below 0.0005%.

The work of De Kazinczy and Axnäs[39] clearly shows the effect of aluminium additions to a semi-killed Open Hearth steel on strain ageing, both in the hot-rolled (finish rolled at 1000°C) and normalised (at 900°C) states, see Figures 4.1 and 4.2. Aluminium has had only

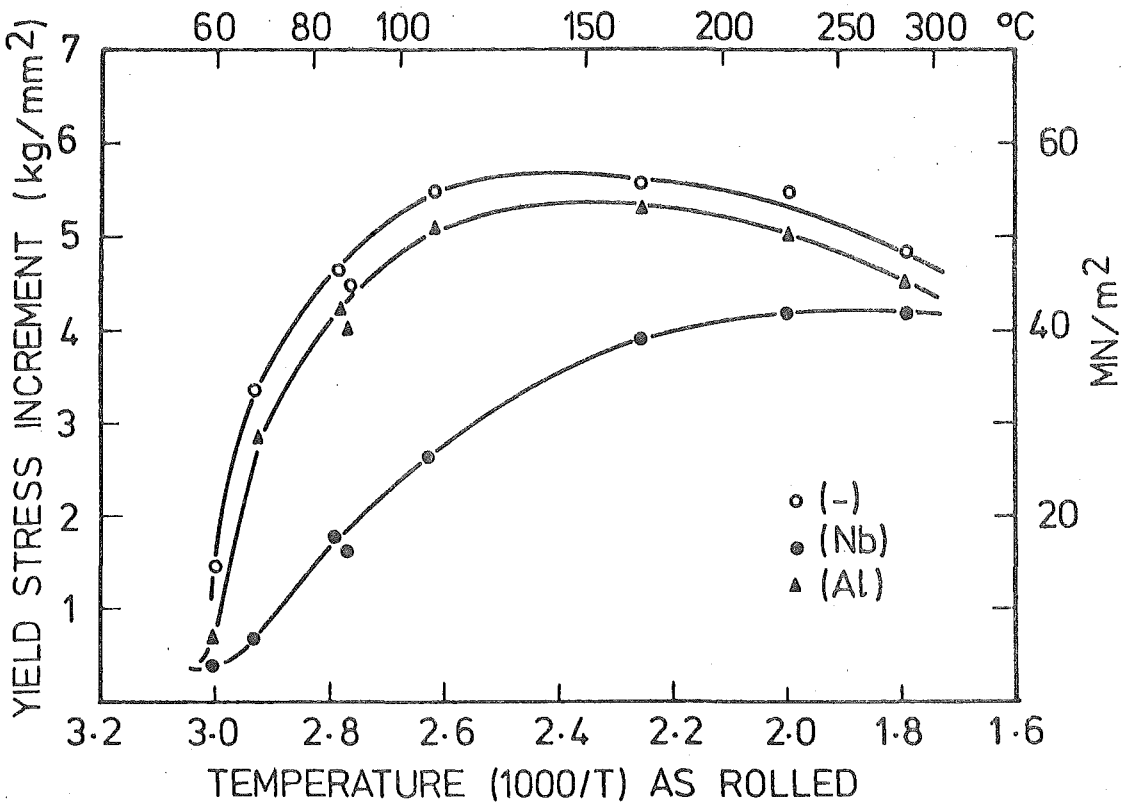

Figure 4.1: Yield stress increment (ΔY) after strain ageing (10% pre-strain, aged for 30 min.) in semi-killed Open Hearth C-Mn steels with temperature. (De Kazinczy and Axnäs[39]).

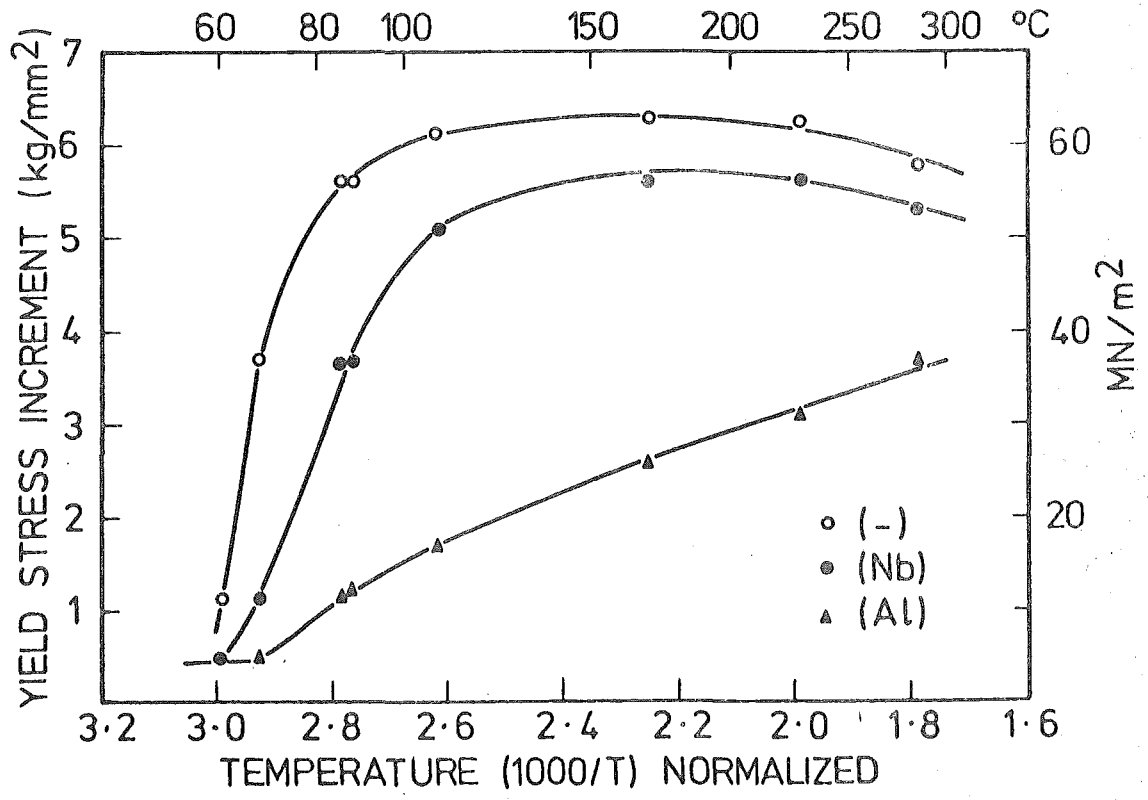

Figure 4.2: Yield stress increment (ΔY) after strain ageing (10% pre-strain, aged for 30 min.) in semi-killed Open Hearth C-Mn steels with temperature. (De Kazinczy and Axnäs[39]).

a slight effect on strain ageing (i.e., on the increase in yield stress, ΔY) in the as-rolled steel at all ageing temperatures up to 300°C. However, strain ageing was considerably reduced in the normalised condition. Similar trends were also shown in the increase in the impact transition temperature after strain ageing, see Figure 3.12. An aluminium content of 0.05% in hot rolled reinforcing steels had little effect on strain ageing characteristics after an ageing treatment of one hour at 100°C[44]. In contrast, strain ageing was completely eliminated in a normalised Al-killed low-carbon steel as a result of the low active nitrogen content (i.e. below 0.0009%), when aged at 110°C for three hours[31]. These observations clearly show that the precipitation of aluminium nitride is not always complete in Al-killed steels.

Birkbeck[45] has compared the properties of an Al-killed steel and a similar semi-killed steel in the annealed condition. His results show that the Al-killed steel has an impact transition temperature of approximately 20°C below that of the semi-killed steel after correcting for grain size (Figure 4.3) and also has a lower value of k_y (Figure 4.4). The reduction in k_y may be caused by a reduction in active nitrogen content. This reduction in k_y may partly be responsible for the consistently lower transition temperature of the Al-killed steel.

It is widely accepted that a method of controlling austenite grain size is by pinning grain boundaries with fine precipitate particles. On the basis of energy changes which occur during grain growth, Gladman[46] has shown that the critical second phase particle size (r_{crit}) for unpinning of a grain boundary is given by

$$r_{crit} = \frac{6\,R_o f}{\pi}\left(\frac{3}{2} - \frac{2}{z}\right)^{-1} \qquad 4.1$$

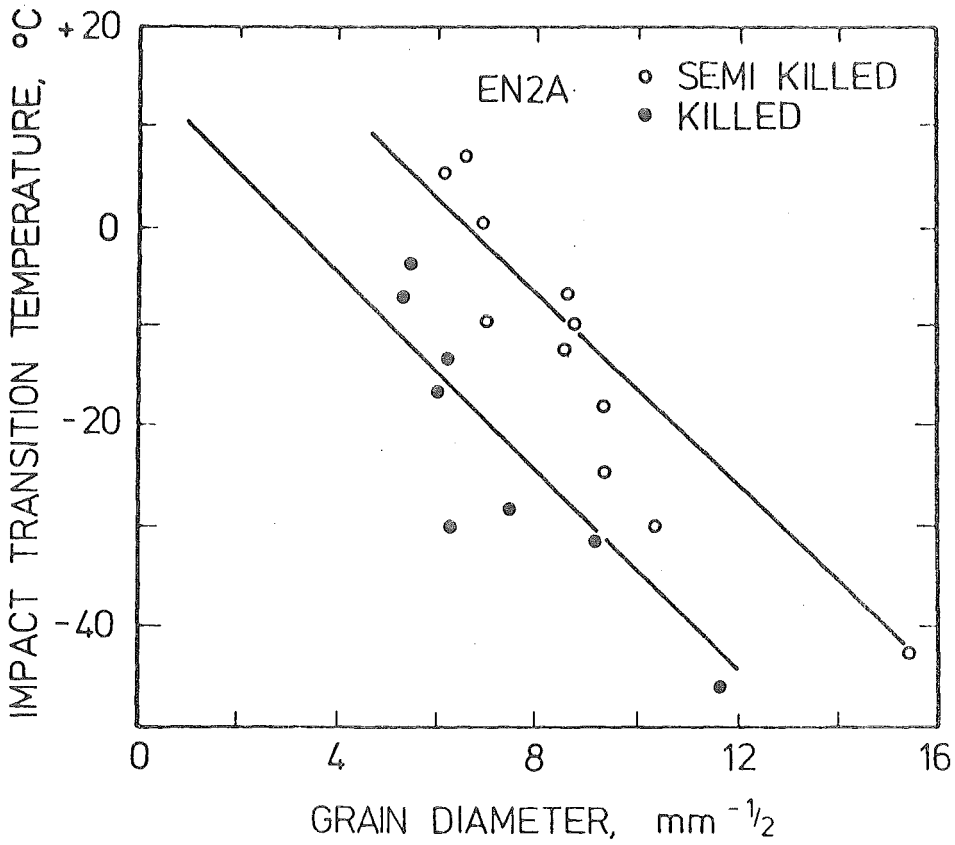

Figure 4.3: The variation in impact transition temperature (75% cleavage fracture) with grain size for an Aℓ-killed steel and a semi-killed steel. (Birkbeck[45]).

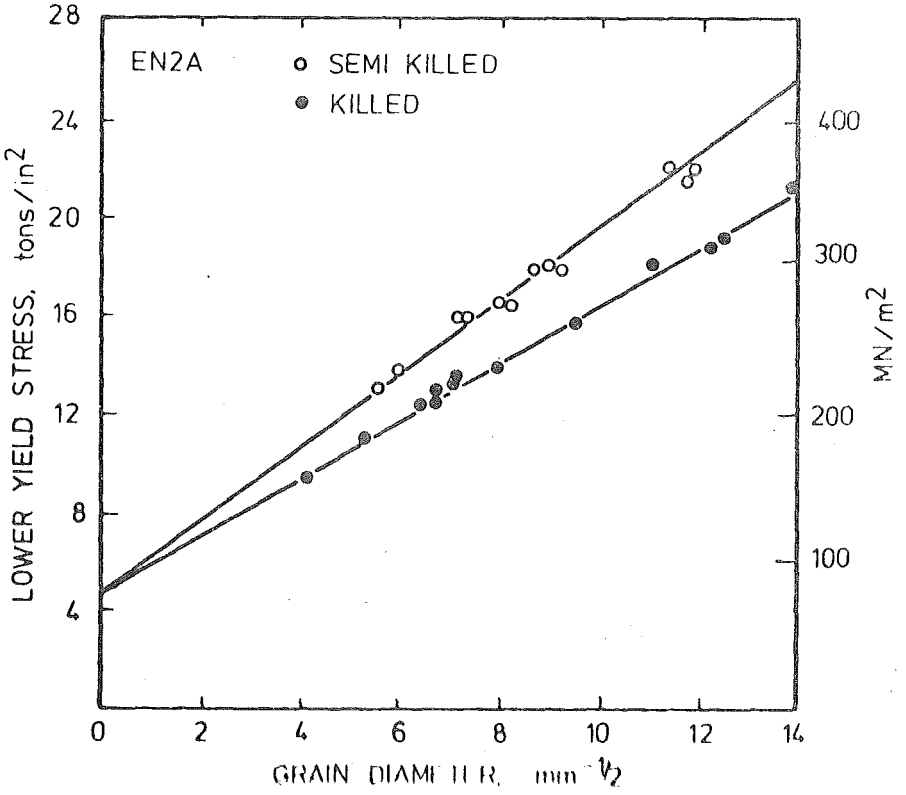

Figure 4.4: The variation in lower yield stress with grain size for an Aℓ-killed steel and a semi-killed steel. (Birkbeck[45]).

where r_{crit} = critical particle radius above which grain growth can occur spontaneously

R_o = matrix grain size

f = volume fraction of second phase particles

z = ratio of the radii of growing grains to matrix grains.

This theory suggests that there is a critical precipitate particle radius which depends on the volume fraction of the precipitates, the matrix grain size and the heterogeneity of the matrix grains. If the actual particle size exceeds the critical value, grain growth can occur because the pinning effect of the particle is eliminated. The use of an AlN precipitate as a grain refiner by the above mechanism has been investigated by Gladman and Pickering[47]. Their experimental observations of precipitate size at the grain coarsening temperatures appear to be in agreement with the above theory. They have shown that grain coarsening starts at temperatures below the solution temperature of AlN (i.e., the dissolution temperature of AlN precipitates) and suggests that this is due to the coarsening of the AlN precipitate. Earlier work by Erasmus[48] on grain coarsening temperature of steels containing AlN precipitate is in agreement with these observations.

The precipitation of AlN has been investigated[49,50] both for isothermal 'down quenching' (i.e., quenching to some intermediate temperature and holding at that temperature for isothermal precipitation of AlN) and 'up quenching' (i.e., rapid heating to the isothermal precipitation temperature after the specimen has been quenched to ambient temperature from the solution temperature of AlN). During 'up quenching' precipitation of AlN is rapid when compared with 'down quenching' where precipitation is very sluggish[49]. The work of

Erasmus[50] is in close agreement with this. Gladman and Pickering[47] have also confirmed that the precipitation of AlN is very slow when cooling through the austenite range and that the aluminium and nitrogen in equilibrium solution at a particular re-heat temperature, and as given by the solubility product, is largely retained in solution at all cooling rates. However,it is precipitated fairly rapidly by re-heating to 950^{o}C, see Figure 4.5. These investigations have shown that the formation of AlN as a precipitate in low-carbon steels is largely dependent on:

(a) Solubility product of AlN in the steel.

(b) Re-heating temperature in the austenitic region.

(c) Time at that austenizing temperature.

(d) The 'up quenching' or normalizing temperature.

It can be seen from Figure 4.6 that a low carbon steel containing 0.04% Al and 0.006% N (representative of the reinforcing steel produced in New Zealand) will have most of the aluminium and nitrogen in solution (i.e., the aluminium and nitrogen will be in the uncombined form) at soaking temperatures in the range 1100^{o} - 1200^{o}C (representative of the soaking temperatures used in the production of reinforcing steel in New Zealand) and hence the 'active' nitrogen content will be more than sufficient to produce strain ageing in the as-rolled state. However, by normalizing this steel at 900^{o}C the precipitation of fine AlN will lower the active nitrogen content to around 0.0005%.

The preceeding discussion on the effects of aluminium in low-carbon steel confirms that precipitation of AlN is completed only after normalizing at approximately 900^{o}C. Hence, in conclusion, it may be said that the normal aluminium contents in as-rolled

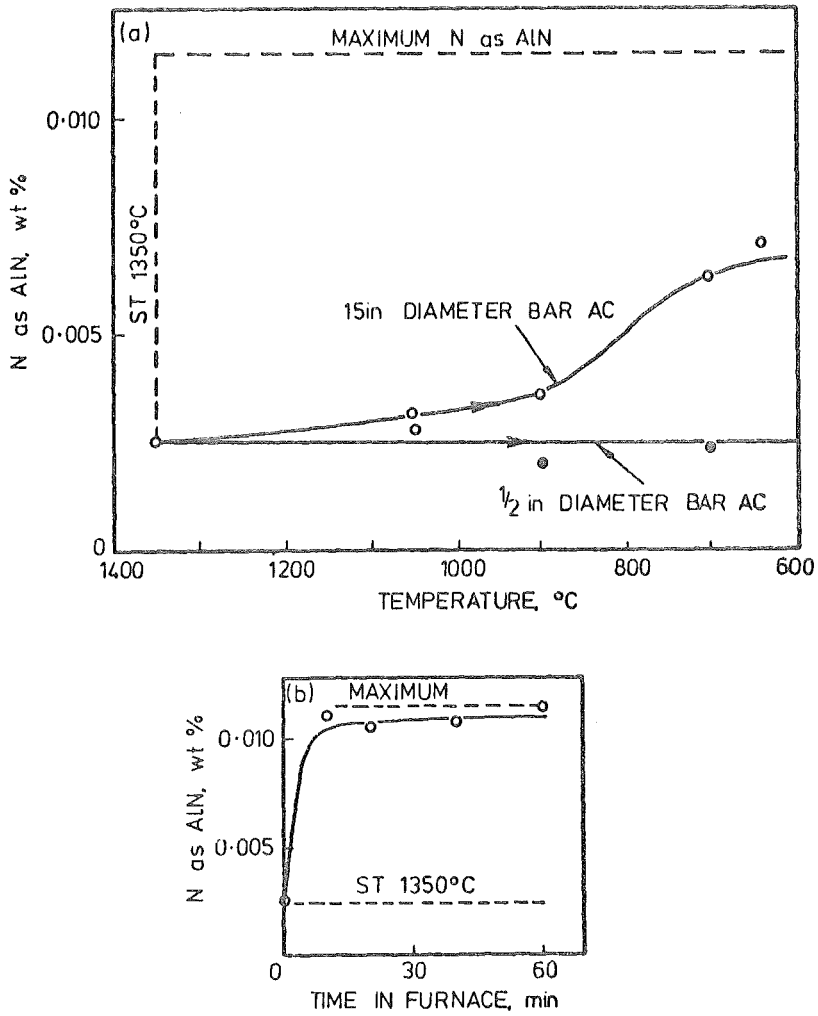

(a) Continuous Cooling
(b) Up-quenching to 950°C.

Figure 4.5: Precipitation characteristics of AlN in a 0.08% Al steel. (Gladman and Pickering[47]).

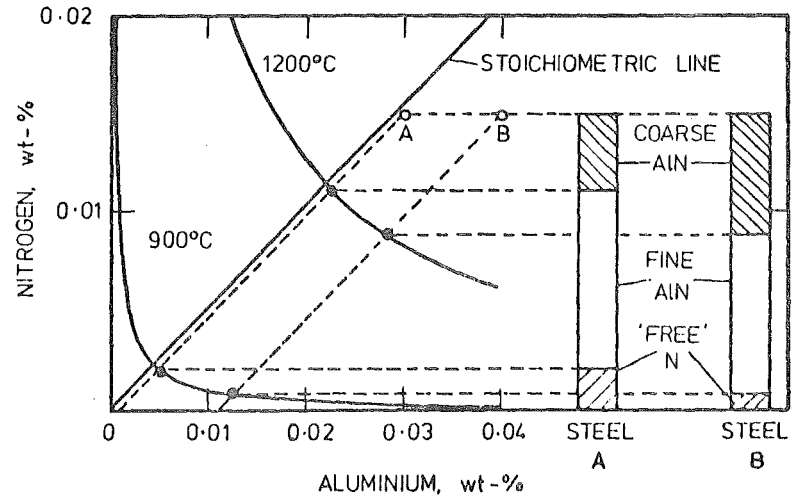

Figure 4.6: The relationship between the solubility product (at 1200°C and 900°C) of AlN, Al and N composition in the steel and the formation of a particle dispersion. The particle (AlN) dispersions of steels A and B are obtained by rolling after re-heating to 1200°C and then normalising the rolled steel. (Gladman and Dulieu[51]).

carbon-manganese reinforcing steels has no effect on strain ageing.

4.2.2 Boron

Boron had been used as a strain age inhibitor in Open Hearth sheet steels used for deep-drawing and pressings in the automobile industry during the latter part of the 1950's and early 1960's. The main reason for using boron for this purpose was because the quantities that had to be added had no significant effect on the rimming action of these steels.

The use of boron to produce non-strain ageing low-carbon steels has been advocated by Morgan and Shyne[52, 53]. They drew attention to the fact that aluminium and titanium additions require the steel to be killed, and vanadium, though it does not affect the rimming action, is expensive. They investigated the effect of boron additions to a steel (0.06% C, 0.55% Mn, and 0.004 - 0.006% N) on strain ageing. The steel was hot rolled at 980^{o}C, and then given a slight reduction through cold rolling and finally box annealed at 705^{o}C for 15 hours before testing. Increasing the boron content initially reduced strain ageing, but with further increases, strain ageing reappeared, see Figure 4.7. This may be due to boron itself acting as an interstitial solute and thus locking dislocations when in excessive quantities[54]. From the view of strain age inhibition, the optimum boron content for this steel appears to be in the range 0.01% to 0.02%. However, when the boron content is >0.007% it starts affecting the rimming action, even when added in two stages[53]. Also, while the rimmed steel strain aged slightly and had a lower boron yield, the semi-killed steels were non-strain ageing and had higher boron yields.

The solubility and precipitation of BN in Fe-B-N alloys studied by Fountain and Chipman[55] has shown that the solubility of BN is

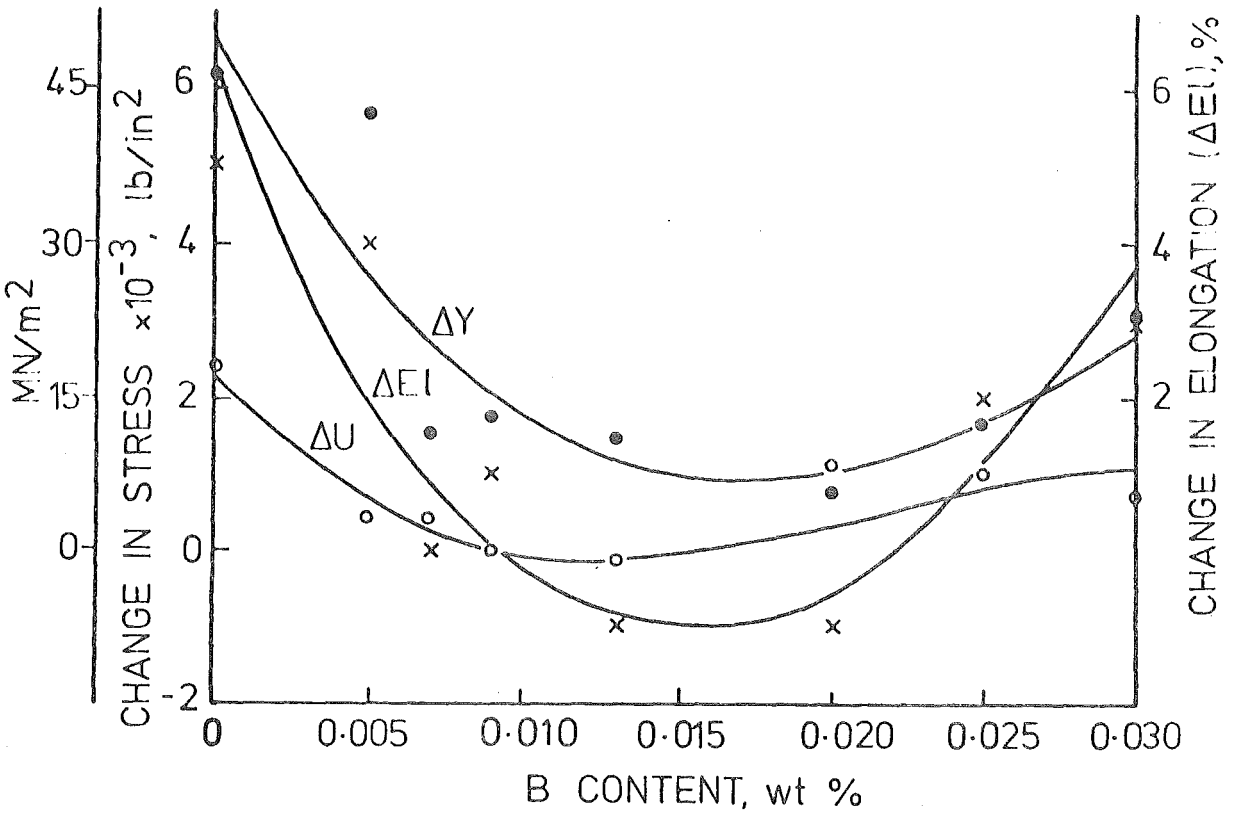

Figure 4.7: Effect of the B content on strain ageing characteristics (ΔY, ΔU, and $\Delta E\ell$) in a low-carbon steel. (Pre-strained 7½% and aged at 100°C for 1 hour). (Morgan and Shyne[52]).

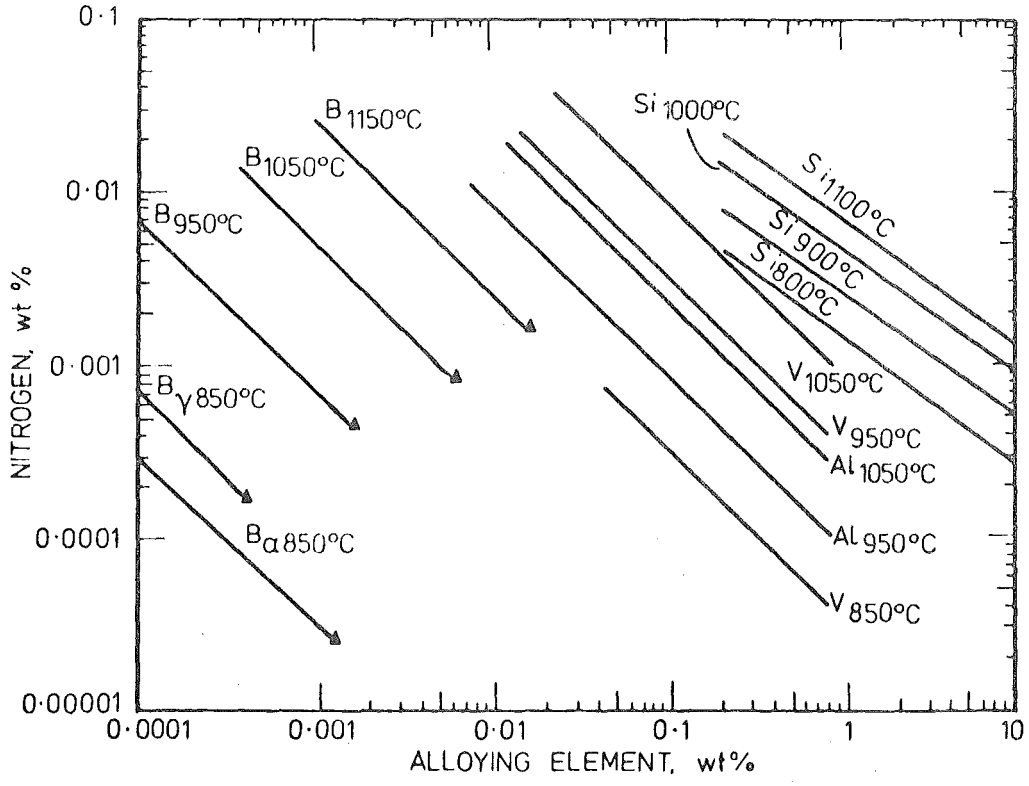

Figure 4.8: The solubility products for BN, AℓN, VN, and Si_3N_4. (Fountain and Chipman[55]).

comparatively lower than that of AlN and VN, both in ferrite and austenite, see Figure 4.8. They have suggested that the solubility may be further reduced in commercial steels, hence very small additions of boron may be more effective in reducing the 'active' nitrogen content of these steels than similar amounts of aluminium or vanadium. Hexagonal BN precipitates 2-5μm in size have been detected in low carbon steels containg boron by means of light microscopy and electron microscopy and diffraction[56]. According to hot tensile test results, hot rolled semi-killed steel strip containing boron in excess of 0.006% is non-strain ageing whether it has been spray cooled or hot coiled.[57] It is suggested that this indicates a relatively high temperature of nitride formation, since spray cooling in both Al-killed and vanadium rimmed steels tends to suppress the formation of nitrides.

It appears from the literature that boron, when added in sufficient quantities, may be effective in precipitating most of the nitrogen as BN during the processing of hot-rolled low carbon steels, and hence reduce the active nitrogen content. However, a recent attempt[58] at producing such a reinforcing steel was unsuccessful, due to the formation of deep tears scattered over the surface and edges (generally known as hot shortness) during primary rolling of ingots to billets. Hot shortness has also been encountered during primary rolling of a semi-killed low carbon steel when the boron content was increased above 0.012%[57].

4.2.3 Titanium

Titanium is a strong and stable nitride former, and TiN particles have sometimes been found in molten steel[59]. Literature on solubility of TiN in steel is extremely scarce, and appears to be due to it being virtually insoluble in austenite at temperatures as

high as 1350°C[60, 61]. In contrast, the solubility of TiC is much greater and its solubility product in structural steel has been determined[60]. George and Irani[61] have reported that X-ray diffraction data show no TiC with low Ti/N ratios (i.e., Ti/N ratios less than the stoichiometric ratio), while two distinct phases, TiN and TiC with different lattice parameters, were identified with high Ti/N ratios (i.e., greater than the stoichiometric ratio) in titanium-bearing steels. Shiraiwa *et al*[62], using electron probe micro-analysis, detected only TiN precipitates in low titanium steels, while titanium carbo-nitride (a solid solution of TiN and TiC) was detected in higher titanium steels. These observations confirm that TiC may only form when the Ti/N ratio is greater than the stoichiometric requirement, so that excess titanium is available for the formation of TiC.

Due to the extremely low solubility and high stability of TiN when compared with most other precipitates from nitride formers, precipitation of TiN may take place independent of the prior heat treatment given to the steel. Hence it may be possible to precipitate nearly all the active nitrogen in low carbon steel as TiN by the addition of the necessary amount of titanium, independent of the subsequent processing conditions.

Consequently, titanium additions in excess of the Ti/N stoichiometric ratio almost completely eliminate strain ageing in the Al-killed as-rolled C-Mn reinforcing steels[4]. The removal of strain ageing characteristics has been caused by the reduction of the 'active' nitrogen content to below 0.0005% due to the precipitation of TiN. Hence, strain ageing almost entirely caused by 'active' nitrogen at ageing temperatures of 100°C or less[2], is eliminated by the addition of sufficient titanium. However, when the ageing

temperature is increased to 205°C, commercial as-rolled high-strength low-alloy (HSLA) steels with titanium contents well in excess of the Ti/N stoichiometric ratio results in strain ageing[63]. The increase in yield stress (ΔY) with pre-strain in two steels containing titanium (Ti-HSLA-1 and Ti-HSLA-2) show that they have lower values of ΔY when compared with a low-carbon steel, especially at larger pre-strain (Figure 4.9). This strain ageing of titanium-bearing HSLA steels may be caused by carbon dislocation locking, as a result of the re-solution of Fe_3C to provide interstitial carbon atoms at high ageing temperatures[2], and strain induced precipitation of TiC at dislocation sites[64].

Investigations into the use of titanium as a grain refining additive to structural steels has given varying results. This appears to be due to its efficiency as a grain refining element being dependent on two main conditions:

(a) The quantities in which it is added to structural steels, and
(b) the processing conditions, especially the rolling schedule.

George and Irani[61, 65] have reported that grain coarsening temperatures (GCT - the temperature range where a rapid transition occurs from a fine austenite grain size to a coarse grain size) greater than 1200°C were obtained in C-Mn steels with low Ti/N ratios. However, when the Ti content was increased above the Ti/N stoichiometric ratio, the grain coarsening temperature decreased by ~200°C, giving similar GCT's of the more conventional grain refining additives like aluminium and niobium. The extremely high grain coarsening temperatures of low Ti/N steels may be due to the very fine precipitates of TiN[65] which are extremely resistant to coarsening. According to particle coarsening kinetics, extremely low concentration of titanium, together with extremely low solubility of TiN,

provides high resistance to particle coarsening[51]. The significantly lower grain coarsening temperatures of the high Ti/N steels are attributed to the coarsening of TiC precipitates at considerably lower temperatures than in the case of TiN precipitates when the latter is present on its own and that as the TiC goes into solution, it provides a sink of titanium in the austenite matrix which would enhance the agglomeration of the fine TiN particles[61].

George and Irani[61] investigated the effect of thermal cycling in a C-Mn steel with low Ti/N ratio, and suggested that to obtain full benefit from grain refinement only one reheat through the ferrite/austenite transformation is permissible during processing. An investigation[66] on different processing conditions during hot-rolling of an Al-killed C-Mn steel with low Ti/N ratio showed that:

(a) Final rolled products produced by conventional rolling practice (i.e. cycling twice through the ferrite/austenite transformation temperature) gave no grain refinement.

(b) Ingots charged into the soaking pits before the transformation temperature is reached and then rolled in the conventional way (in this case the steel is taken only once through the transformation temperature) gave improvement in grain refinement.

(c) Ingots cooled to ambient conditions and directly rolled to finished product (i.e., taken once through the transformation temperature) gave the best grain refinement.

(d) A continuous cast, killed low-carbon steel with similar quantities of titanium and nitrogen, gave impact properties very similar to those obtained in the case of (c).

Reinforcing steels with low Ti/N ratios gave grain refinement when a rolling schedule similar to (c) above was used; however, as the

titanium content was increased above the Ti/N stoichiometric ratio, this refinement was significantly reduced[4].

George and Kennon[67], investigating the effects of thermal cycling on grain coarsening temperature of C-Mn steels with low Ti/N ratios, have confirmed the previous observation[61] that a reduction in grain coarsening temperature ~200°C occurs when the steel is taken through the austenite/ferrite transformation twice. Using their observations, they have deduced that this decrease in grain coarsening temperature is caused mainly by a refinement of grain size during austenite/ferrite transformation rather than by coarsening of TiN precipitates. This explanation appears to be valid when considering the effect of mean grain size (R_o) on critical particle size (r_{crit}) in Gladman's equation 4.1. It appears from the literature that the beneficial effects of fine TiN particles in providing a very high grain coarsening temperature is limited only for steels taken once through the austenite/ferrite transformation, although the reason for this is not fully understood.

It is clear that sufficient addition of titanium to low carbon steel almost completely eliminates nitrogen strain ageing in hot rolled steels. However, commercial production of grain refined structural steel appears to be only permissible with specific rolling practice and specific titanium additions.

4.2.4 Vanadium

Vanadium is both a strong nitride and carbide forming element. As a result of the difficulty in distinguishing between vanadium nitride and vanadium carbide precipitates in steel because of similar lattice parameters, molecular weight and precipitate size, there is little agreement on the structure and composition of these precipitates in steel[68]. Considering the free energies of formation

of vanadium nitride and vanadium carbide in ferrite and austenite, Fountain and Chipman[69] have shown that there will be a greater tendency for the formation of vanadium nitride than for vanadium carbide. Stephenson *et al*[70] have found VN precipitates (by using chemical methods) in hot rolled semi-killed steel containing 0.05% V and 0.014% N, while in the absence of a high nitrogen content, fine precipitates of vanadium carbide were also present. Solubility relationships for VN in C-Mn steels have been determined by chemical methods[60, 71], which confirms that titanium is a stronger nitride former.

In 1950 Epstein *et al*[72] reported on the commercial production of a rimmed non-strain ageing sheet steel containing 0.03% to 0.05% V, for deep drawing purposes. The steel was considered non-strain ageing due to its good drawability after cold reduction and annealing. The susceptibility to strain ageing was also checked by tensile testing both at room temperature and in the blue brittleness temperature range. Their results show that the V-steel has a lower TS at 180^{o}C when compared with its value at room temperature, whereas the base steel has a much higher TS at 180^{o}C when compared with its value at room temperature. These indications that the V-steel was non-strain ageing was confirmed by the absence of a discrete yield point after strain ageing at 100^{o}C for one day. Frame and Schunk[73] recommended a vanadium content of 0.02% to 0.03% and an annealing temperature of 700^{o}C for the prevention of strain ageing in low carbon steels. Jones and Coombs[74] have reported that the change in yield stress (ΔY) and TS (ΔU) after strain ageing (ageing temperature <100^{o}C) was negligible in low carbon steels having vanadium contents ranging from 0.03% to 0.1%. In this case the steel had been treated at 680^{o}C for 20 hours after hot rolling. However, when the annealing temperature was increased to 930^{o}C, this material showed signs of

strain ageing. When the ageing temperature was increased well above 100°C, the steels were highly susceptible to strain ageing. Rashid[63] has reported that a commercial as-rolled high strength low-alloy (HSLA) steel containing 0.11% V was susceptible to strain ageing when aged at 205°C. The increase in yield stress (ΔY) with pre-strain for this steel (V-HSLA) shows that the values of ΔY are similar to those for a low carbon steel, see Figure 4.9. The susceptibility to strain ageing in vanadium-bearing steels as the ageing temperature is raised above 100°C may result from carbon dislocation locking due to the re-solution of Fe_3C[2].

The work of Erasmus[71] on grain coarsening temperature of austenite shows that the 'final' GCT closely follows the solution temperature of VN, while the 'initial' GCT is lower than the solution temperature of VN. The 'initial' and 'final' coarsening points follow the solution curve for VN when the vanadium content is <0.1%; however, at higher vanadium contents, the 'initial' coarsening points appear to follow the solution curve for V_4C_3. These observations suggest that the GCT is controlled by VN precipitates, especially with vanadium contents <0.1% and that VN is formed in preference to V_4C_3 in this steel.

It is well established that small additions of vanadium improve the mechanical properties of as-rolled structural steel. These improvements are brought about by both grain refinement and precipitation hardening, caused by precipitates of VN and V_4C_3. Grain refinement improves both yield stress and impact properties, while precipitation hardening causes an increase in friction stress (σ_i), and hence increases yield stress but deteriorates impact properties. However, precipitation of VN may have a beneficial effect on impact properties due to the reduction of 'active' nitrogen.

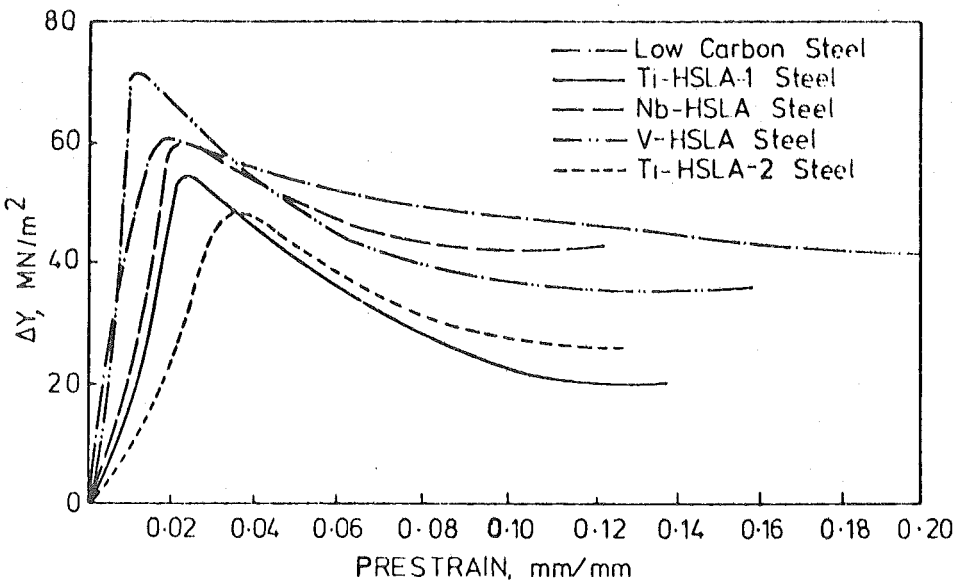

Ti-HSLA-1:- 0.09% C, 0.35% Mn, 0.16% Ti, and 0.008% N.
Ti-HSLA-2:- 0.09% C, 0.51% Mn, 0.23% Ti, and 0.004% N.
Nb-HSLA :- 0.11% C, 1.19% Mn, 0.11% Nb, and 0.007% N.
V -HSLA :- 0.13% C, 1.21% Mn, 0.11% V, and 0.016% N.
Low carbon:- 0.05% C, 0.32% Mn and 0.006% N.

ΔY - The increase in 0.2% yield stress over the pre-strain stress.

Figure 4.9: Change in ΔY with pre-strain after strain ageing. (Aged at 205°C for 1 hour). (Rashid[63]).

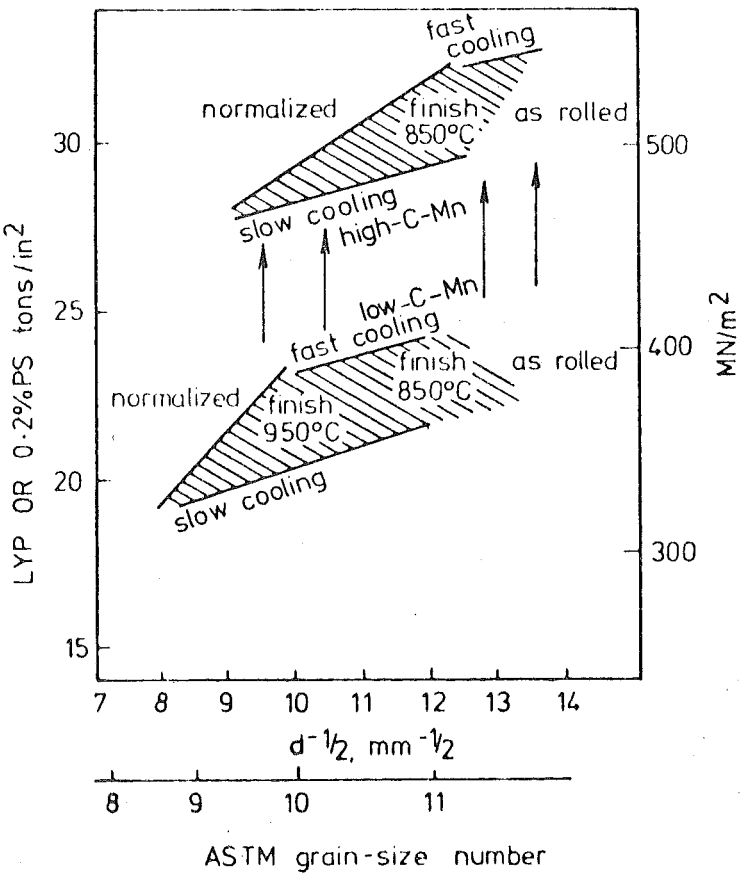

Figure 4.10: Effect of the rolling variables and composition on the lower yield point-grain size relationship (i.e. the Hall-Petch equation) of C-Mn structural steel containing 0.095% vanadium. (Irvine *et al*[60]).

An investigation by Irvine *et al*[60] into the effect of rolling conditions on the lower yield stress of C-Mn structural steels containing 0.095% V is summarised in Figure 4.10. In this investigation the conventional rolling schedule with two re-heat temperatures (1100°C and 1250°C) were used. In general, at a particular cooling rate and composition, the LYS is increased by a lower finish rolling temperature, mainly due to grain refinement. The results of Chapman and Phillips[75] show that decreasing the finish rolling temperature from 1050°C (hot rolling) to 800°C (controlled rolling, i.e. controlling the rolling temperature after the re-heating stage), improves both impact transition temperature and yield strength of a low carbon steel containing 0.06% V, see Figure 4.11. Baker[76] has reported that controlled rolling of low carbon steels with 0.1% V and 0.01% N produced progressive increases in lower yield stress when the finish rolling temperature was decreased. However, the impact transition temperature had a minimum when the finish rolling temperature was just above the ferrite transformation temperature (i.e., the Ar_1 temperature, below which the structure is ferrite). These investigations were made on very low carbon steels with three different Mn contents to give a range of Ar_3 (i.e., the temperature above which the structure is austenite) and Ar_1 temperatures.

In a low carbon steel containing 0.06% V, increasing the rolling reductions at low temperature led to a ferrite grain refinement, a decrease in impact transition temperature and an increase in yield strength[77]. It is suggested that this may be due to refinement of ferrite grains during the austenite/ferrite transformation resulting from the deformation of austenite below its re-crystallisation temperature (i.e., the temperature below which re-crystallisation of austenite is inhibited). It is also

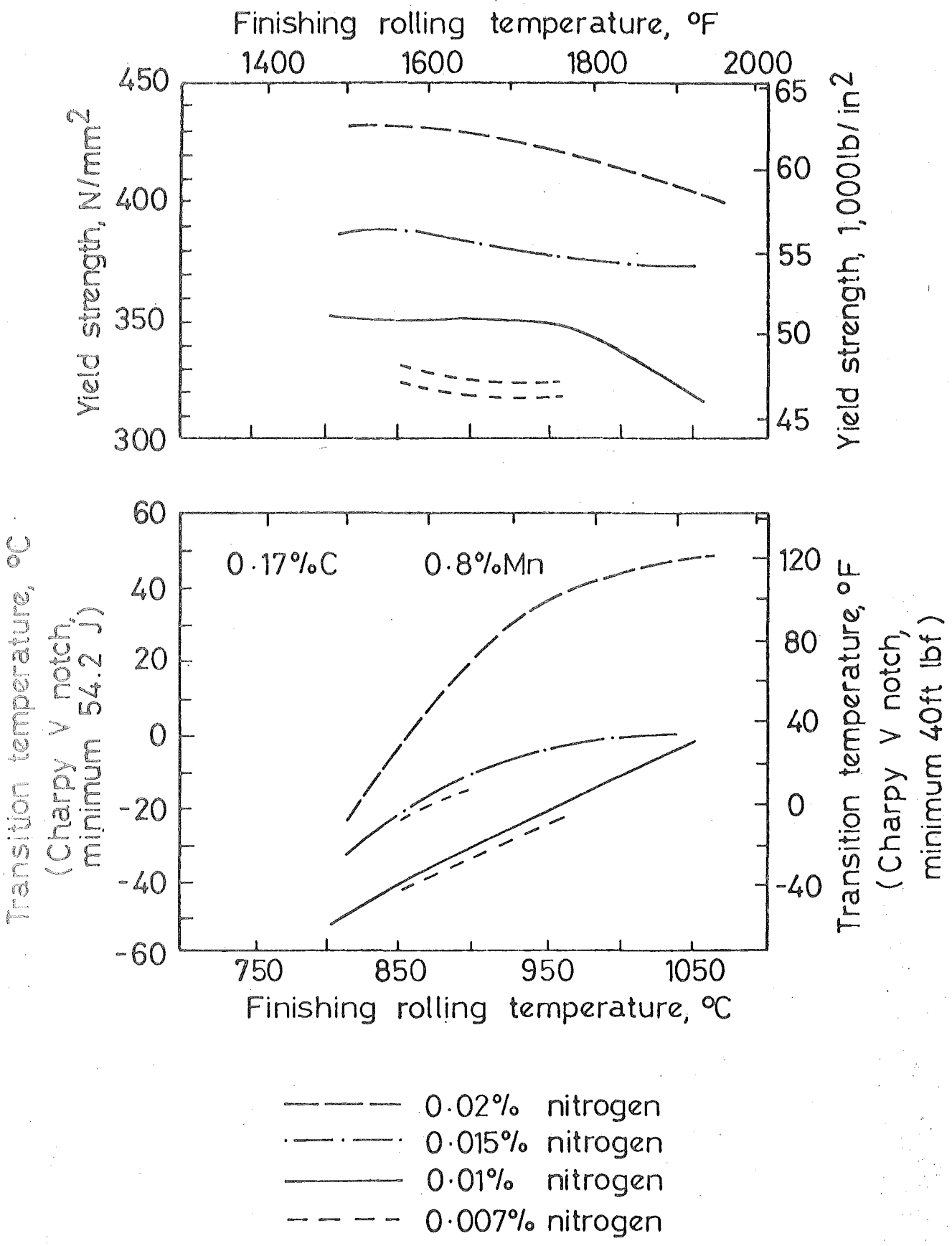

Figure 4.11: Effect of finish rolling temperature on yield strength and impact transition temperature of 0.06% V-N steels. (Chapman and Phillips[75]).

reported that the vanadium addition effectively raised the re-crystallisation temperature of austenite. Coreda and Hook[78] reported that vanadium addition to HSLA steel was effective in retarding the re-crystallisation of austenite after deformation at ~900°C. In this case, one of the suggested mechanisms for this behaviour was strain induced precipitation of V_4C_3 on sub-grain boundaries. This observation and suggestion has, to some extent, been confirmed by Kozasu *et al*[79]. Kozasu[80] reports that most literature on re-crystallisation of austenite after deformation is in agreement that vanadium raises the re-crystallisation temperature of austenite by retarding the progress of re-crystallisation and hence it enables the effects of controlled rolling to be achieved at comparatively high rolling temperatures.

The preceding discussion of literature on the effects of small additions of vanadium to low carbon steel clearly indicates that the vanadium is precipitated as vanadium nitride and vanadium carbide in the as-rolled state. However, the maximum grain refinement appears to be obtained by controlled rolling.

4.2.5 Niobium

As niobium carbide and niobium nitride are mutually soluble, a niobium carbo-nitride Nb(C,N) is formed in structural steels, and there is no marked tendency to form a separate nitride phase[60]. Hence the solubility product for Nb(C,N) in austenite was determined in terms of an equivalent carbon content.

De Kazinczy and Axnäs[39] investigated the effect of 0.036% Nb addition to a semi-killed Open Hearth steel with a basic composition of 0.11% C, 1.0% Mn and 0.004% N. The strain ageing characteristics in both hot-rolled and normalized conditions were examined, and the respective increases in yield stress (ΔY) after ageing for 30 minutes at various ageing temperatures, are shown in Figures 4.1 amd 4.2.

The results show that niobium addition appears to have reduced the strain ageing propensity of the base steel, when the ageing temperature is below 100°C in the as-rolled state. A similar trend of a lower susceptibility of strain age embrittlement is shown by the lower increase in transition temperature (ΔT_{27}) of this steel, see Figure 3.12. However, these values of ΔT_{27} are larger than those obtained for a non-ageing aluminium-treated steel (i.e., the aluminium-treated in the normalized condition) also shown in Figure 3.12. The work of Morrison[81] on the effect of niobium additions to a low carbon steel (0.13% C, 0.5% Mn, 0.16% Si and 0.005% N) on strain ageing is shown in Figure 4.12. The variation of ΔY after a strain ageing treatment of 4% pre-strain followed by ageing at 100°C for an hour with niobium content, shows that a niobium content of about 0.06% is required to start reducing ΔY in the hot-rolled and normalized conditions. However, a heat treatment of 30 minutes at 650°C has almost eliminated strain ageing at the above niobium content in the as-rolled steel. It has been estimated from these observations that the niobium precipitate in the as-rolled and normalized steel contains typically below 5% of the nitride, but may reach 50% by annealing at 650°C. It has been reported[39] that the Nb(C,N) precipitate in a niobium-treated mild steel consisted of 90% NbC and 10% NbN. A commercial HSLA steel containing 0.1% niobium was susceptible to strain ageing when aged at 205°C[63]. The variation in ΔY with pre-strain for this steel (Nb-HSLA) shows that it closely follows the curve for the low carbon steel, see Figure 4.9. This may be due to the additional availability of interstitial carbon for dislocation locking at 205°C.

It is well established that small additions of niobium improve the mechanical properties of as-rolled structural steel by grain

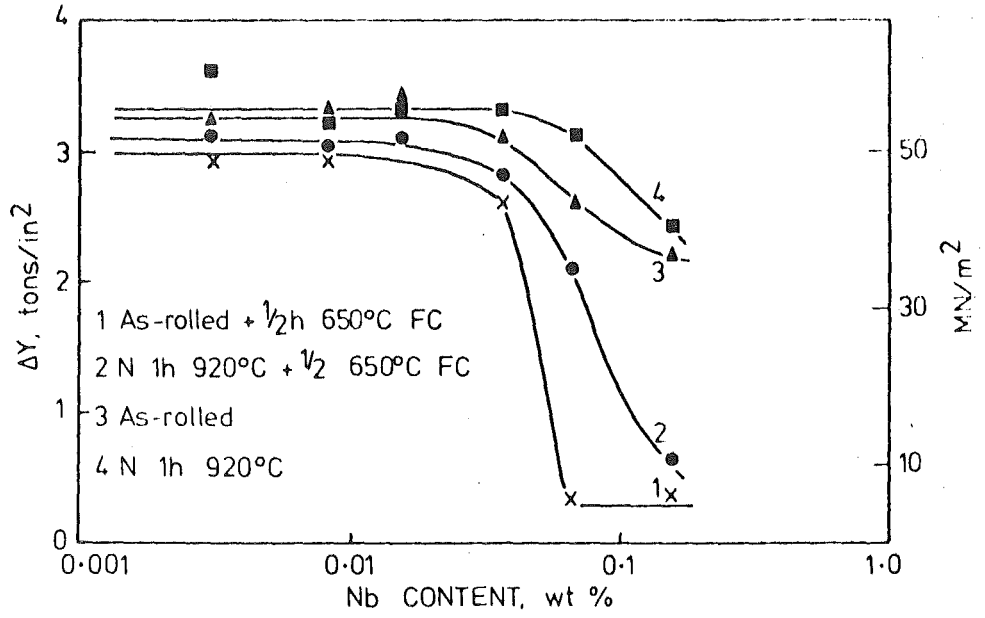

Figure 4.12: Effect of Nb content on the increase in lower yield stress (ΔY) after strain ageing in a low-carbon steel. (Pre-strained 4% and aged at 100°C for 1 hour). (Morrison[81]).

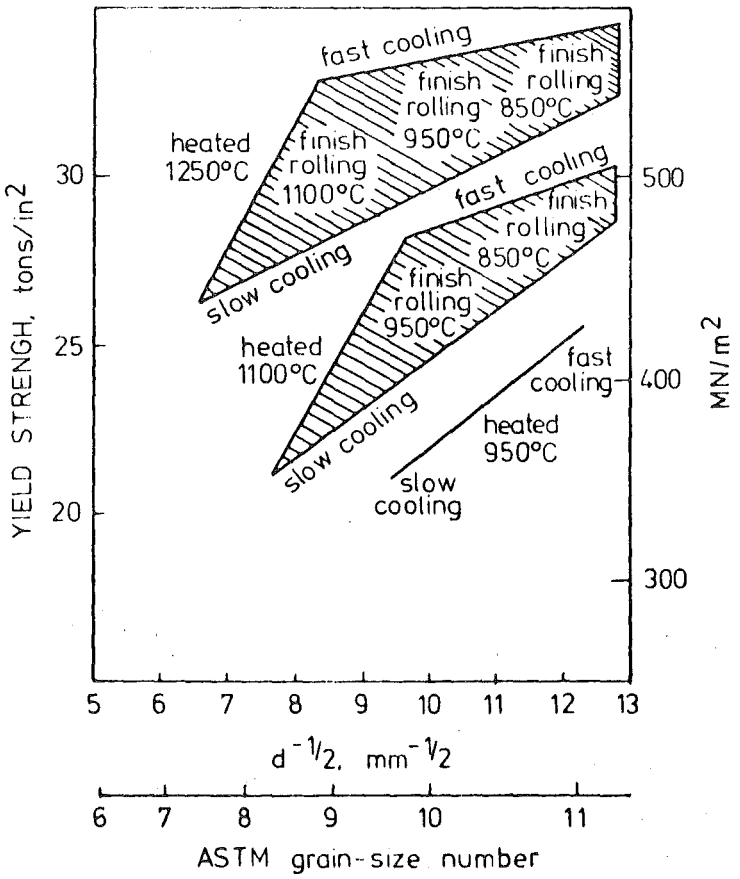

Figure 4.13: Effect of rolling variables on the yield strength-grain size relationship (i.e., the Hall-Petch equation) of C-Mn structural steel containing 0.08% Nb. (Irvine *et al*[60]).

refinement and precipitation hardening. Work by Irvine *et al*[60] on the effect of rolling practice on the lower yield stress of a C-Mn structural steel containing 0.08% niobium is summarized in Figure 4.13. In this work the conventional rolling schedule with two re-heat temperatures (1100°C and 1250°C) were used. In general, at a particular re-heat temperature and cooling rate, the LYS is increased by decreasing the finish rolling temperature, mainly due to grain refinement. The LYS is also increased by increasing the re-heat temperature for a given grain size, resulting from niobium being taken into solution and re-precipitating as a coherent niobium precipitate, hence causing precipitation hardening. Jones and Rothwell[82] have shown the effect of niobium content on the mechanical properties of a C-Mn steel for two finish rolling temperatures, see Figure 4.14. Their results show the remarkable improvement in the impact transition temperature which could be obtained by controlled rolling (i.e., by finish rolling at 850°C). At the high finishing temperature (i.e., hot-rolling) niobium gives maximum precipitation strengthening effect, but no grain refinement, while at low finishing temperature niobium gives significant grain refinement. The precipitation strengthening effect of niobium in hot-rolled steel has also resulted in similar increases in transition temperature in earlier work[39, 81].

It appears to be clearly established that small additions of niobium cause a retardation in the re-crystallization of deformed austenite[64, 77 - 79, 83]. The investigations of Weiss *et al*[64] on the re-crystallization characteristics of a niobium-titanium bearing low carbon steel strongly suggest that the retardation in the re-crystallization of deformed austenite is brought about by strain induced precipitation. They suggest that niobium precipitates, and possibly TiC, are responsible for this process. The results show

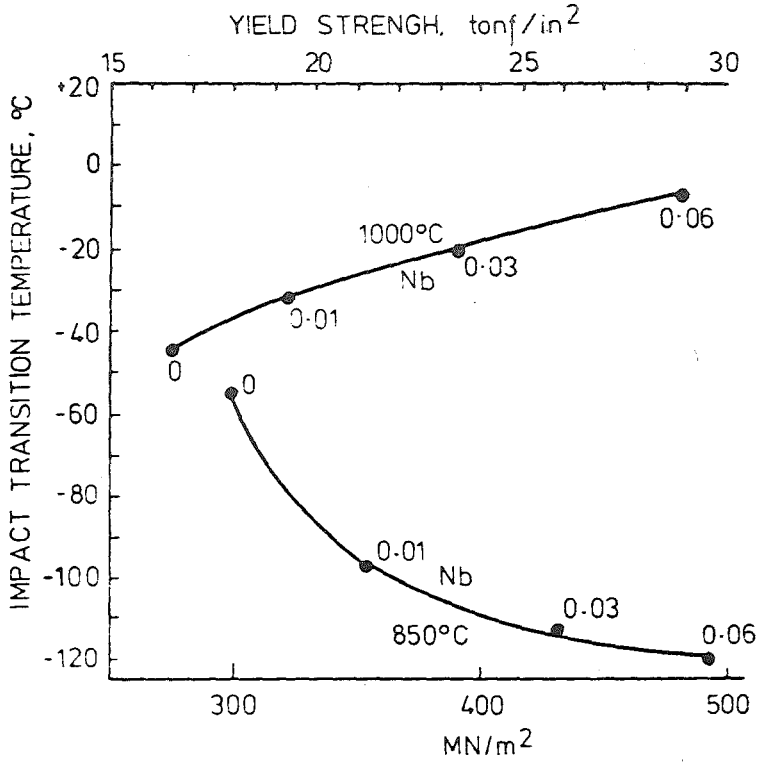

Figure 4.14: Effect of Nb content on the yield strength and impact transition temperature of 0.04% C, 1.5% Mn steel, for two finish rolling temperatures. (Jones and Rothwell[82]).

that strain induced precipitation could be increased by increasing the austenizing temperature and reducing the deformation temperature. A study on re-crystallization of austenite and niobium precipitation during hot working of a niobium HSLA steel, has shown that ~900°C niobium is precipitated at a much faster rate in deformed austenite than in un-deformed austenite[83]. The precipitate size in deformed austenite was ~30-50Å, while in the undeformed austenite it was ~1000 - 3000Å. The retardation in the re-crystallization of deformed austenite in the Ar_3 temperature region may be the cause for grain refinement at low finish rolling temperatures.

In conclustion, it appears from the literature that niobium precipitates formed by small additions of this element to low carbon steels contains only a small fraction of the nitride in the as-rolled state, the rest being carbide. Hence niobium contents in excess of 0.1% may be required, to reduce strain ageing due to nitrogen, to a negligible level. It is also clear that niobium additions cause an increase in LYS at the expense of impact properties in hot-rolled steel, due to precipitation strengthening. The major advantages of niobium additions appear to be obtained by controlled rolling.

4.2.6 Zirconium

Although zirconium is a nitride forming element, literature on the effects of zirconium on low carbon steel is scarce. It has been reported that additions of approximately 0.1% zirconium to as-rolled steels have been found to reduce strain ageing appreciably[3]. The work of Sage and Copley[84] indicates that the addition of 0.06% zirconium to C-Mn steel has reduced the active nitrogen content.

The addition of zirconium to low carbon steel has had no effect on grain size[84, 85], and has been attributed to the larger size on ZrN precipitates compared with the precipitates of conventional

grain refining elements like aluminium or niobium[85]. A 0.6% zirconium content had no effect on the tensile properties[84], which shows that the ZrN precipitates are non-coherent and do not cause precipitation strengthening.

4.3 Summary

As a result of the preceeding discussion on the effects of nitride forming elements in low carbon steels, the following two elements were chosen for the addition to reinforcing steels in order to investigate their efficiency in eliminating nitrogen strain ageing:

(a) Titanium, as a result of it being the strongest nitride former, and when added in controlled amounts, gives improved impact properties and at the same time, increases the yield strength in the as-rolled steel.

(b) Vanadium, as a result of the greater tendency to predipitate the nitride in preference to the carbide, and as the addition can be made to a semi-killed steel. It is also believed that vanadium gives a finer grain size.

CHAPTER 5

EFFECT OF TITANIUM ADDITIONS TO AS-ROLLED C-Mn REINFORCING STEELS

5.1 Preparation of the Steels

The steels were made from casts produced by the BEA process to conform to the Grades 275 and 380 standards of NZS 3402 P, 1973. The cast analysis is given in Table 5.1. Pre-determined amounts of titanium ranging from zero to 0.1% were added to both grades during teeming. The experimental steel ingots were cogged to square billets which were fed directly into a re-heat furnace. This was followed by final rolling to 25.4 mm diameter deformed bar.

5.2 Stabilization of Nitrogen by Titanium

The effect of titanium content on the stabilization of nitrogen for the Grade 275 steel is shown in Figure 5.1. For those steels which contain 0.005 - 0.006% total nitrogen, a 0.02 - 0.03% titanium content appears to be sufficient to effectively stabilize them against strain ageing by nitrogen[4], i.e., titanium contents slightly in excess of the stoichiometric compositon are required. This may be due to some of the titanium being present in the form of TiO_2 and TiC. Similar results were obtained for the Grade 380 steel[4].

5.3 Grain Refinement and Luder's Strain

The use of titanium as a grain refining additive in as-rolled structural steels appears to be dependent on titanium content as well as the rolling schedule[61, 66]. Grain refinement has been observed in this investigation[4], especially in the Grade 380 steels, i.e., the higher manganese steels. (Figure 5.2). However, the extent of the refinement appears to be subjected to the titanium content, best results being obtained at or just below the titanium/nitrogen stoichoimetric ratio. Also, the rolling schedule was such that only one ferrite/austenite transformation occurred during processing, giving the best possible grain refinement conditions[61, 66]. The Luder's strain can also be seen to be closely related to grain size, the maximum yield point

TABLE 5.1: Cast Analysis of Grades 275 and 380 Steels.

(Element, % wt)

Steel	C	Mn	Si	S	P
Grade 275	0.21	0.45	0.16	0.030	0.007
Grade 380	0.25	1.33	0.30	0.025	0.010

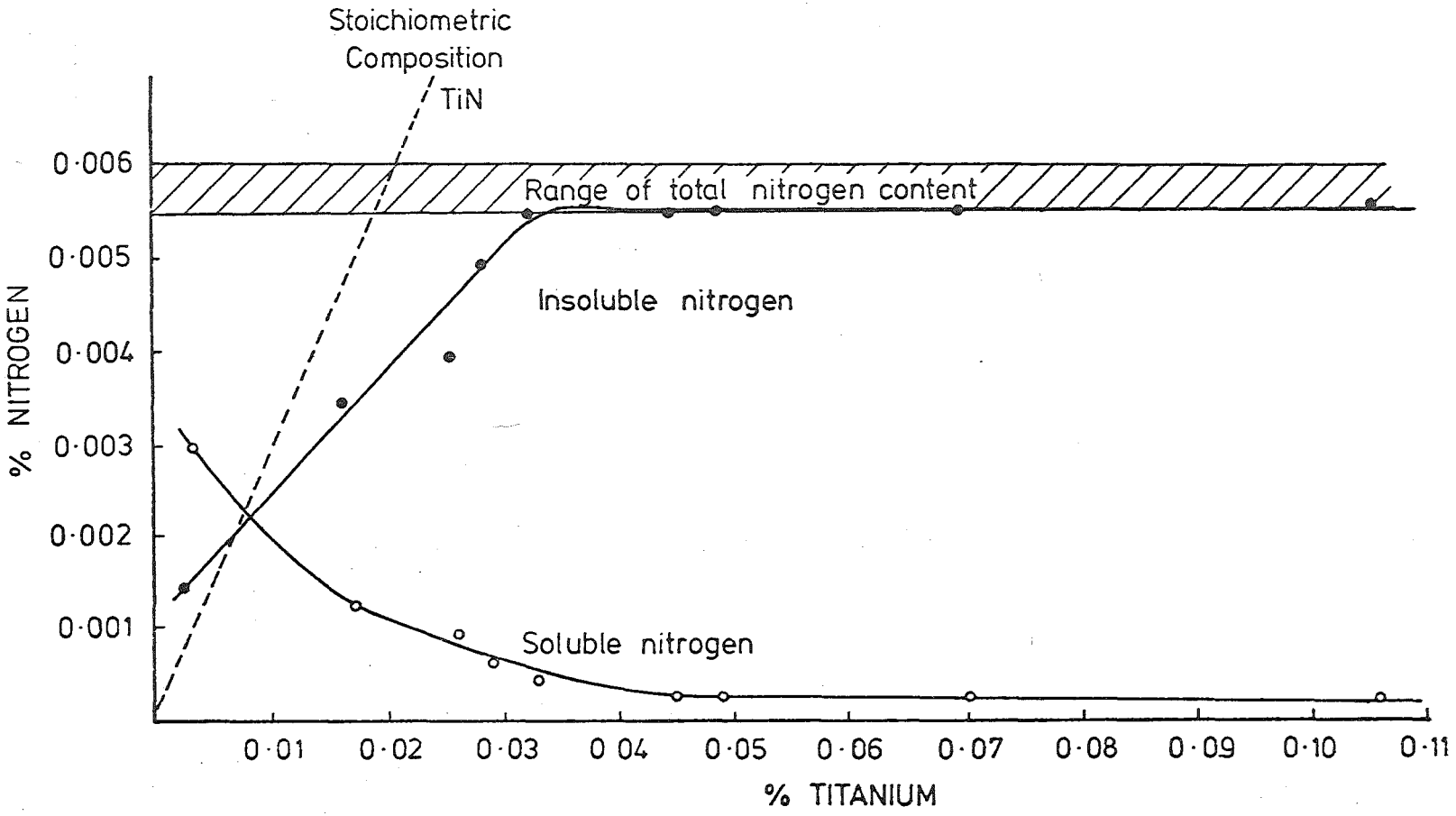

Figure 5.1: Effect of titanium content on the stabilisation of nitrogen in as-rolled reinforcing steel (Grade 275). (Smaill *et al*[4]).

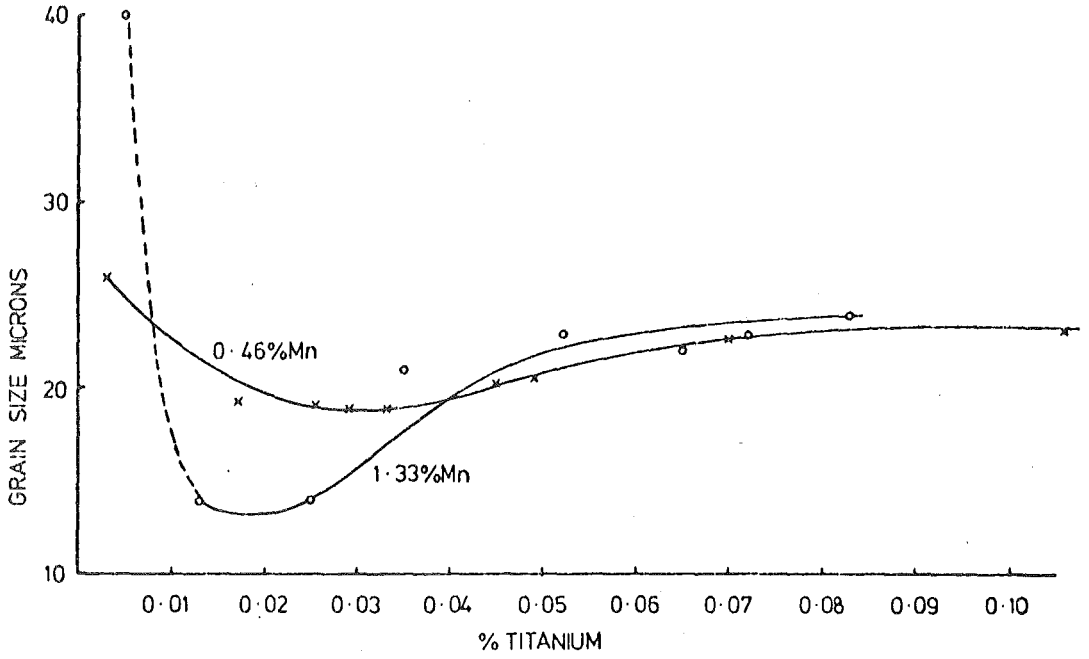

Figure 5.2: Effect of titanium content on grain size, at two manganese contents (0.46% Mn corresponds to Grade 275 and 1.33% Mn corresponds to Grade 380).

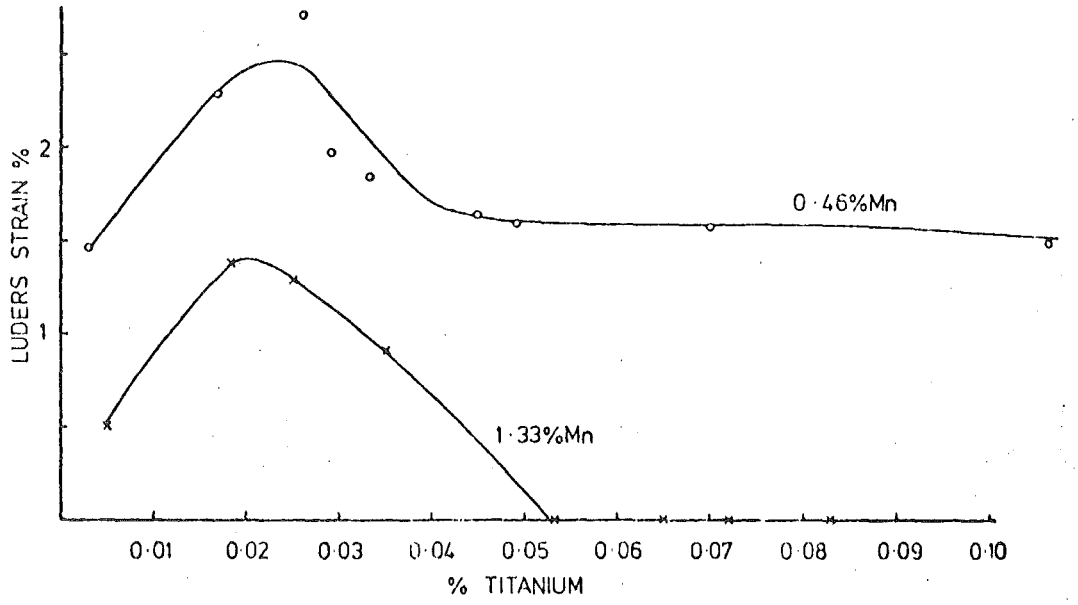

Figure 5.3: Effect of titanium content on Luder's strain, at two manganese contents.

elongation occurring with the TiN stoichiometric composition (Figure 5.3).

5.4 Effect of Titanium Content on Strain Ageing Characteristics

5.4.1 Tensile Properties

The effect of strain ageing on tensile properties has been obtained after pre-straining 5% and subsequently ageing at 100°C for three hours. This ageing treatment is equivalent to 9 months at 15°C[30]. Also, strain ageing at 100°C is almost entirely caused by 'active' nitrogen, which is responsible for natural strain ageing[2].

The increase in lower yield stress (ΔY), increase in tensile strength (ΔU), and the decrease in elongation ($\Delta E\ell$) after strain ageing with titanium content, is shown in Figures 5.4 to 5.6 for the steels with the Grade 275 base composition. It is clear from these results that increasing the titanium content from trace levels to around that of the TiN stoichiometric composition is sufficient to almost eliminate strain ageing caused by nitrogen, and that further increases in titanium content have no added advantage. Similar results were obtained with the Grade 380 base composition, except that in the case of ΔY, first stage ageing appeared to return when the titanium content was increased above the TiN stoichiometric compositon (Figure 5.7). This increase in ΔY was attributed to the precipitation of TiC with excess titanium during the artificial ageing treatment[4].

5.4.2 Impact Properties

The variation in the 27 Joule fracture transition temperature (T_{27}) with titanium content shows that the transition temperature decreases to a minimum at around the TiN stoichiometric composition for both Grades 275 and 380 base compositions, in the as-rolled steels. (See Figures 5.8 and 5.9.) However, with further increase in titanium content, the transition temperature increases steadily. The decrease in the as-rolled transition temperature appears to be related to the grain refinement which occurs

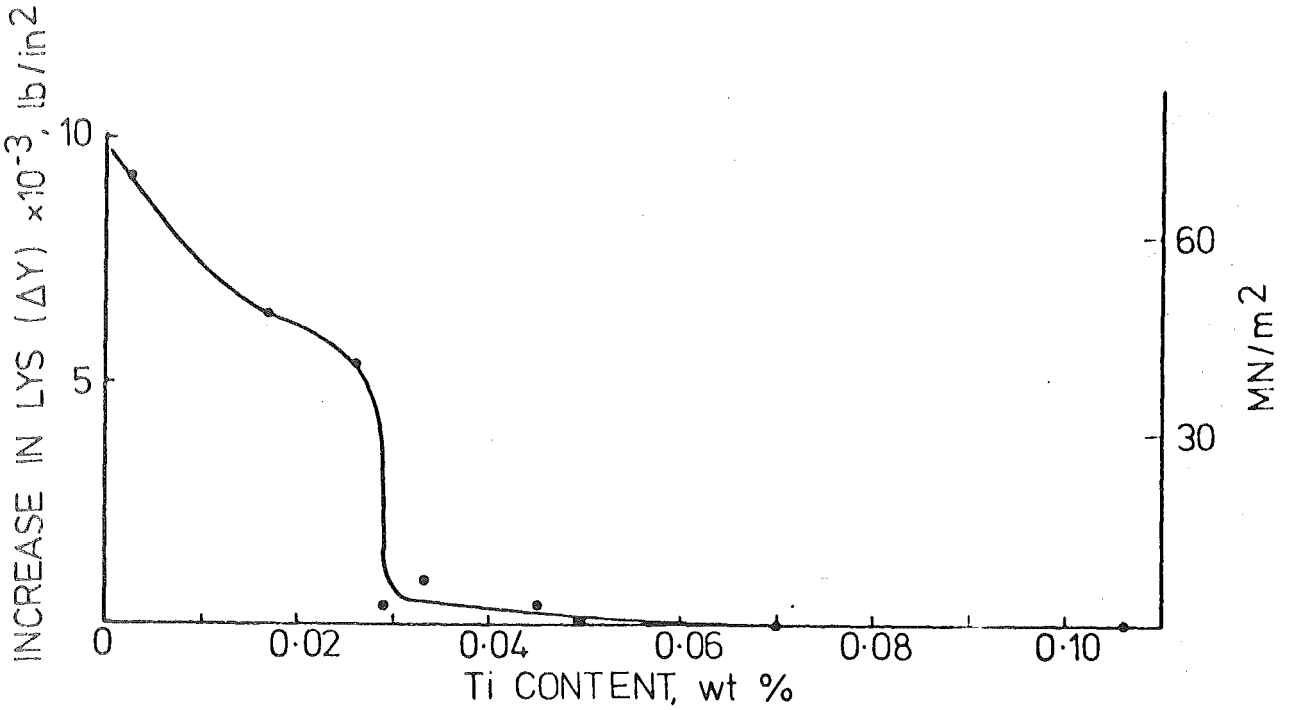

Figure 5.4: Effect of titanium content on the increase in lower yield stress (ΔY)after strain ageing. (Grade 275). (Chong and Lim[86]).

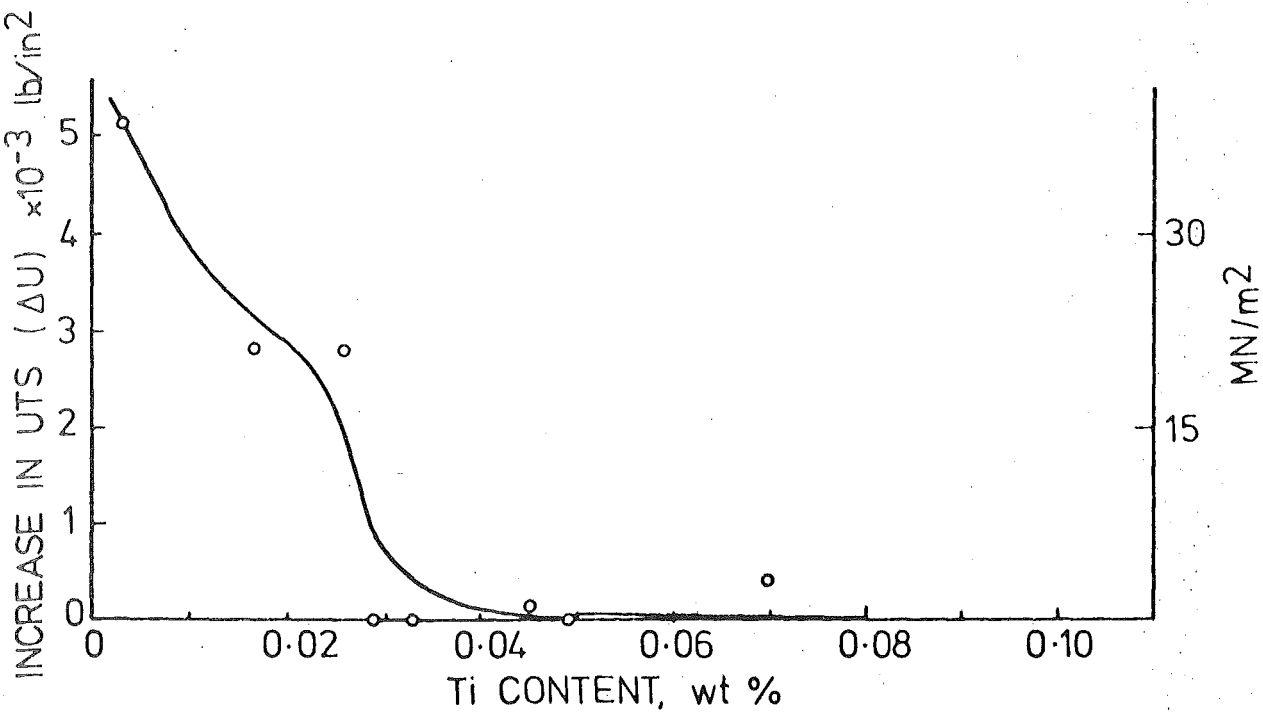

Figure 5.5: Effect of titanium content on the increase in TS (ΔU) after strain ageing. (Grade 275). (Chong and Lim[86]).

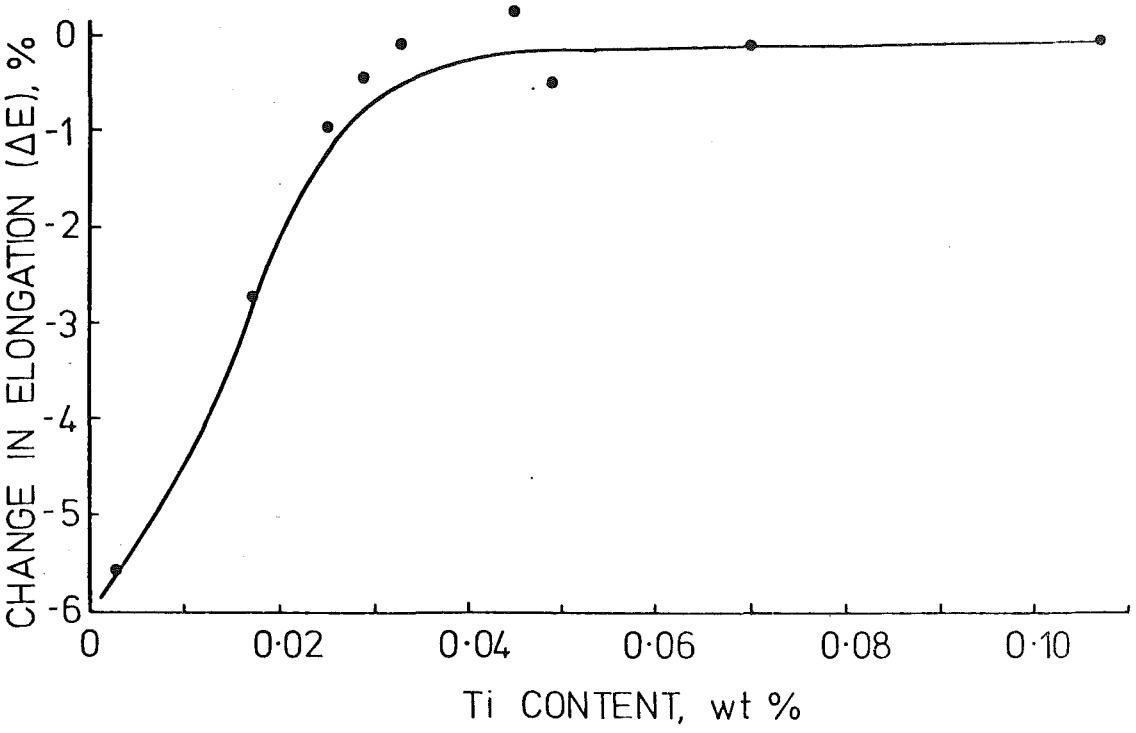

Figure 5.6: Effect of titanium content on the change in elongation ($\Delta E\ell$) after strain ageing. (Grade 275.) (Chong and Lim[86]).

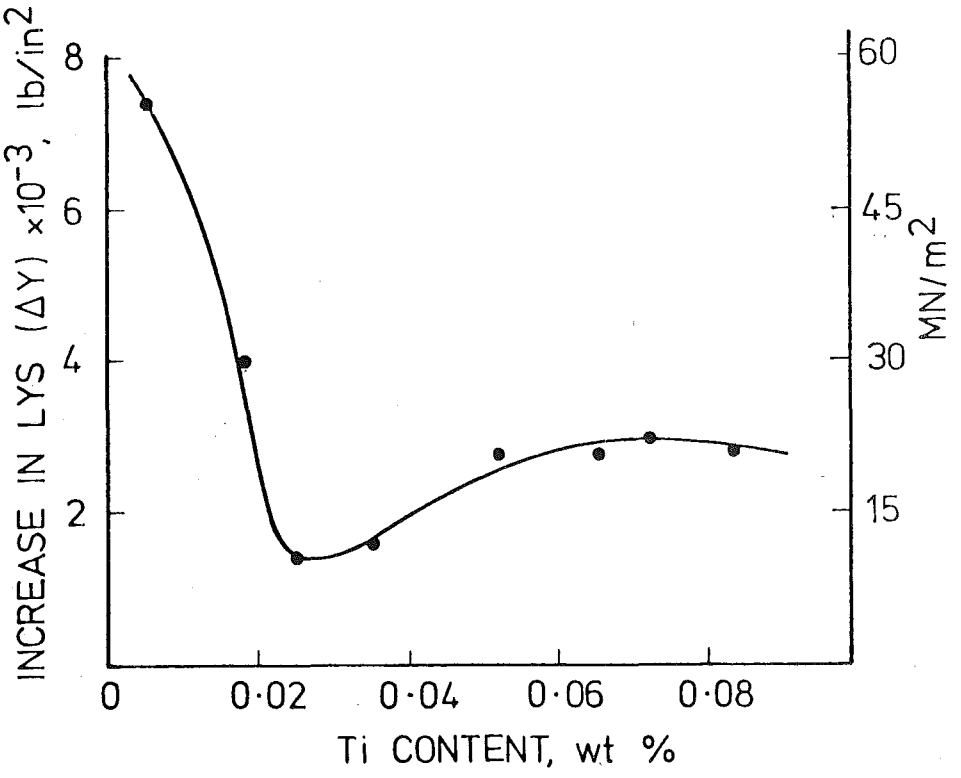

Figure 5.7: Effect of titanium content on the increase in lower yield stress (ΔY) after strain ageing. (Grade 380). (Smaill *et al*[4]).

with titanium additions up to the TiN stoichiometric composition. However, this reduction in transition temperature cannot be fully accounted for by grain refinement and it is suggested that the removal of active nitrogen also plays an important role[4]. The increase in transition temperature with increased titanium contents above the TiN stoichiometric composition has been attributed to fine precipitate particles of TiC in the ferrite matrix, especially in the higher titanium steels.

It is clear from Figures 5.8 and 5.9 that the increase in fracture transition temperature (ΔT_{27}) due to strain ageing (i.e., strain embrittlement), has been considerably reduced from its initial values of 26^{o} and $29^{o}C$ for Grades 275 and 380 base steels, when the titanium content was increased to approximately the stoichiometric composition. This is obviously as a result of the elimination of strain ageing by the effective stabilization of nitrogen. However, further increase in titanium content above the TiN stoichiometric composition resulted in a continuous increase in ΔT_{27}, which appears to be caused by the increased flow stress at 5% pre-strain resulting from precipitation hardening by TiC precipitates in the ferrite matrix[4].

5.5 Summary

As a result of the very strong affinity of titanium for the formation of TiN, sufficient titanium additions to C-Mn reinforcing steels has been successful in almost eliminating nitrogen strain ageing of these steels, in the as-rolled state. The optimum titanium content appears to be in the region of 0.02 - 0.03%, which is the stoichiometric requirement for these steels containing 0.005 - 0.006% nitrogen. Increasing the titanium content above this optimum level results in an increase in the fracture transition temperature from its minimum value.

In addition to eliminating strain ageing, the steels containing this

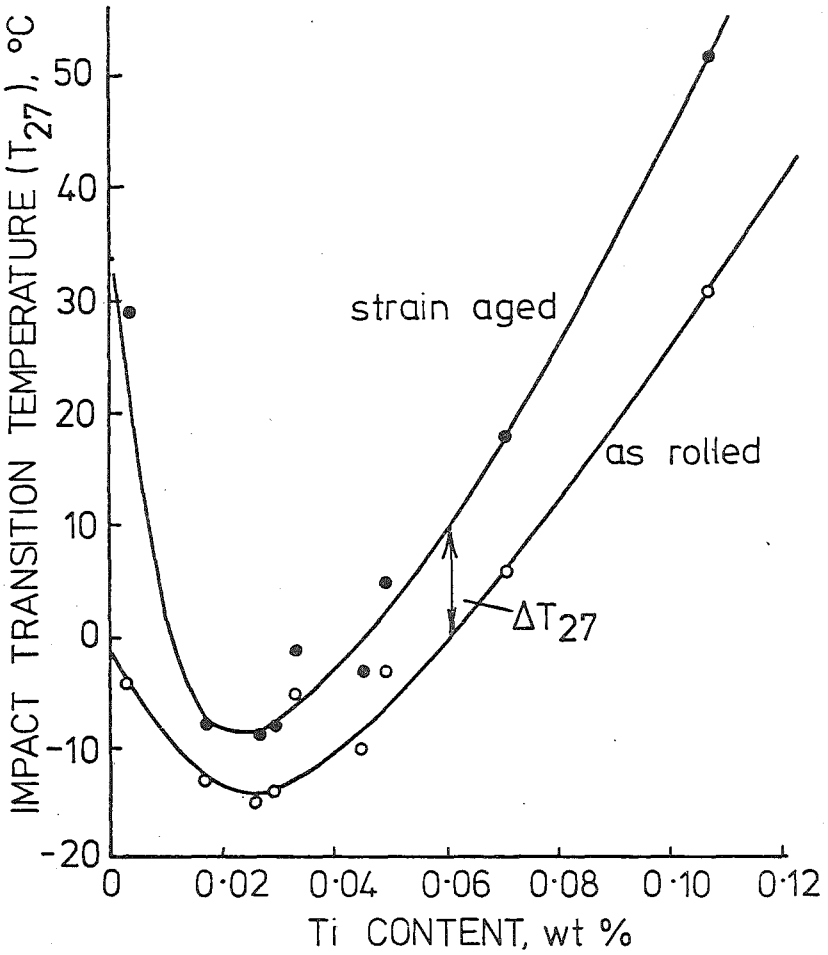

Figure 5.8: Effect of titanium content on impact transition temperature in the as-rolled and strain aged conditions. (Grade 275). (Chong and Lim[86]).

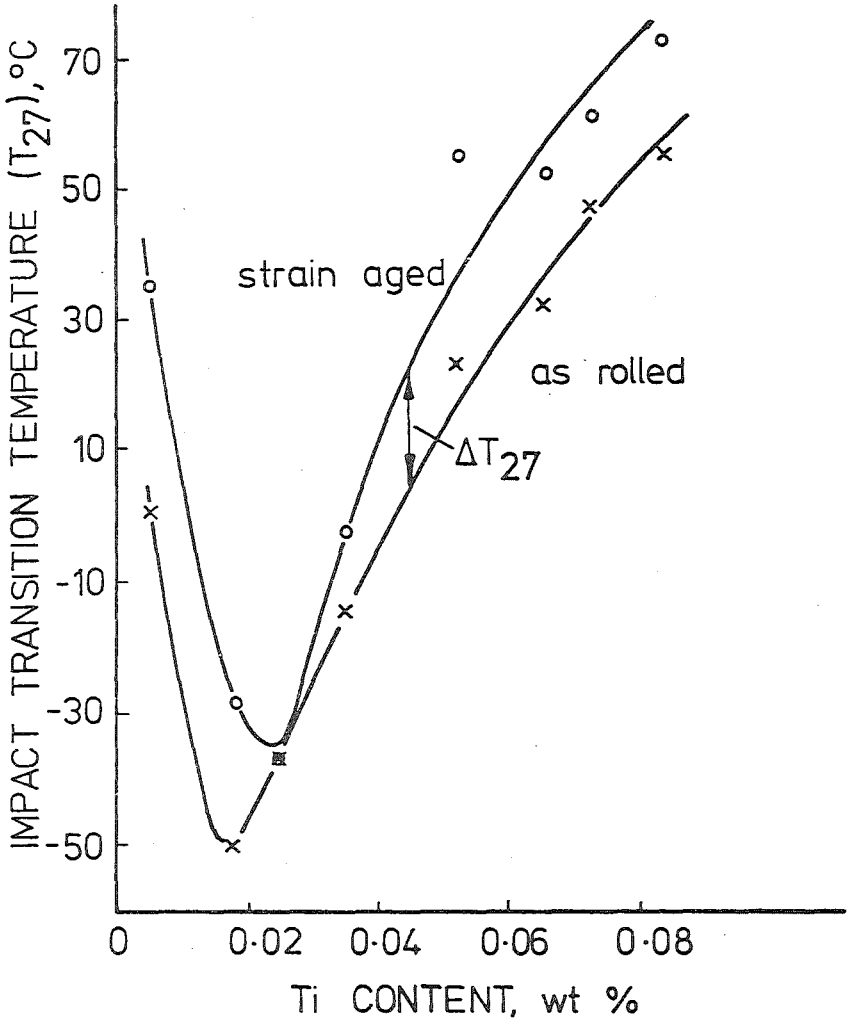

Figure 5.9: Effect of titanium content on impact transition temperature in the as-rolled and strain aged conditions. (Grade 380). (Smaill *et al*[4]).

optimum titanium content gave remarkable improvements in fracture transition temperature in the as-rolled state. Further, this level of titanium content also gives the maximum Luder's strain. Hence it is obvious that C-Mn structural steels containing this optimum level of titanium has tremendous prospects to be used as a reinforcing steel in earthquake resistant concrete structures.

However, in the commercial production of this steel, as titanium is a strong deoxidizer, it is essential that the steel be fully killed so that most of the titanium is available for the formation of TiN.

CHAPTER 6

EFFECT OF VANADIUM ADDITIONS TO AS-ROLLED C-Mn REINFORCING STEELS - EXPERIMENTAL PROCEDURE, RESULTS AND DISCUSSION

6.1 Preparation of the Steels

The steels were made from a cast produced by the BEA process to conform to Grade 275 standard of NZS 3402 P (1973). Two groups of experimental steels were made from this cast during a normal production run. Group A was made with the normal aluminium addition used in commercial production at present and consisted of a series of ingots, each having a pre-determined nominal vanadium addition ranging from zero to 0.1%. Group B had a similar vanadium range. However, the aluminium additions were limited to what would normally be present in a semi-killed steel. Both aluminium and vanadium (in the form of ferro-vanadium) was added to the ingots during teeming. The pre-determined amounts of finely ground ferro-vanadium were separated into six equal portions and added at equal intervals during the teeming operation.

The molten steel was tapped from the furnace at a temperature of approximately 1600^{o}C into a ladle from which it was teemed to the ingot moulds. The cooled ingots were soaked at ~1100^{o}C for three hours and then cogged to 100 mm square billets, which were fed directly into a re-heat furnace at 1050^{o}C. This was followed by final rolling to 20 mm diameter plain bar and then cooled on a cooling bed.

6.2 Chemical Analysis

6.2.1 Composition of the Steels

A detailed composition of the steels was obtained spectrographically from the ARL Spectrometer at New Zealand Steel Ltd. The approximate base compositions of the two groups of steel obtained by this analysis is given in Table 6.1. The vanadium and Al_{sol} contents of these steels

were also determined by a chemical method described in Appendix A using atomic absorbtion (AA) Spectrophotometry. The results from this chemical analysis and those obtained spectrographically for vanadium and aluminium are given in Table 6.2. When examining these results, it is clear that in the case of the aluminium determinations, the chemical method always gave a lower value in comparison with the spectrographic determinations. This difference may be mainly due to aluminium in the form of Al_2O_3, which is not dissolved by the chemical method (see Appendix A) and hence excluded in the organic extract from which the aluminium content is determined by the atomic absorbtion spectrophotometer.

6.2.2 Determination of Nitrogen in the Steels

The nitrogen content of the steels was accurately separated as 'acid soluble' nitrogen (N_{sol} - representing nitrogen in solid solution, as iron nitride and as AℓN) and 'acid insoluble' nitrogen (N_{insol} - representing nitrogen combined as stable nitrides, in this case mostly VN) by the solution of a drilled sample in two stages; namely, by dilute H_2SO_4 and fuming H_2SO_4. A drilled sample from each steel was also used for the determination of nitrogen in the form of AℓN ($N_{A\ell N}$).

The total nitrogen content is given by,

$$N_{tot} = N_{sol} + N_{insol} \qquad 6.1$$

The 'active' nitrogen content (representing nitrogen in solid solution and as iron nitride) is given by

$$N_{'active'} = N_{sol} - N_{A\ell N} \qquad 6.2$$

The resultant nitrogen determination of the steels is given in Table 6.3. The details of the methods[87] used for these determinations is given in Appendix A.

TABLE 6.1: Approximate Base Compositions of the two Groups of Vanadium Steels (Element, % wt)

Steels	C	Mn	Si	S	P	Aℓ
Group A	0.21	0.44	0.17	0.036	0.013	0.04
Group B	0.22	0.46	0.18	0.036	0.013	0.01

TABLE 6.2: Vanadium and Aluminium analysis of the Vanadium Steels (Element, % wt)

Steels	AA Spectrophotometer		Spectrographic	
	V	$Aℓ_{sol}$	V	Aℓ
0A	Trace	0.026	Trace	0.037
1A	0.007	0.034	0.013	0.057
2A	0.019	0.016	0.024	0.013
4A	0.033	0.024	0.046	0.040
6A	0.060	0.022	0.069	0.035
8A	0.091	0.026	0.088	0.042
10A	0.102	0.020	0.110	0.039
0B	0.002	0.005	0.001	0.012
1B	0.013	0.005	0.013	0.013
2B	0.024	0.005	0.030	0.018
4B	0.039	0.004	0.049	0.009
6B	0.067	0.018	0.037	0.039
8B	0.082	0.005	0.100	0.009
10B	0.095	0.006	0.100	0.009

TABLE 6.3: Nitrogen determinations of the Vanadium Steels (% wt)

Steel	N_{sol}	N_{insol}	N_{tot}	$N_{A\ell N}$	N_{active}
0A	0.0053	0.0005	0.0058	0.0002	0.0051
1A	0.0048	0.0013	0.0061	0.0005	0.0043
2A	0.0040	0.0017	0.0057	0.0005	0.0035
4A	0.0031	0.0029	0.0060	0.0011	0.0020
6A	0.0019	0.0037	0.0056	0.0011	0.0008
8A	0.0016	0.0038	0.0054	0.0010	0.0006
10A	0.0014	0.0039	0.0053	0.0010	0.0004
0B	0.0050	0.0005	0.0055	0.0001	0.0049
1B	0.0045	0.0007	0.0052	0.0002	0.0043
2B	0.0040	0.0016	0.0056	0.0003	0.0037
4B	0.0024	0.0030	0.0054	0.0011	0.0013
6B	0.0021	0.0033	0.0054	0.0010	0.0011
8B	0.0016	0.0037	0.0053	0.0014	0.0002
10B	0.0018	0.0043	0.0061	0.0013	0.0005

Table 6.4: Grain Size Measurements of some Vanadium Steels.

Steel	Grain Size	
	d (μm)	$d^{-\frac{1}{2}}$ $(mm)^{-\frac{1}{2}}$
0A	15.2	8.12
2A	14.6	8.28
6A	13.5	8.59
10A	13.5	8.59
0B	14.8	8.23
1B	15.1	8.15
2B	14.7	8.25
4B	13.1	8.74
8B	13.0	8.78

6.3 Grain Size Measurements

The 'effective ferrite grain size' was estimated in accordance with the ASTM standards (Designation E112-74). The modified lineal intercept method was used for the determinations, considering the steels to be of a two phase metal (i.e., ferrite and pearlite). This method essentially consists of the following procedure:

(a) Drawing a set of parallel straight lines on a photomicrograph of known magnification.

(b) Determining the total length of these lines which fall in the ferrite area.

(c) Determining the number of intercepts made in the ferrite area by these lines.

(d) From (b) and (c), and the magnification the mean intercept length is calculated and the 'effective ferrite grain diameter' is determined from this length.

Ferrite grain size estimations were made in some of the steels and these results are given in Table 6.4. To ensure consistency in the results, these grain sizes were estimated from photomicrogrphs taken from areas at the mid-radius of the as-rolled 20 mm bar. However, in a few of the steels, estimations made on different areas on the longitudinal section of the bar showed no significant variation in grain size across the section.

6.4 Tensile Test Results

Tensile testing was performed on specimens with a diameter of 10 mm and gauge length 50 mm, machined from 20 mm bar. The detailed specimen dimensions and the method of preparation are given in Appendix B. In order to eliminate any effects of artificial ageing itself, the as-rolled bar was given a pre-strain ageing treatment of 3 hours at $100^{\circ}C$ before machining the tensile specimens.

All testing was carried out at a strain rate of 0.04/min. on an Instron Testing Machine. The load-extension curves were directly plotted on the recorder using a 50 mm gauge length extensionmeter on the specimens.

Tensile tests were carried out on a set of specimens comprising one from each steel (i.e. 14 specimens in all) in the as-rolled condition. For all specimens the lower yield stress (LYS), Luder's strain (or yield point elongation) and tensile strength (TS) were determined from the corresponding load-extension plots. The percentage elongation at fracture (%Eℓ) was determined from the extension of a 50 mm gauge length of the fractured specimen. These results are given in Table 6.5.

To investigate the effect of strain ageing on tensile properties, a second set of specimens comprising one from each steel were pre-strained by 5%, unloaded and subsequently aged at 100^{o}C for 3 hours before finally testing them to fracture. The resultant variation in tensile properties (i.e. ΔY, ΔU and ΔEℓ) were determined and are given in Table 6.6.

6.5 Charpy V-notch Impact Test Results

Standard Charpy V-notch specimens were machined to BS 131, Part II of 1972. A brief account of the method of prepration is given in Appendix B. Impact testing was performed on an Avery Impact Testing machine at a striking energy of 298 Joules (220 ft lbs) and a striker velocity of 5 m/s (16 ft/s), in accordance with BS 131.

As earlier, to eliminate any effects of the artificial ageing treatment, the as-rolled bar was given a pre-strain ageing treatment. In order to obtain the as-rolled fracture transition temperature of the steels, Charpy specimens were machined from as-rolled 20 mm bar and a full Charpy impact transition curve determined for each steel. The 27 Joule fracture transition temperatures (T_{27}) of the as-rolled steels are given in Table 6.7.

To investigate the effect of strain ageing on the increase in fracture

TABLE 6.5: Tensile Properties of the Vanadium Steels

Steel	LYS (MN/m^2)	Luder's Strain (%)	TS (MN/m^2)	El (%)
0A	309	1.4	483	36.5
1A	296	1.2	480	37.0
2A	320	1.4	489	37.5
4A	333	1.1	509	35.0
6A	357	1.0	636	32.0
8A	379	1.0	558	32.0
10A	397	0.9	570	30.5
0B	312	1.7	481	38.0
1B	316	2.0	486	37.0
2B	333	1.9	488	36.5
4B	351	1.5	518	34.0
6B	367	0.9	547	32.5
8B	398	1.5	555	31.0
10B	405	1.4	560	30.0

TABLE 6.6: Variation in Tensile Properties due to Strain Ageing in Vanadium Steels.

Steel	ΔY (MN/m^2)	ΔU (MN/m^2)	ΔEl (%)
0A	63	38	-7.5
1A	58	28	-6.0
2A	49	19	-4.0
4A	18	4	-2.5
6A	13	1	0.5
8A	12	0	0
10A	9	0	0
0B	61	31	-9.0
1B	62	30	-7.0
2B	54	21	-5.0
4B	14	3	-2.0
6B	8	6	-4.5
8B	10	1	0
10B	12	1	-1

TABLE 6.7: Charpy V-Notch Fracture Transition Temperature of as-rolled and strain-aged Vanadium Steels.

Steel	As rolled T_{27} (^{o}C)	Strain-aged T_{27} (^{o}C)	Increase in T_{27}, i.e. ΔT_{27} (^{o}C)
0A	-13	19	32
1A	-11	14	25
2A	-12	14	26
4A	-1	13	14
6A	-2	13	15
8A	6	19	13
10A	11	24	13
0B	-17	12	29
1B	-14	14	28
2B	-12	12	24
4B	-10	4	14
6B	-1	17	18
8B	9	22	13
10B	12	21	9

transition temperature, strain aged Charpy specimens of each steel were obtained in the following manner:

(a) An as-rolled 20 mm bar was pre-strained by 5% in tension using a Baldwin testing machine.

(b) A set of Charpy specimens were machined from within the gauge length of the pre-strained bar.

(c) Finally the Charpy specimens were aged at 100°C for 3 hours.

The 27 Joule fracture transition temperatures of the strain aged steels were obtained from the determination of the full Charpy impact transition curves. The resultant increase in the fracture transition temperature (ΔT_{27}) due to strain ageing (i.e. strain age embrittlement) was determined for each steel, is given in Table 6.7.

6.6 Discussion of Results

6.6.1 Stabilization of Nitrogen by Vanadium

Figures 6.1(a) and 6.1(b) show the effect of vanadium content on the stabilization of nitrogen in the two groups of steel. It appears from these results that, for effective stabilization of nitrogen in these steels, a vanadium content greater than about 0.06% is required. For those steels which contain 0.005 - 0.006% total nitrogen, the V/N stoichiometric ratio suggests that a vanadium content of 0.018 - 0.021% should be sufficient to reduce the 'active' nitrogen content to a negligible level (i.e., <0.0005%) if all the vanadium is used in the formation of VN. As these results show that vanadium well in excess of the stoichiometric requirement is necessary for the effective stabilization of nitrogen, it is clear that only a part of the vanadium is used in the formation of VN. This is confirmed from the variation of N_{insol} with vanadium content (see Fig. 6.1(a) and 6.1(b)), which show that although

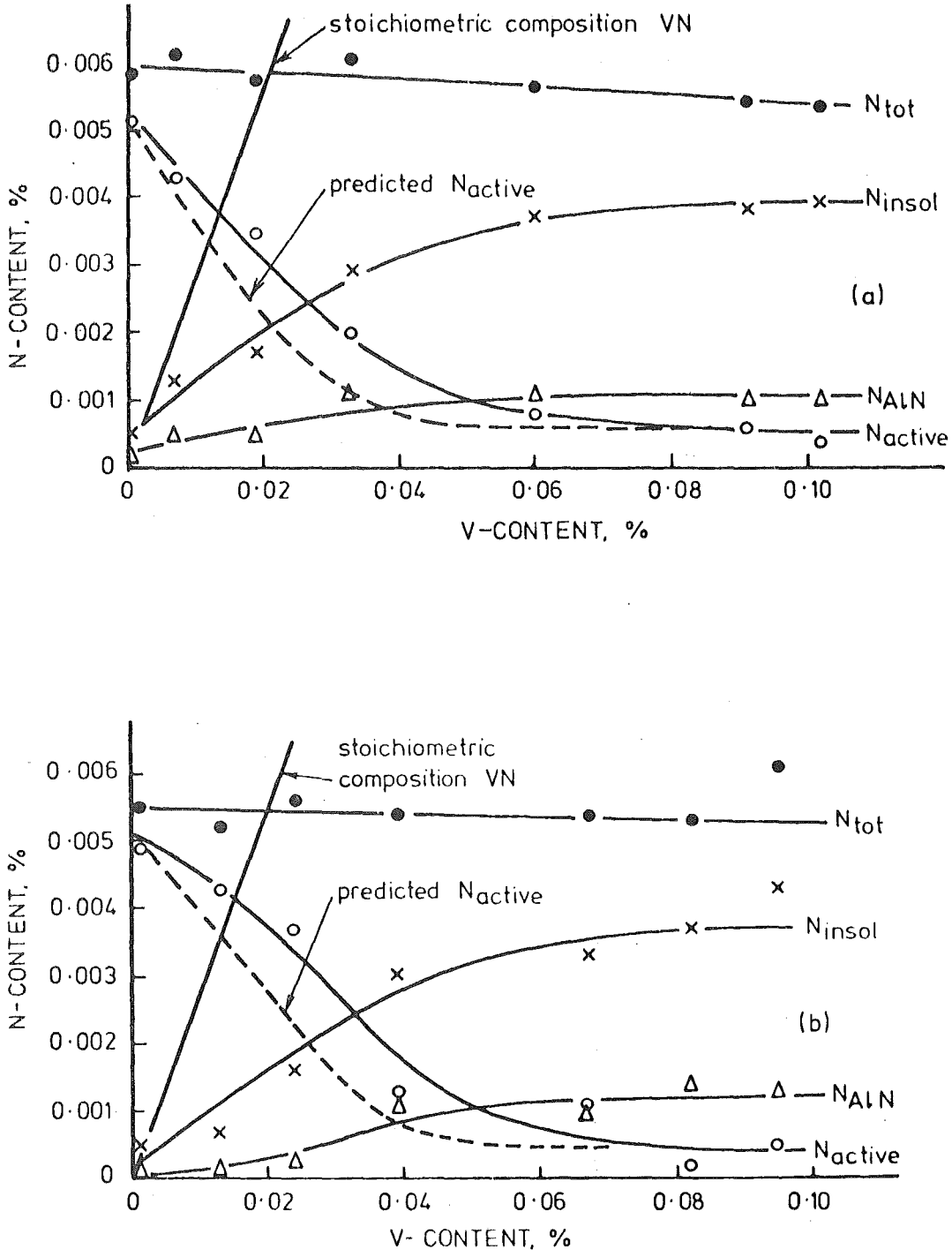

Figure 6.1: Effect of vanadium content on the stabilisation of nitrogen in as-rolled reinforcing steel with (a) 0.025% Al_{sol} and (b) 0.005% Al_{sol}.

N_{insol} (which is almost entirely nitrogen in the form of VN) increases with vanadium content up to 0.06%, only a portion of the vanadium is used up in the formation of VN.

Comparing these results with those observed by Smaill *et al*[4] shows the greater efficiency of titanium in stabilizing nitrogen when compared to vanadium. In the case of titanium, the N_{insol} curve follows the stoichiometric composition line more closely than in the case of vanadium.

6.6.2 Effect of Vanadium on as-rolled Tensile Properties

The variation in lower yield stress with vanadium content for the two groups of steel is shown in Figure 6.2. These results show an approximate linear increase in LYS with vanadium content for both groups of steel. Decreasing the $A\ell_{sol}$ content from approximately 0.025 to 0.005% appears to have no significant effect on the LYS, although the lower $A\ell_{sol}$ steels show a slightly higher value for a constant vanadium content. This difference in LYS, when corrected for vanadium content, may be resulting from a decrease in k_y, observed with an increase in aluminium content[45].

Figure 6.2 also shows that increasing the vanadium content from trace levels to about 0.1% raises the LYS from approximately 306 to 402 MN/m^2. A similar increase in LYS (i.e., from 288 to 380 MN/m^2) has been obtained by the addition of 0.1% titanium to a base steel made to Grade 275 standard[86]. The increase in LYS with vanadium content appears to be almost entirely due to precipitation strengthening by precipitates of V_4C_3 and/or VN in the ferrite matrix, as additions of vanadium had negligible effect on grain size,(see Table 6.4). As expected, associated with the increase in yield strength is a decrease in elongation (see Table 6.5). These results are in close agreement with a recent investigation by Sage[88] on hot-rolled reinforcing steels, which showed

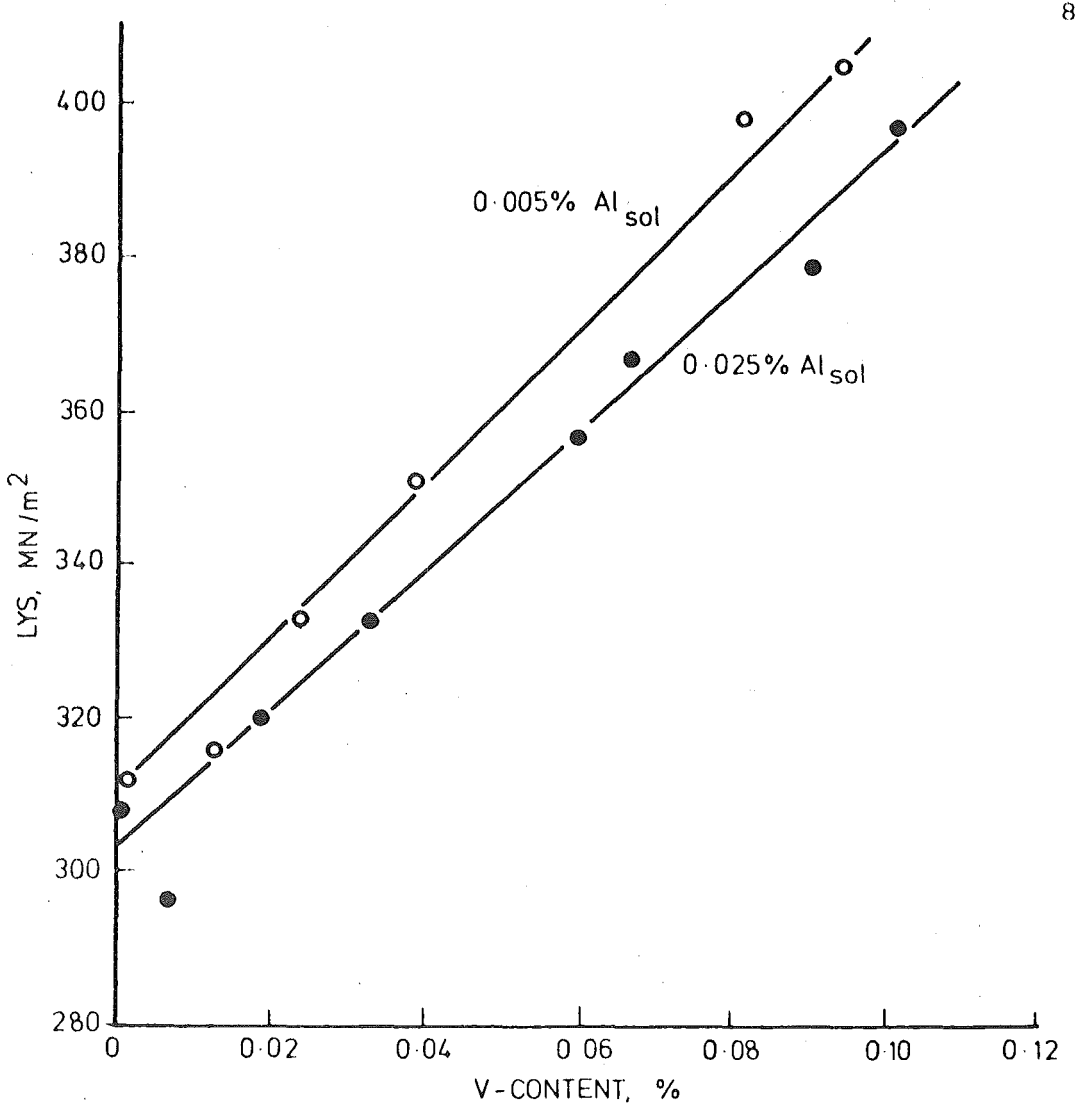

Figure 6.2: Variation in LYS with vanadium content of as-rolled reinforcing steels having two levels of $A\ell_{sol}$.

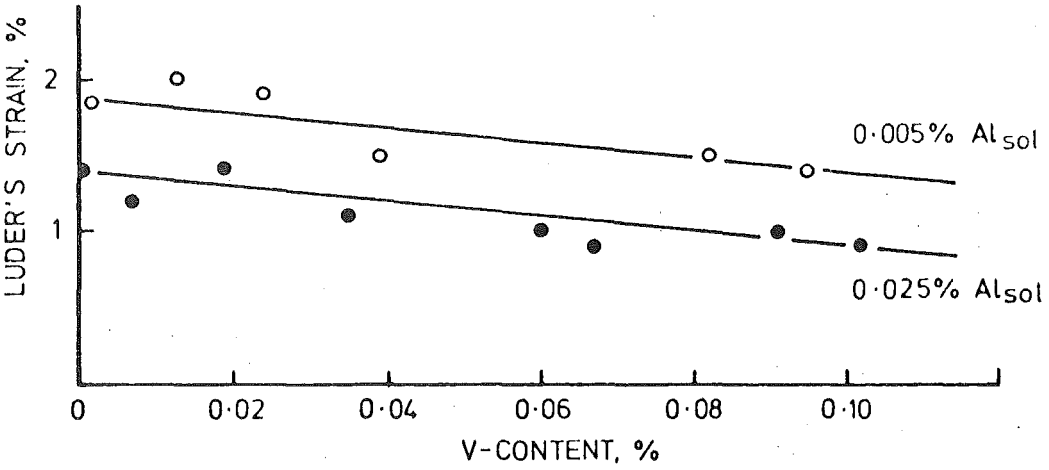

Figure 6.3: Variation in Luder's strain with vanadium content of as-rolled reinforcing steels having two levels of $A\ell_{sol}$.

(a) A similar increase in LYS with vanadium content.

(b) That addition of aluminium (up to 0.02%) had no significant effect on tensile properties.

(c) A reduction in elongation with increase in vanadium content.

(d) That vanadium additions had no effect on grain size.

Figure 6.3 shows the effect of vanadium content on the Luder's strain for the two groups of steel. It is clear from these results that the group of steel with lower $A\ell_{sol}$ content has a larger Luder's strain at a constant vanadium content. This difference in Luder's strain may be attributed to the corresponding difference in LYS on the assumption that the basic flow curve at a constant vanadium content is independent of the $A\ell_{sol}$ contents of these two groups. This assumption can be supported by Figure 6.4, which shows that the variation in tensile strength with vanadium content appears to be independent of the $A\ell_{sol}$ content. Hence, this observed difference in Luder's strain at constant vanadium content also suggests a decrease in k_y with an increase in aluminium content.

6.6.3 Effect of Vanadium on changes in Tensile Properties due to Strain Ageing

The main features of strain ageing on tensile properties represented in Figure 6.5(A), are of a steel having the normal Grade 275 base composition. It is clear from Figure 6.5(B) (Steel 6A), that a vanadium content of 0.06% is sufficient to almost eliminate strain ageing due to nitrogen.

The increase in LYS (ΔY), increase in tensile strength (ΔU), and the decrease in elongation ($\Delta E\ell$) after strain ageing in the two groups of steel (i.e., with $A\ell_{sol}$ contents of approximately 0.025 and 0.005%), with varying vanadium contents, are shown in Figures 6.6(a) and 6.6(b). These results show that increasing the vanadium content from trace levels to

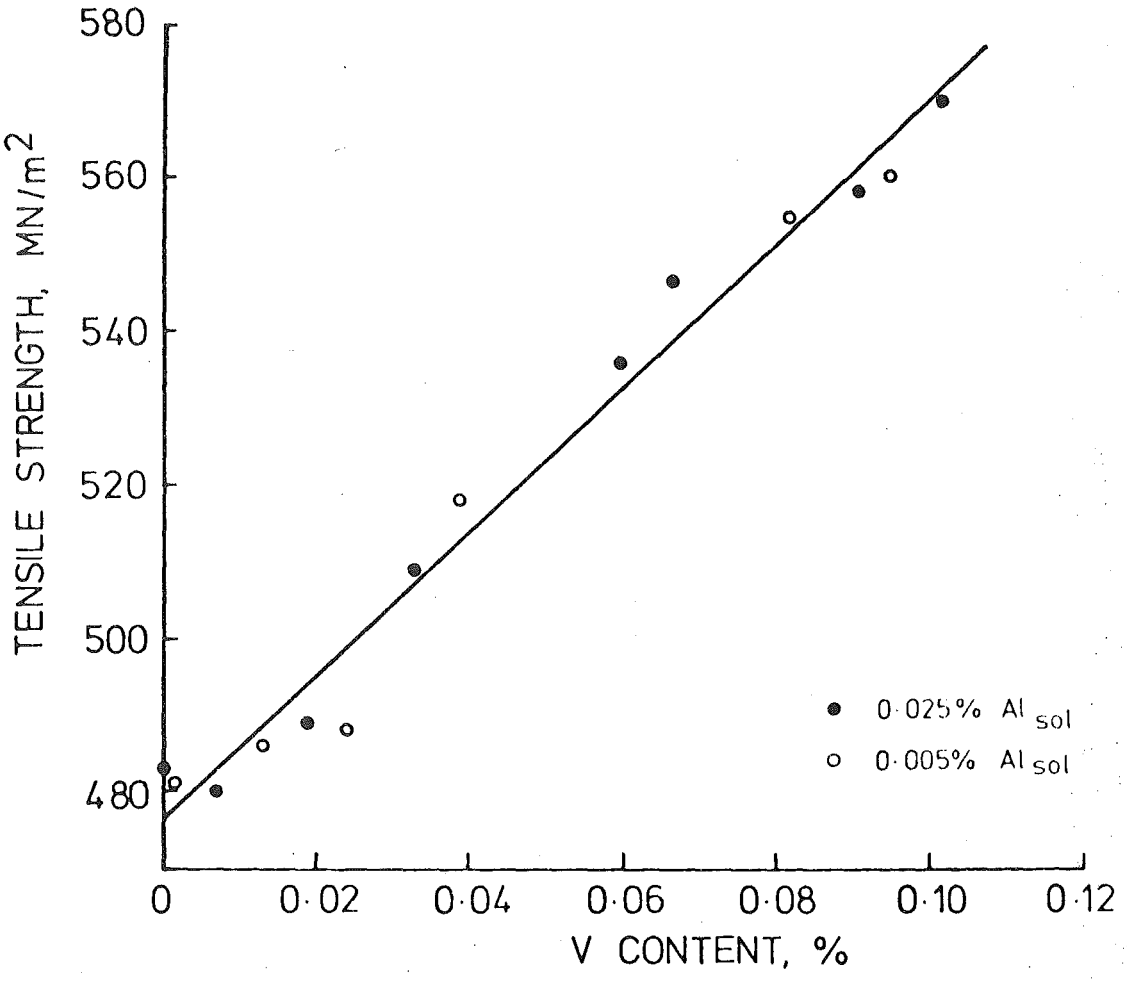

Figure 6.4: Variation in tensile strength with vanadium content of as-rolled reinforcing steels having two levels of Al_{sol}.

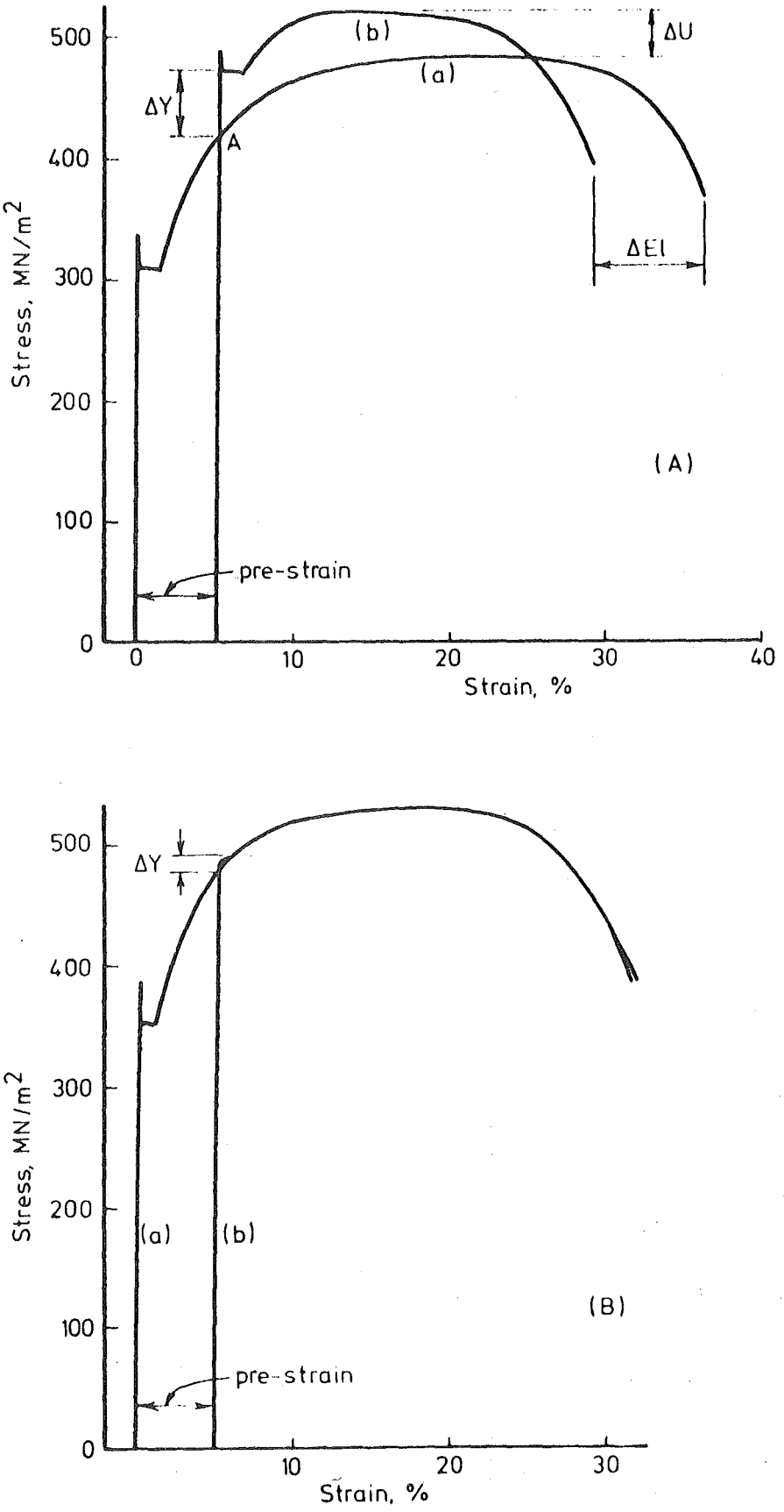

Figure 6.5: Effect of strain ageing (5% pre-strain, aged 3 hours at 100°C) on changes in the stress-strain curve. Curve (a) as-rolled condition, curve (b) strain aged condition.
(A) Normal Grade 275 steel.
(B) 0.06% vanadium steel.

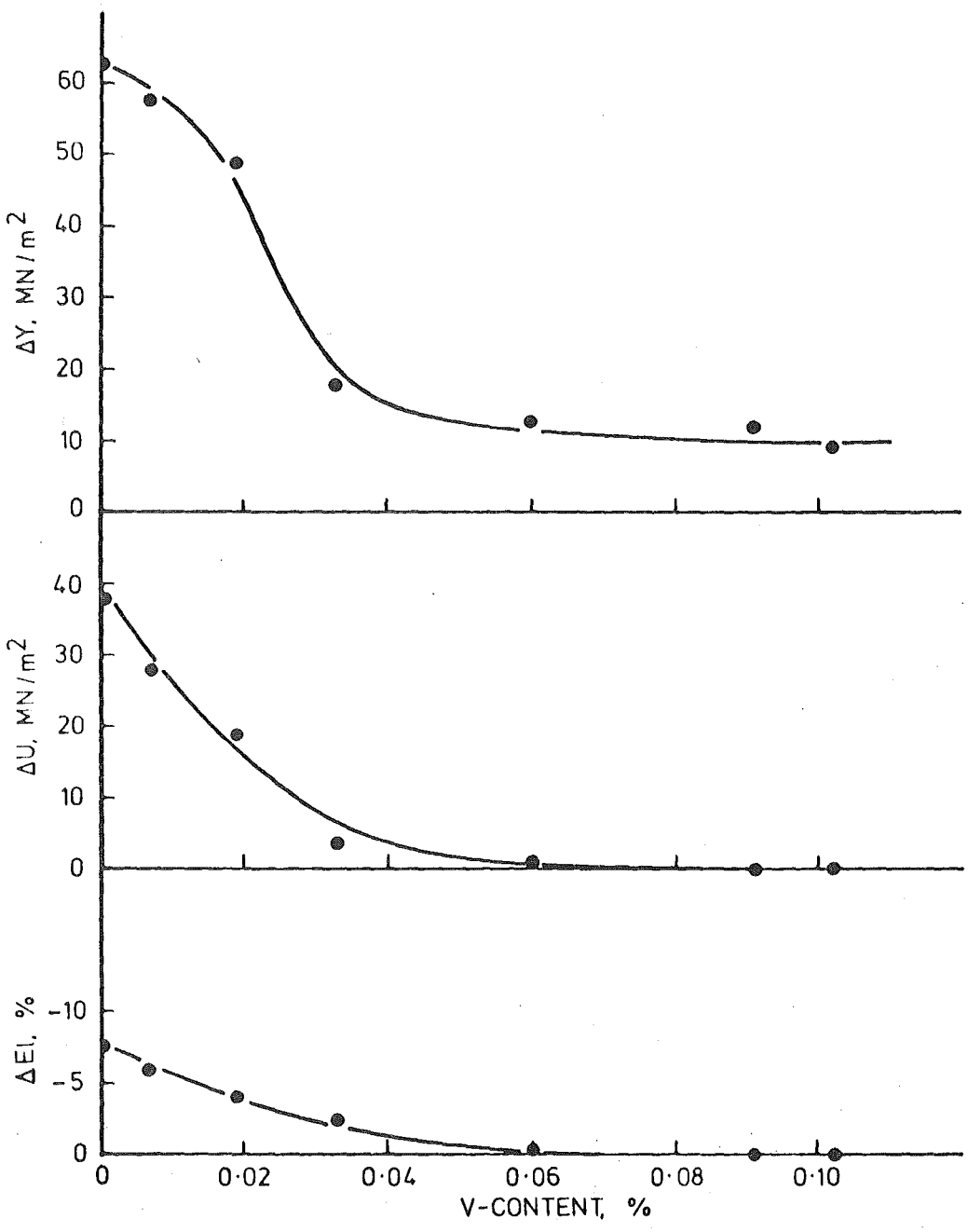

Figure 6.6(a): Effect of vanadium content on the changes in tensile properties due to strain ageing in Group A steels.

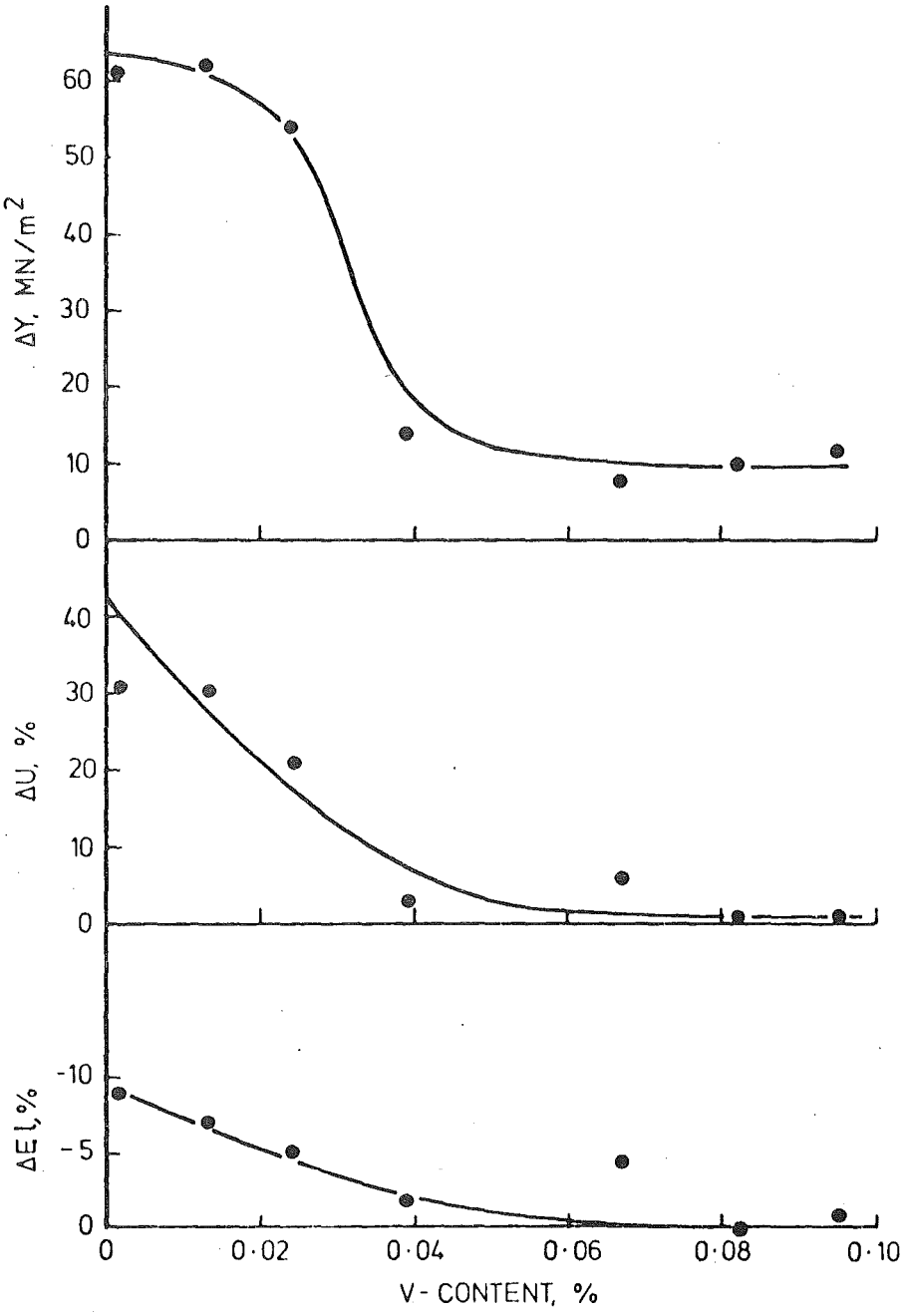

Figure 6.6(b): Effect of vanadium content on changes in tensile properties due to strain ageing in Group B steels.

around 0.06% is necessary for virtual elimination of strain ageing due to nitrogen in these steels. Further increases in vanadium content have no added advantage. The variation of ΔY with vanadium content shows that it reaches a stable value of approximately 10 MN/m^2, and this indication of partial first-stage ageing may be a result of partial dislocation locking by residual nitrogen and any interstitial carbon at 100°C. Recent work by Rashid[89] has shown a similar increase in yield stress after strain ageing at room temperature in a HSLA steel having 0.11% vanadium.

When comparing these results with the nitrogen determinations of these steels (Figures 6.1(a) and 6.1(b)) certain interesting features result. The changes in tensile properties (i.e., ΔY, ΔU, and $\Delta E\ell$) appear to closely follow the 'active' nitrogen content with increases in vanadium content. However, although 0.04% vanadium appears to be sufficient to reduce ΔY to approximately 15 MN/m^2, it only reduces the 'active' nitrogen content to approximately 0.0013%. This level of 'active' nitrogen is sufficient to provide complete first stage ageing[4, 15, 16] (i.e. $\Delta Y \sim 40$ MN/m^2). Hence the 'active' nitrogen content obtained by chemical determinations appears to give higher values than those which may be predicted by the strain ageing characteristics, especially in the 0.02 - 0.04% vanadium range. This may be due to the decomposition of fine precipitates of VN during the solution of the sample in dilute acid, i.e., N_{sol} will contain some nitrogen from VN, as fine precipitates of stable nitrides may not be completely insoluble in dilute acid[87]. The proportion of fine VN precipitates would tend to reduce with increases in vanadium content as a result of the VN precipitation being completed at higher temperatures. Hence, with increases in vanadium content, the proportion of nitrogen from VN in N_{sol} will be reduced. As a result of the preceeding discussion, a speculative prediction of the 'active' nitrogen curves from the curves of ΔY are shown in Figures 6.1 (a) and 6.1 (b). Inaccuracies of the analytical technique used for the determination of nitrogen in the form of $A\ell N$ will

also affect the determination of the 'active' nitrogen content. For example, it has been shown that this technique sometimes entails some losses involved in the course of the dissolution of the sample and filtering of the solution with precipitates[90].

6.6.4 Effect of Vanadium on as-rolled Transition Temperature

Figure 6.7 shows a progressive increase in the 27 Joule fracture transition temperature (T_{27}) with increases in V/N ratio. It also appears that the different $A\ell_{sol}$ content in the two groups of steel have no effect when corrected for the V/N ratio. These results confirm that increases in vanadium causes precipitation hardening in the absence of grain refinement in hot-rolled reinforcing steels. This figure also shows that precipitation hardening appears to be enhanced as the vanadium content is increased.

When comparing Figure 6.7 with Figures 6.1(a) and 6.1(b) it can be seen that the increase in T_{27} in the range of vanadium where the active nitrogen content decreases (i.e. by forming VN) is small when compared with its increase in the higher vanadium range where the active nitrogen content remains almost constant (i.e., below 0.0005%). This shows that vanadium carbide is the major cause for precipitation hardening of ferrite because at vanadium contents in excess of approximately 0.04%, no more vanadium is used for precipitation of VN. It may also be argued that the initial low rate of increase in T_{27} is partly due to the reduction of active nitrogen in that vanadium range.

These results show a contrasting difference to those of titanium additions[4], which gave a pronounced minimum transition temperature at the TiN stoichiometric composition.

6.6.5 Effect of Vanadium on Strain Age Embrittlement

Figures 6.8(a) and 6.8(b) show the effect of strain ageing on the

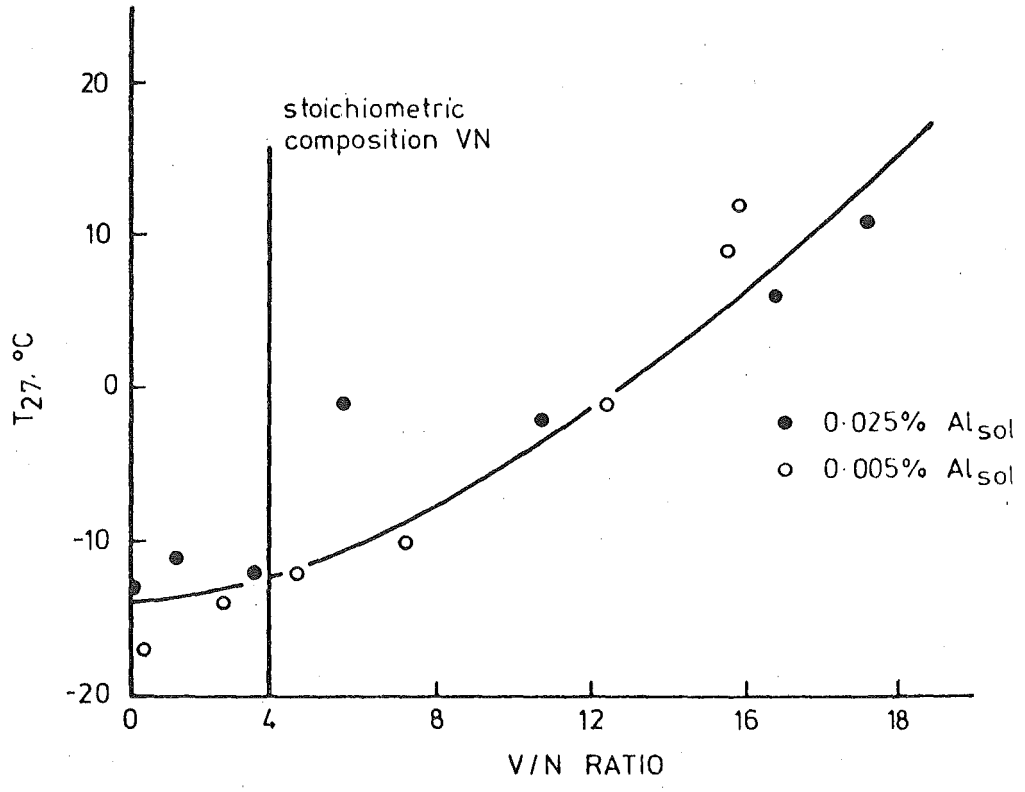

Figure 6.7: Effect of the V/N ratio on the fracture transition temperature (T_{27}) of as-rolled vanadium steels.

27 Joule fracture transition temperature in the two groups of steel as a function of vanadium content. These results show that, although the as-rolled fracture transition temperature does increase progressively with vanadium content, the transition temperature after strain ageing has a minimum approximately at 0.04% vanadium.

The effect of strain ageing is clearly shown by the two steels containing trace quantities of vanadium. The increase in the 27 Joule fracture transition temperature after strain ageing (ΔT_{27}) was 32° and 29°C respectively for steels with 0.025 and 0.005% $A\ell_{sol}$. This effect of strain ageing (i.e. strain age embrittlement) is considerably reduced as the vanadium content is increased.

Figures 6.9(a) and 6.9(b) show more clearly the effect of strain age embrittlement (ΔT_{27}) in the two groups of steel at different vanadium content. In these figures, the curves have been plotted from the approximate difference between the curves for the as-rolled and strain aged conditions from Figures 6.8(a) and 6.8(b) respectively. Figures 6.9(a) and 6.9(b) show that increasing the vanadium content from a trace level to about 0.06% results in the reduction of ΔT_{27} from approximately 32°C to 14°C, which is obviously due to the reduction of 'active' nitrogen content from approximately 0.005% to below 0.0005%. Further increases in vanadium content appear to have little effect on strain age embrittlement. This latter result is in contrast to the increases in ΔT_{27} which occurred at high titanium content in similar as-rolled reinforcing steels[4]. These results show that, although high vanadium additions increases the as-rolled transition temperature due to precipitation hardening mainly by coherent precipitates of V_4C_3, these precipitates appear to have no appreciable effect on strain hardening of these steels when compared with the TiC precipitates in similar high titanium steels, which appeared to have increased strain hardening.

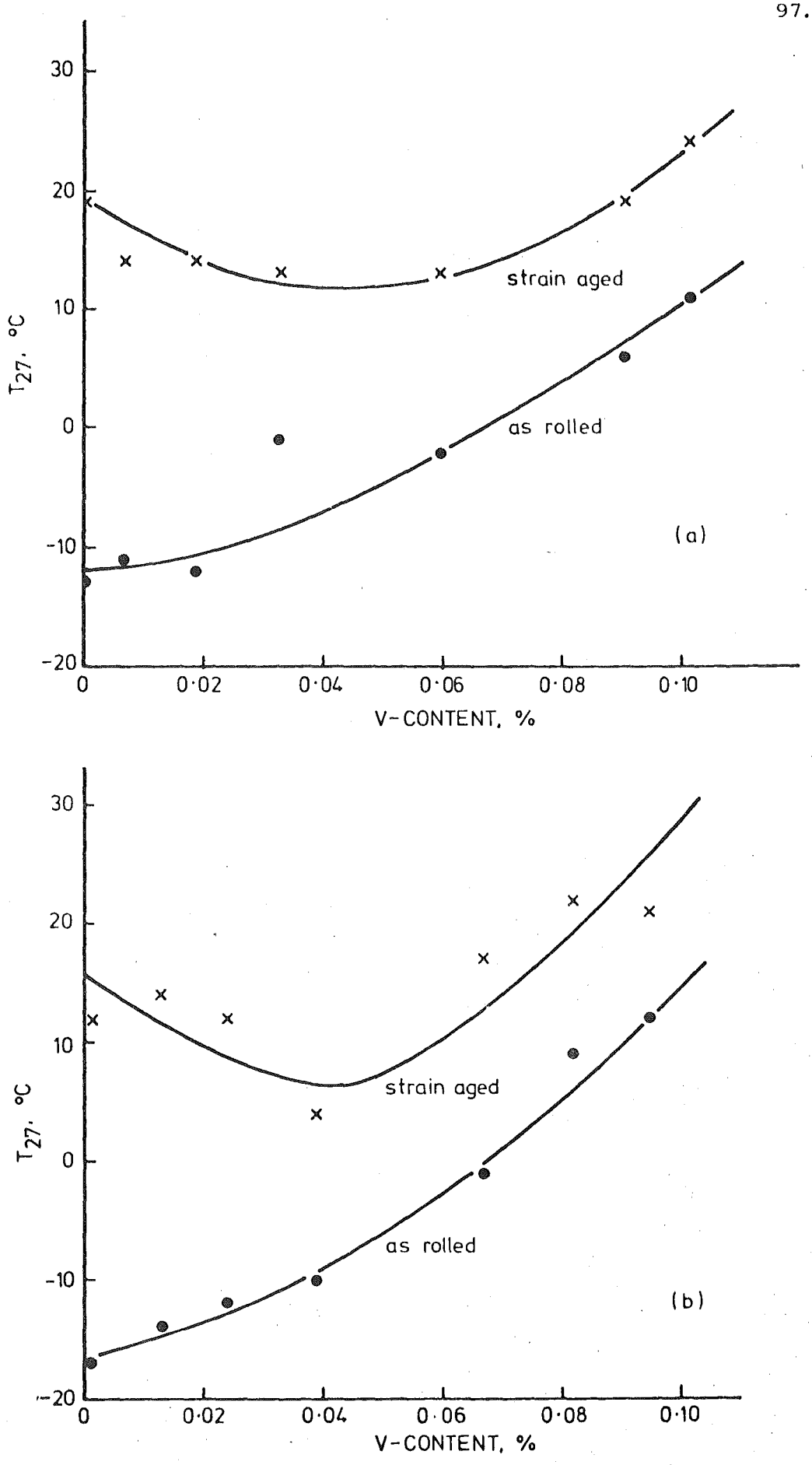

Figure 6.8: Effect of strain ageing on the fracture transition temperature as a function of vanadium content in reinforcing steel with (a) 0.025% Al_{sol} and (b) 0.005% Al_{sol}.

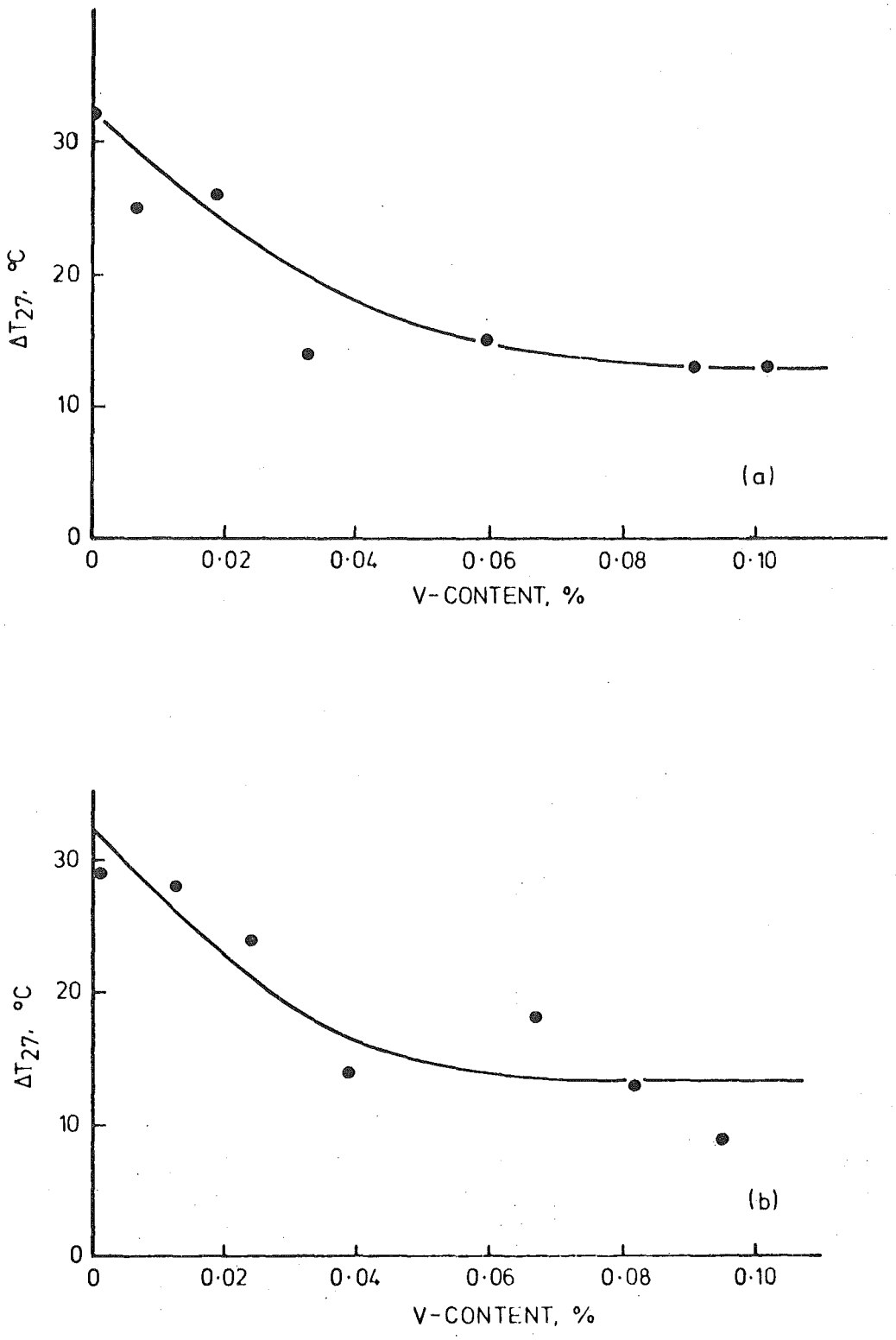

Figure 6.9: Effect of vanadium content on strain age embrittlement of as-rolled reinforcing steel with (a) 0.025% Al_{sol}, (b) 0.005% Al_{sol}.

From the viewpoint of strain age embrittlement, the optimum vanadium content appears to be in the range 0.04 - 0.05%, i.e., the vanadium content which gives the minimum T_{27} in the strain aged condition, see Figures 6.8(a) and 6.8(b). However, due to precipitation strengthening, this amount of vanadium slightly increases the as-rolled fracture transition temperature. These observations confirm the results from chemical analysis and tensile testing that vanadium well in excess of the VN stoichiometric composition is required for the elimination of strain ageing by nitrogen.

6.7 Summary

As a result of the affinity of vanadium for the formation of VN, sufficient vanadium addition to C-Mn reinforcing steels has been successful in almost eliminating nitrogen strain ageing of these steels in the as-rolled state. This investigation has shown that the optimum vanadium content appears to be in the region of 0.04 - 0.05%, which is well in excess of the stoichiometric requirement for those steels which contain 0.005 - 0.006% nitrogen.

The optimum vanadium addition also increases the yield strength of the base steels from approximately 306 to 350 MN/m^2, thought to be due to precipitation strengthening of the ferrite which also results in an increase in the transition temperature by approximately $7^{o}C$. Such an increase in transition temperature, although generally an undesirable change for a reinforcing steel, will not cause serious embrittlement in the as-rolled state, i.e., the ductility requirements for a reinforcing steel to be used in earthquake resistant concrete structures are not seriously affected by such an increase in the as-rolled transition temperature. As the critical conditions arise only in plastically strained regions such as at bends, the optimum vanadium bearing steel will have an advantage over the normal reinforcing steel. Also, due to its stabilized characteristics, the possibility of re-allocation of the 'plastic hinges' or brittle shear failure at 'plastic hinges' during subsequent earthquakes, will be minimised.

It is clear when comparing these results with those from the effect of titanium additions, that although vanadium does eliminate strain ageing due to nitrogen as titanium, the latter element has considerable advantages due to the remarkable improvements in the as-rolled fracture transition temperature and the Luder's strain. However, as a result of the optimum vanadium content not being affected by reducing the aluminium content from 0.04 to 0.01% and the recovery of vanadium not being reduced by reducing the aluminium content, the efficiency of the vanadium addition does not depend on the aluminium content of these reinforcing steels. This effect of vanadium has an advantage over titanium in commercial production as it could be added to the ladle without reducing its recovery or efficiency.

When comparing these results obtained from hot-rolled steels with literature on controlled rolling of vanadium-bearing steels[60, 75-79], some interesting speculations may be made.

(a) It appears that the significant improvements in fracture transition temperature obtained by controlled rolling, due to grain refinement, is caused by strain induced precipitation of V_4C_3 in austenite[78, 79] instead of it mostly precipitating in ferrite as appears to be the case in hot-rolled steel and hence resulting in the deterioration of fracture properties.

(b) VN is precipitated in austenite in preference to V_4C_3 and hence less vanadium being available for V_4C_3 precipitation in ferrite at low vanadium contents. This may be a result for the initial lower rate of increase in the as-rolled transition temperature in the range where the V/N ratio is less than about 8, when compared with the rate of increase at higher vanadium contents, see Figure 6.7. The work of Erasmus[71] also appears to be in agreement with the above suggestion.

Although the base steel was made to Grade 275 standard, this investigation has shown that the yield stress of the as-rolled steel was 308 MN/m^2 and the

27 Joule fracture transition temperature was -13^{o}C. The higher yield strength and lower transition temperature of this steel, when compared with the results from a similar base steel used for titanium additions[86] (i.e., LYS 288 MN/m^{2} and ITT -3^{o}C), is mainly a result of the smaller grain size. The smaller grain size may be expected from the faster cooling rate due to the smaller diameter of the bars, i.e., 22 mm compared to 25.4 mm bar.

CHAPTER 7

STRAIN AGEING CHARACTERISTICS OF NORMAL AND TITANIUM-BEARING AS-ROLLED REINFORCING STEELS - EXPERIMENTAL PROCEDURE, RESULTS AND DISCUSSION

7.1 Introduction

It is clear from the preceeding two chapters that titanium additions have greater advantages over vanadium additions to reinforcing steels, especially because it improves the as-rolled properties, i.e., it reduces the fracture transition temperature and increases the Luder's strain when added in controlled amounts.

Therefore, in the systematic study of the effects of plastic strain, ageing temperature and ageing time on the mechanical properties of normal reinforcing steel, is also included a similar steel containing controlled addition of titanium. This chapter reports the results of such a study.

7.2 Experimental Procedure

The steels were made from a cast produced by the BEA process, to conform to the Grade 275 standard of NZS 3402 P, 1973. The Normal (N) and Titanium bearing (Ti(a)) reinforcing steels were obtained from two adjacent ingots, a pre-determined amount of titanium (in the form of ground ferro-titanium) was added to one ingot during teeming. The molten steel was tapped from the furnace at a temperature of approximately 1600^{o}C into a ladle from which it was teemed to the ingot moulds. The cooled ingots were soaked at ~1100^{o}C for 3 hours and then cogged into 100 mm square billets, which were fed directly into the re-heat furnace at 1050^{o}C. This was followed by final rolling to 28 mm diameter plain bar and then cooled on a cooling bed. The titanium-bearing steel (Ti(b)) was made by the identical procedure from a different cast produced to the Grade 275 standard.

The resultant composition of these steels given in Table 7.1 was obtained

spectrographically. Also given is the titanium content determined by a chemical method described in Appendix A, using atomic absorbtion spectrophotometry. The nitrogen content of the steels was accurately separated as 'acid soluble' nitrogen (N_{sol}), and 'acid insoluble' nitrogen (N_{insol}) and nitrogen in the form of AlN (N_{AlN}), using the method described in Appendix A. The resultant nitrogen determinations are given in Table 7.1.

The 'effective ferrite grain size' was estimated in accordance with the ASTM standards (Designation E112-74), using the modified lineal intercept method. These estimations were made on photomicrographs taken approximately at the mid-radius of a longitudinal section from the as-rolled bar. The results given in Table 7.2 show a clear indication of grain refinement in titanium-bearing steels, (especially in the Ti(b) steel), although the extent of the refinement is small.

7.3 As-Rolled Mechanical Properties

Tensile tests were performed on specimens with a diameter of 12 mm and gauge length 50 mm, machined from 28 mm bar. The detailed specimen dimensions and the method of preparation is given in Appendix B. Testing was carried out at a strain rate of 0.04/min. on an Instron testing machine and the load-extension curves were plotted on the recorder using a 50 mm gauge length extensionmeter on the specimens.

Standard Charpy V-notch specimens were machined from the 28 mm bar to BS 131, Part II of 1972. Impact tests were performed on an Avery Impact Testing Machine at a striking energy of 298 Joules (220 ft lbs) and a striker velocity of 5 m/s (16 ft/s), in accordance with BS 131. A full Charpy impact transition curve was determined for each steel and the 27 Joule fracture transition temperature (T_{27}) was determined.

In order to eliminate any effects of artificial ageing itself, the as-rolled bar was given a pre-strain ageing treatment of 3 hours at 100°C before machining test specimens. The results from these tests are given in Table 7.2.

mposition and the Nitrogen determinations of the Titanium and Normal Steels (Element, % wt)

Mn	Si	S	P	Ti	Ti^*	N_{sol}	N_{insol}	N_{tot}	$N_{A\ell N}$	N_{active}
0.46	0.09	0.03	0.01	Nil	<0.003	0.0051	0.0009	0.0060	0.0002	0.0049
0.45	0.10	0.03	0.01	0.035	0.032	0.0004	0.0061	0.0065	0.0001	0.0003
0.44	0.16	0.02	0.01	0.029	0.026	0.0010	0.0056	0.0066	0.0004	0.0006

Ti^* = Titanium content determined by AA spectrophotometry

TABLE 7.2: Mechanical Properties and Ferrite Grain Size

LYS_2 (MN/m^2)	Luder's Strain (%)	TS_2 (MN/m^2)	$E\ell$ (%)	T_{27} (^oC)	Grain Size $d^{-\frac{1}{2}}$ ($mm^{-\frac{1}{2}}$)
276	1.2	448	40.4	-3	7.33
310	1.4	459	39.0	-6	7.83
292	1.5	459	39.0	-12	8.42

7.4 Tensile Test Results

7.4.1 Effect of Pre-strain

To investigate the effect of the amount of pre-strain on strain ageing, a set of tensile specimens from each steel was pre-strained by pre-determined amounts ranging from 2.5 to 15% in tension. The specimens were subsequently aged at 100°C for 3 hours before finally testing them to fracture. The resultant variations in tensile properties (i.e. ΔY, ΔU and $\Delta E\ell$) after strain ageing were determined and are given in Table 7.3.

7.4.2 Effect of Ageing Temperature and Time

To investigate the effect of ageing temperature on strain ageing, a group of tensile specimens consisting of sets of specimens from Normal (N) and Titanium-bearing (Ti(a)) steels were pre-strained by 5%. Specimens from each set were subsequently aged for one hour at a range of temperatures from 60° to 350°C before testing them to fracture. The resultant variation in tensile properties was determined from the results of the aged specimens (see Table 7.4). A second group of tensile specimens was used to examine the combined effect of ageing temperature and time after pre-straining them by 5%. The specimens were aged at pre-determined temperatures for the corresponding times selected from Table 7.5. The variation in tensile properties after these strain ageing treatments is given in Table 7.6.

7.5 Charpy V-Notch Impact Test Results

7.5.1 Effect of Pre-Strain

In order to investigate the effect of pre-strain on the increase in fracture transition temperature, V-notch Charpy specimens were machined from 28 mm bar, which had been pre-strained by pre-determined amounts ranging from 2.5 to 15% in tension. These specimens were aged at 100°C for 3 hours before testing to obtain a full Charpy

TABLE 7.3: Effect of Pre-Strain on Changes in Tensile Properties due to Strain Ageing in Normal and Titanium Steels.

Steel	Pre-Strain (%)	ΔY (MN/m^2)	ΔU (MN/m^2)	ΔEl (%)
Normal	2.5	58	27	-6.0
	5.0	59	48	-9.0
	7.5	61	58	-9.6
	10.0	58	51	-10.0
	12.5	58	56	-8.4
	15.0	57	61	-9.4
Ti(a)	2.5	22	-1	1.0
	5.0	21	1	-0.4
	7.5	19	3	0.8
	10.0	14	3	0
	12.5	10	5	-1.0
	15.0	9	11	-1.0
Ti(b)	5.0	15	-9	1.0
	10.0	7	-5	0.5
	15.0	6	-5	0

TABLE 7.4: Effect of Ageing Temperature on Changes in Tensile Properties due to Strain Ageing in Normal and Titanium Steel.

Steel	Ageing Temperature (^{o}C)	ΔY (MN/m^2)	ΔU (MN/m^2)	ΔEl (%)
Normal	60	45	14	-3.4
	100	55	39	-7.9
	150	60	41	-8.4
	200	65	49	-8.9
	250	58	54	-9.4
	300	52	71	-9.4
	300	49	43	-8.4
	350	38	45	-8.4
Ti(a)	60	8	-2	-1.0
	100	26	-9	-6.0
	100	20	-9	-1.0
	150	22	1	-1.0
	200	42	4	-3.0
	250	37	18	-4.0
	250	38	14	-5.0
	300	40	12	-5.0
	350	27	18	-5.0

TABLE 7.5: Equivalent ageing times for a one-hour ageing time at higher temperatures as determined using Hundy's Equation 3.7 with an average H value of 4200.

One Hour Ageing Temperature (^{o}C)	Equivalent Ageing Times (Hours)						
	$60^{o}C$	$100^{o}C$	$150^{o}C$	$200^{o}C$	$250^{o}C$	$300^{o}C$	$350^{o}C$
60	1						
100	20	1					
150	380	18.9	1				
200	38.1×10^{2}	189.4	10	1			
250	24.3×10^{3}	12.1×10^{2}	64	6.4	1		
300	11.1×10^{4}	55.4×10^{2}	293	29.3	4.58	1	
350	39.7×10^{4}	19.8×10^{3}	10.5×10^{2}	104	16.3	3.56	1

TABLE 7.6: Combined Effect of Ageing Temperature and Time on Changes in Tensile Properties due to Strain Ageing in Normal and Titanium Steels.

Steel	Ageing Temp. (^{o}C)	Time (Hours)	ΔY (MN/m^2)	ΔU (MN/m^2)	ΔEl (%)
Normal	60	20	55	39	-8.4
	60	380	56	43	-8.4
	100	18.9	59	61	-10.4
	100	189.4	62	39	-7.9
	150	10	68	48	-8.4
	150	64	61	46	-9.9
	200	6.4	58	46	-8.9
Ti(a)	60	20	16	1	0
	60	380	16	-1	-2.0
	100	18.9	19	3	-4.0
	100	189.4	23	3	-1.0
	150	10	34	11	-3.0
	150	64	37	11	-3.0
	200	6.4	34	11	-5.0
Ti(b)	60	380	12	-3	0
	100	18.9	14	-4	-1.0
	100	189.4	20	-10	-1.0
	150	1	18	-12	-1.0
	150	10	32	-4	1.0
	200	1	28	2	-3.0
	200	6.4	37	11	-3.0

TABLE 7.7: Effect of Pre-Strain on ΔT_{27} due to Strain Ageing in Normal and Titanium steels.

Pre-Strain (%)	Normal		Ti(a) Steel		Ti(b) Steel	
	T_{27} (^{o}C)	ΔT_{27}	T_{27}(^{o}C)	ΔT_{27}	T_{27}(^{o}C)	ΔT_{27}
2.5	20	23	8	14		
5.0	24	27	13	19	0	12
7.5	38	41	17	23		
10.0	34	37	20	26	16	28
12.5	40	43.	19	25		
15.0	47	50	28	34	23	35

NOTE: T_{27} represents the fracture transition temperature of the strain aged steels.

TABLE 7.8: Effect of Ageing Temperature on ΔT_{27} due to Strain Ageing in Normal and Titanium Steel.

Ageing Temperature (^{o}C)	Normal		Ti(a) Steel	
	T_{27}(^{o}C)	ΔT_{27}	T_{27}(^{o}C)	ΔT_{27}
60	21	24	10	16
100	20	23	9	15
150	24	27	12	18
200	28	31	17	23
250	29	32	23	29
300	32	35	20	26
300			35	41
350	34	37	31	37

NOTE: T_{27} represents the fracture transition temperature of the strain aged steels.

TABLE 7.9: Combined Effects of Ageing Temperature and Time on ΔT_{27} due to Strain Ageing in Normal and Titanium steels.

Ageing Temp. (^{o}C)	Time (Hours)	Normal		Ti(a) Steel		Ti(b) Steel	
		T_{27} (^{o}C)	ΔT_{27}	T_{27} (^{o}C)	ΔT_{27}	T_{27} (^{o}C)	ΔT_{27}
60	20	24	27	10	16		
60	380	22	25	13	19	10	22
100	18.9	26	29	12	18	4	16
100	189.4	25	28	12	18	7	19
150	1					8	20
150	10	28	31	18	24	10	22
150	64	35	38	29	35		
200	1					12	24
200	6.4	32	35	30	36	18	30

Note: T_{27} represents the fracture transition temperature of the strain aged steels.

impact transition curve for each steel and pre-strain. The resultant increase in the 27 Joule fracture transition temperature (ΔT_{27}) was determined (see Table 7.7).

7.5.2 Effect of Ageing Temperature and Time

To examine the effect of ageing temperature and the combined effect of ageing temperature and time on the increase in fracture transition temperature, the identical strain ageing treatments described in Section 7.4.2 were used. The pre-strained specimens were machined from 28 mm bar which had been pre-strained by 5%. The resultant increase in the 27 Joule fracture transition temperature was determined from a full Charpy impact transition curve for each steel and strain ageing treatment (see Tables 7.8 and 7.9).

7.6 Discussion of Results

7.6.1 The Effect of Pre-Strain

The effect of pre-strain on changes in tensile properties (ΔY, ΔU and $\Delta E\ell$) of specimens aged at 100°C for 3 hours is shown in Figure 7.1 for normal and titanium-bearing steels. This ageing treatment is equivalent to nine months at 15°C[30]. It can be seen that the strain ageing characteristics of the titanium-bearing steels are significantly different to those of the normal Grade 275 steel, confirming that titanium additions in excess of the Ti/N stoichiometric ratio reduces strain ageing to negligible levels[4].

The changes in tensile properties of the normal steel show that the ageing treatment is sufficient to give complete second stage strain ageing. Figure 7.1 shows that ΔY for the normal steel is independent of the pre-strain, while ΔU and $\Delta E\ell$ are more affected. These results are similar to those of Hundy[29] (see Figure 3.9) and in agreement with those of Wilson and Russell[15]. By contrast, the titanium-bearing steels give only partial first stage ageing (see Figures 7.2(A) and 7.2(B)).

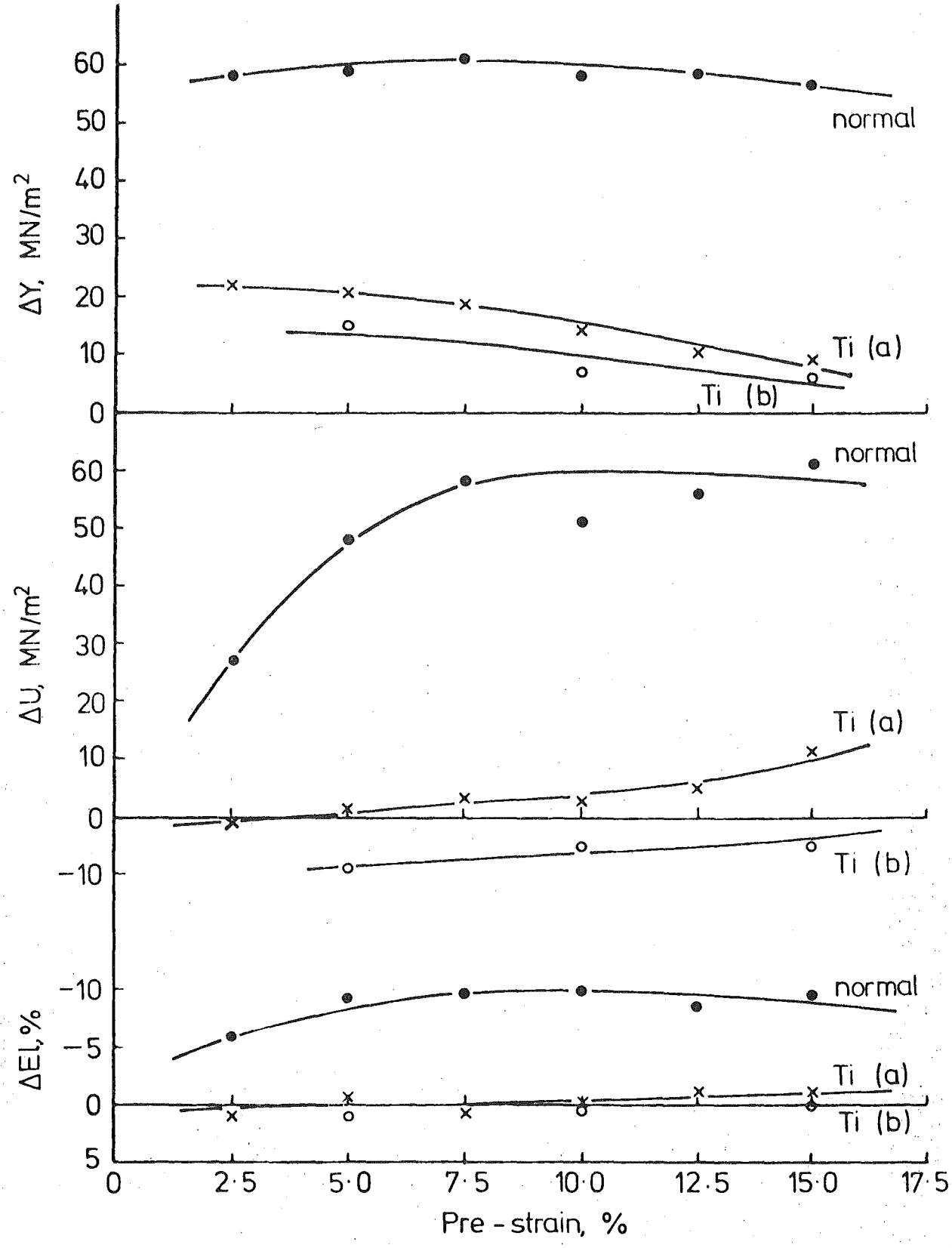

Figure 7.1: Effect of pre-strain on changes in tensile properties due to strain ageing in normal and titanium steels.

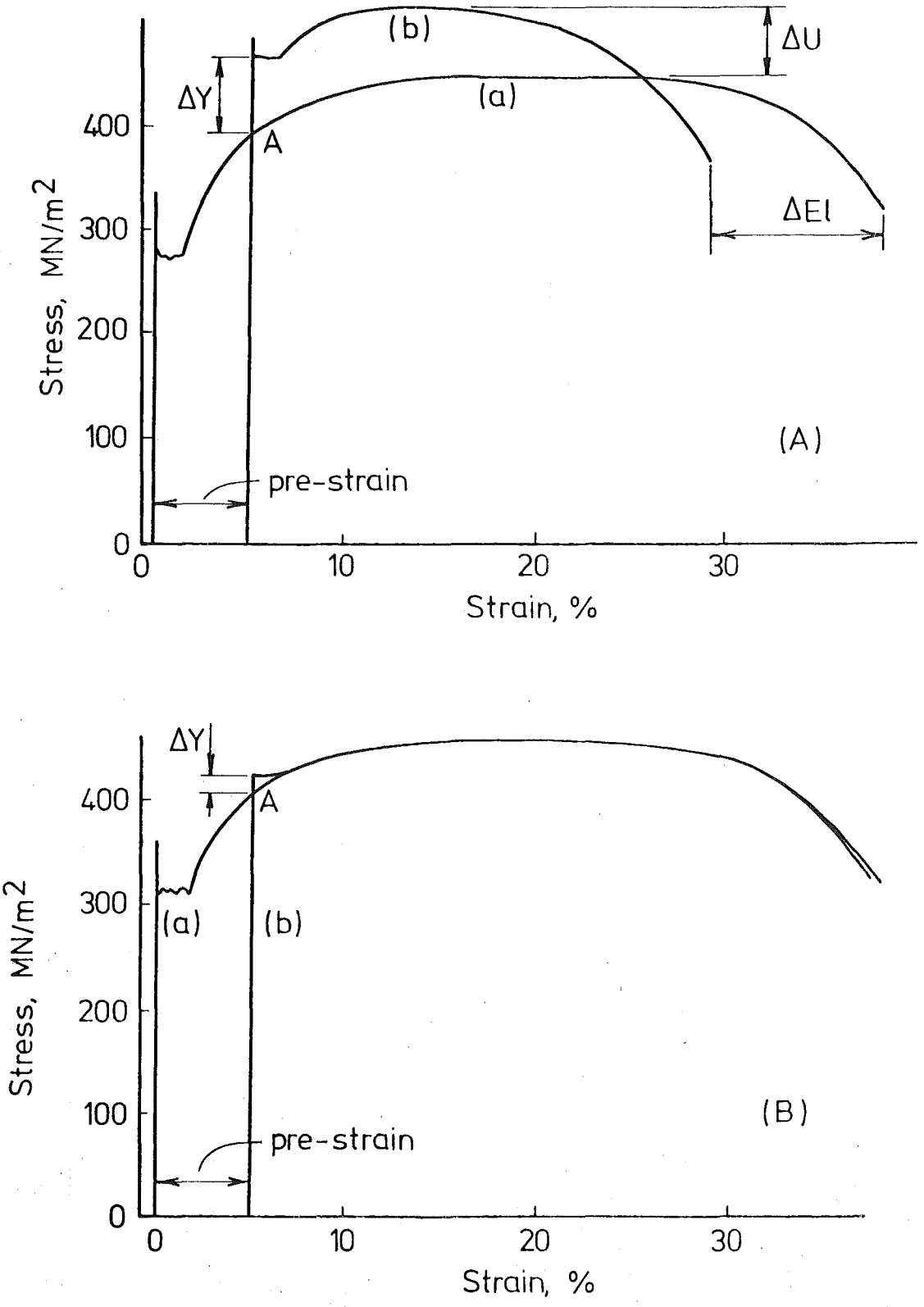

Figure 7.2: Effect of strain ageing (5% pre-strain, aged 3 hours at 100°C) on changes in the stress-strain curve. Curve (a) as-rolled condition, curve (b) strain aged condition.

(A) Normal Grade 275 steel.
(B) Ti(a) steel.

The partial first-stage ageing of the titanium-bearing steels appears to be mainly a result of partial 'atmosphere formation' on mobile dislocations, introduced during plastic straining, by 'active' nitrogen and any interstitial carbon atoms in solid solution in ferrite at 100°C. This is in agreement with the work of Wilson and Russell[15], showing that only partial first-stage ageing takes place in steels with low interstitial contents (see Figure 3.5).

Figure 7.1 shows a slight decrease in ΔY with increases in pre-strain for the titanium-bearing steels. This would appear to be a function of the low 'active' nitrogen content of these steels coupled with the increased availability of dislocation sites with increasing pre-strain, i.e., more precipitation sites (unlocked dislocations) competing for the relatively small amount of 'active' nitrogen (and any carbon) available. Hence the efficiency of mobile dislocation locking will be reduced with increases in pre-strain. This suggestion appears to be confirmed by the curves for ΔU and $\Delta E\ell$ shown in Figure 7.1, where the titanium-bearing steels show some degree of strain age hardening with increasing pre-strain (i.e., an increase in tensile strength (ΔU) and a decrease in elongation ($\Delta E\ell$). Although the changes in ΔU are small when taking into consideration the slight variation in as-rolled properties between individual specimens, the trend of increase in ΔU with pre-strain for both titanium-bearing steels is clear. This strain age hardening is due to increased precipitate density formed after ageing, i.e., the precipitate density is increased with an increase in the precipitation sites, resulting from increased pre-strain. However, where ΔU for the normal grade steel with ample available 'active' nitrogen reaches saturation after approximately 7.5% pre-strain, the titanium bearing steels show only a gradual and relatively minor degree of strain age hardening corresponding to only small increases in precipitate density with increased pre-strain. This apparent strain age hardening in the titanium-bearing steels may be partly

resulting from strain induced precipitation of TiC[64] during ageing, as the titanium content in these steels is in excess of the Ti/N stoichiometric ratio, especially in the Ti(a) steel.

The effect of pre-strain on strain age embrittlement, i.e., the increase in the 27 Joule fracture transition temperature (ΔT_{27}) is shown in Figure 7.3 for specimens aged at 100°C for 3 hours. These results show that, although there is a steady increase in the transition temperature of normal and titanium-bearing steels, with increasing pre-strain, this increase is significantly smaller for the titanium-bearing steels, especially at larger pre-strains. When this smaller increase in ΔT_{27} is considered in conjunction with the lower 'as-rolled' transition temperature of the titanium steels (see Table 7.2), the lesser susceptibility of strain age embrittlement of these steels is apparently increased. The smaller values of ΔT_{27} for the titanium steels, when compared with the normal Grade 275 steel, is obviously a result of its non-ageing characteristics. However, it is reasonable to take into account the limited strain ageing that takes place in the titanium-bearing steels, especially the 'strain age hardening' at larger pre-strains, which may affect the values of ΔT_{27}, i.e., a completely non-strain ageing steel may have still smaller values of ΔT_{27}.

The increases in ΔT_{27} with pre-strain, shown in Figure 7.3, correspond to 2.2°C/1% pre strain and 1.5°C/1% pre-strain for the normal and the titanium-bearing steel (Ti(a)) respectively. This compares reasonably well with approximately 3.4°C/1% pre-strain and 2.0°C/1% pre-strain for a low carbon steel (0.07% C, 0.27% Mn, and 0.003% N), aged at 230°C for 30 minutes and the same steel where the temperature was maintained below -40°C after pre-straining to retard ageing[91]. The latter observations were made from a slow V-notch bend test by obtaining the temperature at which fracture coincides with 'general yield'.

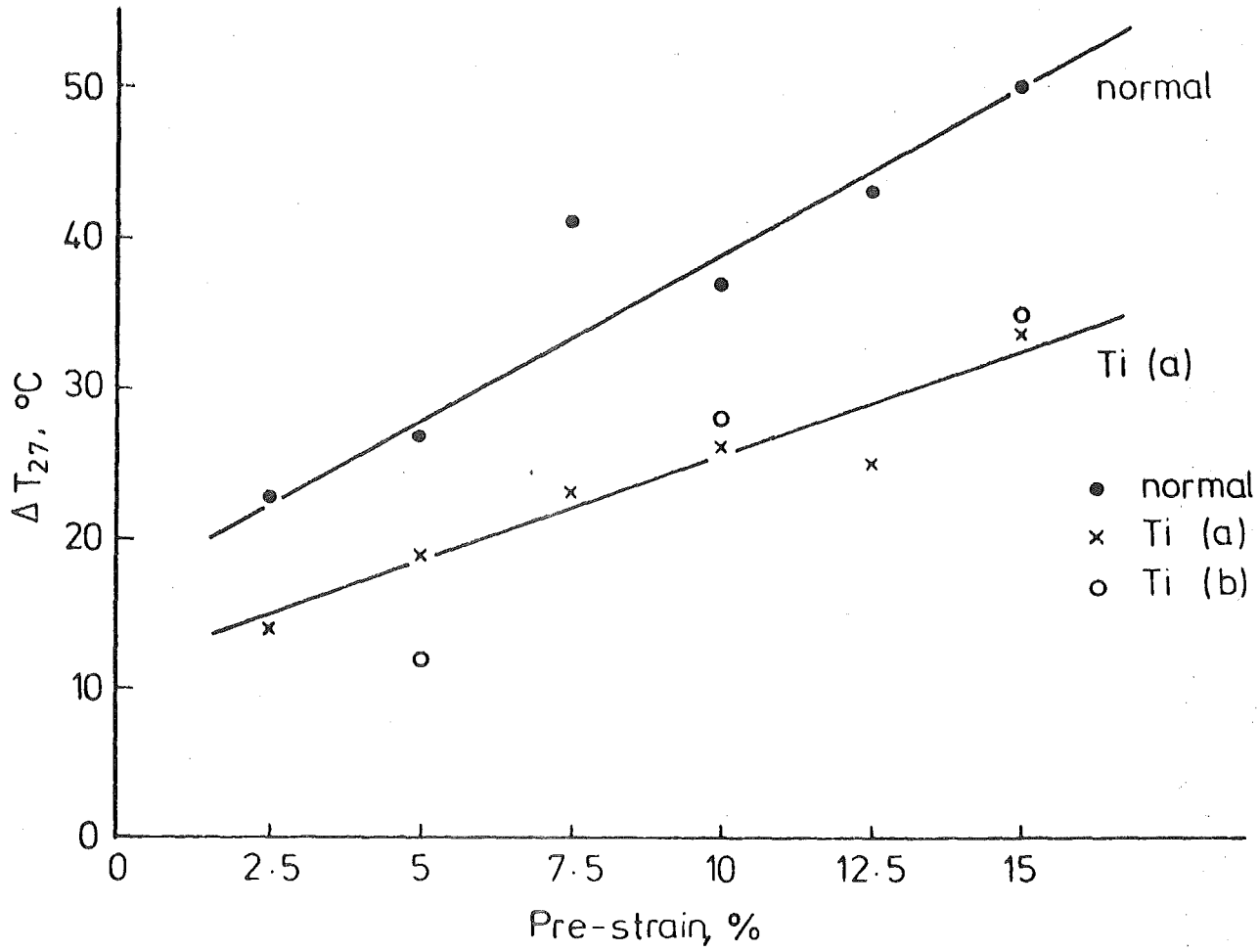

Figure 7.3: Effect of pre-strain on the increase in the fracture transition temperature (ΔT_{27}) due to strain ageing in normal and titanium steels.

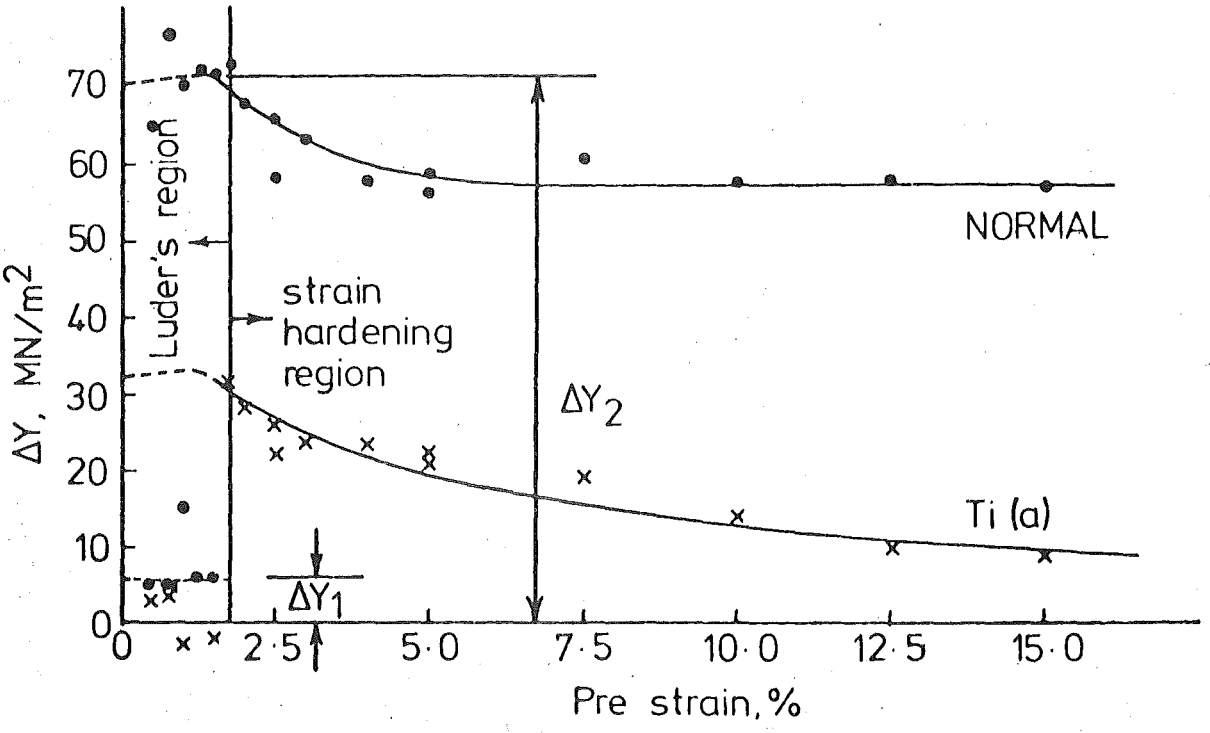

Figure 7.4: Effect of pre-strain (including the yield strain region) on ΔY due to strain ageing in normal and Ti(a) steel.

Although some ageing is likely to have occurred in the titanium steels as a result of the small residual 'active' nitrogen content, and by a small contribution from interstitial carbon (at 100^{o}C), it is obvious that the transition temperature appears to increase with increasing pre-strain, even in the absence of subsequent ageing, probably at a still smaller rate (i.e., <1.5^{o}C/1% pre-strain). The mechanism responsible for this increase cannot be fully explained in quantitative terms at present, but logically would be associated with changes in the 'effective surface energy' (γ_{eff}), required in the creation of two new surfaces during cleavage fracture. This term is orders of magnitude greater than the 'free surface energy' (γ) and should combine the effects of:-

(a) plastic deformation occurring during the propagation of a cleavage crack, which is manifest in the 'river pattern' seen on cleavage facets; and

(b) plastic deformation occurring at the notch root during the nucleation and growth of a micro-crack and shown to always precede cleavage crack propagation[92, 93].

It may be argued that prior plastic strain would increase 'γ_{eff}' by increasing the density of 'river pattern' lines on the cleavage facets which results in an increase in the fracture stress (σ_F), required to propagate a cleavage crack nucleus[91]. However, it is fairly well accepted that the growth of a micro-crack in the notch root area is the critical event of slip-initiated cleavage fracture[92, 93]. Hence, when both initiation and propagation of a cleavage crack in a V-notched Charpy specimen is taken into account 'γ_{eff}' may be separated into two components, i.e.,

$$\gamma_{eff} = \gamma_{plastic} + \gamma_{prop} \qquad 7.1$$

where, $\gamma_{plastic}$ results from plastic deformation that takes place in the

notch root area preceeding cleavage crack propagation and γ_{prop} is the 'effective surface energy' term during propagation of the cleavage crack. Although prior plastic strain (uniform) may increase 'γ_{prop}' it also makes the creation of dislocations (plastic deformation) around a crack nucleus more difficult because the dislocation back stresses are higher, which result in a decrease in the term '$\gamma_{plastic}$'. This may result in the overall reduction in 'γ_{eff}' and consequently increase the fracture transition temperature. The additional increase in the transition temperature during subsequent ageing may be explained by the increase in k_y from its value in the pre-strained condition. There may also be a contribution from a further reduction in 'γ_{eff}' due to dislocation locking.

An attempt made on separating the embrittlement caused by plastic straining in the absence of ageing and during subsequent ageing in semi-killed Open Hearth C-Mn steels, has show that steels containing low 'active' nitrogen (e.g., aluminium-treated normalised steel) give only a relatively small increase in the transition temperature during ageing below $100^{o}C$[39] (see Figure 3.12).

7.6.2 Effect of Pre-Strain within the Yield Strain Region

In the previous discussion, pre-straining had been carried out in the strain hardening region of the load-extension curve. The results from an investigation[58] into the effect of pre-strain within the yield strain region, have been combined with the results from the strain hardening region and are shown in Figure 7.4.

It was observed that initial yielding after strain ageing occurred almost at the yield stress of the unstrained material in both steels, and this yield point elongation extended up to the strain hardening curve of the as-rolled steel[58] (see Figure 7.5). Figure 7.6 shows that this yield point elongation (YPE_1) is approximately the difference between the YPE of the as-rolled material and the pre-strain. These results confirm that

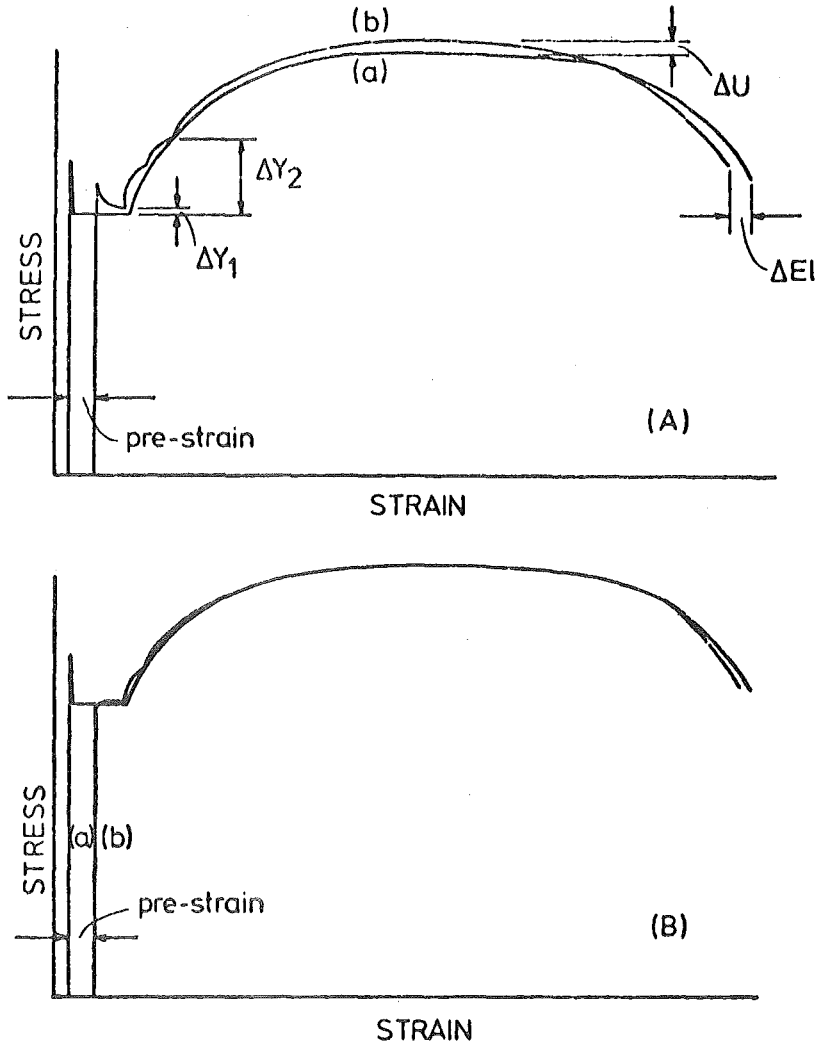

Figure 7.5: Effect of pre-strain in the yield strain region on changes in the stress-strain curve after strain ageing. Curve (a) as-rolled condition, curve (b) strain aged condition.
(A) Normal Grade 275 steel.
(B) Ti(a) steel.

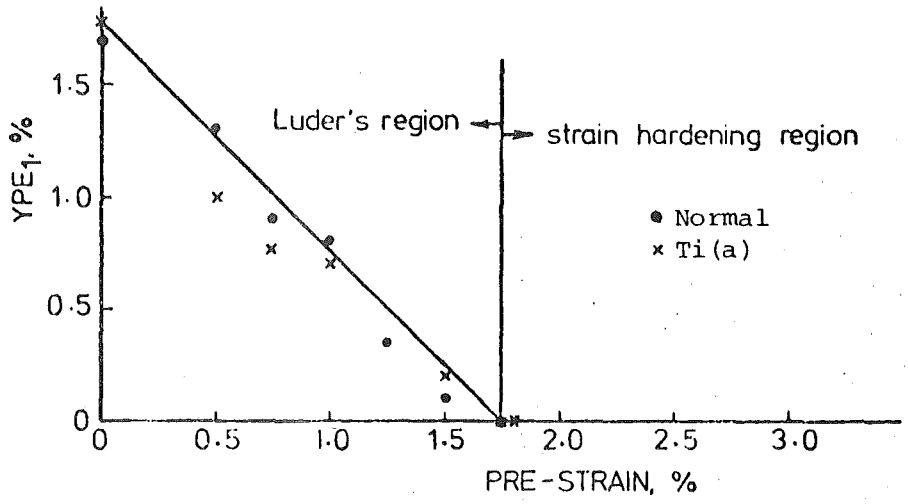

Figure 7.6: The relationship between pre-strain in the yield strain region and the first yield point elongation (YPE_1), after strain ageing in normal and Ti(a) steel.

when a low carbon steel is pre-strained (in tension) in the yield strain region (or Luder's region), certain regions of the specimen accommodate the full YPE while the rest of the specimen remains undeformed and yields at the original yield stress when tested after subsequent ageing.

The strain aged specimens of the normal steel show a second yield point at a higher stress ($\Delta Y_2 \approx 70$ MN/m^2) at which the final yielding of the initially deformed regions of the specimens takes place, while the titanium steel shows no apparent second yield point. Figure 7.4 shows the increases in stress at the first and second yield points (ΔY_1 and ΔY_2) in the Luder's region. The testing of normal Grade 275 deformed bar (i.e., without machining) in the yield strain region, gave similar results to those shown in Figures 7.4 and 7.6[58]. However, the upper yield point was always absent as a result of the stress concentration at the base of the deformations (protrusions).

7.6.3 Effect of Ageing Temperature and Time

The effect of ageing temperature on changes in tensile properties after a 5% pre-strain and with constant ageing time (one hour) is shown in Figure 7.7 for both normal and titanium steel (Ti(a)). The titanium steel can again be seen to show almost negligible strain ageing when compared with the normal Grade 275 steel at temperatures below approximately 100°C to 150°C. Above this temperature range the strain ageing characteristics approach those of the normal steel, although the normal steel consistently shows a higher degree of strain age hardening.

Strain ageing in the normal steel will be due almost entirely to nitrogen at temperatures below 100°C, and the effect of carbon becomes progressively greater above this temperature range. As the titanium steel has only a very small amount of 'active' nitrogen (0.0003%), the difference between the curves (Figure 7.7) for the normal and titanium bearing steel may be attributed almost entirely to the effect of nitrogen

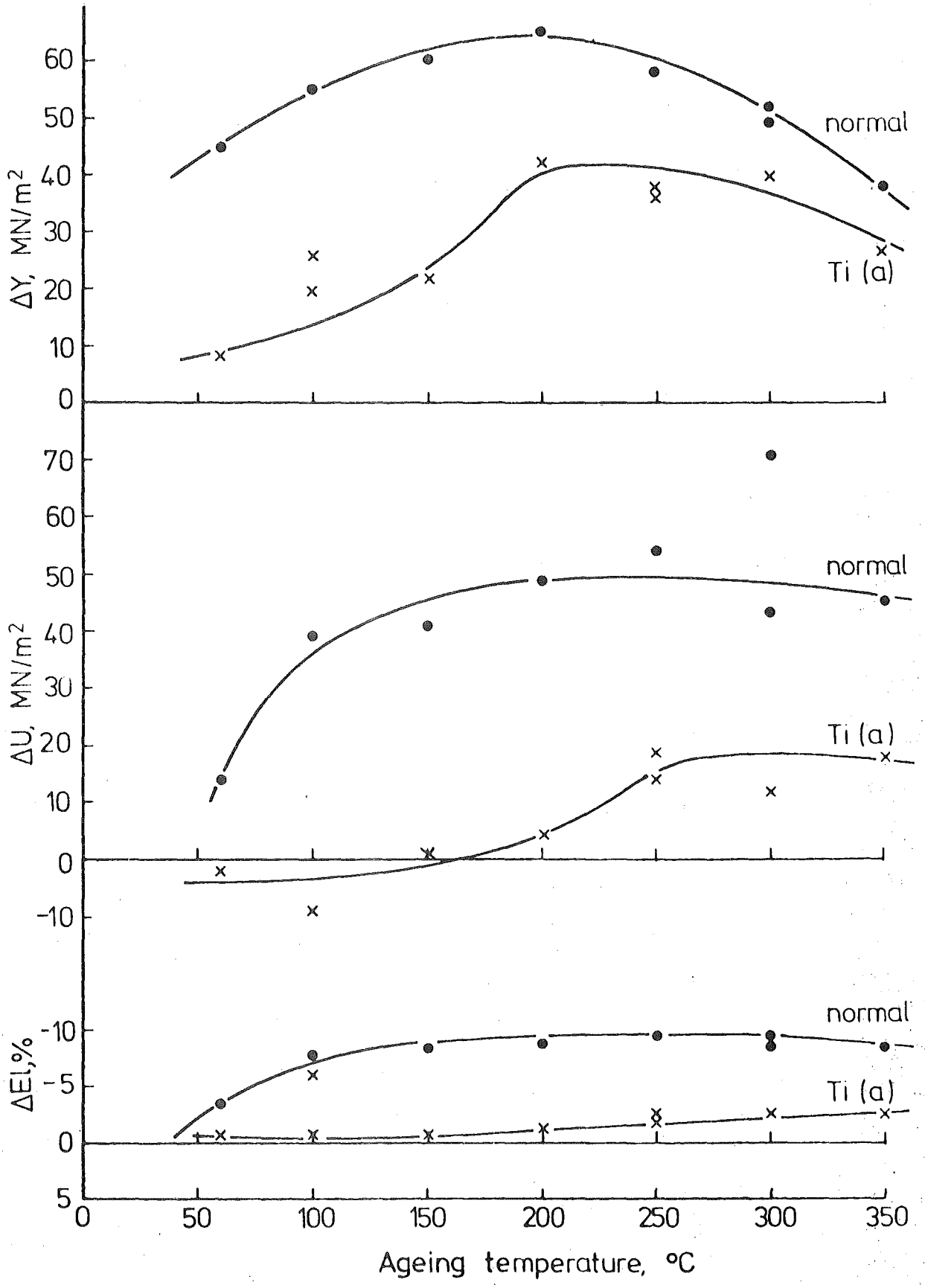

Figure 7.7: Effect of ageing temperature on changes in tensile properties due to strain ageing in normal and Ti(a) steel.

locking and precipitation. In other words, the strain age hardening effects (i.e., increases in ΔU and decreases in $\Delta E\ell$) which begin to show for the titanium steel above approximately 200°C are caused almost entirely by carbon, although there may be some degree of first stage ageing due to residual 'active' nitrogen shown in the curve for ΔY at low temperatures. Consequently these curves appear to show that locking and precipitation hardening effects of nitrogen are strong by comparison with carbon. Codd and Petch[54] have also reported that nitrogen atoms lock dislocations with more severity than carbon. This difference may also be partly due to the lower interstitial content of the titanium steel.

Comparison of curves for ΔY and ΔU for the titanium steel show that only partial first stage ageing occurs at temperatures below approximately 150°C, i.e., no apparent increase in tensile strength (ΔU) or decrease in elongation ($\Delta E\ell$) is shown. The curve for ΔY shows that first stage ageing is almost complete at 200°C, and is confirmed by the complete return of the discontinuous yield point[15] in the specimen aged at 200°C, while this characteristic is absent in specimens aged below 200°C, see Figures 7.8(A) and 7.8(B). Second stage ageing (i.e. precipitate formation) occurs above this temperature as carbon becomes progressively available for dislocation locking and precipitation.

The curve for ΔY for the normal steel (Figure 7.7) shows that initially ΔY increases up to a maximum of approximately 65 MN/m^2 at 200°C and then steadily drops to approximately 40 MN/m^2 at 350°C. The decrease in ΔY as the ageing temperature is increased above 200°C (also observed for the titanium steel) may be due to 'over-ageing', as suggested by Wilson and Russell[15], and internal stress relaxation (recovery), both processes being enhanced at higher temperatures. Figure 7.7 also shows that an ageing treatment of one hour at 60°C (equivalent to approximately 3 days at 15°C[30]) is sufficient to complete first stage ageing, and one hour at 100°C (equivalent to 68 days at 15°C[30]) is sufficient to almost

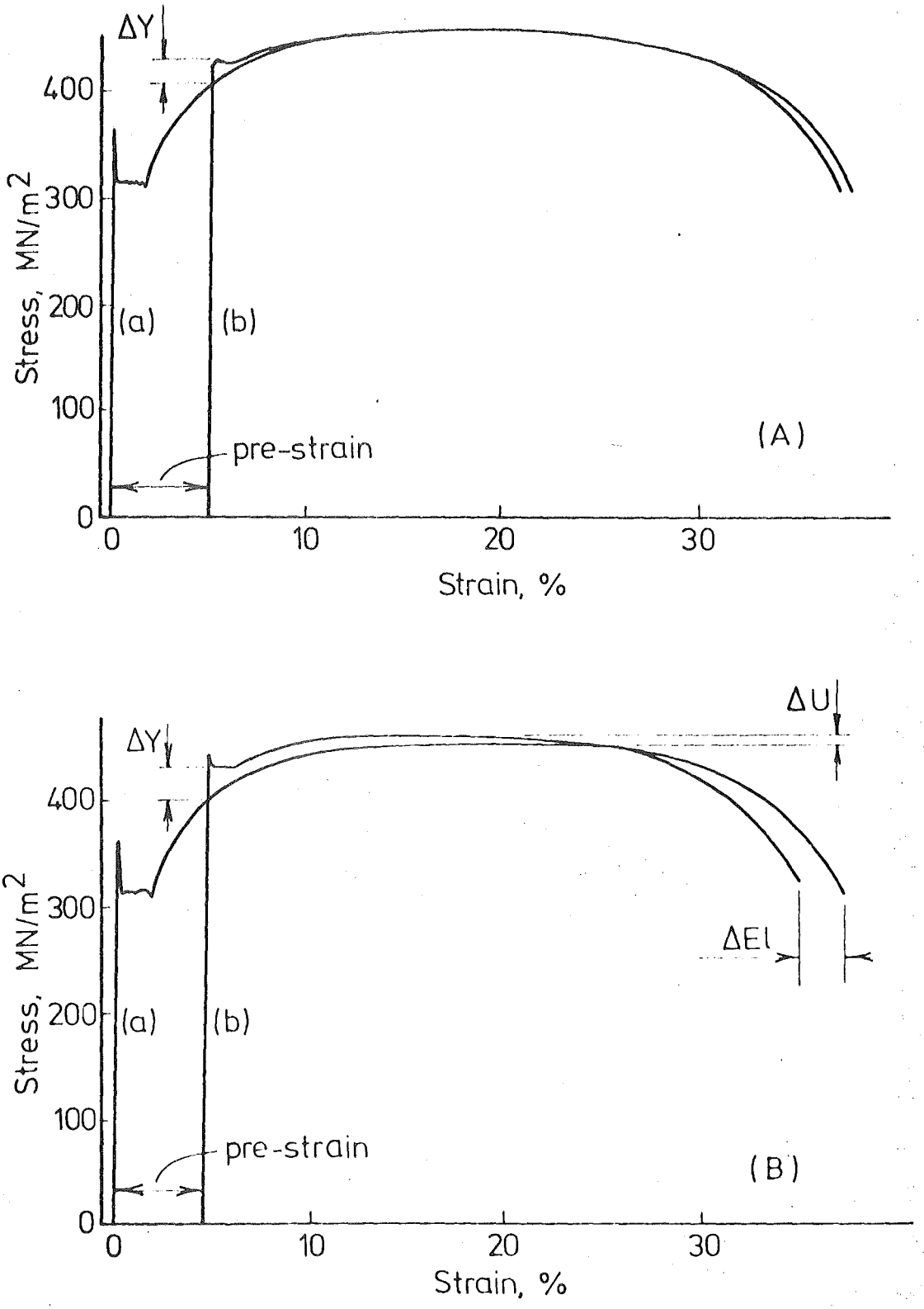

Figure 7.8: Effect of strain ageing on changes in the stress-strain curve for Ti(a) steel, curve (a) as-rolled condition, curve (b) strain aged condition.

(A) Aged at 150°C for one hour.
(B) Aged at 200°C for one hour.

complete second stage ageing for normal steel. When Hundy's Equation 3.7 is used to convert this data for normal steel to equivalent ageing times at 60°C (see Figure 7.9), close agreement is obtained with the results of Wilson and Russell[15] (Figure 3.4) for a low-carbon steel, thus showing the applicability of Hundy's equation for the normal steel in the temperature range 60° - 350°C.

Using Hundy's equation with an average H value of 4200, equivalent times were calculated for a one hour ageing time at higher temperatures ranging from 100 to 350°C, and specimens aged accordingly at selected temperatures and times. These results are shown in Figure 7.10, where the ageing time-temperature combinations are plotted as equivalent temperatures for one hour ageing treatments.

These experimental data show good agreement with the experimental curves derived for the one hour ageing treatments (Figure 7.7) also shown in Figure 7.10, for the normal steel and hence generally confirm the validity of Hundy's equation. The deviation of some results of ΔU (namely ageing at 100°C, giving an hour's equivalent ageing at 150 and 200°C) may be a result of the variation in tensile strength between individual specimens. It is clearly noticeable, however, that values of ΔY for the titanium steel are consistently lower than the curve for the one hour ageing treatment for that steel. This may be expected where two overlapping diffusing species (nitrogen and carbon atoms) are being considered, and one is absent, or virtually absent, as in the case of the titanium steel and the other (i.e., carbon) increases from insignificant levels with the increase in temperature. The reduction in the solubility of carbon in ferrite at the lower temperatures (i.e. below approximately 100°C) means simply that carbon is not available to take place in the diffusion proces, and Hundy's equation is consequently no longer valid, since it assumes constant interstitial content with temperature.

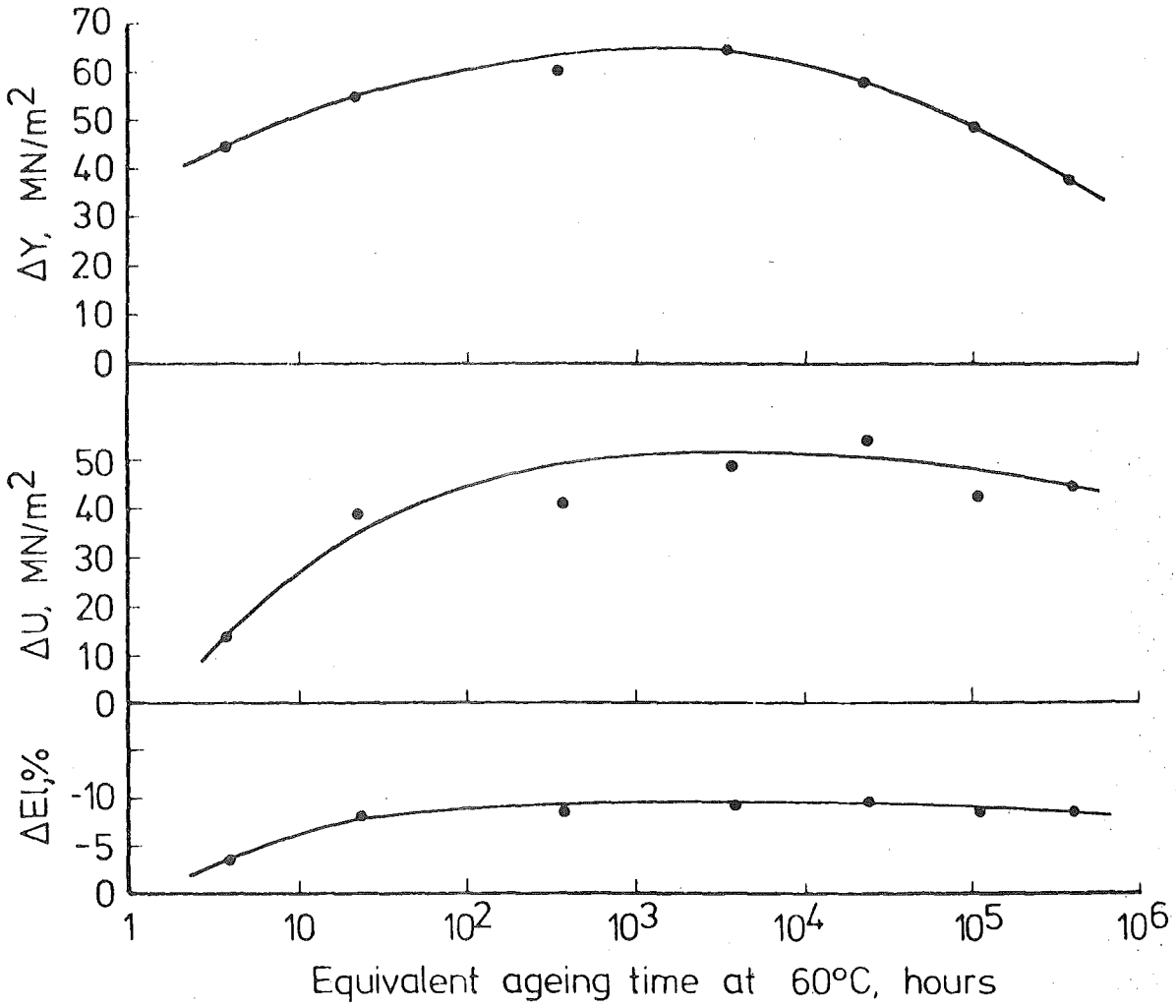

Figure 7.9: Effect of equivalent ageing time at 60°C as determined by Hundy's equation (using an average H value of 4200), on changes in tensile properties of normal steel.

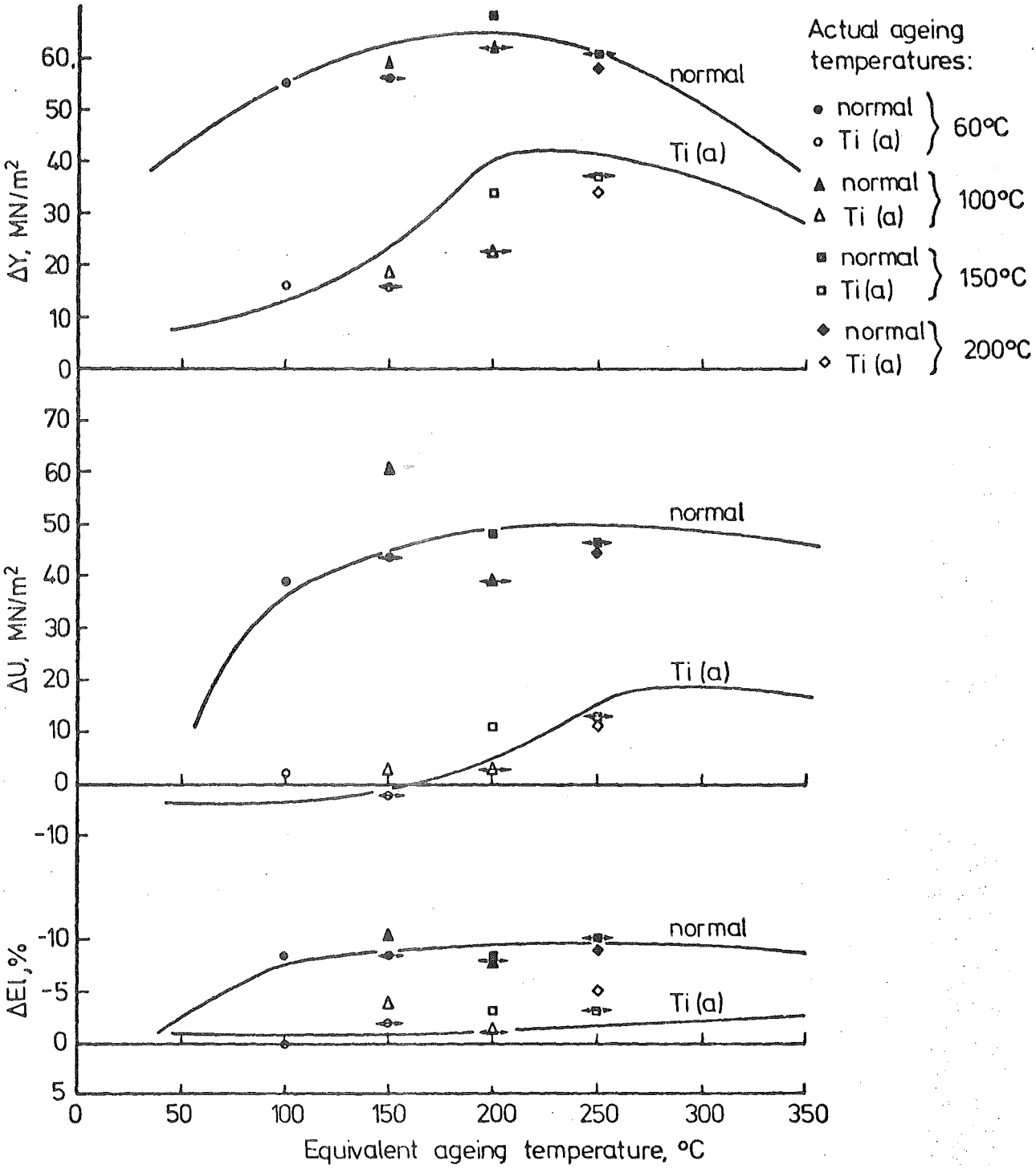

Figure 7.10: Changes in tensile properties obtained from selected ageing temperature-time combinations, superimposed on the curves from Figure 7.7 using Hundy's equation with an average H value of 4200. Also shown are the deviations when using H values of either carbon or nitrogen.

Reservations must be made on the applicability of Hundy's equation for steels containing strong nitride formers[2]. A closer look at the results from titanium steel show that, from tests carried out after ageing at 100°C and 150°C, giving the equivalent of one hour's ageing at 200°C, ageing at 100°C produces only partial first stage ageing of almost the same degree as 3 hours at 100°C, (i.e., $\Delta Y \sim 20$ MN/m^2), but as the temperature is increased to 200°C, first stage ageing is complete and signs of second stage ageing have appeared. However, the tests carried out after ageing at 150°C and 200°C, giving the equivalent of one hour's ageing at 250°C, show that these ageing treatments give almost the same degree of ageing. It therefore appears that strain ageing characteristics at ageing temperatures of above approximately 150°C are significantly different from those below approximately 100°C. Considerable evidence is available that in steels containing strong nitride formers, ageing below 100°C may differ in character from ageing above 100°C [2,3].

For the titanium steel, ageing at 150°C appears to show some interesting features. An ageing treatment of one hour at 150°C gives only partial first-stage ageing; however, increasing the ageing time to 10 hours is sufficient to almost complete the first stage of the ageing process. A further increase in ageing time to 64 hours provides strain age hardening of the titanium steel. This may be a result of a dynamic process where, due to the precipitation of carbon on dislocations, a continuous supply of interstitial carbon, governed by the equilibrium solubility of carbon at 150°, will be available in the ferrite matrix resulting from the re-solution of Fe_3C. This suggested process will be enhanced when the temperature is further increased beyond 150°C, due to:

(a) the higher equilibrium solubility of carbon;

(b) the higher diffusion rate of carbon; and

(c) a faster rate of precipitation on dislocations, as suggested by Wilson and Russell[15].

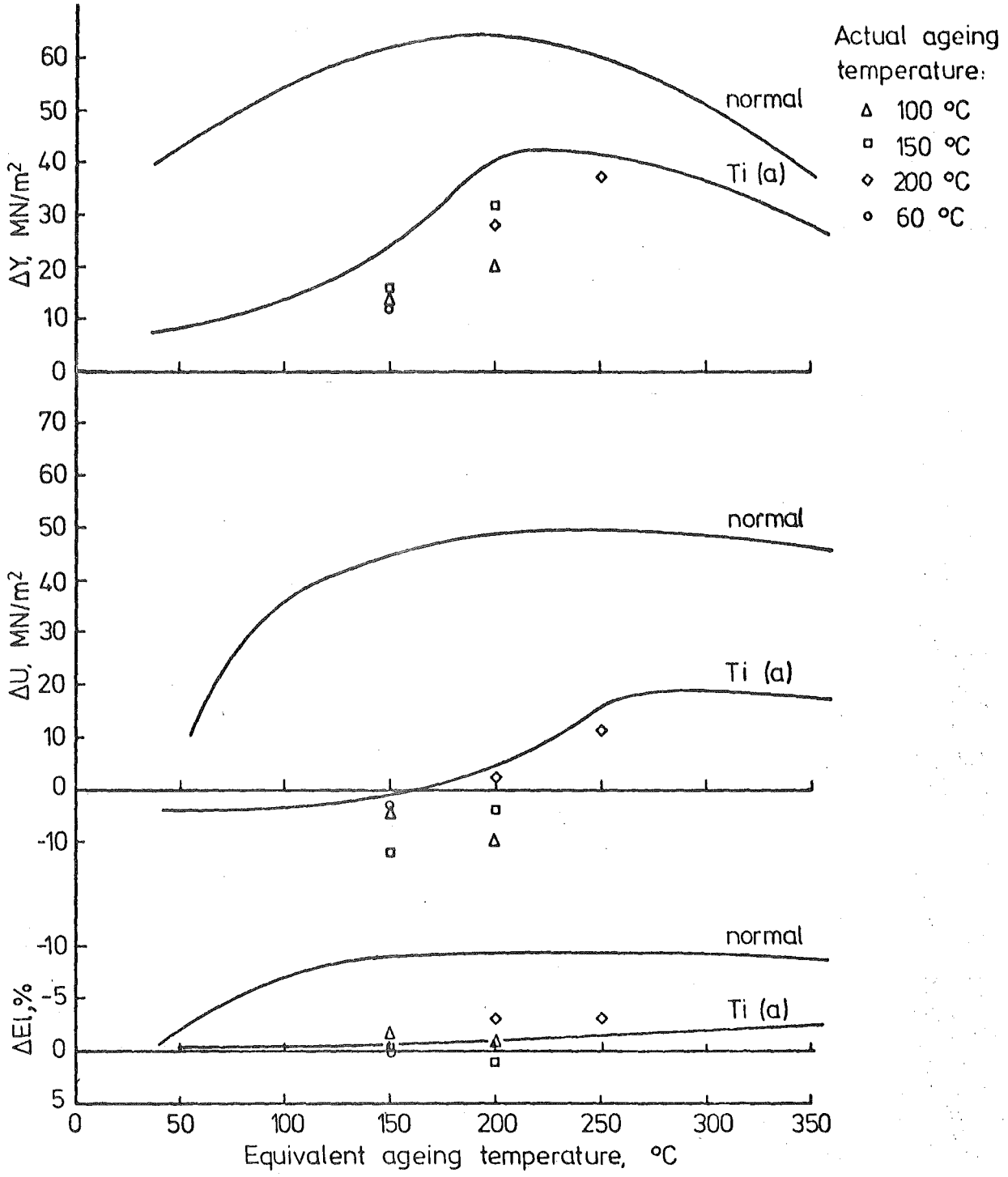

Figure 7.11: Changes in tensile properties of Ti(b) steel obtained from selected ageing temperature-time combinations, superimposed on the curves from Figure 7.7 using Hundy's equation with an average H value of 4200.

Figure 7.11 shows some results obtained from the titanium (b) steel, where the ageing time-temperature combinations are plotted as equivalent temperatures for one hour ageing treatments superimposed on the curves from Figure 7.7, using Hundy's equation with an average H value of 4200. These results confirm that titanium steels give consistently lower values than the curve derived for the one hour ageing treatments. They also confirm that ageing below approximately 100°C, even for very long periods (~300 hours), causes only partial first stage ageing in titanium steels, i.e, these steels are 'stabilised' below 100°C.

The effect of ageing temperature on strain age embrittlement, i.e., the increase in the 27 Joule Charpy transition temperature (ΔT_{27}), is shown in Figure 7.12, after 5% pre-strain and a one hour ageing treatment for both normal and titanium (a) steel. The titanium steel can again be seen to have a lower ΔT_{27} than the normal Grade 275 steel, although the difference between the ΔT_{27}'s becomes progressively smaller as the ageing temperature is raised above approximately 150°C, the curves for the two steels becoming coincident at temperatures of 300°C and above. These results may be generally expected as the 'stabilised' characteristics of the titanium steel at low temperatures do not hold when ageing temperatures of above approximately 100°C are used.

Hundy's equation is again used with an average H value of 4200 to calculate equivalent times for a one hour ageing treatment at higher temperatures and the Charpy specimens aged accordingly at pre-selected temperatures and times. The resultant increases in Charpy transition temperature (ΔT_{27}) are plotted in Figure 7.13, superimposed on the experimental curves derived for the one hour ageing treatments from Figure 7.12. These results show reasonable agreement with the curves from Figure 7.12, except for a few cases in the titanium steels, again showing the general validity of Hundy's equation for the normal steel.

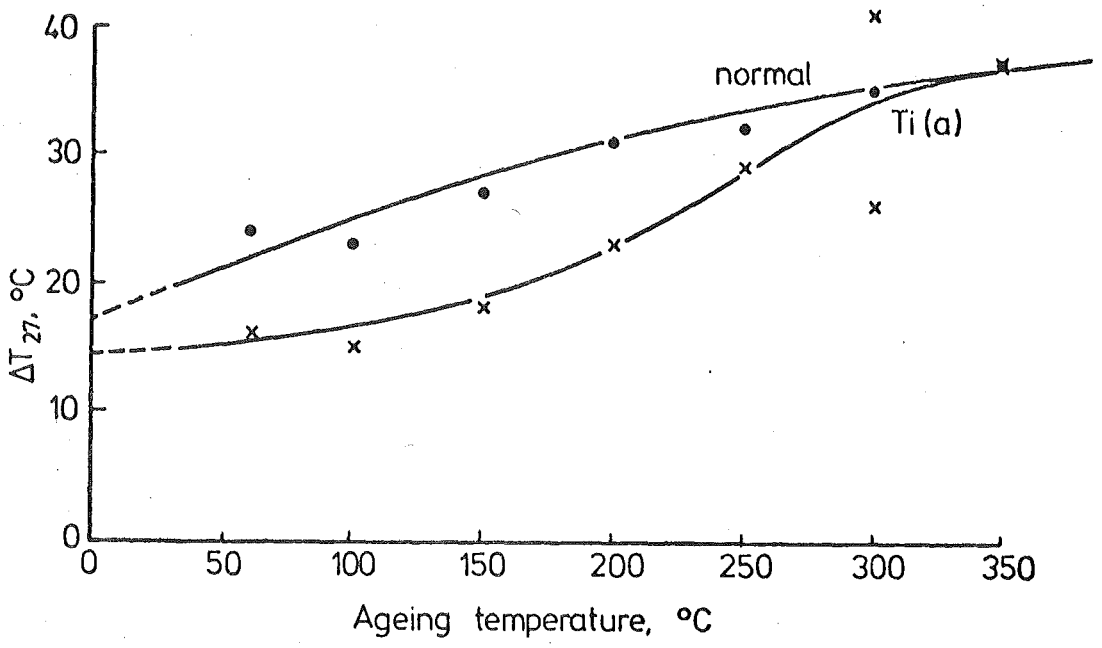

Figure 7.12: Effect of ageing temperature on ΔT_{27} due to strain ageing in normal and Ti(a) steel.

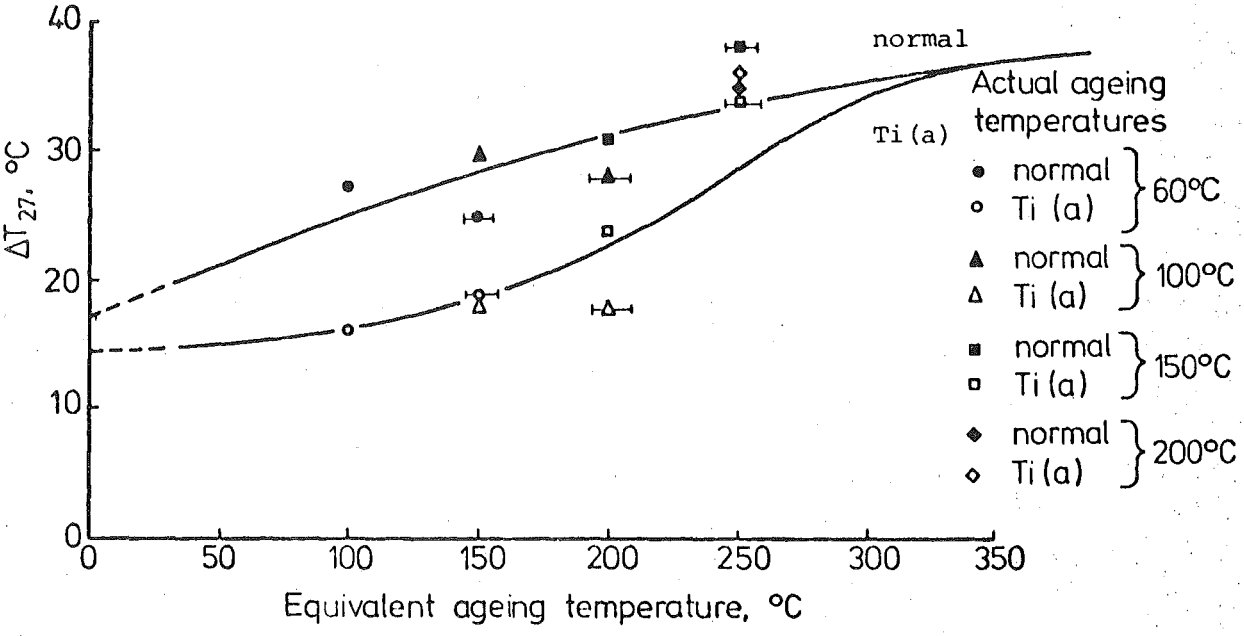

Figure 7.13: ΔT_{27} obtained from selected ageing temperature-time combinations, superimposed on the curves from Figure 7.12 using Hundy's equation with an average H value of 4200. Also shown are the deviations when using H values of either carbon or nitrogen.

However, again its applicability for the titanium steel appears suspect. For example, ageing for approximately 190 hours at 100°C causes embrittlement to only the same degree as one hour at 100°C, as a result of the non-availability of interstitials to take part in the diffusion process and cause further dislocation locking.

It appears from Figure 7.12, that dislocation locking and precipitation by carbon in the titanium steel at temperatures above approximately 300°C has an almost identical effect to nitrogen and carbon together in the normal steel, despite the differences in ΔY and ΔU of these steels, shown in Figure 7.7, in the case of strain age embrittlement. It would appear, therefore, that the increase in the 27 Joule fracture transition temperature is dependent mainly on a critical minimum degree of dislocation locking and precipitation (i.e., a critical minimum degree of 'strain age hardening') and further strain age hardening above this critical minimum does not affect the fracture transition temperature significantly. When comparing the curves in Figures 7.7 and 7.12 for the normal steel, it appears that this critical minimum degree of strain age hardening has been almost achieved by an ageing treatment of one hour at 60°C, i.e., equivalent to approximately 3 days at 15°C. From curves in Figures 7.10 and 7.13, for the titanium steel, it appears that this minimum degree of strain age hardening is accomplished by an ageing treatment of one hour at 250°C or a equivalent temperature-time combination, with a temperature of 150°C or above. An interesting feature can also be seen when comparing the curves for the titanium steel in Figures 7.7 and 7.12, i.e., the transition of ΔT_{27} from approximately a non-ageing value to a fully aged value, which occurs in the temperature range of 150 to 250°C, is closely followed by the transition shown in the curve for ΔU. Figure 7.14 shows the results obtained from the titanium (b) steel, where the ageing temperature-time combinations are plotted as equivalent temperatures for one hour's ageing treatment, superimposed on the curves from Figure 7.12, using Hundy's

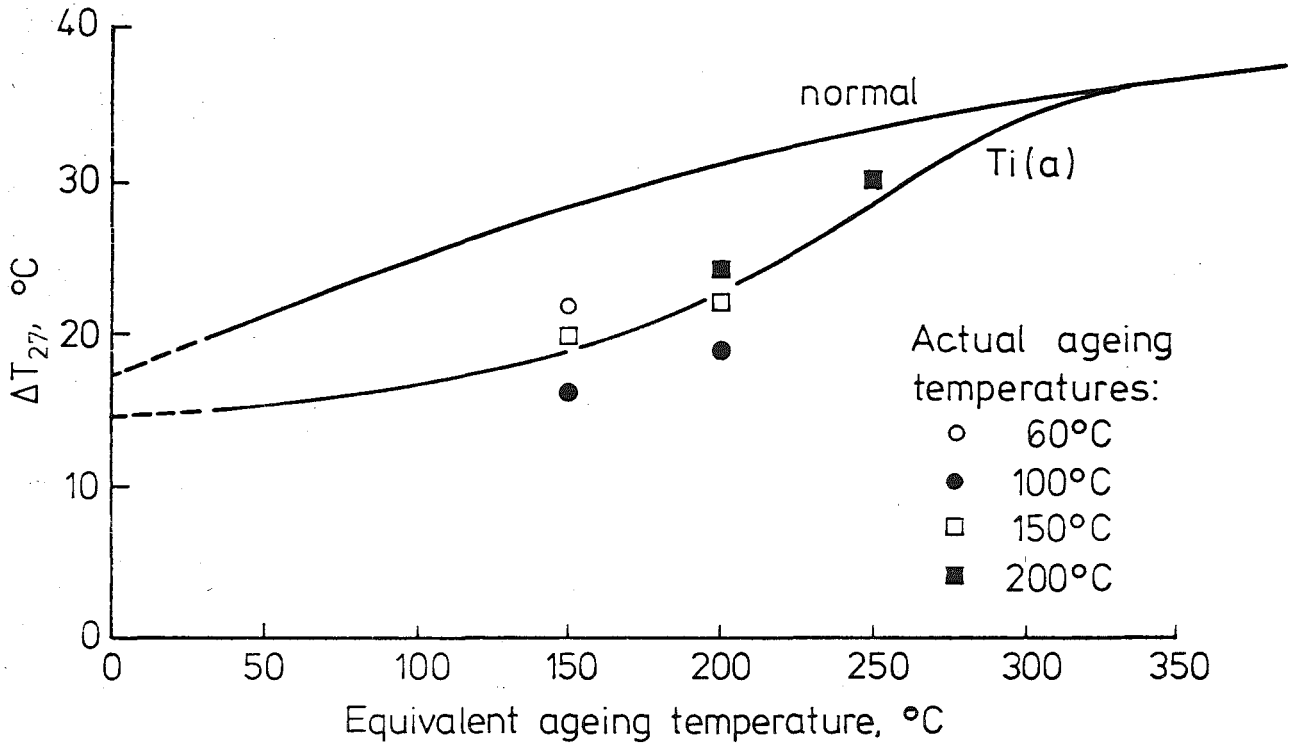

Figure 7.14: ΔT_{27} for Ti(b) steel obtained from selected ageing temperature-time combinations, superimposed on the curves from Figure 7.12 using Hundy's equation with an average H value of 4200.

equation with an average H value of 4200. These results confirm the existence of a critical minimum degree of strain age hardening above which the transition temperature is not affected significantly (compare Figure 7.14 with Figure 7.11), and that this minimum degree of strain age hardening is accomplished by an equivalent ageing treatment of one hour at 250°C.

It is not clear from Figures 7.12 and 7.13 whether the 'overageing' and 'recovery' shown in the curves for ΔY in Figure 7.7 have had any influence in the increase in fracture transition temperature up to ageing temperatures of 350°C, although a reduced rate of increase in ΔT_{27} is speculated in the curves shown in Figures 7.12 and 7.13 at the higher ageing temperatures. Although 'overageing' and 'recovery' have been observed at higher ageing temperatures, i.e., in the range 200-300°C, for semi-killed Open Hearth carbon-manganese steels in the curves for ΔY, no such 'recovery' was observed in the impact properties[39]. However, when the ageing temperature is further increased, considerable recovery in the impact properties occurred in normal carbon-manganese reinforcing steels[94].

The curve for ΔT_{27} for the titanium steel in Figure 7.12 is expected to become asymptotic with the temperature axis at low temperatures, due to the retardation of the strain ageing process resulting from the inhibition of the diffusion process. This asymptotic value of ΔT_{27}, which is approximately 14°C would hence correspond to the increase in the 27 Joule fracture transition temperature resulting from pre-strain in the absence of any subsequent ageing. When this value is compared with Figure 7.3 at the 5% pre-strain level, it appears that ageing by residual nitrogen and some carbon (at 100°C) has had a small influence on the curve for the titanium steel in Figure 7.3 (i.e., an increase of approximately 4°C); hence suggesting a greater difference between the curves for the titanium-bearing and normal Grade 275 steel, if ageing had been at ambient temperature. A speculative extrapolation of the curve for the normal steel in

Figure 7.12 to become coincident with the asymptotic part of the curve for the titanium steel, suggests that temperatures as low as -40°C to -70°C would be necessary to prevent embrittlement due to nitrogen diffusion in normal steels.

7.7 Summary

The effect of pre-strain and ageing temperature variation on the mechanical properties of normal Grade 275 and a similar titanium steel has shown the following:

(a) Titanium reduces changes in tensile properties due to strain ageing to negligible levels in steels plastically pre-strained and aged at 100°C or less.

(b) Titanium-bearing steels are less susceptible than normal steels to strain age embrittlement especially at larger pre-strains, and when aged at 100°C or less.

(c) Tensile pre-strain in the yield strain region has no effect on the stress-strain curve after strain ageing in the titanium-bearing steel.

(d) Titanium-bearing steels lose their 'stabilised' characteristics when the ageing temperature is increased above 100°C, and the properties approximating to those of normal reinforcing steel at ageing temperatures of 250°C and above.

(e) Although Hundy's equation is applicable to normal steels, its validity is limited in the case of titanium steels.

(f) Although 'overageing' and internal stress relaxation are shown in tensile test results at high ageing temperatures (i.e., in the range 200 - 350°C), Charpy impact test results show no clear effect of this recovery.

(g) Plastic straining in the absence of ageing brings about an increase in the fracture transition temperature, a further increase occurring during ageing.

CHAPTER 8

EMBRITTLEMENT IN COLD BENT REINFORCING BAR

8.1 Embrittlement Testing of Deformed Reinforcing Bar

8.1.1 Chemical Analysis

Some of the steel reinforcing bar used for embrittlement testing which was obtained commercially, was analysed for carbon and manganese content. Nitrogen determinations were also carried out on these steels by the method given in Appendix A. The resultant carbon, manganese and nitrogen contents of the steels are given in Table 8.1.

8.1.2 Testing Procedure

The deformed reinforcing bar was cut to pre-determined lengths and then bent through 90^{o} around formers of different diameters followed by re-straightening to approximately 45^{o}. These tests were performed in two series: in the first the re-straightening operation was carried out immediately after making the initial 90^{o} bend, and in the second, the bars were aged at $100^{o}C$ for 3 hours between making the initial bend and carrying out the re-straightening operation. This ageing treatment gives an almost fully aged condition and is equivalent to nine months at $15^{o}C$[30]. The above bend tests were repeated but with the temperature during re-straightening lowered to between $0\text{-}4^{o}C$. The propensity of the test bars to crack on the inner surface was assessed according to the depth of any crack formed and the corresponding failure mode, i.e., digits 1 to 5 indicate crack depths of approximately 1 to 5 mm, the digit 6 indicating complete fracture, and the letters D and C indicating ductile tearing and cleavage fracture respectively. C6 consequently represents catastrophic fracture within the first degree or two of re-straightening.

The above slow bend tests were performed on commercially available deformed reinforcing bars from both Grades 275 and 380 (NZS 3402 P) on a

TABLE 8.1: Chemical Analysis of Commercially obtained Reinforcing Bar (Element, % wt)

Steel	d(mm)	C	Mn	N_{sol}	N_{insol}	N_{tot}	$N_{A\ell N}$	N_{active}
Grade 275	16	0.22	0.51	0.0049	0.0009	0.0058	0.0002	0.0047
	22	0.21	0.51	0.0049	0.0004	0.0053	0.0002	0.0047
	28	0.23	0.40	0.0049	0.0007	0.0056	0.0003	0.0046
Grade 380	16	0.34	1.16	0.0051	0.0007	0.0058	0.0003	0.0048
	22	0.38	1.06	0.0075	0.0006	0.0081	0.0002	0.0073
	28	0.38	1.15	0.0059	0.0005	0.0064	0.0005	0.0054

NOTE: d = bar diameter

TABLE 8.2(a): Results from Slow Bend Tests on Deformed Reinforcing Bar, Grade 275 Steel.

Bar Diameter (d), mm	FORMER DIAMETER						
	1d	1.5d	2d	2.5d	3d	3.5d	4d
UN-AGED, TESTING TEMPERATURE ~20°C							
10			N	N			
16		N	N	N			
22	D2	D2	D1	D1			
28		C1,D4	C1,D4	D3	D1	D1	
AGED, TESTING TEMPERATURE ~20°C							
10			N	N			
16		N	N	N			
22	D2	D2	D2	D2			
28		C6	C1,D6	D4	D2	D2	
UN-AGED, TESTING TEMPERATURE 0 - 4°C							
10							
16		N	N				
22	C2,D4	D2	D1				
28		C3,D6	C1,D2	C2,D3	D1		
AGED, TESTING TEMPERATURE 0 - 4°C							
10							
16		C1,D3	D1				
22	C6	D2	D3				
28		C6	D4	C6	C6	D2	D1

TABLE 8.2(b): Results from Show Bend Tests on Deformed Reinforcing Bar, Grade 380 Steel.

Bar Diameter (d), mm	FORMER DIAMETER							
	1.5d	2d	2.5d	3d	3.5d	4d	4.5d	5d
UN-AGED, TESTING TEMPERATURE ~20°C								
10				D1	D1	N	N	
16				D1	D1	N	N	
22		D3	D2	N	D1	D1	N	
28				D3	D1	N		
AGED, TESTING TEMPERATURE ~20°C								
10			D1	N	N	N		
16			D2	D1	N	N		
22			C6	C6	D1	D1		
28			D4	C6	D3	D1	N	
UN-AGED, TESTING TEMPERATURE 0 - 4°C								
10								
16	D2	D1		N	N	N		
22				C6	C6	D2	D2	
28				C1,D4		D1		
AGED, TESTING TEMPERATURE 0 - 4°C								
10								
16	D3	D2		N	N	N		
22				C6	C6	C6	C6	D1
28				C6		D4	D3	N

range of bar sizes, the results of which are given in Tables 8.2(a) and 8.2(b).

8.2 Estimation of Plastic Strain in Cold Bent Reinforcing Bar

8.2.1 Specimen Preparation

Grade 275 deformed reinforcing bar was bent through 90^{o} around formers of different diameter. The bends were then sectioned longitudinally into two equal halves, and one half was used for the preparation of a metallographic specimen containing the sharpest notch in the surface inner radius of the bend, formed between the deformations (protrusions) and the bar, as well as a plain area between adjacent deformations. Specimens were also prepared from bends in 20 mm diameter plain reinforcing bar.

8.2.2 Quantitative Metallographic Estimation of Plastic Strain

The method used is essentially a measurement of ferrite grain profiles in plastically strained areas, as unstrained hot-rolled reinforcing steels have ferrite grain profiles with no directionality.

The plastic strain in the tangential direction of the longitudinal section was estimated below the notch in the following manner:

(a) Photomicrographs were taken on an area just below the notch, or in a severe bend just below the "compression crack".

(b) A 10 mm square grid was drawn just below the notch, or "compression crack", covering a 50 x 50 mm square area as shown in Figures 8.1(a) and 8.1(b) respectively. The grid lines were drawn in the tangential and traverse directions of the longitudinal section.

(c) The number of ferrite grain intersections made by the two sets of perpendicular grid lines was obtained separately.

(d) The average compressive plastic strain in the tangential direction was determined from the deviation of the intersection count in the

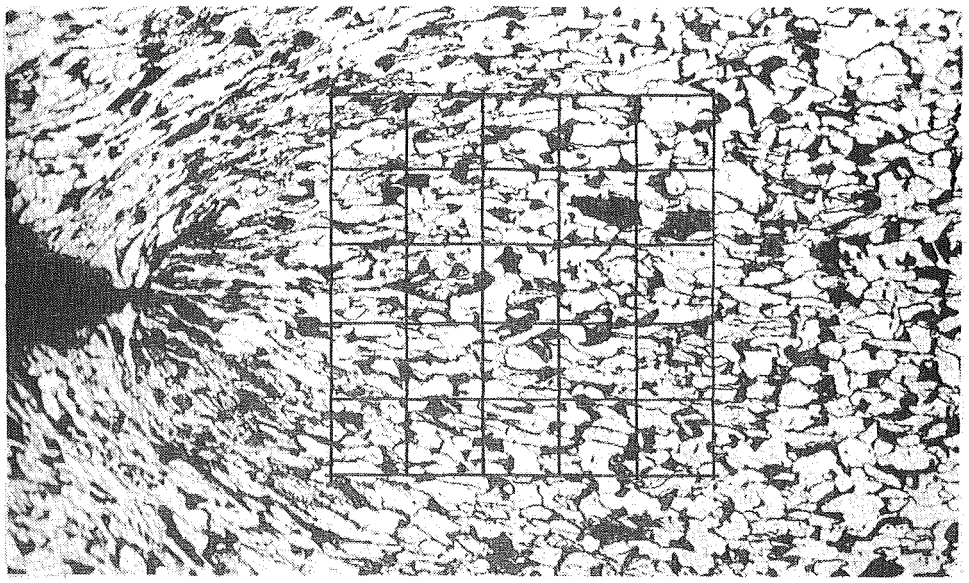

(a) Notch root formed in a 16 mm diameter deformed bar bent around a 1.5d former. x 220.

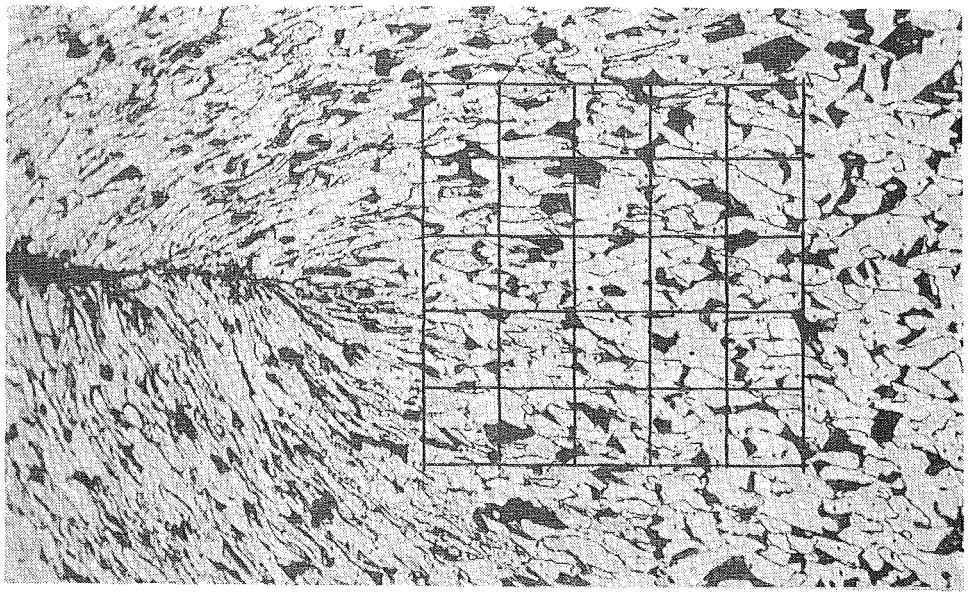

(b) "Compression crack" formed in a 22 mm diameter deformed bar bent around a 2.5d former. x 220.

Figure 8.1: Photomicrographs of areas below (a) notch root and (b) "compression crack", formed adjacent to a deformation on the inner radii surface of bends, showing the 10 mm x 10 mm strain measurement grid.

TABLE 8.3: Tangential Plastic Strain at the Inner Surface Radii of Cold Bent Reinforcing Bar (Plastic Strain, %).

(a) 20 mm Plain Reinforcing Bar.

Bar diameter (d), mm	Former Diameter (D),			
	1d	2d	3d	4d
20	35.7	20.0	17.9	17.1

(b) Deformed Reinforcing Bar, Plain Area.

Bar diameter (d), mm	Former Diameter (D),				
	1d	1.5d	2.5d	3.5d	4d
16	31.0	31.9	26.7	12.1	17.1
22	32.2	28.2	25.7	22.1	21.8
28		33.7	26.9	17.3	

(c) Deformed Reinforcing Bar, Notch Root Area.

Bar diameter (d), mm	Former Diameter (D),				
	1d	1.5d	2.5d	3.5d	4d
16	38.6	37.8	32.1	22.3	22.6
22	41.1	40.0	34.0	29.8	24.6
28		49.6	34.6	30.1	

tangential direction from the mean intersection count obtained from both directions.

The same method was adopted to estimate the compressive plastic strain in the tangential direction at the surface inner radius from a photomicrograph of a plain area between adjacent deformations. Quantitative metallographic estimations of the tangential plastic strain at the surface inner radii of bends in 20 mm diameter plain reinforcing bar were made from photomicrographs taken on areas containing the inner surface radii. In the case of deformed reinforcing bar, these estimations were made on three different bar sizes, and the resultant plastic strains are given in Table 8.3.

8.3 Examination of Fracture Profiles

The specimens used for this examination were prepared from test bars subjected to the embrittlement test. The bends selected for the examination of fracture profiles were from the 28 mm bar of Grade 275 steel having a bend diameter (i.e., former diameter) of 2.5d (d - diameter of bar) which were tested at 0 - 4°C. These specimens produced cracks of C6 (i.e., a complete cleavage fracture) in the aged bend and C2, D3 in the un-aged bend (see Table 8.2(a)).

Specimens for microscopic examination were obtained by sectioning the bends longitudinally into two equal halves and using one half for the preparation of a metallographic specimen containing the fracture profile. Photomicrographs of the fracture profiles were taken on the initial portion of the fractures and are shown in Figure 8.2.

In both fractures, the initiation of the crack appears to have taken place from the notch root that is formed between the deformations (ribs) and the bar at the inner radius surface. The predominantly cleavage failure produced in the aged specimen shows that only very limited plastic deformation has taken place adjacent to the fracture surface during the propagation of the fracture (Figure 8.2(a)). In contrast, although the un-aged specimen shows limited

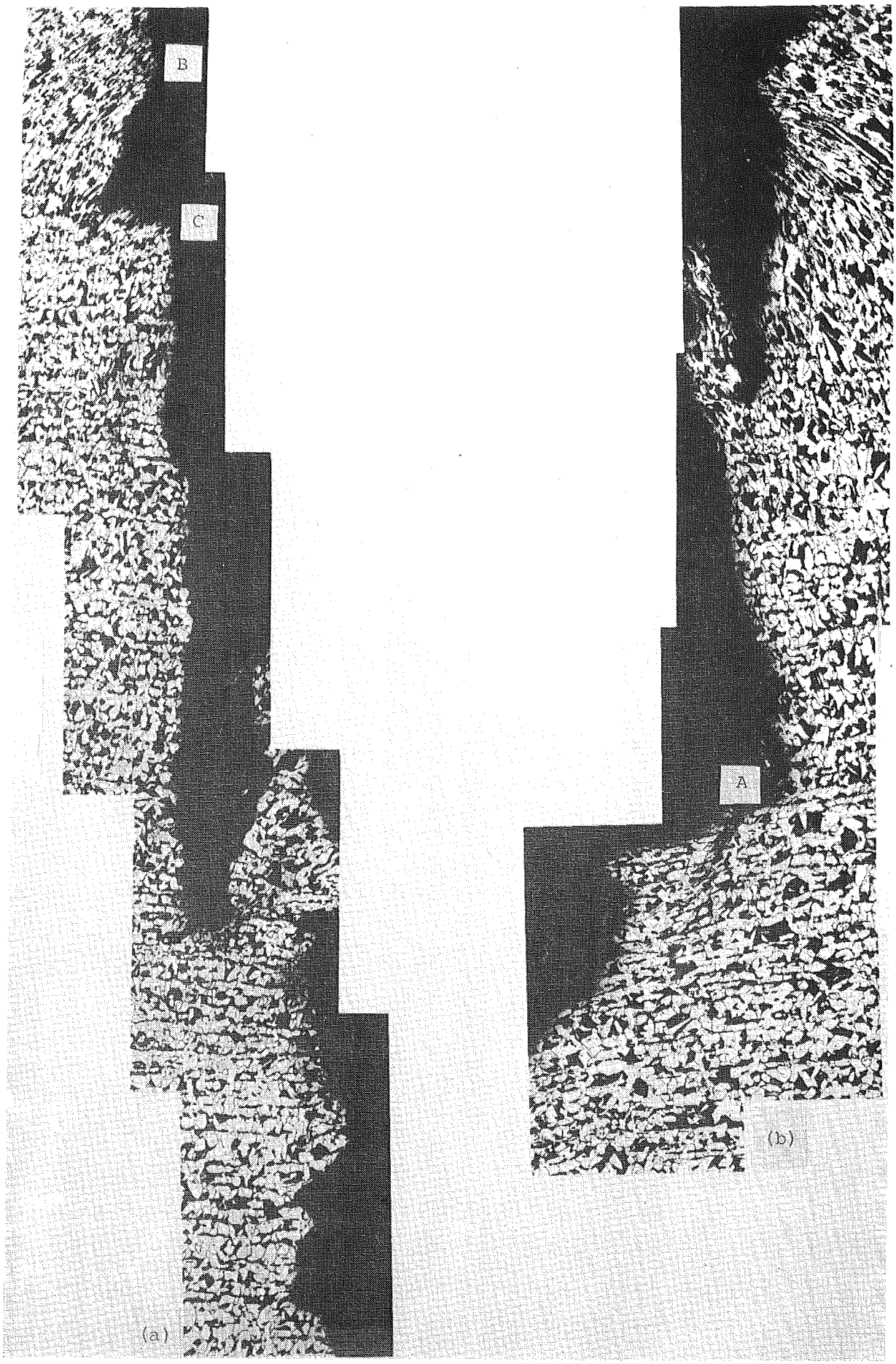

Figure 8.2: Initial fracture profiles of (a) an aged bend, (b) an un-aged bend, in 28 mm deformed bar with a bend diameter of 2.5d, after re-straightening. x 110.

plastic deformation in the initial portion of the fracture during re-straightening, the fracture changes to a ductile mode showing gross plastic deformation from then on, the transition occurring approximately at A (see Figure 8.2(b)).

8.4 Examination of Fracture Surfaces

Typical fracture surfaces for scanning electron microscopic examination were obtained from 22 mm diameter Grade 275 deformed reinforcing steel bar. The reinforcing bar was bent through 90° around formers of different diameters and then re-straightened after subsequent ageing, in a similar manner to the embrittlement test. The re-straightening was done at different sub-zero temperatures, and the fractures were immediately coated with a 'clear plastic' spray to prevent any atmospheric attack on the fracture surface during subsequent preparation of the specimens for electron microscopic examination. Finally, a very light gold coating was given after removing the 'clear plastic' by washing in acetone.

The fractures examined were:

(a) A complete cleavage failure of a 1.5d bend.

(b) A crack in a 1.5d bend that may be classified as C3, D2.

(c) A complete cleavage failure of a 3.5d bend.

The fracture surfaces of (a) and (c) were predominantly cleavage having the typical 'river pattern' lines of cleaved facets. However, these surfaces also had ductile fracture areas showing the typical dimples of a ductile fracture, which appeared to result from ductile tears after the surfaces on either side had cleaved at different topographic levels (Figure 8.3). Examination of the area of fracture initiation showed that the facets in the very initial stages of the fracture had no clear sign of the typical 'river pattern' lines of a cleaved surface. Instead, the fracture facets were comparatively plain, having a shallow ripple pattern with boundaries of ductile tear in the plane of the fracture facet (Figure 8.4). These fracture

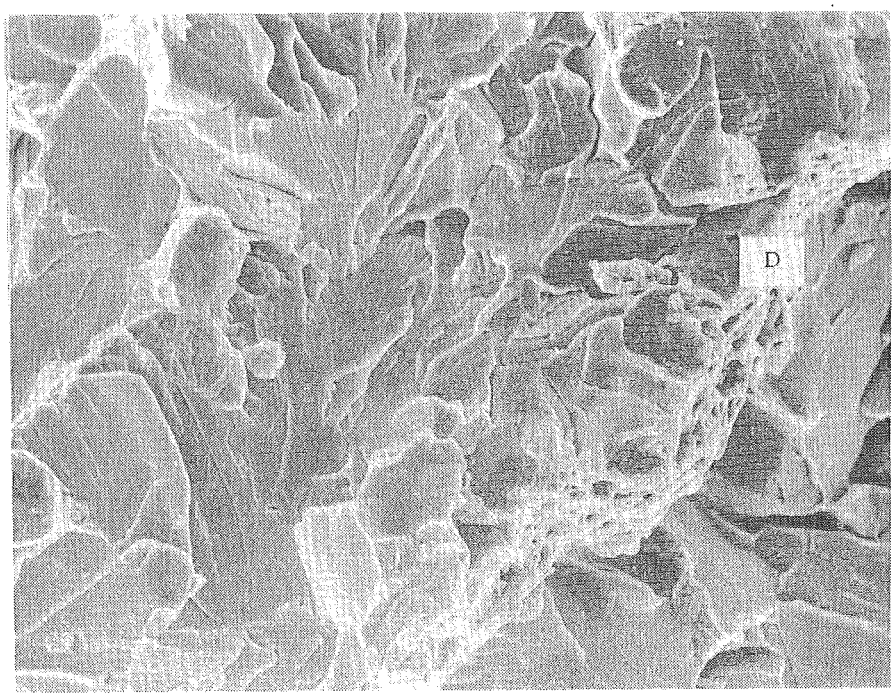

Figure 8.3: A typical ductile tear (D) in the predominantly cleavage fracture of the 3.5d bend in 22 mm deformed bar. x 810.

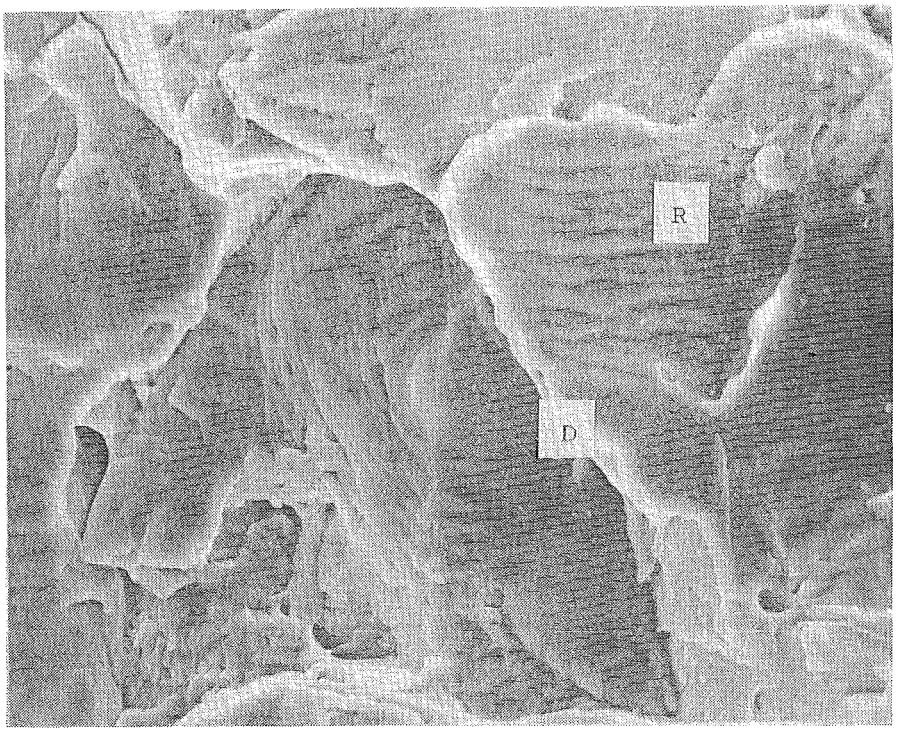

Figure 8.4: A "compression crack" area adjacent to the inner radius surface of a 1.5d bend in the 22 mm deformed bar. x 2210.

R - the ripple pattern: D - the ductile tear boundary.

facets appear to be from areas of the "compression crack" which are normally present in severe bends. This may be confirmed by the significantly smaller area having this type of fracture facets in specimen (c) compared with the area in specimens (a) and (b), i.e., the compression crack area increases with the severity of the bend. Figure 8.5 shows a transition area having the "compression crack" facets preceding the cleavage facets. However, the transition from the "compression crack" facets to the cleavage facets are not so abrupt and regions having mixed fracture areas were also observed.

The fracture surface of specimen (b) was similar to that of (a) for the initial portion of the fracture, showing the "compression crack" facets preceding the cleavage fracture surface with the typical 'river pattern' lines. However, the mode changes to a ductile form after a crack depth of approximately 3 mm. This fracture is very similar to the one shown in Figure 8.2(b), and hence the surface above A in Figure 8.2(b) should be predominantly cleavage, except for the portion of the "compression crack".

The fracture surfaces of specimens (a) and (c) showed irregularity both in the macroscopic and microscopic scales. The fractrographic examination of these surfaces showed that areas with high pre-strain had a larger density of 'river pattern' lines when compared with areas with low pre-strain such as close to the neutral axis of the bend, see Figures 8.6 and 8.7. No smooth facets seen in Figure 8.7 were observed in areas of high pre-strain. These features have also been reported by Groom and Knott, carrying out fractographic investigation on cleavage fracture of uniformly pre-strained low carbon steels[91].

8.5 Discussion

8.5.1 Embrittlement Test Results

The results of the embrittlement test performed on commercially obtained deformed reinforcing bar given in Tables 8.2(a) and 8.2(b) show the following trends:

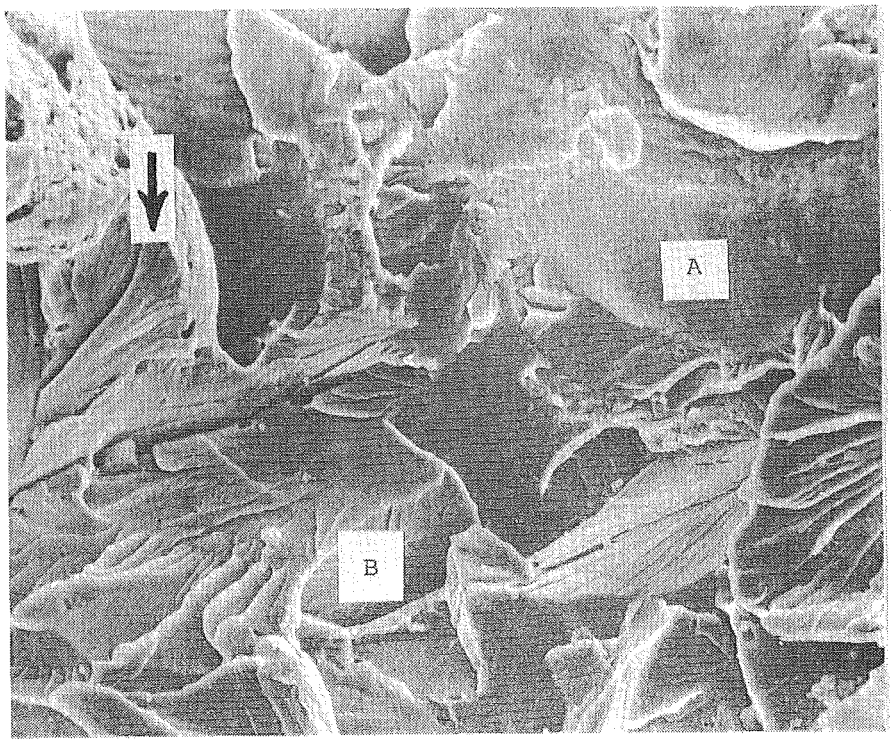

Figure 8.5: A transition area with "compression crack" facets (A) preceding cleavage facets (B), from the fracture of a 1.5d bend in 22 mm bar. x 1480. Arrow shows the direction of crack propagation.

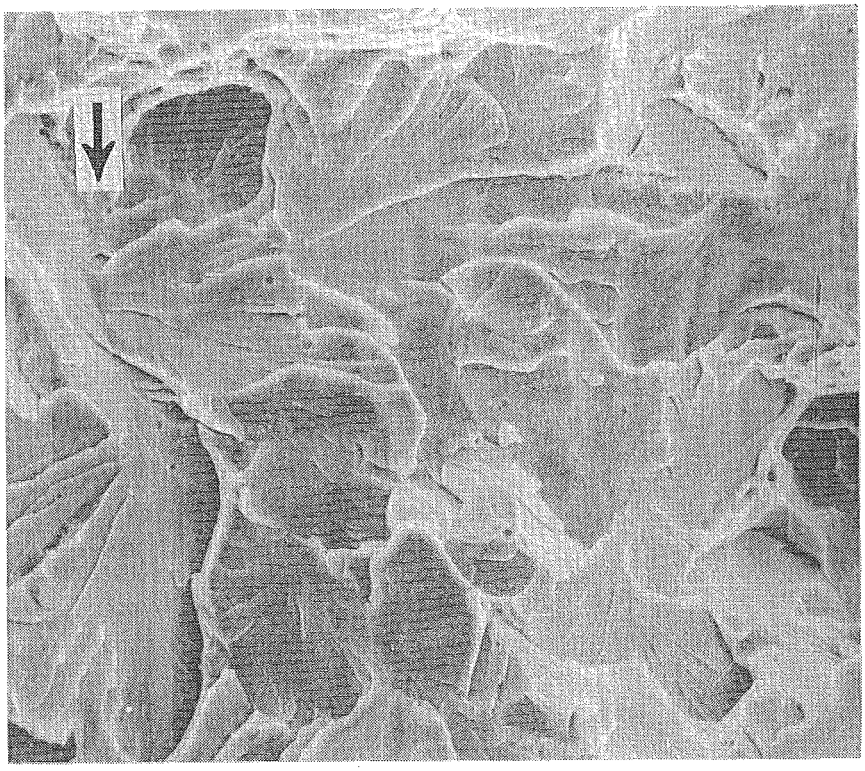

Figure 8.6: An area of high pre-strain adjacent to the compression crack, of the 3.5d bend, having a high density of 'river pattern' lines. x 1480. Arrow shows direction of crack propagation.

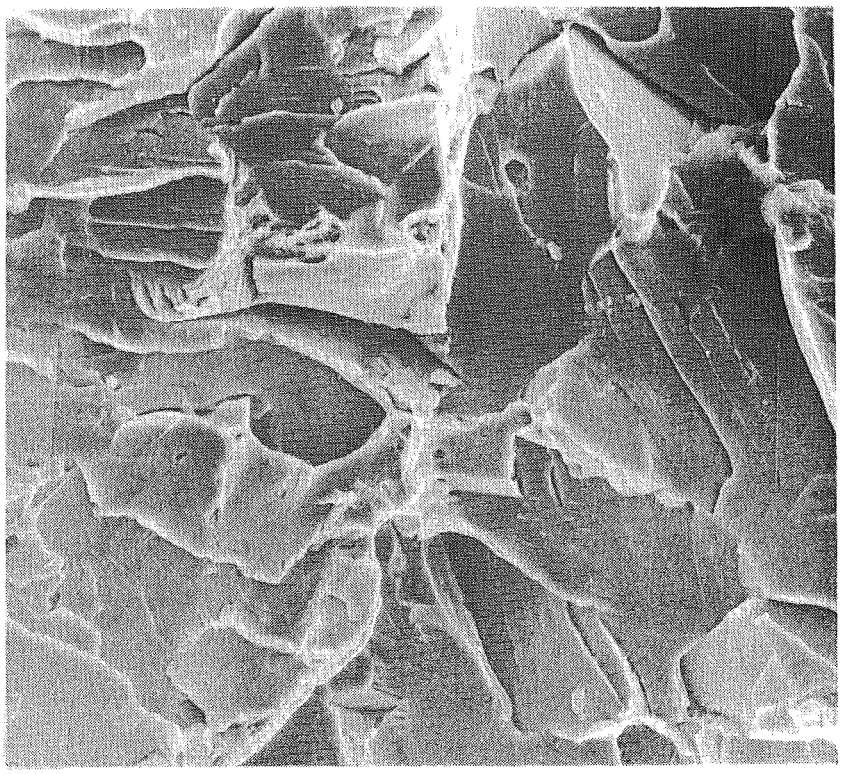

Figure 8.7: An area of low pre-strain close to the neutral axis of the 1.5d bend, having a low density of 'river pattern' lines. x 1480.

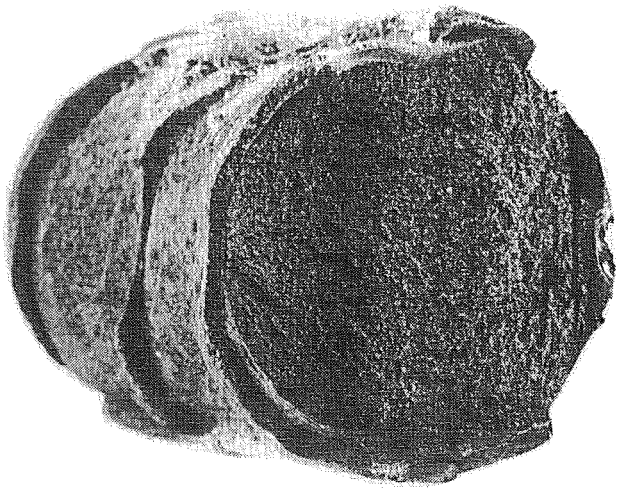

Figure 8.8: Cleavage fracture in 28 mm diameter deformed bar, showing crack nucleation area adjacent to flattened deformation.

(a) Decreasing the former diameter for a particular bar size increases the tendency to more severe cracking.

(b) Increasing the bar diameter at a constant former diameter/bar diameter ratio increases the tendency to more severe cracking, except in one instance (i.e., 22 mm bar of Grade 380 steel) due to a high initial fracture transition temperature.

(c) Cracking, whether by cleavage or ductile tearing, is always more severe after ageing, and the incidence of cleavage cracking increases after ageing. This is particularly noticeable in the tests conducted in the temprature range 0 - 4^{o}C.

(d) Decreasing the re-straightening temperature enhances cleavage fracture.

(e) Grade 380 steel in general has a greater tendency for cleavage fracture when compared with Grade 275 steel.

The trends (a) and (c) are consistent with the predictions that may be made from the results of strain age embrittlement obtained from V-notch Charpy impact testing, shown in Figure 7.3. Increasing the severity of the bend, i.e., decreasing the former diameter, results in an increase in the plastic strain at the inner surface radius of the bend from where the crack always initiates, and consequently increases the susceptibility of embrittlement both in the aged and un-aged conditions. These steels, which have sufficient 'active' nitrogen to cause natural strain ageing, (see Table 8.1), will have a higher transition temperature in the aged condition than in the un-aged state. The effect (d) is the normal fracture mode transition characteristic that is inherent in low carbon steels, and (e) results mainly from the higher initial (as-rolled) transition temperature of the Grade 380 steel[4], due to the higher carbon content of this steel (see Table 8.1).

A very important observation that resulted from these tests is that although the existing Standards (NZS 3402 P, 1973) for bend properties of deformed reinforcing bar are safe for the initial bend, they are in the critical range when considering the re-bend properties, especially at low temperatures that have to be encountered in service. The most critical cases being:

(a) the 28 mm diameter bar of the Grade 275 steel, and

(b) the 22 mm diameter bar of the Grade 380 steel.

NZS 3402 P specifies a minimum bend diameter of 3d for the bar (a) and 4d for the bar (b). The results (see Table 8.2(a) and 8.2(b)) show that these specified bend former diameters produced complete cleavage fractures in the lower temperature range. Although the bar (b) has a significantly higher nitrogen content (i.e. 0.0081%) than normally present in the New Zealand made reinforcing steels (produced by the BEA process), both steels are within the specifications of NZS 3402 P. Although the embrittlement tests were conducted only up to the 28 mm bar size, it is clear from the trend (b) that the specified minimum bend former diameters of 3d and 5d for 40 mm bar of Grades 275 and 380 respectively, (i.e., the largest bar size presently produced in New Zealand), will not be safe.

This is obviously the cause for construction site failures at bends in deformed reinforcing bar reported from many parts of New Zealand. In one such case where all the necessary information was available, a detailed study has been done[6]. These results and discussion show that both existing Standards NZS 3402 P, 1973, and NZS 1900, Chapter 9.3A, 1970 (a standard for structural concrete) are inadequate and should be modified so that such failures are eliminated in future.

8.5.2 Cleavage Fracture at Bends

The examination of complete fractures at bends (designated as (b)

obtained from the embrittlement test, showed that in each instance, fracture nucleation was from an area on the bend inner radius surface and adjacent to a deformation (rib), i.e., the deformation has acted as a tensile stress raiser for the nucleation of fracture. Figure 8.8 shows a typical fracture having the crack nucleation area adjacent to a flattened deformation. The mechanism of formation of the notch between the deformations (ribs) and the bar at the surface inner radius during making the initial bend, has been explained in detail[6]. This tendency for notch formation increases with decreasing bend former diamter, and with increase in bar size. In extreme cases "compression cracks" form between deformations and the bar, resulting from intensive localised shear due to compressive flattening of the deformations. A typical "compression crack" formed adjacent to a deformation on the inner radius surface of a 22 mm diameter deformed bar, is shown in Figure 8.1(b). In this instance, the crack formed when the bar was bent around a former of diameter 2.5d.

The investigation carried out on the construction site failures in bent deformed reinforcing bar has shown that the failures were by cleavage as a result of strain age embrittlement at the bend, usually associated with stress concentrations (notches) formed by the deformations on the bend inner radii surfaces, when the bend radii were increased[6]. The results from the embrittlement test confirm that cleavage fracture during re-straightening is enhanced by:

(a) decreasing the bend former diameter (D),

(b) subsequent ageing of the bend, and

(c) decreasing the re-straightening temperature,

and when the conditions below the notch are critical, cleavage fracture results. The smaller critical inner bend radius for the 28 mm bar of the Grade 275 steel, for the embrittlement test compared with the

construction site failures[6], i.e. 1.5d compared with 2.6d, results from the higher strain rate, due to the shock loading, applied on the bend at the construction site.

8.5.3 The Mechanism of Fracture

When a bend in deformed reinforcing bar is re-straightened or opened by increasing the bend radius, initial yielding initiates from the points of stress concentration, such as at the base of the deformations. This may be illustrated using a deformed bar rolled from a low carbon, high nitrogen steel, which is initially bent through 90^{o} around a former and then normalised at $910^{o}C$ for 30 minutes in order to relieve plastic deformation that is introduced during the initial bending, before finally re-straightening through a degree or two. The resulting yield zones can be revealed macroscopically by ageing the bend at $250^{o}C$ for 30 minutes and polishing a section that is cut along the longitudinal axis of the bend down to 400 grade emery paper, and macro-etching this section using Fry's reagent, see Figure 8.9. The darker regions show the yield zones. In this instance the steel used had a composition, 0.04% C, 0.2% Mn, 0.005% $A\ell_{sol}$, and 0.012% N, and was hot rolled to 24 mm deformed bar. The Fry's reagent used was a solution containing 45 gr of $CuCl_2$ dissolved in 100 ml of water and 180 ml of HCl. However, a bend that is not stress relieved as in the embrittlement test, will not have the identical yield zone pattern, due to the variation in the degree of hardening resulting from the initial bend.

When the bend is being opened out by decreasing the bend angle, the critical regions from the view point of cleavage are the notch root areas at the inner surface radii, as in addition to being the initial regions of plastic deformation which always precedes cleavage fracture[92, 93], they also create a triaxial stress system in the region, thus effectively increasing the tensile stress/shear stress ration which enhances cleavage

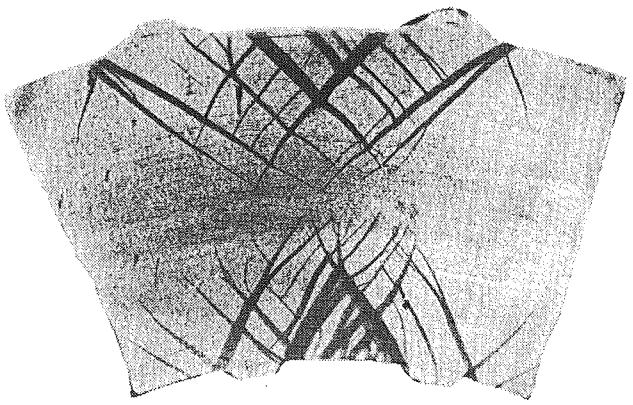

Figure 8.9: Localised plastic yielding from stress concentration points adjacent to deformations, of a 3d bend in 24 mm deformed bar, during the very initial stages of re-straightening.

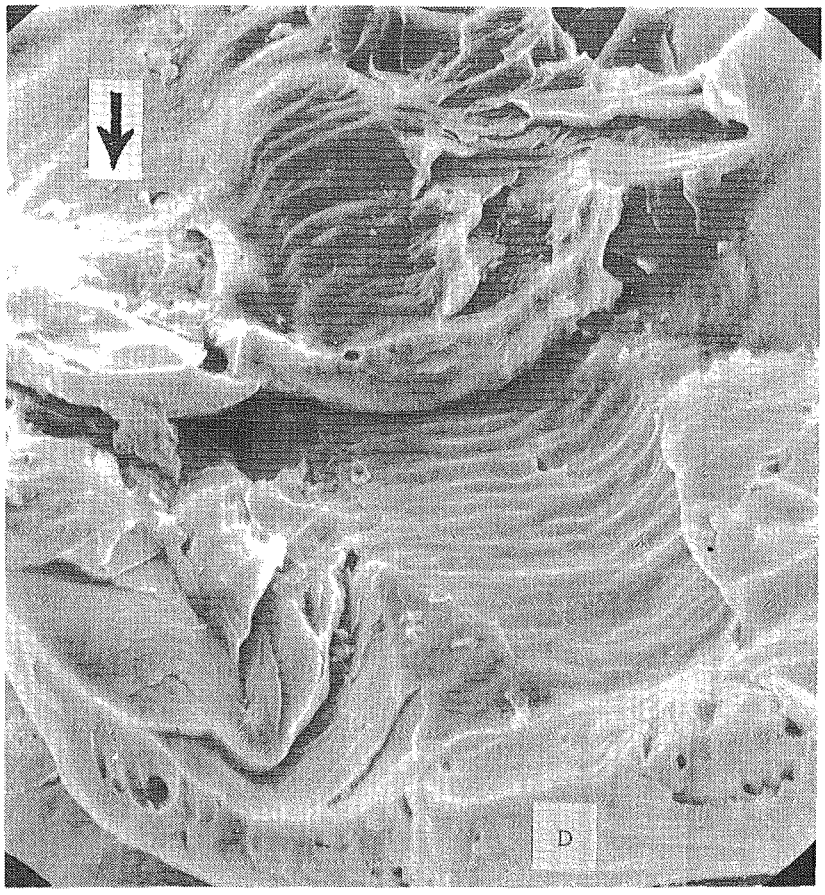

Figure 8.10: A "compression crack" area of the 1.5d bend with the fracture surface tilted 20°, showing areas of ductile tear (D) normal to the fracture surface. x 3350.
Arrow shows the direction of crack propagation.

fracture. Hence the behaviour of the bend during re-straightening is critically dependent on the conditions prevailing in the notch root area, i.e., if the transition temperature of this area is higher than the temperature of the bar, cleavage fracture may result, giving a fracture surface predominantly consisting of cleavage facets. In bends which result in the formation of "compression cracks" during initial bending, this critical area lies below the root of the compression crack, i.e., if cleavage fracture results it will initiate below the compression crack, generally showing a transition area from a compression crack to a predominantly cleavage fracture, see Figure 8.5.

The fine ductile tears seen in the compression crack facets (Figure 8.4) may form as a result of intensive localised shear that takes place during initial bending, and hence no plastic deformation occurs in these regions during opening out the bend (the region from B to C in Figure 8.2(a) appears to be such an area). However, in some regions of the compression crack, the ductile tearing may not be completed during initial bending, and hence result in ductile tears approximately normal to the fracture surface, that appear to have taken place during opening of the bend, see Figure 8.10. The fracture surface at C normal to the main crack in Figure 8.2(a) appears to be such an area. This form of ductile tearing probably takes place after the formation of the unstable cleavage crack below the compression crack.

The results of fracture profile examination (Figure 8.2) and fractrographic examination of specimens (a) and (b) show that a fracture which originally commences as a result of cleavage with limited plastic deformation may not propagate to give a complete cleavage failure. However, such fractures would be produced in the ductile to brittle fracture transition region and are undesirable in the cases of designed bends and hence must be avoided. Therefore, fracture criteria must be based on the prevailing condition at the notch root area or below the

"compression crack" whichever is the case.

8.5.4 Methods of Reducting the Susceptibility of Cleavage Fracture

Embrittlement at bends in cold bent reinforcing bar is a result of the combined effects of:

(a) the amount of plastic strain,

(b) subsequent ageing of the bend,

(c) the triaxial stress system (stress constraint) at the notch root, in the case of deformed bar,

(d) strain rate, and

(e) temperature at the bend, when decreasing the bend angle.

The results from the quantitative estimation of plastic strain at bends in reinforcing bar given in Table 8.3, are plotted with the former diameter/bar diameter ($^{D}/_{d}$) ratic for 20 mm plain bar, and 28, 22 and 16 mm deformed bar in Figures 8.11 to 8.14 respectively. Also shown in these figures is the theoretical curve for the compressive plastic strain in the tangential direction at the inner surface radii of the bends, obtained by Lubahn and Sachs[95], and may be expressed in the form:

$$\varepsilon_T = \frac{1 - K}{1 + K} \qquad 8.1$$

where $$K = \frac{^{D}/_{d}}{1 + \sqrt{(^{D}/_{d})^2 + 2\,(^{D}/_{d})}}$$

Results from the 20 mm plain bar (Figure 8.11) show that, in general, the experimental values for the plastic strain are lower, especially at the smaller $^{D}/_{d}$ ratios. This may be a result of:

(a) The strain estimation being done in a two-dimensional area outside the inner surface of the bend, while the theoretical solution gives the plastic strain at the inner surface radius.

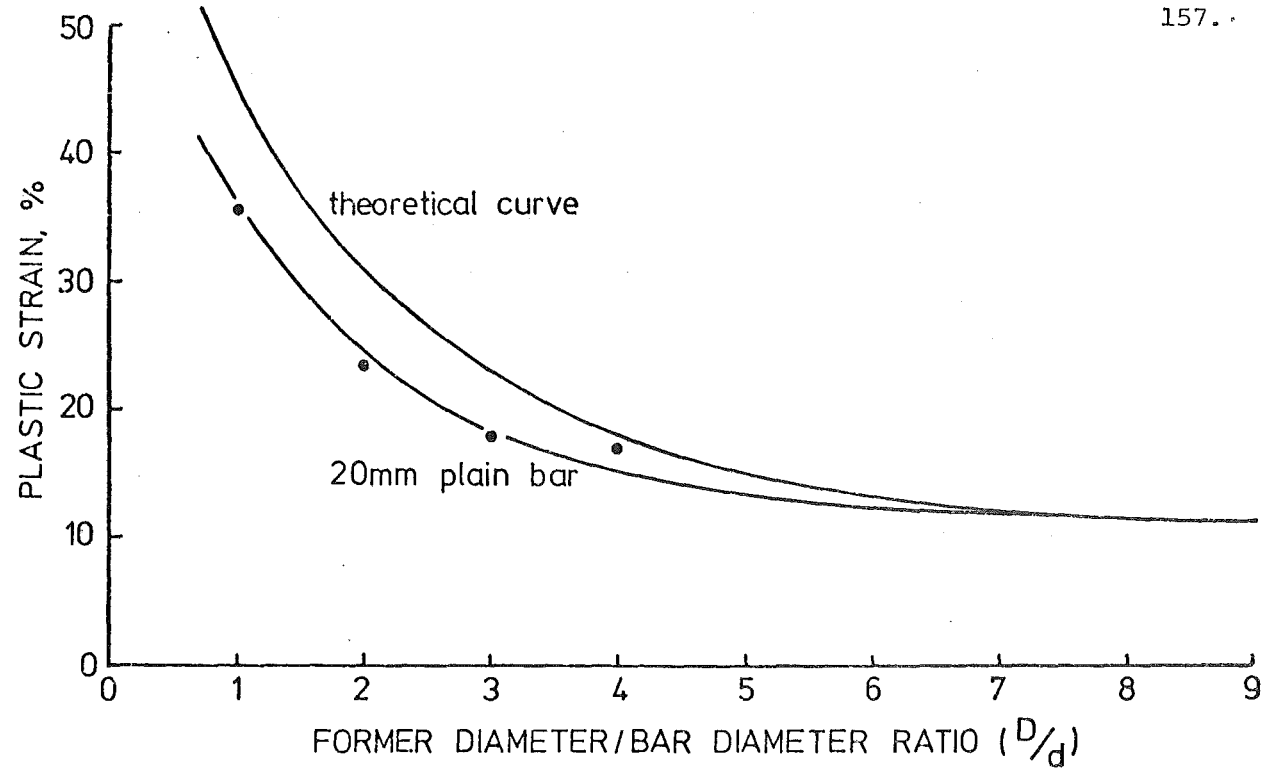

Figure 8.11: Variation in tangential plastic strain on bend inner radius surface of 20 mm diameter plain reinforcing bar, with former diameter/bar diameter ratio.

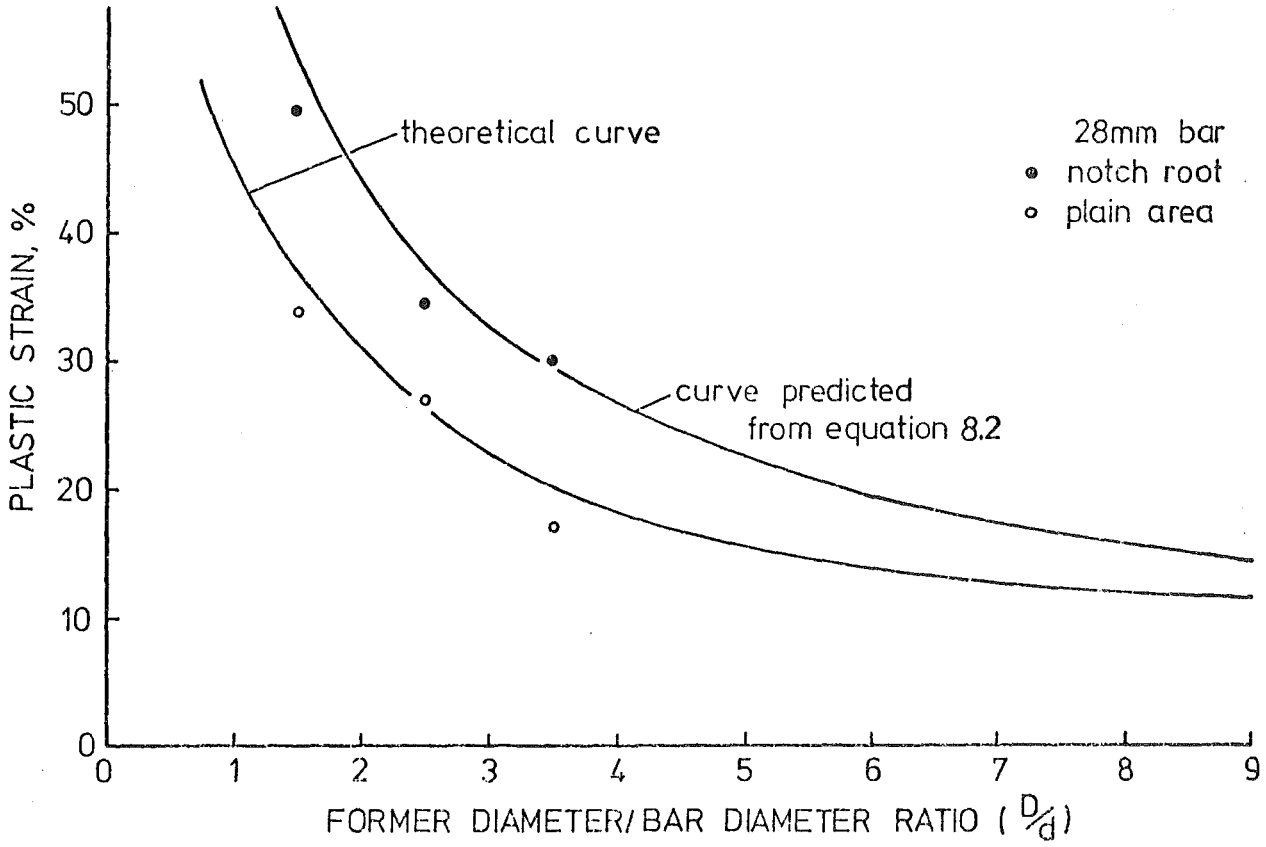

Figure 8.12: Variations in tangential plastic strain adjacent to deformations on bend inner radius surface, i.e. at the notch root, and on bend inner radius surface, i.e. on the plain area between adjacent deformations, with former diameter/bar diameter ratio, for 28 mm deformed reinforcing bar.

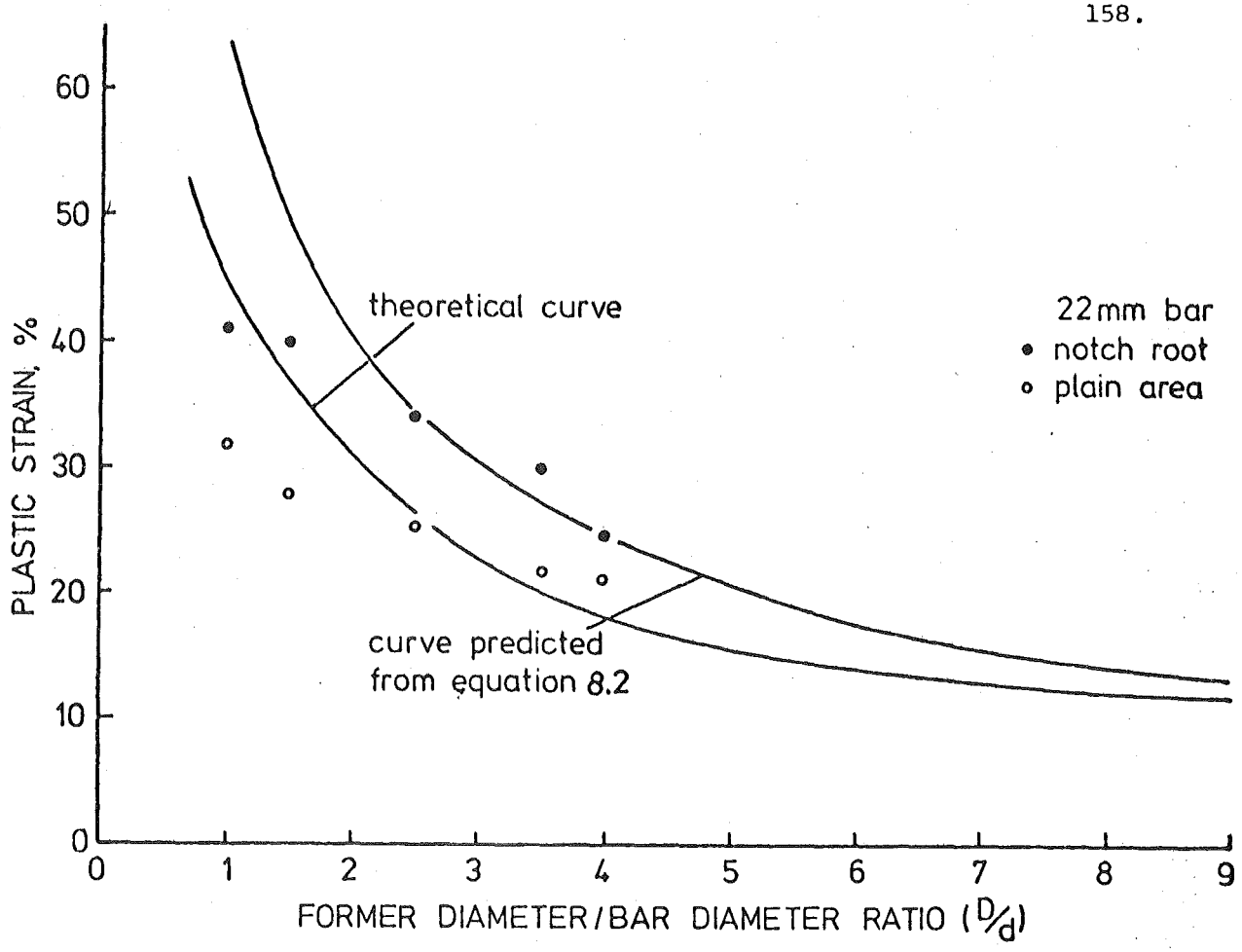

Figure 8.13: Variation in tangential plastic strain with former diameter/ bar diameter ratio for 22 mm deformed bar, both at the notch root and bend inner radius surface.

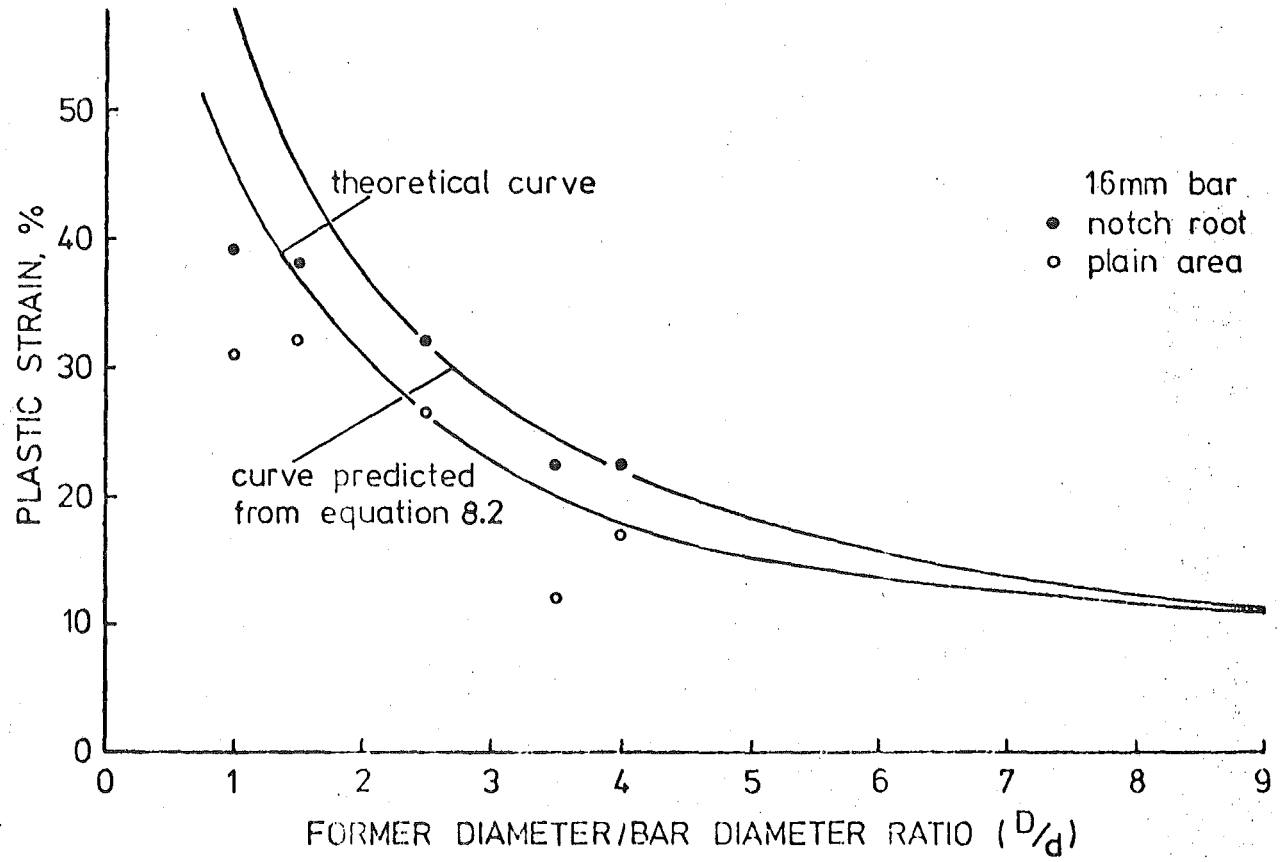

Figure 8.14: Variation in tangential plastic strain with former diameter/ bar diameter ratio for 16 mm deformed bar, both at the notch root and bend inner radius surface.

(b) The deviation from plain strain conditions in regions adjacent to the inner surface radius, which has been assumed in the method used for quantitative estimation of the plastic strain.

Both these effects have a greater significance when the $^{D}/_{d}$ ratio decreases, i.e., when the tangential strain increases.

Figures 8.12 to 8.14 show that the plastic strain below the notch root (or below the compression crack) increases with the decrease in $^{D}/_{d}$ ratio as would be expected, and also that, in general, it is greater than the corresponding theoretical value for a plain bar. These figures also show that the plastic strain at the notch root increases with bar diameter at constant $^{D}/_{d}$ ratio, i.e., at a constant value of $^{D}/_{d}$, the increase in bar diameter (d) causes increased localised shear below the notch root. Hence the compressive plastic strain below the notch root appears to be a function of:

(a) The corresponding theoretical strain at the inner surface radius of a plain bar (ε_T).

(b) The severity of the bend, i.e., the $^{D}/_{d}$ ratio.

(c) The nominal bar diameter (d).

Taking the above factors into consideration, an analytical expression for the plastic strain below the notch root (ε) was derived to obtain a close fit to the experimental data, resulting in the expression given below:

$$\varepsilon = \varepsilon_T + 0.7\ (^{d^2}/_{D}) + 0.2d - 3 \qquad 8.2$$

The curves obtained from the above expression are shown in Figures 8.12 to 8.14. When the experimental data and the corresponding predictions from Equation 8.2 were subjected to a statistical analysis, the results showed that correlation exists at the 99% confidence limits. The results from the plastic strain estimations made without assuming plain

strain conditions appear to fit the predicted curves from Equation 8.2 (see Appendix C). Although Equation 8.2 appears to give conservative predictions at the smaller $^{D}/_{d}$ ratios, this is a desirable result, because

(a) figure 8.11 shows that the experimental results give lower values at the smaller $^{D}/_{d}$ ratios, and

(b) in areas of intensive localised shear, as for example, below compressive cracks, the quantitative estimations become very approximate.

The dependence of the compressive plastic strain in the tangential direction, at the notch root on bar diameter (d) at constant $^{D}/_{d}$ ratios, may be the cause for trend (b) obtained from the embrittlement test results (Section 8.5.1).

Figure 7.3 shows that increasing the plastic strain produces a steady increase in the degree of strain age embrittlement both in the aged and non-aged conditions. Hence, one method of reducing the susceptibility of cleavage fracture at bends is to reduce the plastic strain at the notch root area, which may be done by increasing the bend radius. Another feasible method is to produce a non-strain ageing steel, as subsequent ageing after plastic straining brings about a further increase in the degree of embrittlement. The formation of notches between the bar and the deformations at the inner surface radius, during initial bending, cannot be avoided unless extremely large bend radii are used. Increasing the sharpness of the notch beyond a critical geometry may not cause any additional deteriorating effects on embrittlement as a result of the plastic deformation that occurs at the notch root before the growth of the unstable cleavage crack, i.e., the stress constraint below the notch root is not affected beyond a critical notch root geometry in slip-initiated cleavage. Finally, the contributory

causes (d) and (e) are predominantly governed by natural conditions, namely the characteristics of seismic ground motions and the environment temperature, when considering bends in reinforcing bar that are embedded in reinforced concrete structures.

It is clearly evident from the previous sections of this discussion that the existing standards for designed minimum bend radii of reinforcing bar used by constructors in the field, as well as those specified for bend tests, needs critical investigation and that such an investigation should be based on the prevailing conditions below the notch root area. Using available data on the plastic strain below the notch root, i.e., Equation 8.2, the increase in the fracture transition temperature with plastic strain (Figure 7.3) and the as-rolled transition temperature, in conjunction with results from a construction site failure at bends in deformed reinforcing bar[6], an attempt has been made to determine safe bend radii for deformed reinforcing bar, to be used when detailing reinforcements in concrete structures in order to avoid failure by strain age embrittlement (see Appendix C). Also determined in this paper (Appendix C) are the bend former diameters to be used as a test for strain age embrittlement in deformed reinforcing bar, using the results from the slow bend embrittlement test. These determinations show that, although the existing standards for minimum bend radii (i.e., NZS 1900 9.3A (1970) and ACI 318-71) specify safe values for smaller bar sizes (i.e. up to 28 mm in Grade 275 and 20 mm in Grade 380), they appear to be unsafe at larger bar sizes. Based on these determinations, recommendations are made for the modification of the existing standards (see Appendix C). NZS 1900 9.3A and ACI 318-71 Standards specify different bend radii for stirrups, tie hooks, etc. which are generally smaller than the corresponding standard bends; however the determinations made are applicable to all deformed bars independent of their use. Hence, when smaller bend radii are required, as may be in the case of stirrups, plain bar may have to be used, because

the susceptibility of cleavage fracture is immensely reduced as a result of the absence of the triaxial stress constraint.

This paper (Appendix C) also shows the advantages of non-strain ageing reinforcing steels as they may be bent to smaller safe bend radii, especially for larger bar sizes, compared with the corresponding normal reinforcing steels, as a result of the lower increase in transition temperature (ΔT_{27}) and the lower as-rolled transition temperature. To ensure that all reinforcing bars are safe at the recommended bend radii to be used when detailing reinforcements in concrete structures, a V-notch Charpy impact test has been specified for the as-rolled steels.

Other possible methods of reducing the susceptibility of cleavage fracture at bends in deformed reinforcing bar are:

(a) by giving a stress relieving treatment in the bend area, by heating them to 650° - 700°C; or

(b) grinding off the deformations on the bend inner radius *before* making the initial bend.

Both these methods are not feasible operations to be carried out as a standard practice; however, they may be used in special instances when the earlier methods suggested cannot be used.

CHAPTER 9

CONCLUSIONS AND RECOMMENDATIONS

9.1 The Significant Effects of Strain Ageing

9.1.1 The Effect of Increase in Yield Strength

To ensure the formation of the 'plastic hinge' on the beam adjacent to the beam-column joint during earthquake loading on a reinforced concrete structure, use is made of an 'overstrength' factor at the potential plastic hinge[1]. The overstrength factors presently used range from 1.2 to 1.3[1, 5]. As well as determining the flexural strength of the column, this factor also determines the necessary transverse reinforcement both for the column and the beam to prevent the possibility of brittle shear failure.

Strain ageing of the flexural steel at the plastic hinge subsequent to the initial formidable seismic loading may increase the yield strength of the steel by approximately 70 MN/m^2. As the steel used at present for flexural reinforcement in beams is of Grade 275[5], this increase in yield strength can increase the flexural strength by a factor of 1.25. Hence the overstrength factor used at present may not be sufficient when consideration is given to the possibility of strain ageing in flexural steel. However, increasing the overstrength factor above what is presently used will further increase the reinforcement of the present heavily reinforced strong column-weak beam joint as well as being an expensive exercise.

9.1.2 The Effect of Strain Age Embrittlement

When considering the ductility requirements from a reinforcing steel to be used in earthquake resistant reinforced concrete structures, it is clear from this investigation that the existing standards for minimum bend radii in deformed reinforcing bar are inadequate. Recommendations have been made for safe bend radii in deformed reinforcing bar, to be used when detailing reinforcements in concrete structures (see Appendix C). These

recommended minimum bend radii are strictly applicable in all bending practices, i.e., both for longitudinal and transverse reinforcing steels. When it is essential to use smaller bend radii as may be in the case of stirrups, it is recommended that plain bar be used. However, in certain regions of the structure, the use of plain bar for transverse reinforcement may not be advisable[1]; for example, in columns close to the column-beam joint, where there is always a possibility of formation of a plastic hinge which may result in an anchorage failure, if plain bar is used.

The effect of welding at or near bends cannot be completely predicted from the data available from this investigation. As strain ageing is both a time and temperature dependent process, to study the effect of welding bent reinforcing bar from the viewpoint of strain age embrittlement at bends, a time-temperature history at the bend is required. With this data it will be possible to predict the effect of welding at or near bends using the relation between increase in the fracture transition temperature (ΔT_{27}) and ageing temperature - ageing time combinations (Figures 7.12 and 7.13). However, when welding close to bends in Grade 275 reinforcing bar, the long term effect may be the same as for natural ageing, as there appears to be a minimum degree of strain age hardening above which the fracture properties are not significantly affected, and this minimum degree is achieved by natural ageing of this steel.

A very important result of this investigation is that: strain age embrittlement, combined with the stress constraint at the notch roots in the inner surface radii of bends, i.e., the development of the triaxial stress system together with a stress concentration at the notch, can cause brittle (cleavage) fracture during service. This fact must be brought to the knowledge of all structural engineers, so that both in design and in detailing of reinforcement, consideration is given to the effects of strain age embrittlement of bent reinforcing bar in order that such failures are

eliminated; for example, minimise the use of sharp bend radii in critical regions of the structure.

9.2 The Advantages of Non-Strain Ageing Steels

9.2.1 The Effect of Increase in Yield Strength

Although natural strain ageing cannot be completely eliminated by the addition of nitride formers due to the residual nitrogen and any carbon in solid solution at atmospheric temperature, the increase in yield strength is limited to 10 - 15 MN/m^2. This increase is insignificant when compared to approximately 70 MN/m^2 that results from natural strain ageing in normal reinforcing steels, and hence the overstrength factor that is used at present may be sufficient to account for any strain ageing of flexural reinforcement, when using non-strain ageing steels.

9.2.2 The Effect of Strain Age Embrittlement

This investigation has shown that strain age embrittlement (i.e., the increase in fracture transition temperature) has been considerably reduced in non-strain ageing steels. The difference in strain age embrittlement, between a non-strain ageing steel and a similar normal reinforcing steel, is steadily increased with increases in plastic strain. As a result of this difference, smaller safe bend radii may be used when using non-strain ageing deformed reinforcing bar. Recommendations have been made for minimum bend radii for non-strain ageing reinforcing steels to be used in detailing reinforcements in concrete structures (see Appendix C).

The smaller bend radii that may be used in non-strain ageing deformed reinforcing bar makes it possible for them to be used in stirrups on more occasions than when using the correponding normal deformed reinforcing bar. This is an extremely desirable proposition, especially in regions where anchorage of transverse reinforcement is essential.

Welding at or near bends in non-strain ageing reinforcing bars can

have an undesirable effect on strain age embrittlement even in the long term, as natural ageing in non-strain ageing steels causes negligible effect on the fracture properties, as the minimum degree of strain age hardening is not achieved, while ageing at elevated temperatures for sufficient time achieves this minimum degree. However, for a more accurate prediction, a temperature-time history at the bend is required.

Although titanium and vanadium additions have produced reinforcing steels with negligible strain ageing, they are susceptible to some degree of strain age embrittlement when aged at 100°C. Also this susceptibility is increased with increases in plastic strain. As these results cannot be quantitatively explained at present, it would be appropriate to check them from a normal reinforcing steel and the corresponding non-strain ageing steel, where testing is carried out with a minimum degree of ageing practically possible by holding the specimens at low temperature to eliminate ageing between plastic straining and testing. Other valuable data could be obtained by the relationship between ΔT_{27} and plastic pre-strain for the same steels after natural ageing, as well as at a higher ageing temperature when the non-strain ageing steel is expected to have sufficient interstitials to provide the necessary minimum degree of strain age hardening. As the derivation of safe bend radii for Grade 380 steel and the corresponding titanium bearing steel (classified as Grade 415) given in Appendix C, has been based on the ΔT_{27} vs plastic pre-strain relationship for the Grade 275 steel and the corresponding titanium bearing steel, and it is essential that this relationship be checked for the previous steels.

9.3 Comparison of the Elements that may be used to Prevent Strain Ageing

In Chapter 4, a comprehensive discussion has been made on the methods available for reducing or preventing natural strain ageing in as-rolled low carbon steels. The results of this discussion may be summarised as follows:

(a) Alloying elements normally present in reinforcing steels have no effect on

strain ageing characteristics in the quantities that they are present in as-rolled steels. Although heat treatments may alter these effects, for example, normalising the as-rolled steel at 900°C may reduce strain ageing to a negligible level, these processes are not feasible economically.

(b) The best method would be to use a strong nitride former which combines with the nitrogen present in the steel independent of the processing conditions. The best elements for this purpose appeared to be titanium, vanadium, and boron; although Nb is a nitride former, it is required in larger quantities as it forms the carbide in preference to the nitride. However, the use of boron causes problems during hot-rolling of the steel.

The addition of titanium and vanadium to normal reinforcing steels has shown that both these elements are capable of reducing strain ageing to a negligible level when added in sufficient quantities. However, titanium is the stronger nitride former, as titanium slightly in excess of the TiN stoichiometric requirement is sufficient to precipitate almost all the nitrogen as TiN, while vanadium well in excess of the VN stoichiometric ratio is required for this purpose.

Optimum titanium additions, i.e. titanium requirement for TiN stoichiometric composition, also have other advantages for a reinforcing steel to be used in earthquake resistant reinforced concrete structures. This titanium content gives grain refinement which results in a larger Luder's strain when compared with the normal steel, and is partially responsible for the lowering of the as-rolled fracture transition temperature. As the overstrength factor is used to account for factors that may cause strength increase, one of which is additional steel strength due to strain hardening at large deformation[1], a larger Luder's strain reduces the possibility of overstrength, which is a desirable event at plastic hinges. The reduction of the as-rolled transition temperature further reduces the susceptibility of brittle (cleavage) fracture at bends in deformed reinforcing bar. As the present Grade 380 steel has only a very limited Luder's strain (i.e. a yield strain of approximately 0.5%[4]) it is not being used for

reinforcement in earthquake resistant structures[5], especially as longitudinal reinforcement in flexural members designed for plastic hinge formation. However, the optimum titanium addition to this steel increases the Luder's strain considerably (i.e., to approximately 1.3%[4]), and hence it may be used for longitudinal reinforcement of flexural members designed for plastic hinges. The production of such a steel has tremendous economic advantages in addition to many other desirable results; for example, the reduction in reinforcement steel content in regions that are at present heavily reinforced, such as the column-beam joint.

Although sufficient addition of vanadium does reduce strain ageing to a negligible level, this optimum level of vanadium increases the as-rolled fracture transition temperature by approximately $7^{o}C$. This increase in transition temperature, although generally an undesirable change for a reinforcing steel, will not cause any serious embrittlement in the as-rolled steel, i.e., the ductility requirements for a reinforcing steel to be used in earthquake resistant structures are not seriously affected by such an increase in the as-rolled transition temperature when the other advantages such as the reduction in strain age embrittlement, increase in yield strength, are taken into consideration. This vanadium content has little effect on the Luder's strain when compared with the value for normal reinforcing steel. Therefore, vanadium additions also produce a reinforcing steel with better properties than the corresponding normal reinforcing steel. However, the major benefit of vanadium addition, i.e. grain refinement, appears only to be obtained by controlled rolling.

This investigation has proved that controlled titanium additions provide the best solution for producing a hot-rolled reinforcing steel that has the most desirable properties that would be required from a steel used for reinforcement of earthquake resistant concrete structures. Therefore, it is strongly recommended that steps be taken for the immediate trial commercial production of this steel.

REFERENCES

1. PARK, R., and PAULAY, T., "Reinforced Concrete Structures", John Wiley & Sons, New York, 1975.
2. BAIRD, J.D., Iron & Steel, vol.36, 1963, pp.186, 326, 368, 400.
3. BAIRD, J.D., Metallurgical Rev., vol.16, 1971, p.1.
4. SMAILL, J.S. *et al*, Metals Technology, vol.3, 1976, p.194.
5. PARK, R., Proc. 27th Conf. of the Australian Institute of Metals, Christchurch, New Zealand, 1974, p.136.
6. ERASMUS, L.A., and PUSSEGODA, L.N., New Zealand Engineering, vol.32, 1977, p.178.
7. FAHY, F.W., and ERASMUS, L.A., Engineering Metallurgy Seminar Notes, University of Canterbury, New Zealand, 1967.
8. COTTRELL, A.H., and BILBY, B.A., Proc. Phy. Soc., vol.A62, 1949, p.49.
9. HALL, E.O., "Yield Point Phenomena in Metals and Alloys", MacMillan, London, 1970.
10. PETCH, N.J., Journ. Iron & Steel Inst., vol.174, 1953, p.25.
11. FISHER, R.M., Ph.D. Thesis, Cambridge University, 1961.
12. COTTRELL, A.H., "The relation between structure and mechanical properties of metals", N.P.L. Symp., No.15, H.M.S.O., 1963, p.456.
13. WILSON, D.V., Acta. Met., vol.16, 1968, p.743.
14. NACKEN, M., and HELLER, W., Arch. Eisenh., vol.27, 1956, p.45.
15. WILSON, D.V. and RUSSELL, B., Acta. Met., vol.8, 1960, p.468.
16. WILSON, D.V., and RUSSELL, B., *ibid*, vol.8, 1960, p.36.
17. THOMAS, W.R., and LEAK, G.M., Proc. Phy. Soc., vol.B68, 1955, p.1001.
18. LEAK, G.M., Iron & Steel Inst., Spec. Rep. No.68, 1960, p.270.
19. MORGAN, E.R., and SHYNE, J.C., Trans. AIME, vol.209, 1957, p.65.
20. KOSTER, W., *et al*, Arch. Eisenh., vol.25, 1954, p.567.
21. KOSTER, W., and KAMPSCHULTE, G., *ibid*, vol.32, 1961, p.809.
22. BUTLER, J.F., Trans. Metallurgical Soc. AIME, vol.224, 1962, p.89.
23. LOW, J.R., and GENSAMER, M., Trans. AIME, vol.58, 1944, p.207.
24. STEPHENSON, E.T., and COHEN, M., Trans. ASM, vol.54, 1961, p.72.

25. WILSON, D.V., Acta. Met., vol.5, 1957, p.293.

26. HUNDY, B.B., Journ. Iron & Steel Inst., vol.178, 1954, p.127.

27. TARDIF, H.P., and BALL, C.S., *ibid*, vol.182, 1956, p.9.

28. WILSON, D.V., and OGRAM, G.R., *ibid*, vol.206, 1968, p.911.

29. HUNDY, B.B., Metallurgia, vol.53, 1956, p.203.

30. HUNDY, B.B., Journ. Iron & Steel Inst., vol.178, 1954, p.34.

31. ERASMUS, L.A., Ph.D. Thesis, University of Cape Town, South Africa, 1972.

32. BERGSTRÖM, Y., Materials Sci. Eng., vol.9, 1972, p.101.

33. COTTRELL, A.H., Trans. Metallurgical Soc., AIME, vol.212, 1958, p.192.

34. PETCH, N.J., Phil. Mag., vol.3, 1958, p.1089.

35. LIEBOWITZ, H., Ed., "Fracture", vol.6, Adacemic Press, New York, 1969.

36. ERASMUS, L.A., M.Sc. Thesis, University of Cape Town, South Africa, 1971.

37. HESLOP, J., and PETCH, N.J., Phil. Mag., vol.3, 1958, p.1128.

38. KOCHENDÖRFER, A., *et al*, Int. Journ. of Fracture, vol.11, 1975, p.365.

39. DE KAZINCZY, F., and AXNÄS, A., Jernkont. Ann., vol.147, 1963, p.931.

40. ENRIETTO, J.F., Journ. Iron & Steel Inst., vol.204, 1966, p.252.

41. RITCHIE, I.G., and RAWLINGS, R., Acta. Met., vol.15, 1967, p.491.

42. LEAK, D.A. *et al*, *ibid*, vol.3, 1955, p.501.

43. ROBERTS, W., *et al*, Journ. Iron & Steel Inst., vol.210, 1972, p.931.

44. LEE, R. McL., and PARLANE, A.J.A., Proj. Report, Department of Mechanical Engineering, University of Canterbury, New Zealand, 1970.

45. BIRKBECK, G., Journ. Iron & Steel Inst., vol.206, 1968, p.909.

46. GLADMAN, T., Proc. Roy. Soc., vol.294A, 1966, p.298.

47. GLADMAN, T., and PICKERING, F.B., Journ. Iron & Steel Inst., vol.205, 1967, p.653.

48. ERASMUS, L.A., *ibid*, vol. 202, 1964, p.32.

49. KÖING, P., *et al*, Arch. Eisenh., vol.32, 1961, p.541.

50. ERASMUS, L.A., Iron & Steel, vol.39, 1966, p.477.

51. GLADMAN, T., and DULIEU, D., Metal Science, vol.8, 1974, p.167.

52. MORGAN, E.R., and SHYNE, J.C., Journ. Iron & Steel Inst., vol.185, 1957, p.156.

53. MORGAN, E.R., and SHYNE, J.C., Trans. AIME, vol.209, 1957, p.781.

54. CODD, I., and PETCH, N.J., Phil. Mag., vol.5, 1960, p.30.

55. FOUNTAIN, R.W., and CHIPMAN, J., Trans. AIME, vol.224, 1962, p.599.

56. BUTLER, T.F., *ibid*, vol.224, 1962, p.84.

57. SHOENBERGER, L.R., Trans. Metallurgical Soc. AIME, vol.212, 1958, p.402.

58. CHAN, B.K., Proj. Report (MM/69/76), Department of Mechanical Engineering, University of Canterbury, New Zealand, 1976.

59. COMSTOCK, G.F., Sheet Metal Industries, vol.20, 1943, pp.1527, 1723

60. IRVINE, K.J., *et al*, Journ. Iron & Steel Inst., vol.205, 1967, p.161.

61. GEORGE, T.J., and IRANI, J.J., Journ. Australian Inst. Metals, vol.13, 1968, p.94

62. SHIRAIWA, T., *et al*, Trans. Iron & Steel Inst. Japan, vol.10, 1970, p.406.

63. RASHID, M.S., Metallurgical Trans., vol.6A, 1975, p.1265.

64. WEISS, H., *et al*, Journ. Iron & Steel Inst., vol.211, 1973, p.703.

65. GEORGE, T.J., and IRANI, J.J., BISRA Report No. MG/C/32/68.

66. BASHFORD, G., and GEORGE, T.J., BHP Technical Bull., vol.15, 1971, p.18.

67. GEORGE, T.J. and KENNON, N.F., Journ. Australian Inst. Metals, vol.17, 1972, p.73.

68. SAGE, A.M., and EVANS, D.W., "Vanadium structural steels" - a review of Pub. Literature on the structure and properties of as-rolled and normalised steels, Pub. Highweld Steel & Vanadium Corp., London, 1970.

69. FOUNTAIN, R.W., and CHIPMAN, J., Trans. AIME, vol.212, 1958, p.737.

70. STEPHENSON, E.T., *et al*, Trans, ASM, vol.57, 1964, p.208.

71. ERASMUS, L.A., Journ. Iron & Steel Inst., vol.202, 1964, p.128.

72. EPSTEIN, S., *et al*, Journ. Metals, vol.188, 1950, p.830.

73. FRAME, J.W., and SCHUNK, F.B., "Deep drawing steels", IMD Spec. Rep. Series No.6, AIME, 1958, p.57.

74. JONES, W., and COOMBS, G., Journ. Iron & Steel Inst., vol.174, 1953, p.9.

75. CHAPMAN, J.A., and PHILLIPS, R., BISRA Report No. MG/C/104/65.

76. BAKER, T.N., Journ. Iron & Steel Inst., vol.211, 1973, p.502.

77. KUBOTA, H., Nippon Kokan Tech. Report - Overseas, Dec.1971, p.23.

78. COREDA, J.N., and HOOK, R.E., Metallurgical Trans., vol.1, 1970, p.111.

79. KOZASU, I., *et al*, Trans. Iron & Steel Inst. Japan, vol.11, 1971, p.367.

80. KOAZSU, I., *ibid*, vol.12, 1972, p.241.

81. MORRISON, W.B., Journ. Iron & Steel Inst., vol.201, 1963, p.317.

82. JONES, R.D., and ROTHWELL, A.B., Iron & Steel Inst. Publication 108, 1968, p.78.

83. LE BON, A., *et al*, Metal Science, vol.9, 1975, p.36.

84. SAGE, A.M., and COPLEY, F.E., Journ. Iron & Steel Inst., vol.195, 1960, p.422.

85. STUART, H., *et al*, BISRA Reports No . MG/C/54/69 and MG/C/55/69.

86. CHONG, C.J., and LIM, K.H., Proj. Report (MM/3/74), Department of Mechanical Engineering, University of Canterbury, New Zealand, 1974.

87. The United Steel Companies Ltd, Research & Development Dept., Swinden Labs, Moorgate, Rotherham, England, Jan.1962, Ref.No.A.3763/-/62.

88. SAGE, A.M., Metals Technology, vol.3, 1976, p.65.

89. RASHID, M.S., Metallurgical Trans., vol.7A, 1976, p.497.

90. KAWAMURA, K., *et al*, Trans. Iron & Steel Inst. Japan, vol.14, 1974, p.347.

91. GROOM, J.D.G., and KNOTT, J.F., Metal Science, vol.9, 1975, p.390.

92. KNOTT, J.F., and COTTRELL, A.H., Journ. Iron & Steel Inst., vol.201, 1963, p.249.

93. KNOTT, J.F., *ibid*, vol.204, 1966, p.104.

94. FONG, K.Y., Proj. Report (45/77), Department of Mechanical Engineering, University of Canterbury, New Zealand, 1977.

95. LUBAHN, J.D., and SACHS, G., Trans. ASME, vol.72, 1950, p.201.

APPENDIX A

A.1 Determination of Titanium, Vanadium and Aluminium in Steel*

A.1.1 Summary of the Method

Drillings from a sample are dissolved in HNO_3/HCl mixture and the silicon is precipitated and filtered off after fuming with $HClO_4$. (This process will not dissolve Al_2O_3 and possibly about 15-20% of titanium in the form of TiN.) Most other interfering elements are removed from the dilute acid solution by a mercury cathode separation. The titanium and vanadium is then precipitated with cupferron and extracted into amyl acetate. The organic phase is separated and stabilised by triethanolamine solution in ethonol. The aqueous phase is buffered to a pH of between 4.5 and 5.0 and the aluminium is extracted with cupferron into amyl acetate. The organic extract is stabilised by triethonalamine in ethonol. Finally, these organic extracts are used for the determination by AA spectrophotometry.

A.1.2 Procedure

An accurately weighed gram of the steel sample was dissolved in a mixture of 20 ml of 5N HNO_3 and 10 ml of 6N HCl by warming. This solution was boiled down to about two-thirds of the original volume and 12-13 ml of conc. $HClO_4$ was added. The 250 ml beaker containing this solution was covered with a watch glass and heated to fumes and continued fuming for about 5 minutes with clear vapour refluxing on the sides of the beaker after which the solution was removed from the heat and allowed to cool. The salting out which occurs during cooling, is dissolved by adding about 25 - 30 ml of water. The silicon was removed by filtering this warm solution. The filtrate was transferred to a mercury cathod cell containing about 25 ml of mercury and electrolysed using a 6-8 volt supply at 5 - 10 amps until the iron was removed. (Test for iron in solution using 10% W/v potassium thiocynate.) The electrolyte was then transferred to

a 100 ml separating funnel and any remaining mercury was removed.

2 ml of 6% cupferron solution was added to the cool solution in the separating funnel followed by exactly 10 ml of amyl acetate. After shaking the solution the two phases were allowed to separate. The aqueous phase was collected in a 200 ml separating funnel for aluminium determination (when necessary). The organic phase was washed with 20 ml of 4% $HClO_4$ and after the phases separated, the aqueous phase was removed. After removing all traces of water in the organic phase, it was collected in a dry 25 ml glass vial and stabilised immediately by adding 2 ml of 4.5% W/W triethonalamine solution in ethonol. This solution was kept for determination of titanium or vanadium. To the aqueous phase in the 200 ml separating funnel 8 - 12 ml of mixed acetate solution was added followed by 3 to 4 drops of bromophenyl blue indicator. To this solution 5N ammomia solution was added until the first appearance of pale blue, and the strength was adjusted so that the pH lies between 4.5 and 5.0 using pH paper. From then on the process was identical to the preparation of the stabilised extract of titanium or vanadium except that the organic phase was washed with 25 ml of acetate buffer solution.

A range of organic standards was prepared for each element from a standard solution of that element depending on the expected contents of that element in the steel analysed. The AA spectrophotometer was set up to give the maximum response for the particular element and then the zero adjusted with ethonol. The stabilised organic samples were then nebulised and the readings noted. Another set of readings was taken by nebulising the same samples in the reverse order. From the mean readings, the element content was determined.

* This method has been developed by:

D. Somerville,
Senior Technician,
Department of Mechanical Engineering,
University of Canterbury.

A.2 The Determination of Nitrogen in Steel

A.2.1 Summary of the Method

(a) Determination of Soluble and Insoluble Nitrogen Contents

Drillings from a sample are dissolved in dilute H_2SO_4 by heating in a steam bath. When the acid attack on the drillings is complete, the insoluble residue is separated by centrifuging. The clear solution contains all the 'acid-soluble' nitrogen as an ammonium salt. The insoluble residue is then decomposed by fuming with concentrated H_2SO_4 at its boiling point. This solution is then diluted and contains all the 'acid-insoluble' nitrogen as an ammonium salt. The nitrogen in these two solutions is absorbed as ammonia into a boric acid solution by steam distillation from NaOH solution. The nitrogen contents are then determined from these ammonia solutions colorimetrically with Nessler's reagent.

(b) Determination of Nitrogen Content as AlN (N_{AlN})

The sample is dissolved in methyl acetate-bromine solution. The insoluble residue from this solution is obtained by filtering through two layers of glass fibre filter paper. The bromine absorbed in the filter papers is washed off with methyl acetate. After drying this residue any AlN present in it is hydrolysed by digesting with NaOH in the steam distillation apparatus. The ammonia evolved is collected in a boric acid solution and the nitrogen content of this solution is determined colorimetrically.

A.2.2 Procedure

(a) Determination of N_{sol} and N_{insol}

3.5 gr of the sample was dissolved by the addition of about 40 ml of 18% H_2SO_4 and warming over a steam bath. Once all action had ceased, the solution was cooled and transferred into a 50 ml centrifuge tube and centrifuged at about 2500 r.p.m. for about 8 minutes. 1 ml of 3% $BaCl_2$ was added to the solution and then centrifuged for a further 5 minutes. The clear solution was carefully poured to a 100 ml stopped bottle and kept for steam

distillation.

The insoluble residue was transferred to the original flask washing with ammonia-free distilled water. 10 ml of concentrated H_2SO_4 was added to this insoluble residue and evaporated to fumes using a busen flame. The fuming was continued at its boiling point until all the insoluble residue was decomposed. This solution was cooled and then diluted to about 30 ml by adding ammonia-free distilled water and kept for steam distillation.

The steam distillation was carried out on the apparatus shown in Figure A.1. Initially the apparatus was conditioned by adding about 30 ml of ammonia-free distilled water followed by 40 ml of 50% NaOH solution (containing Devarda's alloy) to the distillation flask E via funnel D and distilling for about 15 minutes by closing Taps 1 and 2. The heat was turned off the steam generator A and the contents in E were allowed to syphon into the evacuation flask C and then drained through Tap 2. A sample kept for distillation was admitted to E followed by 40 ml of 50% NaOH solution. The funnel D was then washed with a little ammonia-free distilled water. The distillation was carried out by closing Taps 1 and 2 and the distillate collected at G in a 100 ml bottle containing 10 ml of 0.1% Boric acid. The bottle was kept with the outlet from the condenser F dipping into the boric acid before closing Taps 1 and 2. The distillation was continued until about 60 - 70 ml were collected. As earlier, the contents of E were drained through Tap 2 after removing the heat from A. This process was repeated for other samples. A blank determination was carried out using 40 ml of 18% H_2SO_4 for each batch of tests.

The distillate solutions were brought up to a standard volume by the addition of ammonia-free distilled water. A set of standard solutions (nitrogen content ranging from 0% to 0.008%) was made from a standard ammonium chloride solution (strength 2 ml = 0.001% N). The standard solutions were

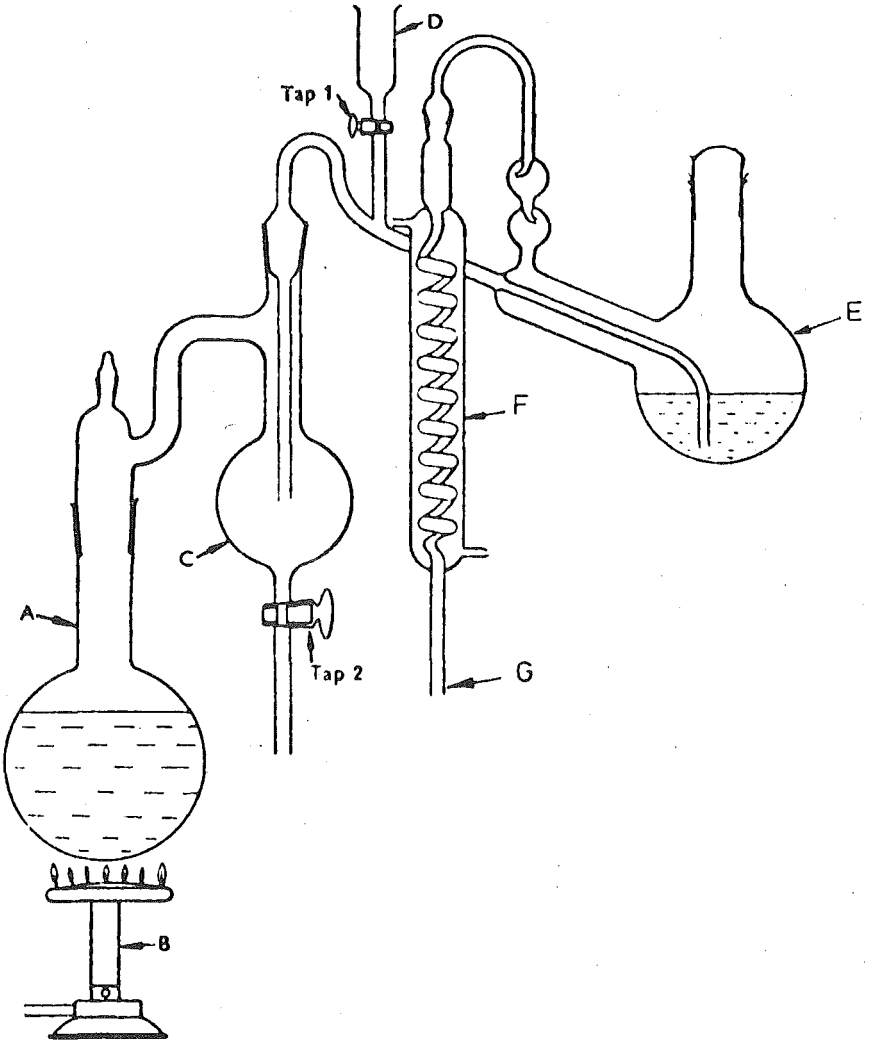

Fig.A.1. Steam Distillation apparatus used for the determination of nitrogen in steel.

made by diluting different volumes of the standard ammonia solution by the addition of 10 ml of 0.1% Boric acid followed by ammonia-free distilled water until the standard volume was reached. 2 ml of Nessler's reagent was added to each of these solutions, mixed and allowed to stand for about 15 minutes. Readings were taken for each solution using a Colormeter. The nitrogen contents of the distillate solutions were determined using the calibration graph which was obtained from the standard solutions.

(b) Determination of $N_{A\ell N}$

3.5 gr of the sample were transferred to a dry 100 ml R.B. flask followed by 8 - 10 ml of bromine. A condenser was attached to the flask and about 40 ml of methyl acetate was added cautiously via the top of the condenser, a few ml at a time. The solution was boiled (at 60°C) gently with the solvent refluxing from the condenser. This process was continued until the sample was fully dissolved (checked using a small magnet). This solution was filtered through two layers of glass fibre filter paper in a dry funnel and filter disc, using suction. The flask was washed with methyl acetate to remove any adhering particles. The filter paper and residue were washed with methyl acetate until it was free from bromine and then transferred to a dry watch glass and dried in an air oven at about 100°C and finally cooled in a desicator.

The dry filter paper containing the residue was transferred to the distillation flask E by opening it at the top, followed by 20 ml of 50% NaOH solution via funnel D. The funnel D was then washed with a little ammonia-free distilled water. The distillation of the sample was then carried out and the distillate collected in a 100 ml bottle, as described in (a). The contents in E were sucked out from top. The nitrogen content of the distillate was determined colorimetrically as in (a).

When carrying out a new set of tests, the distillation apparatus was initially conditioned and a blank determination was made during the tests.

A.2.3 General Precautions in Procedure

The tests were carried out in a Laboratory where every precaution was taken against contamination with ammonia. The reagents and glassware used were specially kept for nitrogen determinations. All reagents used were selected for very low ammonia content. For all dilution of reagents, ammonia-free distilled water was used. The nitrogen content of the blanks (<0.0004%) confirmed that contamination with ammonia was below accepted levels.

APPENDIX B

B.1 Tensile Specimen Preparation

Two sizes of tensile specimens (gauge diameters 12 and 10 mm) were machined. For testing titanium-bearing steel, specimens having a diameter of 12 mm were machined from 28 mm bar, while testing of vanadium-bearing steels was carried out on 10 mm diameter specimens machined from 20 mm bar. The detailed dimensions of these test specimens are shown in Figures B.1 and B.2 respectively. The machining was done by turning and finally giving a ground surface finish along the portion containing the gauge length. (G).

B.2 Charpy V-notch Specimen Preparation

All Charpy V-notch specimens were machined from reinforcing bar to the dimensional requirements of BS 131, Part II of 1972. The machining was done by milling followed by surface grinding. Finally, the standard V-notch was cut by a notching machine.

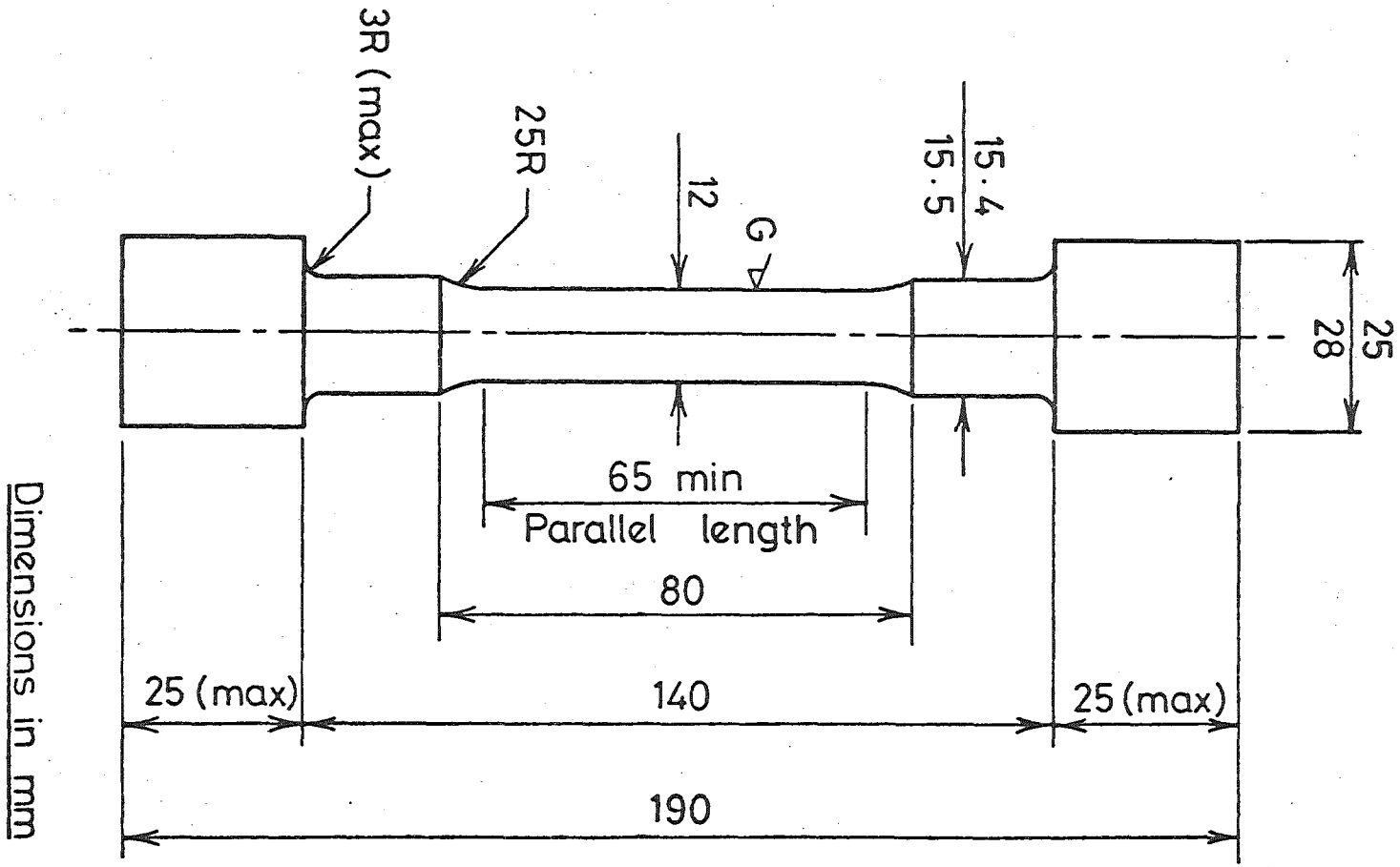

Fig.B.1: Details of the 12 mm diameter tensile specimen.

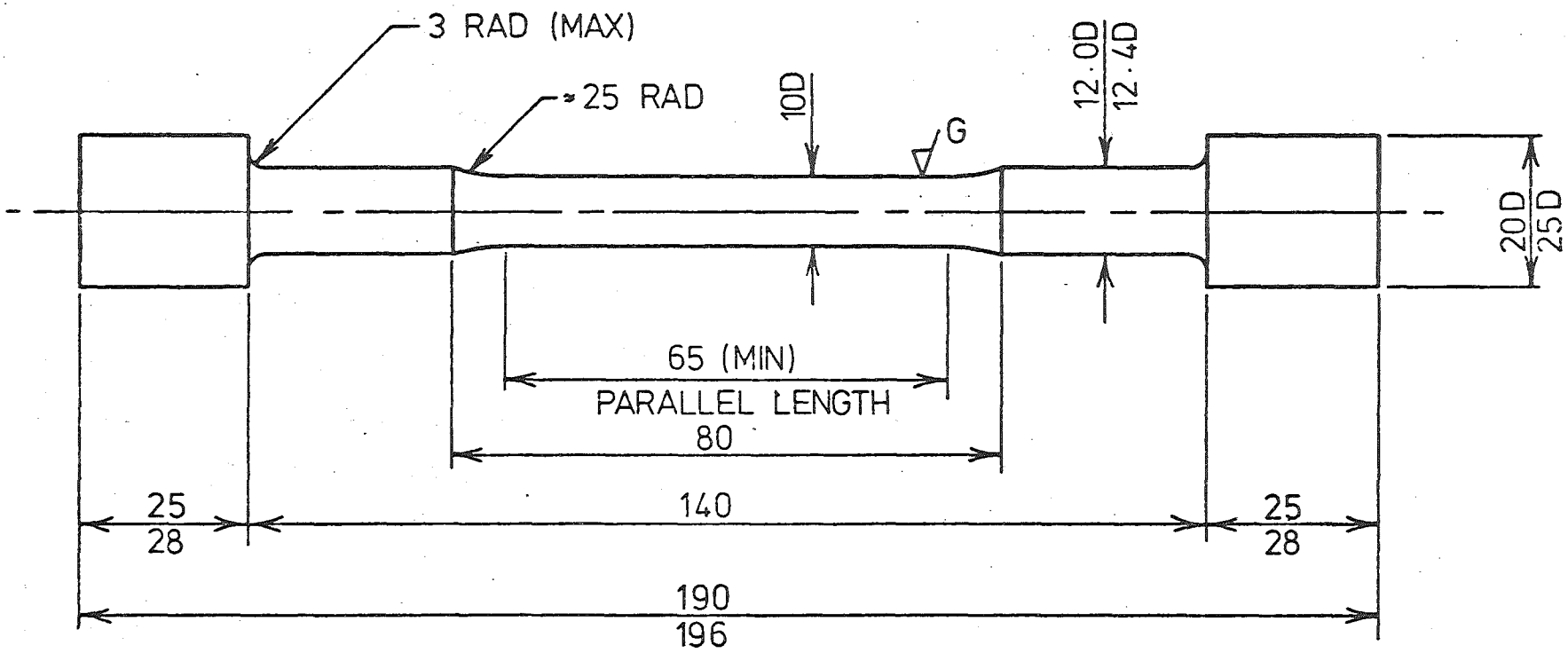

Fig.B.2: Details of the 10 mm diamter tensile specimen.

DIMENSIONS IN MM

APPENDIX C

SAFE BEND RADII FOR DEFORMED REINFORCING BAR TO AVOID FAILURE BY STRAIN AGE EMBRITTLEMENT

L. A. ERASMUS,
M.Sc. (Eng.), Ph.D., C. Eng., M.I.Mech.E., F.I.M.,(Member)*

L.N. PUSSEGODA,
B.Sc.(Eng.)+

SYNOPSIS

Construction site failures of bends as a result of strain age embrittlement suggests that current standards for bend radii in deformed reinforcing bar are inadequate. A method of measuring plastic strain adjacent to the bar deformations has been devised, and an analytical relationship between the bar diameter, the bend former diameter and localized plastic strain determined. This has been used with a relationship between prestrain and Charpy transition temperature to determine safe bend radii for different bar diameters. A considerable advantage in the use of titanium stabilized non-strain ageing grades 275 (Ti) and 415 (Ti) over the existing reinforcing bar grades 275 and 380 has also been shown.

*Reader in Mechanical Engineering, University of Canterbury.

+Postgraduate student.

INTRODUCTION

When structural steel is strained plastically and then allowed to age either at ambient or an elevated temperature, the discontinuous yield point is found to return progressively at a stress substantially above that of the unstrained steel. This return of the discontinuous yield point is accompanied by an increase in the tensile strength and a reduction in ductility, called strain age hardening, and an increase in the ductile to brittle fracture mode transition temperature, called strain age embrittlement.

The above strain ageing effects are brought about by the locking or pinning of mobile dislocations, introduced during plastic straining, by interstitial carbon and nitrogen atoms which diffuse to the dislocation sites during ageing. This locking or pinning effect may be weak when the interstitial content is low or during the early stages of the ageing process, but becomes strong after prolonged ageing with normal interstitial contents. Natural ageing at ambient temperature in slow cooled or as rolled low carbon steels has been shown to be caused by nitrogen only[1]. Hence the addition of a strong nitride forming element such as titanium to low carbon steel reduces its susceptibility to natural ageing [2].

Strain age embrittlement in reinforcing steel has presented spasmodic problems to the building and construction industry in New Zealand for many years. This is usually manifest by sudden and unexpected brittle fractures at design bends or returns in the reinforcing bar during placing or boxing some months after the initial bends are made. Sometimes these failures occur when partially imbedded reinforcing bars are being restraightened after being bent out of the way to allow for working access.

Repair by welding is not recommended, since the weld heat results in accelerated ageing, possibly enhanced by carbon diffusion, in the adjacent

parts of the bend. Subsequent failure in these bends adjacent to the previous repair is consequently possible.

The only reason why strain age embrittlement is not a major construction problem is that the ageing process at ambient temperature is relatively slow, so that in most instances insufficient ageing occurs during the construction period to give strain age embrittlement failures. However, the ageing process continues unnoticed in the region of bends, returns, etc., after they have been embedded in the concrete. Strain age embrittlement should consequently be of major engineering concern, since the occurrence of high tensile stress close to these bends must always be a possibility during earthquakes, and the resultant brittle fractures could lead to the catastrophic collapse of many modern structures, apparently designed to resist seismic loading.

A recent paper on bend fractures during construction in 28 mm diameter deformed reinforcing bar concluded that a number of factors contributed to cleavage fracture at these bends [3]. These were:-

(i) Strain ageing in the plastically deformed material associated with the bend. The increase in plastic strain with decreasing bend radius increases the ductile to brittle transition temperature, see Figure 1.

(ii) The increase in ductile to brittle transition temperature brought about by triaxial stress conditions as found at the root of sharp notches. This notch effect becomes critical when previously made bends are being restraightened, or opened out, since the bar length between deformations (ribs) on the bend inner radius surface is decreased by compressive flow when making the initial bend. This effectively decreases the fillet radius between the bar and the deformations on the bend inner radius surface, and combined with

compressive flattening of these protrusions against the bend former during the bending operation, can result in sharp notches and in extreme cases compression cracks on the bend inner radius surface, see Figure 2.

When these notches are subjected to tensile stress, such as occurs when the bend is being opened out, intense localised plastic deformation occurs at the notches, see Figure 3, resulting in the nucleation of cleavage cracks.

(iii) High strain rates such as occur when previously made bends are struck or as is likely to occur during seismic loading.

(iv) Low temperatures, cleavage fracture being the preferred fracture mode at temperatures below the transition temperature.

Obviously only the first two factors above can be predicted and controlled, although the fracture mode transition temperature of the steel can be substantially lowered by making a small addition of titanium during steel-making which also renders the steel non-strain ageing [2]. The first two factors above are a function of the initial bend radius and for this reason a revision of the minimum bend radii given in Table X of NZS 1900, chapter 9.3A (1970), was recommended [3]. Insufficient data on the plastic strains induced on the inner radii surface of bends was available at that time to allow more specific recommendations on acceptable minimum bend radii.

In the work reported here a method of measuring plastic strain adjacent to the deformations (ribs) has been devised enabling minimum bend former diameters to avoid failure by strain age embrittlement to be calculated. This has been done for grades 275 and 380 (NZS 3402P (1973)), and for the proposed new titanium stablized grades 275 (Ti) and 415 (Ti).

THE MEASUREMENT OF PLASTIC STRAIN IN BENDS

Theoretical solutions for plastic strain in bent bars assuming a non-strain hardening material have been derived by Lubahn and Sachs [4]. Almost identical solutions were obtained for axial surface strain (i.e. tangential to the bar axis) when assuming plane strain or plane stress conditions. They showed that the axial surface strain for the bend inner radius surface could be approximated by the equation:-

$$\varepsilon_c = \frac{1 - K}{1 + K} \qquad \text{Equation 1}$$

$$\text{where } K = \frac{D/d}{1 + \left\{\left(D/d\right)^2 + 2D/d\right\}^{\frac{1}{2}}}$$

d = bar diameter

D = bend former diameter

This equation gives the axial strain for the bend inner radius surface for plain bars, but because of the strain concentration effect of the protrusions (deformations), see Figure 3, it cannot be used directly to calculate the plastic strain on the inner radius surface of deformed reinforcing bar. These areas of intensive localised plastic strain are however the nucleation points for cleavage fracture when the bend is opened out, so that some measure of this strain magnitude and its effect on the ductile to brittle fracture transition temperature is essential for the determination of safe bend radii. Unfortunately, the small size of these localised strain areas precludes the use of conventional strain measurement techniques, e.g. electrical resistance strain gauges. For this reason a measurement technique based on microstructural change during deformation was contrived.

All commercial metallic materials are polycrystalline, and in single phase metals or metals with a relatively small proportion of a second phase such as low carbon steel, the boundary between one grain and the next can readily be shown on a microspecimen by different etching techniques. When a series of parallel lines are constructed on a photomicrograph of the etched microstructure and the number of grain boundary intersections for the total length of line counted, the mean grain size is given by:-

$$\delta = \frac{\text{total line length}}{\text{M x number of boundary intersections}}$$

where M is the photomicrograph magnification.

This method of estimating mean grain size is well established and frequently used on structural steel and other metals, where the lines are normally constructed as a square grid to compensate for any directionality in the structure.

During plastic straining, the metal crystals or grains are elongated in the direction of straining, and if the distance between the boundaries on each grain is considered equal to a small initial gauge length, the strain can be measured from the elongation of each grain, i.e. if the grain size is measured as above but in the direction of straining, then strain can be defined:-

$$\varepsilon_a = \frac{\Delta\delta_a}{\delta_o} \qquad \text{Equation 2}$$

where $\Delta\delta_a = \delta_1 - \delta_o$

δ_1 = mean grain size measured in the direction of straining

δ_o = initial mean grain size

A slight modification of this technique can also be used where the grain size perpendicular to the direction of straining is also measured. Strain can now be defined:-

$$\varepsilon_p = \frac{\delta_1 - \delta_m}{\delta_m} \qquad \text{Equation 3}$$

where $\delta_m = \frac{\delta_1 + \delta_2}{2}$

δ_2 = mean grain size measured after straining, perpendicular to δ_1

The first method (equation 2) suffers experimental inaccuracies due to small variations in grain size from point to point in the bar, normally overcome by increasing the total line length used for grain intersection counts. However, the small area of interest in this instance (taken as approximately 0.23 mm square) precluded this refinement. The experimental inaccuracies are smaller in the second method (equation 3) since all the measurements are made in one specific area and not referred to some other unstrained area. However, this method assumes plane strain conditions, i.e. that the grain size perpendicular to the microspecimen surface is not changed during straining.

Both of these techniques were used in this instance to measure the axial surface strains close to the inner radius surface of 20 mm diameter plain bar and a range of deformed bar sizes. Each bend was sectioned in the plane of the bend (e.g. as for Figure 3) and the grain size measured as near to the inner radius surface as possible. The calculated strains for the 20 mm diameter plain bar are shown in Figure 4 together with the theoretical curve from equation 1. For the deformed reinforcing bars plastic strains were again measured as near the inner radius surface as possible, but adjacent to the protrusions (deformations). These strains were significantly larger than predicted by equation 1, and the results for 16 mm, 22 mm and 28 mm diameter bars are shown in Figure 5(a), 5(b) and 5(c) respectively. Since strain increased more rapidly with decreasing D/d ratio on the deformed bars, and increased also with bar diameter, a combined analytical expression was derived:-

$$\varepsilon_n = \varepsilon_c + 0.7 \left(\frac{d}{D}\right)^2 + 0.2\, d - 3 \qquad \text{Equation 4}$$

where ε_n = notch strain adjacent to the bar protrusion expressed as percentage strain

ε_c = theoretical strain from equation 1 expressed as percentage strain

d and D = bar and bend former diameters respectively (mm)

Curves predicted by equation 4 are also shown in Figures 5(a), 5(b) and 5(c).

Although a better correlation was obtained between equation 1 and the experimental strain measured by equation 2 on the 20 mm diameter plain bar, see Figure 4, a greater degree of scatter was obtained on the deformed reinforcing bar with this technique, see Figure 5. Since Lubahn and Sachs [4] have shown almost identical solutions for plane stress and plane strain bend conditions, the two measurement techniques (equations 2 and 3) were used together to determine equation 4. The resultant correlation coefficient between equation 4 and the experimental results was 0.762, i.e. significance better than the 0.1% level. The variation in the shape distortion of grains even within the small area used for experimental strain measurement suggested that further refinement of equation 4 would not be soundly based, see Figure 6.

THE CALCULATION OF SAFE BEND RADII

To calculate bend radii which will resist failure by strain age embrittlement during seismic loading, some standard or reference point is required. Unfortunately such data is not available, and what little data exists on construction site failures is generally incomplete. The only fully documented failure of this kind occurred in 28 mm diameter deformed reinforcing bar when 90° bends were being struck with a sledge hammer at an ambient temperature of 5°C to 7°C [3]. Approximately 50% of the bends so struck fractured, all in a region

where the bend radius was 2.6d. Adjacent parts of these bends where the radius was 3.1d did not fail. If it is assumed that these conditions approximate to the severest conditions likely to be encountered during construction or subsequent earthquakes, i.e. shock loading at relatively low temperature, a safe bend radius of 3.5d (bend former diameter 7.0d) can be taken as the reference non-failure condition.

Similar fractures were produced in the laboratory on bars from the same batch at test temperatures between $0^{o}C$ and $4^{o}C$ when restraightening artificially aged bends of 1.5d radius (bend former diameter 3d) or less, see Table 1. Restraightening of these bends was by slow bending as opposed to the impact or shock loading of the construction site failures. A reference safe bend former diameter of 3.5d is consequently established for this test. Tests on this steel showed that the chemical composition and mechanical properties were normal for grade 275 reinforcing bar, and that it had a Charpy transition temperature of $-2^{o}C$ [3].

Taking the above safe bend former diameter of 7.0d as the reference standard, the bar surface strain adjacent to the protrusions (deformations) in the region of fracture nucleation can be determined from equation 4, and by referring this strain to Figure 1 an equivalent Charpy transition temperature increase can be obtained. Since the initial as rolled transition temperature of this material is known, the equivalent Charpy transition temperature of the material in the region of fracture nucleation can be obtained, e.g. a D/d ratio of 7.0 gives from equation 4 a notch strain of 17%, corresponding to a Charpy transition temperature increase of $55^{o}C$ (see Figure 1). The material had an initial transition temperature of $-2^{o}C$, so that the final equivalent transition temperature of the material in the region of fracture nucleation was $53^{o}C$.

If it is now assumed that there is no substantial change in the triaxial stress state resulting from the bar deformations on the bend inner radius surface when changing from one bar diameter to the next, the above calculations can be reversed to calculate safe D/d ratios for other bar diameters, i.e. assuming that an equivalent transition temperature of 53°C (or less) will not result in fracture adjacent to the bar deformations. These calculations require also a knowledge of the normal Charpy transition temperatures for all bar sizes in grade 275 and 380 reinforcing bar. This substantial quantity of data is unfortunately not available, but the values shown in Table 2 can be assumed as normal in the absence of better data. This table assumes a range of 30°C change in Charpy transition temperature over the bar size range 10 mm to 40 mm diameter, hinging on actual values obtained on 28 mm diameter reinforcing bar.

Using Table 2 and the reference fracture transition temperature of 53°C, safe bend radii (bend former diameter) have been calculated for deformed reinforcing bars made to grade 275 and grade 380. These bend former diameters, both calculated and recommended, are shown in Tables 3 and 4 for the respective grades, together with former diameters currently recommended by NZS 1900 Chapter 9.3A (1970) and the ACI Standard 318-71.

In making the above calculations it has also been assumed that the data shown in Figure 1 for grade 275 reinforcing bar applies equally to grade 380 steel. The only available data for grade 380 steel is also shown in Figure 1, and supports the above assumption.

THE NEW TITANIUM STABLISED REINFORCING STEELS

It is now well established that a small addition of titanium made during steelmaking to the reinforcing steel grades 275 and 380 will render these steels non-strain ageing by forming stable titanium nitride

precipitates, thus lowering and in most instances completely eliminating active nitrogen in these steels [1, 2]. It has also been shown that this titanium addition, usually in the range 0.020% to 0.035%, will increase the yield strength, increase the yield (Luder) strain, and reduce the as rolled Charpy transition temperature (improved fracture toughness) [2]. This increase in yield strength can be used to advantage by reducing the carbon content of the steel which will result in further improvements in yield strain and fracture toughness whilst still meeting the specified minimum yield strength. Alternatively, this increased yield strength can be used without significant change to the present basic chemical composition to give a new higher strength grade of reinforcing steel.

It is proposed that the former option be adopted to replace grade 275 steel, and this new grade be designated grade 275 (Ti). If the latter option is adopted to replace grade 380 steel, resulting in a new high strength grade 415 (Ti), ACI design charts and tables for concrete reinforced by bars of 60,000 lbs/in^2 (414 MN/m^2) yield strength can be used, resulting in considerable advantage to New Zealand Structural Engineers.

The availability of this steel will also have considerable economic advantage, and the reduced reinforcing volume in joints will aid their design. The improved yield strain of grade 415 (Ti) over the existing grade 380 is also attractive [2], since the low yield strain values obtainable on the present grade 380 reinforcing results in this steel being scarcely used.

Safe bend radii can be calculated for these steels in an identical manner to that adopted above for the normal grades 275 and 380 reinforcing bar, and these results are again shown in Tables 3 and 4. As with grade 380 steel, insufficient data exists on the increase in Charpy transition temperature with prestrain for the new grade 415 (Ti) reinforcing bar, necessitating the use of data shown in Figure 1 for

the 275 (Ti) grade when calculating bend former diameters. What data is available for this grade after 5% prestrain is again shown in Figure 1, and suggests that it will not be substantially different to that for grade 275 (Ti) reinforcing bar. Again a Charpy transition temperature range with changing bar diameter has been assumed in Table 2 to enable the bend former diameter calculations to be made.

It can be seen from Tables 3 and 4 that these new titanium stabilized steels have considerable advantage over the normal reinforcing grades 275 and 380, and bearing in mind the other advantages referred to above, the rapid adoption of these grades seems most desirable.

QUALITY CONTROL

To ensure that reinforcing steel conforms satisfactorily to the material properties assumed as a basis for the calculations of the safe bend radii recommended in Tables 3 and 4, additional testing to that specified in NZS 3402P (1973) is necessary. This would require the introduction of a Charpy test specifying a minimum requirement of 27 Joule at the test temperatures indicated in Table 5. This table has been derived from Table 2 but with the temperatures rounded up to the nearest $5^{o}C$ increment where this is possible without compromising the additional safety factor introduced when rounding up the bend former diameters recommended in Tables 3 and 4.

The only available data on the 27 Joule Charpy transition temperature of New Zealand produced casts is summarised in Appendix 1. Comparison of this data with Table 5 suggests that the requirements of Table 5 are reasonable and could probably be met on most normal production casts made by Pacific Steel Ltd.

An alternative test procedure more suited to field or site testing would be the reversed bend test. For this test the deformed

bar would require bending through 90° around a bend former of specified diameter before being aged at 100°C (boiling water) for 3 hours. This ageing treatment approximates to natural ageing at 15°C for 9 months. The bend is then restraightened without impact to 60° at a test temperature between 0°C and 4°C (water and ice mixture). If the bar has strain aged excessively, cleavage (brittle) fracture will propagate across at least half the bar diameter within the initial few degrees of restraightening. Using the reverse bend test results obtained on the 28 mm diameter grade 275 deformed bar, see Table 1, as a standard or reference point, safe bend radii can again be calculated using Table 2, equation 4 and Figure 1, i.e. assuming a reference safe bend former diameter of 3.5d. The calculated and recommended bend former diameters for this test are shown in Table 6 for grade 275 and 380 deformed reinforcing bar. Unfortunately this test cannot be used on the new titanium stablised grades 275 (Ti) and 415 (Ti) since the calculated bend former diameters are too small and restrictive in range to allow satisfactory discriminations between satisfactory and unsatisfactory material, i.e. a maximum former diameter of 2d for 40 mm diameter bar. These calculations also require extrapolation of the graph shown in Figure 1 for grade 275 (Ti) steel to an unreasonable degree, making its validity questionable.

The results from a series of reverse bend tests on commercially purchased grade 275 and grade 380 steel are shown in Tables 7(a) and 7(b) respectively. The propensity of each test bar to cracking on the inner radius surface was assessed according to the depth of any crack formed and the failure mode, i.e. digits 1 to 5 indicate crack depths of 1 to 5 mm, with the digit 6 indicating complete fracture, and the letters N, D and C indicating no crack, ductile tearing and cleavage fracture respectively. C6 consequently represents catastrophic fractures by cleavage within the first degree or two of restraightening. The predicted safe bend former diameter limit from Table 6 is also indicated

in Tables 7(a) and 7(b), and with the exception of the 22 mm diameter grade 380 bar, fractures classified as C6 do not occur with bend former diameters equal to or greater than those predicted as safe by Table 6. The results of chemical analysis of the test bars from Table 7 are shown in Table 8 where the main difference between the 22 mm diameter grade 380 bar and the other test samples in this grade (see also Appendix 1) is the higher than normal active nitrogen content of this sample. Charpy tests on this reinforcing bar showed that it had a 27 Joule transition temperature of 25^{O}C, giving a calculated safe reversed bend former diameter of 6.0d. This can be seen to be in keeping with the test results shown in Table 7(b).

Since the Charpy test on this reinforcing bar would fail to meet the specification requirement shown in Table 5, this cast would justifiably be rejected by both tests.

CONCLUSIONS

To calculate safe bend radii a number of assumptions have had to be made. These are that:-

(i) the relationship between Charpy transition temperature and prestrain shown in Figure 1 for normal grade 275 and the improved grade 275 (Ti) reinforced steel can be extrapolated to higher prestrains than the experimentally determined 15%. This is necessary since plastic instability leading to localised necking occurs in bars strained in tension to larger strains and results in non-uniform straining. Attempts have been made to prestrain test material in compression [5], but friction between the press plattens and the specimen results again in non-uniform straining and uncertainty in results. There seems, therefore, to be no possibility of extending this experimental data to higher prestrain values other than by extrapolation.

(ii) the increase in Charpy transition temperature with prestrain for grade 380 and the new titanium stabilised grade 415 (Ti) reinforcing bar will be similar to that determined for grades 275 and 275 (Ti) respectively. The limited data currently available (for 5% prestrain) appears to support this assumption.

(iii) the failure conditions used as reference or standard, i.e. the 28 mm diameter deformed bar bent through 90^{o} and struck with a sledge hammer after ageing for nine months [3], corresponds to the most severe conditions likely to be encountered during construction, and approximates to conditions likely to be encountered during earthquakes. There is no possibility of confirming this assumption, however, it is significant that the recommended bend former diameters for grade 275 and 380 reinforcing bar are generally larger and therefore safer than recommended in the existing standards.

By contrast the recommended bend former diameters for the new titanium stablised grades 275 (Ti) and 415 (Ti) reinforcing bar are smaller than those recommended in existing standards, showing considerable advantage over the existing grades. The bend former diameters for the titanium stabilised steels have also been calculated with more conservative estimates of transition temperature than for the normal grades, and in many instances the recommended bend former diameters are more than the normal 1d above the calculated value, see for example Table 4. This has been done deliberately to compensate for a lack of data on production casts of these grades. However, this means that there has been an overall higher factor of safety applied to the titanium stabilised grades.

(iv) the deformations (ribs) on all bar diameters give similar states of triaxial stress on the bend inner radius surface, see Figure 2. Obviously this could vary slightly from one bending machine to the next, and with different bar sizes and production runs, but this variation should be small and random and can therefore be neglected.

In some special circumstances it may be desirable to make bends of smaller radius than those recommended in Tables 3 and 4. The alternatives are then to either use plain bar, or to grind the deformations off the bar inner radius surface before making the bend.

(v) finally it has been necessary to assume a range of Charpy transition temperatures for bars of different diameter (Table 2). Current data indicates that these values, and the amended values given in Table 5, will normally be obtainable on production casts. The large amount of data required to verify these tables, taking statistical variation into consideration, can only be obtained by introducing this requirement into a provisional standard e.g. NZS 3402(P). These tables could subsequently be amended to suit the new data, and the bend former diameters shown in Tables 3 and 4 then recalculated.

ACKNOWLEDGEMENTS

Mr. L.N. Pussegoda has been supported by a Ministry of Works grant whilst pursuing a research programme on strain ageing in structural steel. The authors gratefully acknowledge this assistance. The continued support of the management of Pacific Steel Limited in research on strain ageing undertaken in the Department of Mechanical Engineering, University of Canterbury, is also gratefully acknowledged.

REFERENCES

1. PUSSEGODA, L.N. and ERASMUS, L.A., 1977, Proc. 6th Australasian Conf. on Mechanics of Structures and Materials, Christchurch, p. 445.

2. SMAILL, J.S., et. al., 1976, Metals Technology, Vol. 3, p. 94.

3. ERASMUS, L.A. and PUSSEGODA, L.N., 1977, N.Z. Engineering, Vol. 32, p. 178.

4. LUBAHN, J.D. and SACHS, G., 1950, Trans. A.S.M.E., Vol. 72, p. 201.

5. GROOM, J.D. and KNOTT, J.F., 1975, Metal Science, Vol. 9, p. 390.

TABLE 1 Slow reversed bend tests on grade 275 deformed reinforcing bar at $0^{o}C$ - $4^{o}C$.

Bar Dia. mm.	Former Diameter				
	2.0d	2.5d	3.0d	3.5d	4.0d
28	C6	C6	C6	D1	D1

C6 = Cleavage fracture across cross-section

D1 = Ductile tear 1 mm. deep

TABLE 2 Assumed normal Charpy transition temperatures for reinforcing bar.

27 Joule Transition Temperature (^{o}C)

Grade	275	275 (Ti)	380	415 (Ti)
Bar Dia. (mm.)				
10	-23	-26	-15	-34
12	-21	-24	-13	-32
16	-15	-18	- 7	-26
20	-12	-15	- 4	-23
22	-10	-13	- 2	-21
24	- 7	-10	1	-18
28	- 3*	- 6*	5*	-14*
32	2	- 1	10	- 9
34	4	1	12	- 7
40	7	4	15	- 4

*Experimentally determined values.

TABLE 3 Safe bend former diameters for grades 275 and 275 (Ti) deformed reinforcing bar.

Bar diameter d (mm)	Former diameter D					
	NZS 1900 9.3 A	ACI 318-71	NZS 3402 Grade 275		New Grade 275 (Ti)	
			Calculated	Recommended	Calculated	Recommended
10	5d	6d	2.9d	4d	1.2d	2d
12	5d	6d	3.2d	5d	1.3d	2d
16	5d	6d	3.8d	5d	1.6d	3d
20	6d	6d	4.6d	6d	1.9d	3d
22	6d	6d	5.0d	6d	2.1d	4d
24	6d	6d	5.8d	7d	2.4d	4d
28	8d	8d	7.0d	8d	2.9d	5d
32	8d	8d	9.7d	11d	3.7d	5d
34	8d	8d	11.0d	12d	4.0d	6d
40	-	10d	15.0d	16d	5.4d	7d

TABLE 4 Safe bend former diameters for grade 380 and 415 (Ti) deformed reinforcing bar.

Bar diameter d (mm)	Former diameter D					
	NZS 1900 9.3A	ACI 318-71	NZS 3402 Grade 380		New Grade 415 (Ti)	
			Calculated	Recommended	Calculated	Recommended
10	5d	6d	3.3d	5d	1.0d	2d
12	5d	6d	3.8d	5d	1.1d	2d
16	5d	6d	4.7d	6d	1.3d	3d
20	6d	6d	5.5d	7d	1.6d	3d
22	6d	6d	6.2d	8d	1.7d	4d
24	6d	6d	7.5d	9d	1.9d	4d
28	8d	8d	9.5d	11d	2.3d	5d
32	8d	8d	14.1d	16d	2.9d	5d
34	8d	8d	16.0d	18d	3.1d	6d
40	-	10d	26.0d	28d	3.8d	7d

TABLE 5 Tentative Charpy test temperatures for reinforcing bar quality control.

Charpy Test Temperatures for minimum of 27 Joules

Grade	275	275(Ti)	380	415(Ti)
Bar Dia.(mm)				
10	-20*	-20*	-10*	-30*
12	-20*	-20*	-10*	-30*
16	-10	-15	- 5	-25
20	-10	-10	0	-20
22	- 5	-10	0	-20
24	- 5	- 5	5	-15
28	0	- 5	5	-10
32	0	0	10	- 5
34	5	5	10	- 5
40	5	5	15	0

*20 Joule on 7.5 mm subsidiary Charpy test piece

TABLE 6 Bend former diameters for reversed bend field tests on deformed reinforcing bar to be tested at $0^{\circ}C$ - $4^{\circ}C$ after ageing at $100^{\circ}C$.

Bar diameter d(mm)	Former diameter D			
	NZS 3402 Grade 275		NZS 3402 Grade 380	
	Calculated	Recommended	Calculated	Recommended
10	1.7d	1.5d	2.0d	2.0d
12	1.8d	2.0d	2.2d	2.0d
16	2.2d	2.0d	2.6d	2.5d
20	2.5d	2.5d	3.0d	3.0d
22	2.7d	2.5d	3.2d	3.0d
24	3.0d	3.0d	3.6d	3.5d
28	3.4d	3.5d	4.2d	4.0d
32	4.2d	4.0d	5.1d	5.0d
34	4.7d	5.0d	5.7d	6.0d
40	5.7d	6.0d	6.9d	7.0d

TABLE 7(a) Reversed bend tests at 0°C - 4°C on aged grade 275 deformed reinforcing bar

Bar Dia. mm.	Former Diameter						
	1.0d	1.5d	2.0d	2.5d	3.0d	3.5d	4.0d
16		C1, D3	D1				
22	C6	D2	D3				
28		C6	D4	C6	C6	D2	D1

TABLE 7(b) Reversed bend tests at 0°C - 4°C on aged grade 380 deformed reinforcing bar

Bar Dia. mm.	Former Diameter							
	1.5d	2.0d	2.5d	3.0d	3.5d	4.0d	4.5d	5.0d
16	D3	D2		N	N	N		
22				C6	C6	C6	C6	D1
28				C6		D4	D3	N

TABLE 8 Chemical analysis of commercial reinforcing bar used for slow reversed bend tests in Table 7.

Steel	C (%)	Mn (%)	Nitrogen analysis (wt %)				
			N_{sol}	N_{insol}	N_{tot}	N_{AlN}	N_{active}
Grade 275, 16 mm bar	0.22	0.51	0.0049	0.0009	0.0058	0.0002	0.0047
" " 22 " "	0.21	0.51	0.0049	0.0004	0.0053	0.0002	0.0047
" " 28 " "	0.23	0.40	0.0049	0.0007	0.0056	0.0003	0.0046
Grade 380, 16 mm bar	0.34	1.16	0.0051	0.0007	0.0058	0.0003	0.0048
" " 22 " "	0.38	1.06	0.0075	0.0006	0.0081	0.0002	0.0073
" " 28 " "	0.38	1.15	0.0059	0.0005	0.0064	0.0005	0.0054

APPENDIX 1

Charpy 27 Joule Transition Temperature (T_{27})
for Production Casts

Bar dia.(mm)	%C	%Mn	%Ti	$\%N_{active}$	$T_{27}(^{o}C)$	Ref
Grade 275						
20	0.21	0.51	0	0.0056	-16	A
20	0.23	0.47	0	0.0049	-17	B
20	0.23	0.44	0	0.0051	-13	B
24	0.18	0.63	0	0.005	-35	C
28	0.23	0.46	0	0.0040	-3	D
28	0.23	0.46	0	0.0049	-3	B
28	0.20	0.45	0	0.0045	-2	E
32	0.21	0.45	0	0.005	-17	F
32	0.20	0.45	0	0.004	-20	F
Grade 275 (Ti)						
24	0.18	0.63	Trace	0.003	-42	C
28	0.21	0.44	0.029	0.0005	-12	D
28	0.23	0.45	0.036	0.0003	-6	B
Grade 380						
22	0.38	1.10	0	0.0045	-10	G
24	0.25	1.33	0	0.0039	1	H
32	0.36	1.22	0	0.005	14	F
Grade 415 (Ti)						
24	0.25	1.33	0.018	0.0012	-51	H
24	0.25	1.33	0.025	0.0003	-37	H
24	0.25	1.33	0.035	0.0001	-14	H

References

A Project report 45/77, Dept.Mechanical Engineering

B Ph.D. thesis, L.N. Pussegoda

C Project report 7/72, Dept. Mechanical Engineering

D Project report 3/74, Dept. Mechanical Engineering

E Erasmus L.A. & Pussegoda L.N., 1977, N.Z. Engineering, Vol.32, p. 178

F Lyth C, DSIR/AIDD Report G94, 1972

G Project report 3/71 Dept. Mechanical Engineering

H Project report 36/73 Dept. Mechanical Engineering

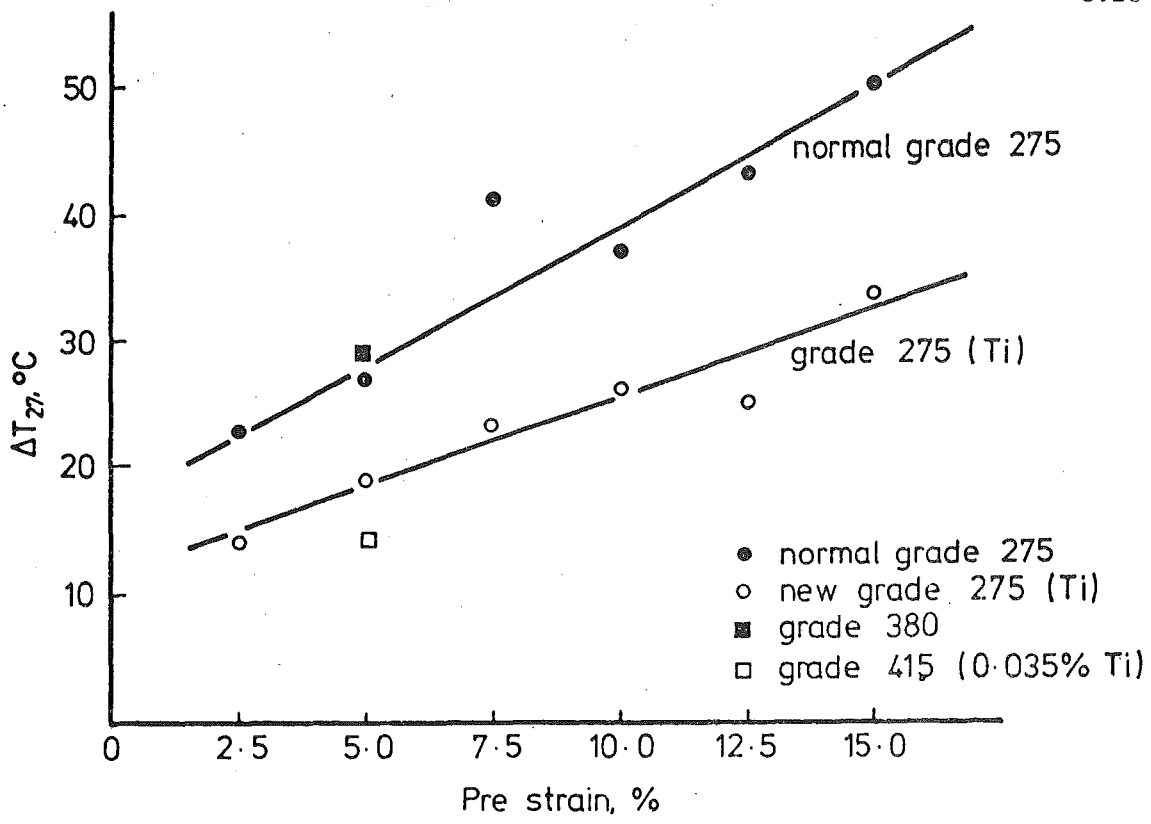

Figure 1: The effect of pre-strain on the increase in Charpy transition temperature (27 Joule energy level) after ageing at 100°C.

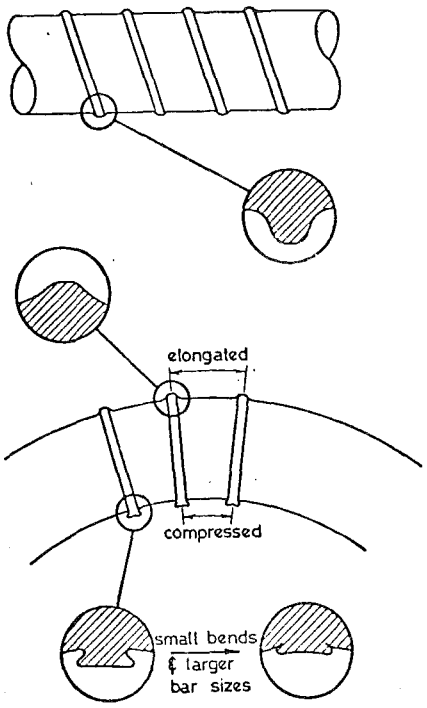

Figure 2: Stress concentration effect decreased by deformation - bar fillet radius being increased on bend outer radius surface, and increased by decreased fillet radius on bar inner radius surface, often intensified by flattening of deformations on bend former (schematic).

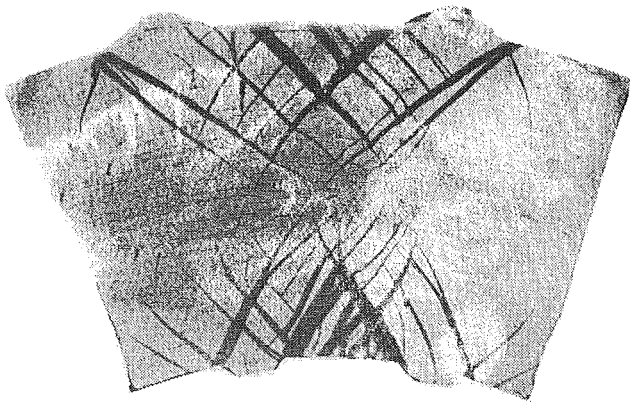

Figure 3: Localised plastic flow from stress concentration points adjacent to protrusions (deformations). 24 mm diameter deformed bar bent on former of diameter 3d. Bend normalised and restraightened approximately 0.5° before sectioning and etching in Fry's Reagent.

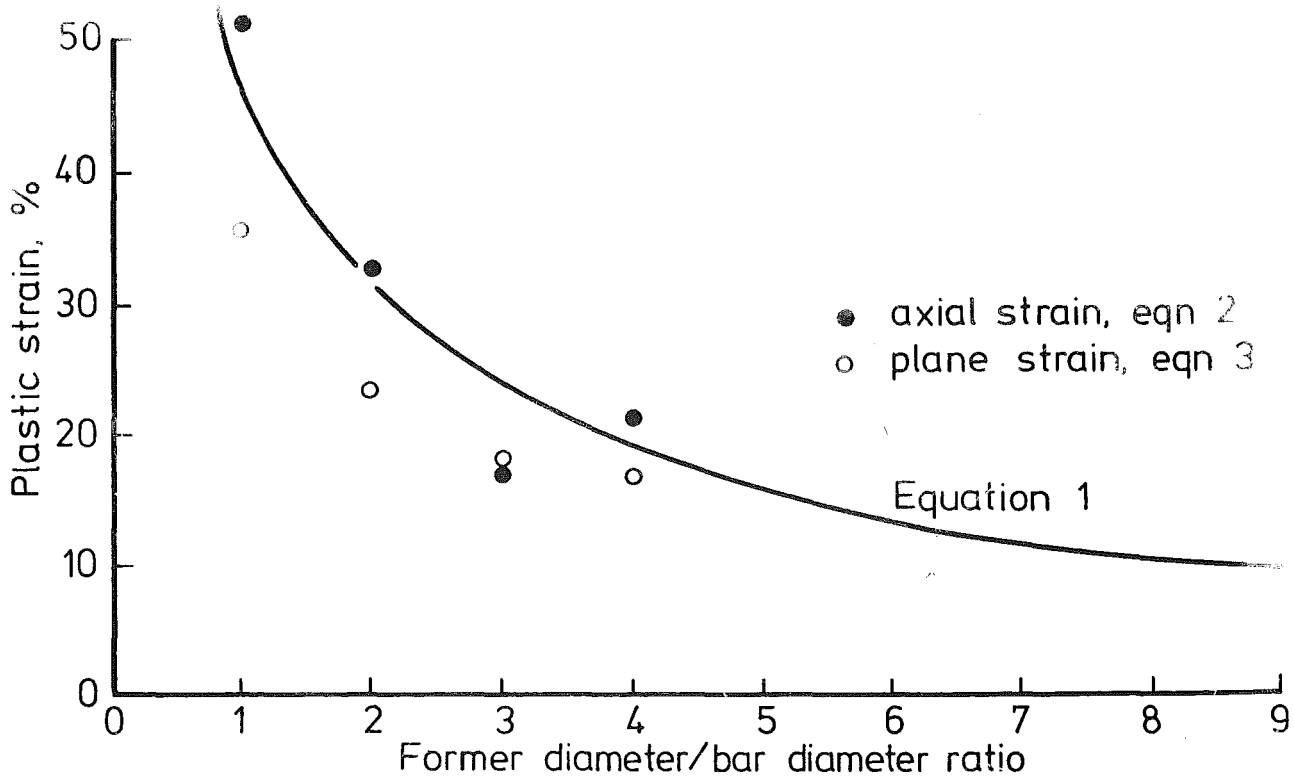

Figure 4: Plastic strain on bend inner radius surface of 20 mm diameter plain reinforcing bar.

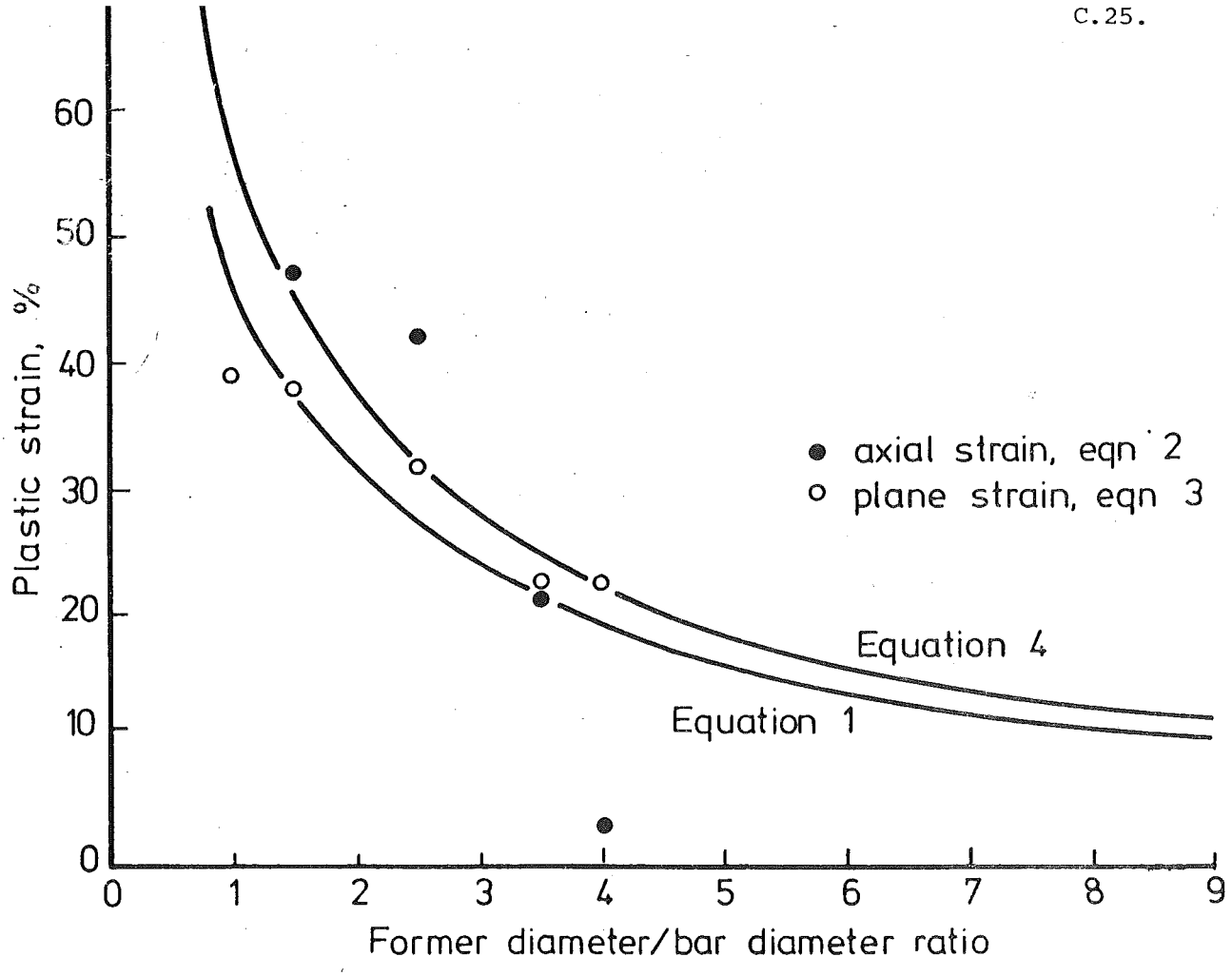

(a) 16 mm diameter reinforcing bar.

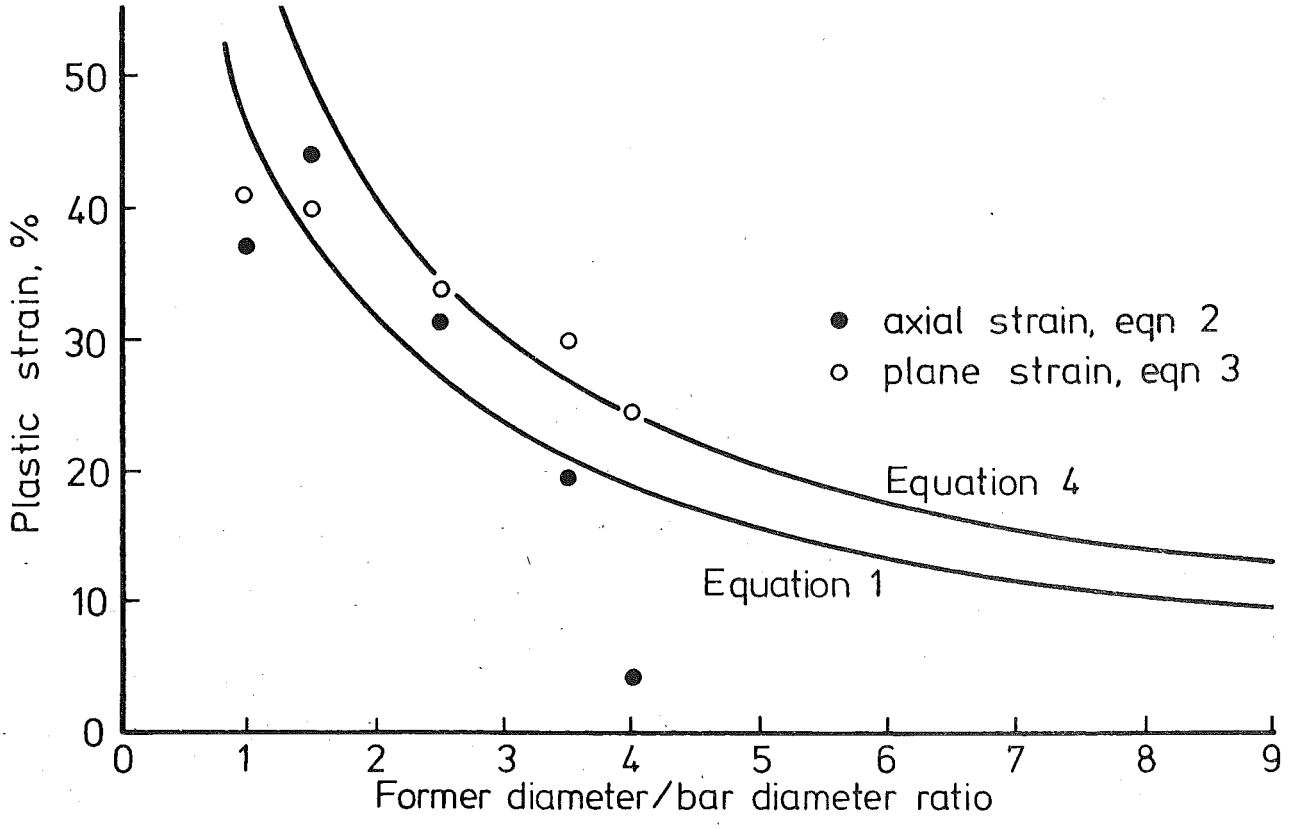

(b) 22 mm diameter reinforcing bar.

Figure 5: Plastic strain adjacent to deformations on bend inner radius surface.

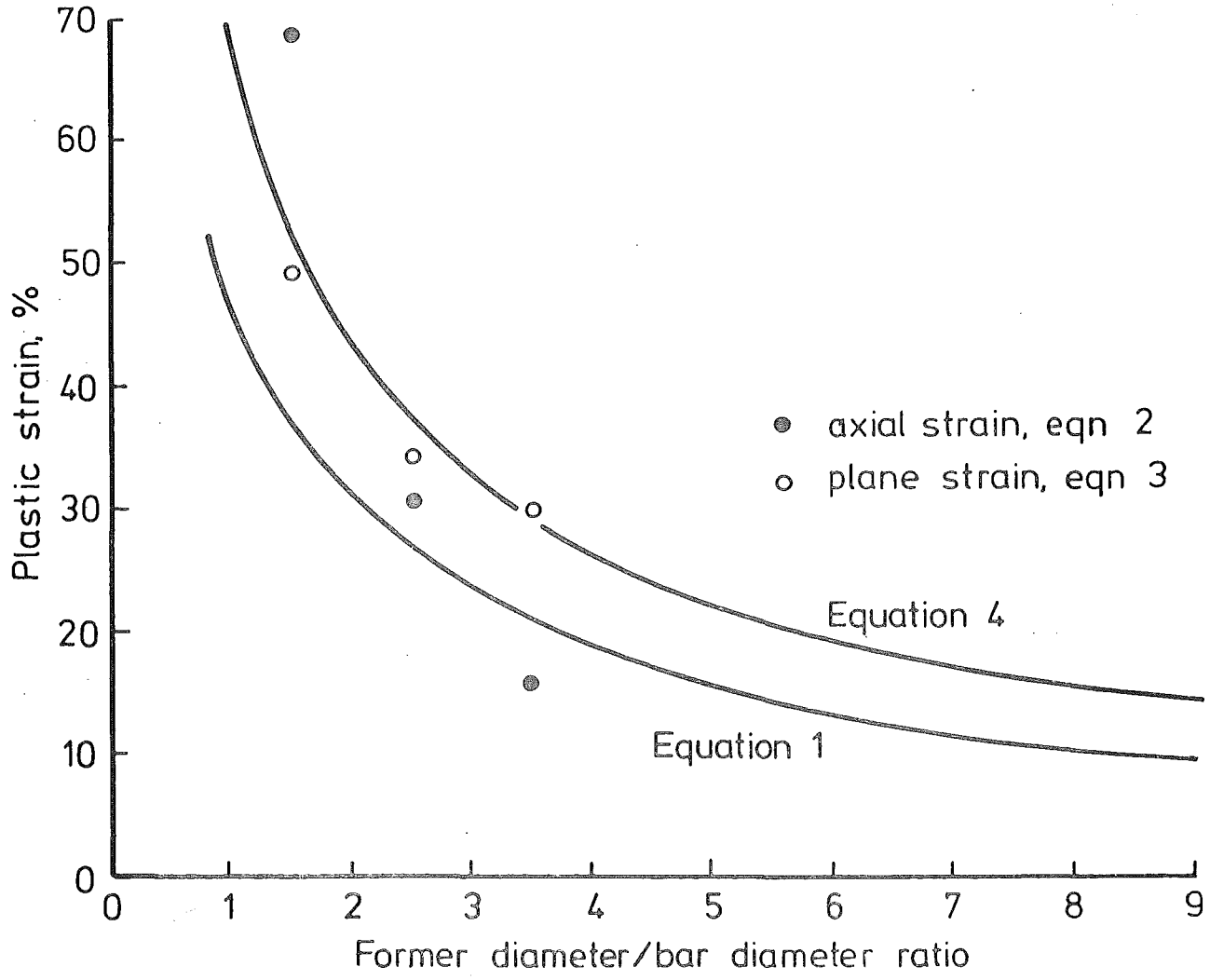

(c) 28 mm diameter reinforcing bar.

Figure 5: Plastic strain adjacent to deformations on bend inner radius surface.

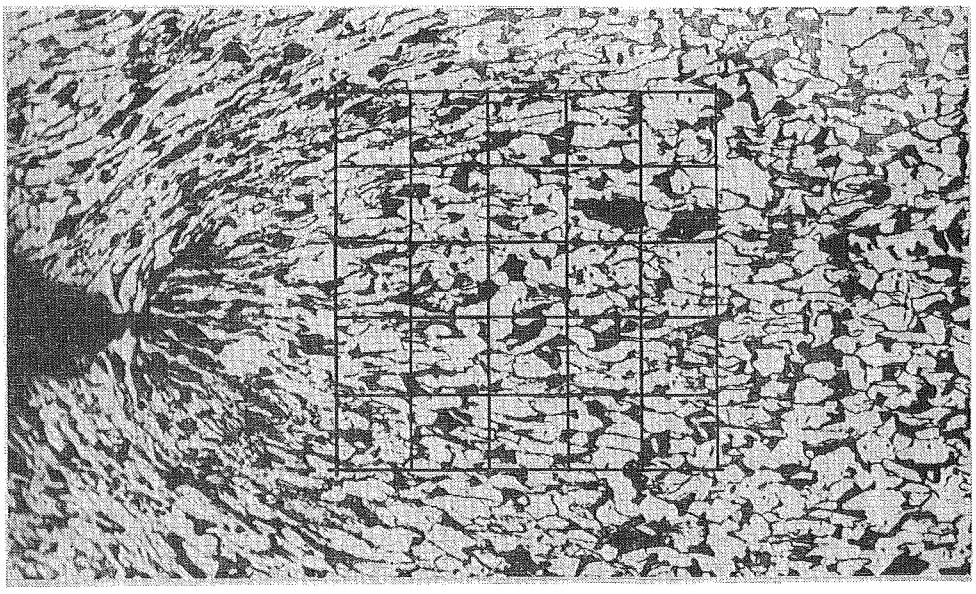

Figure 6: Strain measurement grid on micrograph of bar structure adjacent to deformation. Grid size 10 mm x 10 mm.